Svein Helge Gjøsund

Kinematics in Regular and Irregular Waves based on a Lagrangian Formulation

NTNU Trondheim
Norges teknisk-naturvitenskapelige universitet

Doktor ingeniøravhandling 2000:86
Institutt for konstruksjonsteknikk

KINEMATICS IN REGULAR AND IRREGULAR WAVES BASED ON A LAGRANGIAN FORMULATION

by

Svein Helge Gjøsund

dr.ing. thesis
Trondheim, September 2000

Department of Structural Engineering
Faculty of Civil and Environmental Engineering
The Norwegian University of Science and Technology

ABSTRACT

Kinematics in two-dimensional regular and irregular surface waves is described based on the Lagrangian form of the equations of motion, with particular emphasis on the conditions in the so-called splash zone in irregular waves. A practical method for accurate calculation of kinematics in broad-banded irregular waves is developed based on Gerstner's wave theory, and theoretical calculations are compared with laboratory wave data. A review of basic hydrodynamics has also been called for, and is presented from a Lagrangian as well as Eulerian point of view. The results of the analytical study and the study of the wave data question the applicability of certain universally accepted fluid dynamical principles.

The basic equations of fluid motion are presented on Eulerian and Lagrangian form, including the general Lagrangian form of the Laplacian. The relations governing vortex motion are also presented, including the theorems of Helmholtz, Kelvin and others on the rate of change of vorticity and circulation. Rotation of fluid elements is also studied from a Lagrangian point of view, showing that vorticity is not suited to express how a fluid element actually rotates about itself. It is found reason to question the common Lagrangian form of the continuity equation, namely that the Jacobian must be constant and that it in general can be set equal to 1, since this requirement results in some ambiguities and fundamental inconsistencies. Further, when considered in a Lagrangian frame of reference, we have that the theorems of Helmholtz, Kelvin and others require that a given Lagrangian point always represents the same identifiable material "particle", i.e. that the Jacobian is constant and equals 1. Hence, there is also reason to question the common assumption of irrotational (potential) flow in motions generated by conservative (potential) forces only, since this requirement is based on a material (Lagrangian) interpretation of the theorems on vortex motion. The weaker requirement of zero curl of the acceleration in such flows still applies, irrespective of the behaviour of the Jacobian.

The Lagrangian wave theories of Gerstner and Miche are presented, pertaining to regular waves in deep and intermediate water, respectively. These wave theories represent closed orbital particle motion, i.e. without any net transport of mass. They also contain vorticity (rotationality) at second order, and are therefore traditionally considered invalid beyond first order. The classical solution for surface waves is Stokes 2nd order wave theory. The difference between this theory and the two above is Stokes drift; a second order forward transport of mass. Stokes waves and Stokes drift are here also studied from a Lagrangian point of view. It is found that Stokes waves violate continuity and cause a vorticity at second order within less than one wave period, even for waves of small amplitude. Stokes waves are therefore theoretically inconsistent in the Lagrangian frame of reference, which in turn questions the arguments rendering Gerstner's (and Miche's) theory invalid, i.e. the above-mentioned assumption of irrotational motion. The wave theories of Gerstner and Miche are concluded to be applicable basic solutions for regular waves in the limit of negligible viscosity.

Irregular waves are here modelled as a sum of linear regular Gerstner or Miche waves, superposed in the Lagrangian frame of reference. The Lagrangian approach is better suited to show the physics of the wave motions than the Eulerian approach, and the linear Lagrangian model of irregular waves automatically includes what are known as nonlinear interactions

from an Eulerian point of view. The irregular approach presented here is still only a solution of the linearized Lagrangian problem; it is not a model for nonlinear irregular waves in a mathematical sense.

Iterative methods have been developed that determine which water particle occupies a specific spatial (Eulerian) position at a specific instant in time. This means that also Eulerian quantities can be calculated, in a practical manner, based on the Lagrangian solutions. The iteration methods apply to regular as well as broad-banded irregular waves, and yield theoretically consistent values everywhere, also in the splash zone. Since the models of irregular waves presented in this thesis are based on the linear (first order) parts of the regular solutions only, they are not affected by the above questions regarding continuity, vorticity and mass transport at second order.

The Lagrangian theories and models are compared with laboratory wave data for both regular and irregular wave cases. The wave data include measurements of the surface elevation and LDV-measurements of water particle velocities at different vertical positions, also above the still water level. The mean horizontal velocity in a vertical cross-section has been studied closely, and the instantaneous horizontal velocity in a vertical cross-section beneath individual crests and troughs has also been considered.

The analysis of the experimental data show that distinct transitions in the mean horizontal velocity in the flume take place after a relatively short period of time. These analysis, along with visual observations, also indicate that water particles actually move in more or less closed orbits, i.e. similar to Gerstner and Miche waves, which is fundamentally different from the commonly assumed Stokes drift and associated return current. Again, this supports the above questioning of Stokes waves, Stokes drift and irrotational motion.

For regular waves, the wave theories of Gerstner and Miche are found to compare exceptionally well with the measurements after the transitions have taken place and a relatively steady mean velocity profile has been established. For irregular waves, the Lagrangian models also compare well with the measurements, although these results are more subject to uncertainties. In particular, the horizontal velocity beneath crests and troughs predicted by the Lagrangian approach is compared with calculations according to the widely used Wheeler's method. The Lagrangian approach is generally found to compare better with the measurements than Wheeler's method does, and it accounts for the discrepancies typically observed when Wheeler's method is compared with wave flume measurements. It should be noted that Wheeler's "ad hoc" method does not satisfy the basic equations of motion, while the Lagrangian approach presented here does satisfy the basic equations consistently, even in the splash zone.

Hence, this study raises some fundamental theoretical questions with respect to continuity, vorticity and mass transport. For waves, it is of the utmost importance to resolve the issues of non-uniform mass transport when higher order solutions are sought. Caution should be taken when analyzing wave flume measurements, in particular for irregular wave cases. Such measurements may not be satisfactorily suited for comparisons with, or verification of, theoretical models of irregular ocean waves.

Anyhow, the Lagrangian approach presented herein should be of great practical and theoretical value, very well suited for simulations and design purposes. The potential for further development seems considerable, and may e.g. open for theoretically consistent superposition of nonlinear Lagrangian components and detailed modelling of wave-wave interactions and wave-current interactions.

PREFACE

This thesis is submitted in partial fulfillment of the *doktor ingeniør* degree at the Norwegian University of Science and Technology (NTNU). The work has been carried out at the Department of Structural Engineering at NTNU from 1997 to 2000, and has been fully financed by a scholarship from The Research Council of Norway (NFR). The funding by NFR is thankfully acknowledged.

The present study was initiated as a result of some remarkable findings by Moe and Arntsen (1996). The primary intent of this dissertation has been to further investigate and develop the Lagrangian approach applied on waves there. The basic equations governing wave motion have been examined, and a practical and consistent method for calculating kinematics in irregular ocean waves has been developed. Theoretical predictions of wave kinematics have been compared with laboratory wave data. Comparisons with ocean measurements were also intended, but could not be done within the time frame of this work.

I would like to thank my advisors Professor Geir Moe and Associate Professor Øivind A. Arntsen for their help and encouragement, for constructive criticism of my work and comments on the manuscript, and for valuable discussions.

I would further like to thank Dr. Ove Tobias Gudmestad at STATOIL and Dr. Witold Cieślikiewicz at the University of Gdansk for providing the experimental wave data, and Dr. Gudmestad also for providing substantial literature on the subject.

A few simple experiments were conducted in a wave flume at SINTEF Civil and Environmental Engineering in Trondheim during the course of this work, and the help from the staff there was very much appreciated.

Acknowledgements are also due to Den norske stats oljeselskap a.s (STATOIL) for their financial support (NOK 30.000, contract no. ANS028531) for my participations at the 1998 International OTRC Symposium *Ocean Wave Kinematics, Dynamics and Loads on Structures* in Houston, April 30th - May 1st 1998, and the 28th WEGEMT School *Wave Modelling Applied to the Design of Offshore and Coastal Structures* in Toulon, July 6th - 10th 1998.

Trondheim, September 2000
Svein Helge Gjøsund

NOMENCLATURE & GLOSSARY

Special symbols and notations

2D	two-dimensional, (x, z)-plane
3D	three-dimensional, (x, y, z)-space
∇	nabla/del-operator
$\overline{f}$	overbar denotes mean value of f
$O(f)$	order of magnitude of f
Re[f]	real part of f
Im[f]	imaginary part of f
$sign\{f\}$	sign of f, returning +1 or –1

Subscripts

$_E$	on Eulerian form
$_L$	on Lagrangian form
$_{submerged}$	pertaining to Eulerian points always submerged in water
$_{surface}$	pertaining to Lagrangian points constituting the free surface
$_t$	denoting value at time t
$_{t_0}$	denoting initial value at time t_0

The meaning of other sub- and superscripts are as given by the lists of symbols below, or assumed to be directly apparent from the context in which they are used.

Latin symbols

A	area
C_p	constant in pressure term
C_ω	ratio between the representative narrow band frequency (e.g. ω_{20}) and ω_p, viz. $C_\omega = \dfrac{\omega_{representative}}{\omega_p}$
$D1, D2$	diagonals of a material fluid element
E	energy
E_k	kinetic energy
E_p	potential energy

$\mathbf{G}$	body force
G_x, G_y, G_z	body force components in a right-handed Eulerian Cartesian coordinate system
H	wave height
H_{m0}	significant wave height defined by 0^{th} spectral moment
H_S	significant wave height, identical to H_{m0} in this thesis
J	Jacobi-determinant
N	number of sample points in a timeseries / components in a Fourier-series
P	energy flux
S	surface
$S(\omega)$	wave frequency spectrum
$\mathbf{T}$	stress tensor (surface force)
T	wave period
T_p	spectral peak period
T_{10}	spectral mean period
T_{20}	spectral mean zero crossing period
T_N	duration of timeseries
$U(z_0)$	added drift velocity in Miche's solution
$\mathbf{V}$	velocity vector
V_0	3D Lagrangian region defining a specific volume of mass
Z	complex Eulerian variable
Z_0	complex Lagrangian variable
a	wave amplitude
$\mathbf{a}$	acceleration vector
a_x, a_y, a_z	acceleration components in a right-handed Eulerian Cartesian coordinate system
c	phase velocity / wave celerity
c_g	group velocity
dA	differential Eulerian area
dS	differential surface area in Eulerian coordinates
ds	differential curve segment in Eulerian coordinates
ds_0	differential curve segment in Lagrangian coordinates
dx_i	differential of x_i
$\mathbf{e}_s$	unit tangential vector of ds
$\mathbf{e}_S$	unit normal vector of dS
e	tolerance of error in approximated Eulerian coordinates
$e_{x,m}$	error in approximated Eulerian x-coordinate after m iterations
$e_{z,m}$	error in approximated Eulerian z-coordinate after m iterations
e_m	highest value of $e_{x,m}$ and $e_{z,m}$
e_0	tolerance of error in approximated Lagrangian coordinates
$e_{x0,m}$	error in approximated Lagrangian x_0-coordinate after m iterations
$e_{z0,m}$	error in approximated Lagrangian z_0-coordinate after m iterations
e_{0m}	highest value of $e_{x0,m}$ and $e_{z0,m}$
f	general scalar / function
f	wave frequency (s^{-1})
$f_{Nyquist}$	Nyquist frequency (s^{-1})
f_{Sample}	sampling frequency (s^{-1})
$f_{S(\omega),\text{Gerstner}}$	maximum effective surface steepness in a realization of irregular Gerstner waves
$f_{S(\omega),\text{Miche}}$	maximum effective surface steepness in a realization of irregular Miche waves
$\mathbf{g}$	gravity field
g	gravity constant ($g \cong 9.81$ m/s^2)
h	water depth
$\mathbf{i}$, $\mathbf{j}$, $\mathbf{k}$	Eulerian unit vectors in x-, y- and z-direction, respectively
k	wave number
k_p	wave number associated with spectral peak frequency
k_{10}	wave number associated with spectral mean frequency

k_{20}	wave number associated with spectral mean zero crossing frequency
m	mass
m_i	i^{th} spectral moment of frequency spectrum
p	pressure
$p_x(x)$	Rayleigh distribution function of the parameter x
q	scalar defined by $\mathbf{V} \cdot \mathbf{V} = q^2$
s	curve
t	time
t_0	initial instant in time
$u_{Stokes\ drift}$	Stokes drift, a drift velocity of fluid "particles"
u, v, w	velocity components in a right-handed Eulerian Cartesian coordinate system
w_f	suggested multiplication factor in Wheeler's method
x, y, z	coordinates in a right-handed Eulerian Cartesian coordinate system
x_0, y_0, z_0	coordinates in a right-handed Lagrangian coordinate system
x_i	x, y, z
x_{i0}	x_0, y_0, z_0
$z_{Wheeler}$	stretched vertical coordinate in Wheeler's method

Greek symbols

Δ	difference
Δt	temporal spacing between timeseries sample points
$\Delta\omega$	frequency spacing between components in the wave spectrum
$\Delta z_{Gerstner}$	vertical shift in Gerstner waves
Δz_{Miche}	vertical shift in Miche waves
Γ	circulation
χ	horizontal displacement of Lagrangian point in Gerstner waves
δ	increment, difference
ε_n	constant relative phase of wave components
φ	velocity potential
$\varphi_{acc.}$	acceleration potential
$\varphi_{complex}$	complex potential function
φ_L	Lagrangian velocity potential
$\varphi_{L,complex}$	complex Lagrangian potential function
γ	peakedness parameter in JONSWAP spectrum
η	surface elevation
κ	angle between two curves defined by $x_0 = const.$ and $z_0 = const.$
λ	wavelength
μ	coefficient of viscosity / dynamic viscosity (water: $\mu \cong 10^{-3}$ kg/ms)
θ	phase
θ_0	limiting phase; determining when an Eulerian point is submerged in water
ρ	density (fresh water: $\rho \cong 1000$ kg/m^3, sea water: $\rho \cong 1025$ kg/m^3)
σ_η	standard deviation of the surface elevation
σ_η^2	variance of the surface elevation
υ	kinematic viscosity (water: $\upsilon = \mu/\rho \cong 10^{-6}$ m^2/s)
$\boldsymbol{\omega}$	(rigid body) rotation vector
ω_{D1}	rotation of the diagonal $D1$ of a deformable fluid element
ω_{D2}	rotation of the diagonal $D2$ of a deformable fluid element
ω_M	mean of ω_{D1} and ω_{D2}
$\omega_{(x0,z0)}$	mean rotation of the two basic lines in a material element

ω_i	(rigid body) rotation about i-axis
ω	wave circular frequency (rad/s)
$\omega_{Nyquist}$	Nyquist frequency (rad/s)
ω_p	spectral peak frequency
ω_{10}	spectral mean frequency
ω_{20}	spectral mean zero crossing frequency
ξ	vertical displacement of Lagrangian point in Gerstner waves
ψ	stream function
ψ_L	Lagrangian stream function
ψ_1	scalar whose gradient is the gravity field
ψ_2	scalar representing the "total head", cf. Eq. (3.31)
ζ	vorticity
$\boldsymbol{\zeta}$	vorticity vector
ζ_x, ζ_y, ζ_z	vorticity components in a right-handed Eulerian Cartesian coordinate system

Glossary

It is found appropriate to include a short glossary of some essential terms. Many of them should be well known, and most of them are explained in the text as well. It still seems useful to emphasize their meaning here and foreshadow some of the subtleties involved. Several of the terms are defined and treated in a more formal manner in Sections 3.1 and 3.4, and the reader is also referred to Section 7.1.4 for a historical note on the terms 'rotation' and 'vorticity'.

circulation The line integral of the velocity along a closed curve at a given instant. Note that this is a strictly mathematical definition, **circulation** does not necessarily express a flow of mass along the boundary of a deforming fluid element (shown in Section 4.1.3). **Circulation** is related to **vorticity** through Stokes' theorem.

continuum model/hypothesis (*The following is based on Lin and Segel (1988, their section 13.1) and Batchelor (1967, his section 1.2)*). A continuum may be explained as a medium that is continuously distributed in space. The properties of this medium are smoothly varying functions of position, so that each point in space occupied by the medium is assigned a value of any of these properties. A continuum model disregards molecular variations, and therefore requires that we consider small 'lumps' of fluid that are large enough for molecular variations to be insignificant. For water, the smallest typical dimension for this to be physically correct may be estimated to be of the order 10^{-9} m. The value of a property in a point may thus be considered an average over a small surrounding 'lump' of fluid.

deep water Normally defined by $h/\lambda > 0.5$, where h is the water depth and λ is the wavelength.

emergence effect The effect of a fixed spatial position in the **splash zone** sometimes being submerged in water and sometimes left in air (emerged) due to the waves.

Eulerian current The mean velocity in a point fixed in space, which does not necessarily describe a mass transport.

Eulerian spectrum The amplitude spectrum of the surface elevation measured at a fixed x-position.

first transition The first distinct transition, associated with the passing of the initial wave front, in the horizontal velocity in the experiments in Skjelbreia et al. (1991), cf. Sections 6.2, 6.3, 7.3 and 7.4.

intermediate water Normally defined by the interval $0.05 - 0.1 < h/\lambda < 0.5$, where λ is the wavelength in deep water, i.e. $\lambda \approx 1.56\,T^2$ $[m]$.

irrotational/irrotationality These terms are used exclusively for rotation defined as half the **vorticity**, cf. **rotational/rotationality** also, expressing motion with zero **vorticity**, i.e. $\zeta = 0$.

Jacobian The Jacobi-determinant, also denoted by J, defined in Eqs. (2.19) and (2.24) for the 2D and 3D case, respectively.

Lagrangian current The mean velocity of a Lagrangian point, i.e. a real transport of mass.

Lagrangian (orbital amplitude) spectrum The amplitude spectrum of the vertical displacement in the orbital motion of a given Lagrangian point.

physical rotation The actual rotation (expressed e.g. by an angular velocity) of a fluid element, i.e. how it turns/spins about itself. There are several alternative ways of defining and describing such rotation, and its magnitude will depend on the actual instantaneous shape of the material element under consideration. **Physical rotation** therefore describes e.g. angular velocity qualitatively rather than quantitatively. Note that **physical rotation** is *not* the rotation associated with **vorticity**, **circulation** or **potential flow**.

potential flow A flow with **irrotational** motion, i.e. zero **vorticity**, where the velocity vector may be expressed as the gradient of a scalar function; the velocity potential.

potential force A force that can be expressed as the gradient of a scalar function (also called conservative force).

potential theory The theory of solutions of Laplace's equation. Note that **potential flow** does not necessarily imply that **potential theory** is applicable. **Potential flow** only means that a velocity potential exists, i.e. that the curl of the velocity is zero, while the use of **potential theory** also requires the divergence of the velocity to be zero, i.e that the flow is incompressible. Still, whenever a velocity potential is used it is also normally assumed that the flow is incompressible, making this distinction unnecessary in most cases.

However, the curl of the acceleration in inviscid flow is zero, enabling us to speak of an acceleration potential, while the divergence of the acceleration need not be zero. Hence, **potential theory** cannot generally be applied to determine this acceleration potential.

rigid body rotation The angular velocity of a rigid body.

rotation No specific meaning is associated with this term, its meaning being a matter of definition. In fluid mechanics, rotation is normally defined as half the curl of the velocity, and is then a strictly mathematical quantity equivalent to vorticity. However, by rotation we normally mean how something physically turns about

itself, i.e. what is called **physical rotation** above. It is found that **vorticity** is not suited to express how a deforming fluid element turns about itself, and rotation defined as half the **vorticity** may therefore be physically misleading.

rotational/rotationality These terms are used exclusively for rotation defined as half the **vorticity**, cf. **irrotational/irrotationality** also.

second transition The second distinct transition, taking place after roughly 1-2 minutes, in the horizontal velocity in the experiments in Skjelbreia et al. (1991), cf. Sections 6.2, 6.3, 7.3 and 7.4.

shallow water Normally defined by $h/\lambda < 0.05$ - 0.1, where λ is the wavelength in deep water, i.e. $\lambda \approx 1.56\,T^2\ [m]$.

splash zone The region near the still water level, where, due to the waves, a fixed spatial position is sometimes submerged in water and sometimes left in air.

vertical shift The shift in *mean* vertical position of a Lagrangian point during motion as compared to a state of rest.

vorticity **Vorticity** is defined as the curl of the velocity. Note that this is a strictly mathematical definition, **vorticity** does *not* unambiguously describe how a deforming fluid element turns about itself. **Vorticity** is related to **circulation** through Stokes' theorem.

TABLE OF CONTENTS

CHAPTER 1

INTRODUCTION

1.1 Background and Objectives

Proper modelling of waves and wave kinematics, i.e. the displacements, velocities and accelerations of water particles in waves, is essential in marine engineering and in several other aspects of marine activity. It is also of general interest in any subject related to seas and the motion of fluids. With respect to offshore engineering applications, the importance of accurate information about wave kinematics is especially apparent with respect to calculations of wave forces on slender structures. This is often done according to Morison's formula (Morison et al., 1950), where the total force consists of one term proportional to the fluid acceleration (inertia term) and one term proportional to the square of the fluid velocity (drag term). Reliable information about the kinematics, and thus the pressure in the fluid and the magnitude and geometry of the surface elevation, is also of importance for estimation of wave loads on other types of marine structures, and for prediction and description of specific wave conditions that may be of significance for e.g. conduction of marine operations, safe operation of ships or for coastal matters.

However, due to the nonlinear and irregular nature of the problem, no complete or quite satisfactory models of ocean waves or their kinematics exist. In particular, the conditions in the splash zone in irregular waves are not satisfactorily modelled by the traditional Eulerian approaches. The reason for this is that the surface profile is an unknown in an Eulerian analysis, and the boundary conditions at the free surface can therefore only be satisfied in an approximate manner. By the splash zone is meant the region near the still water level, where, due to the waves, a fixed spatial position is sometimes submerged in water and sometimes left in air. This deficiency in the splash zone is unfortunate, since this is where the water motion due to surface waves is most pronounced. So-called engineering methods have been developed in order to improve the results in the splash zone, e.g. Wheeler's method (Wheeler, 1970), but these methods do not satisfy the basic hydrodynamic equations properly. Their accuracy and reliability is therefore limited. See Gudmestad (1993) for a review of engineering practice and recommendations for further developments. However, the particular problems encountered in the splash zone can be avoided by considering the problem from a Lagrangian point of view, e.g. as in Gerstner's and Miche's wave theories, since the free surface can there be specified at once.

The immediate background for this thesis work is the paper by Moe and Arntsen (1996), where calculations of kinematics based on Gerstner's wave theory were found to compare remarkably well with wave flume measurements, for irregular as well as regular wave cases,

also in the splash zone. Since Gerstner's theory is rotational, and therefore traditionally considered invalid as a basic solution for waves, these findings require some explanation. It would then normally be assumed that the agreement between measurements and Gerstner's theory is a result of Stokes drift and associated return current in a closed flume. However, the measurements and further observations also indicate that the waves in the experiments actually have closed orbits, i.e. as in Gerstner waves, which is fundamentally different from a Stokes drift and return current.

The main objective of this thesis is analytical modelling of regular and irregular surface gravity waves in intermediate to deep water, with particular emphasis on the splash zone kinematics, based on the Lagrangian form of the equations of motion. More specifically, Gerstner's wave theory is applied for regular waves in deep water, and Miche's solution is applied for regular waves in intermediate water. Irregular waves are modelled as a sum of linear regular Gerstner/Miche components. Only the two-dimensional case is treated, and shallow water or varying depth is not considered.

After closer investigations of experimental measurements, the theoretical consequences of Stokes drift and Gerstner's theory itself, it is found reason to question the arguments rendering Gerstner's theory invalid. Therefore, this thesis also includes a rather thorough review of some basic equations and principles, in order to investigate the assumption of irrotational flow.

Also, linear Gerstner waves are better suited to show the physics of wave motion than linear Stokes waves (Airy waves) are. Irregular waves modelled as a sum of linear Gerstner (or Miche) components are seen to automatically include effects that are considered nonlinear from an Eulerian point of view, and allow more extreme wave forms than the common Eulerian approaches. This was shown by Pierson (1961, 1962), cf. Neumann and Pierson (1966) and Kinsman (1965) also, who along with Tick (1963) recommended that the Lagrangian approach be studied more closely with respect to irregular waves. The irregular approach presented here is still only a solution of the linearized Lagrangian problem; it is not a model for nonlinear irregular waves in a mathematical sense. However, it seems that the Lagrangian approach may also open for theoretically consistent superposition of nonlinear wave components.

A state-of-the-art survey for ocean wave kinematics was given in Tørum and Gudmestad (1990), and more recently in Zhang (1998). Comparisons of measured and predicted kinematics that are of particular relevance for the present study are Johnsen (1987), Gudmestad et al. (1988), Skjelbreia (1987, 1988, 1991), Tørum and Skjelbreia (1990), Skjelbreia et al. (1991), Cieslikiewicz and Gudmestad (1994b), Moe and Arntsen (1996) and Moe et al. (1998).

Works on wave modelling, wave interactions and wave kinematics are often based on potential, i.e. irrotational, flow. It is also customary to represent the surface elevation as a sum of linear wave components of different frequencies. Zhang et al. (1996), cf. Spell et al. (1996) also, have recently developed the Hybrid Wave Model for irregular waves, not only adding the components but also accounting for interactions among them. In this model, interactions between two components of close frequencies are modelled by a conventional perturbation approach, while interactions between two components well separated in frequency are modelled by a phase modulation approach. The hybrid model has later been extended to account for directionality (Zhang et al., 1998). Stansberg (1994), cf. Stansberg and Gudmestad (1996) also, presents a 2nd order random wave model. In this model, the first and second order velocity potentials of each component are both included up to the still water level. Above the still water level and up to the free surface, linear extrapolation is employed for the first order potential and vertical extrapolation is employed for the second order potential. A stochastic Eulerian approach is taken by Cieslikiewicz and Gudmestad (1993, 1994a, 1994b, 1995, 1996), taking into account the influence of the *emergence effect* (see

Glossary) on stochastic parameters in the splash zone as well as studying weak nonlinear effects. Baldock et al. (1996) and Swan et al. (1998) give particular attention to accurate laboratory measurements of kinematics beneath steep focused wave groups and compare to numerical calculations. Instead of modelling an irregular sea surface as a sum of different wave components, it may be considered a modulated wave group. This approach is taken by Trulsen and Dysthe (1996), cf. Trulsen et al. (1998) also, modelling irregular waves and their kinematics based on a modified nonlinear Schrödinger equation, and Peregrine et al. (1996), studying kinematics in steep wave events that result from the so-called Benjamin-Feir instability. Finally it may also be noted that Naciri and Mei (1992) have studied the evolution of a short wave on a very long wave of finite amplitude, representing the latter by the rotational Gerstner wave. They conclude that Gerstner's exact solution may serve as a convenient stepping stone towards a better understanding of such aspects.

An essential part of wave modelling is a proper description of the flow, in the sense of real net mass transport, beneath the surface. Theoretical and experimental studies of mass transport in waves have been presented by Longuet-Higgins (1953, 1960), Ünülata and Mei (1970), Mei et al. (1972) and Liu and Davis (1977). These studies are treated in Kinsman (1965, his section 10.4), Sarpkaya and Isaacson (1982, their section 4.8) and Mei (1989, his section 9.6) also. However, neither of the solutions presented in these works appears to be applicable for wave amplitudes that are not very small (Sarpkaya and Isaacson, 1982). Also, the physical processes involved are unclear and the time required establishing the proposed flows appear to be unreasonably long. More recent studies of mass transport in waves include Hudspeth and Sulisz (1991), Cieslikiewicz and Gudmestad (1994b) and Groeneweg and Klopman (1998). These works assume that a return current exists in wave flume experiments. Monismith and co-workers (2000) have studied results from four sets of laboratory experiments. They find that waves generated mechanically in the laboratory do not change the mean Lagrangian velocity until they are sufficiently steep to break, suggesting that these waves have closed orbits and may be better described as Gerstner waves than as Stokes waves. Woltering and Daemrich (1994), cf. Woltering (1996) also, have studied mass transport and orbital velocities in regular and two-component Stokes waves from a Lagrangian point of view. They arrive at similar conclusions as indicated above, i.e. that a low order Lagrangian model is equivalent to a higher order Eulerian model, and that (Eulerian) nonlinearities are automatically included. It is unclear if and how Stokes drift is included in their formulation.

Anyhow, whereas a generally accepted model for mass transport in waves does not seem to exist, wave flume experiments clearly indicate a positive mean Eulerian horizontal velocity near the surface and a negative mean velocity further down in the fluid, also for irregular waves. As shown in Moe and Arntsen (1996), this mean velocity profile is well described by Gerstner's theory. If the depth is not too great compared to the wavelength, a forward creeping flow will also eventually develop at the bottom. An important question is then *if* the mean Eulerian velocity profile in experiments is a result of a Stokes-like drift and associated return current, or if fluid elements actually move in more or less closed orbits, and *why* the motion is the way it is. The actual generation of the waves and the time required establishing a relatively steady mean velocity profile is essential in this respect.

1.2 About the Work, Results and Outline of the Thesis

As stated in Section 1.1, the agreement in Moe and Arntsen (1996) between Gerstner's theory and experimental measurements would normally be assumed to stem from so-called wave flume effects. The motion is then assumed to be irrotational, with a Stokes drift near the surface and, due to the end-walls of the tank, a return current further down in the fluid.

However, the assumption of irrotational motion relies heavily on some quite strict fundamental theoretical assumptions and approximations, in particular the concept of "point particles". When studying these and their consequences more closely, it seems that some misinterpretations and inconsistencies are involved. Examples of this is vorticity not describing the *physical* rotation of fluid elements, cf. Section 3.4, and Stokes drift actually violating continuity and causing a vorticity at second order within less than a wave period, cf. Section 4.3. This, in turn, questions the relevancy of imposing physical conditions on quantities such as the vorticity and circulation, and thus the very foundation for requiring irrotational flow. A large part of the work has therefore been focused on investigations of fundamental theoretical issues like continuity, vorticity and mass transport, primarily from a Lagrangian point of view. Hence, even if the wave problem described in Section 1.1 is limited to two-dimensional inviscid incompressible flow, the basic equations and relations presented in Chapters 2 and 3 pertain to more general fluid flow conditions.

A lot of effort has also been put into "exact" transformation of the Lagrangian solution to the Eulerian frame of reference, also for broad-banded irregular waves, since the use of e.g. Taylor-expansions is not satisfactory for this purpose. Due to the form of the Lagrangian solutions, numerical iteration seem appropriate for the transformation, and such methods have therefore been developed as a part of this thesis work. The performance and speed of the methods are found satisfactory for the present needs, and it has not been prioritized to further optimize the methods with respect to e.g. convergence or computation time. All calculations are performed in MATLAB (version 5.3.1/R11.1), where also all plots are generated.

With respect to calculations and comparisons with measurements, these mainly focus on the horizontal velocity. A few results for the vertical velocity are included, while no results are presented for accelerations or pressure. The results for regular waves have been given more attention than the results for irregular waves. Modelling of irregular waves should be based on a proper understanding of regular waves, and a proper interpretation of the mean horizontal velocity in regular wave experiments is then of the utmost importance. Irregular waves are also subject to more theoretical and practical uncertainties, making it hard to distinguish between deficiencies in the theoretical models and unfortunate effects due to the experimental conditions. The Lagrangian approach for irregular wave kinematics is therefore compared with Wheeler's method as well as with measurements, which should be quite informative with respect to the performance and usefulness of the Lagrangian approach.

The measurements used for the comparisons are from the extensive experiments carried out by Skjelbreia et al. (1991) at the Norwegian Hydrotechnical Laboratory (NHL, now SINTEF Civil and Environmental Engineering, Department of Coastal and Ocean Engineering) in Trondheim. These include measurements of the surface elevation and LDV-measurements of water particle velocities, also in the splash zone, for irregular as well as regular wave cases. While most of the theoretical considerations in this work pertain to Gerstner's theory, and thus deep water, the experiments pertain mainly to waves in intermediate water. The measurements have therefore been compared with Miche waves. However, the differences between applying Gerstner's and Miche's expressions are of a minor quantitative nature for the experimental cases under consideration. The results found when comparing measurements with Miche's theory are therefore representative also for Gerstner's theory.

At an early stage of the work on this thesis, some of the runs in the above-mentioned experiments, and a few more, were reproduced in the same flume and under the same conditions as in the original experiments. No velocity measurements were conducted, but the development of the mean horizontal velocity was observed visually by employing a thread in the glass section of the flume. The thread was fixed at the bottom and above the wave flume, at two points on a straight vertical line above the centerline of the flume, but had sufficient slack to form according to the flow in the flume. Also, short threads were fixed in a transverse manner along the main thread, giving a more detailed picture of the flow. The behaviour of

the thread(s) in these runs was video-filmed. No further presentation of these simple experiments is given in this thesis, but they proved quite helpful in order to interpret and verify the results from the analysis of the LDV-measurements.

It may also be in its place to emphasize the use of a few terms:

- By the term *order*, e.g. of a solution or of the magnitude of a term, is meant the *order in wave amplitude*, meaning that e.g. $k^m a^n$ is of *order n*.

- The reference level of the Eulerian frame of reference is traditionally placed at the so-called still water level. This is also the general rule in this thesis. However, in order to take full advantage of the Lagrangian solutions, it is sometimes necessary to place the reference level a small distance (of second order) above the still water level. It might then seem appropriate to define designated Eulerian variables for each specific reference level. However, it is believed that this would reduce the readability of the thesis. Instead, it has been chosen to emphasize which reference level applies for specific expressions whenever relevant, although it is realized that this may also be a source of confusion.

- In general, the same symbol is used to describe a quantity irrespective of it being Lagrangian or Eulerian, e.g. u for the horizontal velocity. The distinction between a Lagrangian and Eulerian description is apparent from the form of the expressions and which variables are dependent and independent. Still, the variables are not always included along with the symbol. It is then either explicitly stated whether the quantity in question is Lagrangian or Eulerian, or it is assumed to be apparent from the context.

- Finally, it is recommended that the reader take a quick look at the Glossary on pages *x - xii* before commencing with the rest of the thesis. In particular, the definitions and perceptions of the terms **rotation** and **physical rotation** are essential.

The outline of the thesis is as follows:

In Chapter 2, the basic equations of motion are presented on Eulerian as well as Lagrangian form, including the general Lagrangian form of the Laplacian. The relations governing vortex motion are presented in Chapter 3, along with considerations on the existence of a velocity potential and expressions describing the physical rotation of a specific fluid element.

The Lagrangian wave theories of Gerstner and Miche are presented in Chapter 4. By the use of Taylor-expansions they are also given on Eulerian form, correct to second order. In addition, Stokes waves and Stokes drift are considered from a Lagrangian point of view. Modelling of irregular waves in the Lagrangian frame of reference is treated in Chapter 5, including numerical (iterative) methods for transforming the Lagrangian solutions to the Eulerian frame of reference.

In Chapter 6 are presented the results from calculations and comparisons with wave flume measurements. A short description of how to obtain the necessary Lagrangian wave component parameters from Fourier analysis of the measured surface elevation is also given.

Chapter 7 contains a discussion of some of the theoretical issues treated in this thesis as well as a discussion of the results presented in Chapter 6. Conclusions and recommendations for further work are given in Chapter 8.

Appendix A contains the basic form of the inverse partial derivatives needed when applying the chain rule between the Lagrangian and Eulerian frames of reference.

Appendix B contains plots showing the temporal development of the mean Eulerian horizontal velocity in the regular wave experiments, cf. Section 6.2.1 also.

Appendix C contains photocopies (from the proceedings in which they were published) of the papers by Moe and Arntsen (1996) and Moe et al. (1998). This means that the pagination of these is also as in the respective proceedings.

CHAPTER 2

THE BASIC EQUATIONS OF MOTION

This chapter presents the equations of motion on Lagrangian as well as Eulerian form. The fluid is assumed to be a continuum and the motion is assumed to be continuous. The governing equations are derived by ensuring conservation of mass (continuity) and linear- and angular momentum (Newton's second law) of a material fluid element. The fundamental unknowns are the velocity and pressure. Further considerations with respect to vortex motion are presented in Chapter 3.

In the case of ordinary surface gravity waves, water may be considered an incompressible Newtonian fluid. However, starting from a more general point of view will clarify some relations between the different forms of the governing equations.

2.1 Eulerian and Lagrangian Descriptions

The Eulerian frame of reference is a right-handed Cartesian coordinate system (x, y, z), with the positive z-axis pointing vertically upwards. The Lagrangian frame of reference (x_0, y_0, z_0) may also be considered right-handed, with the positive z_0-axis pointing towards the free surface. Directions and absolute lengths are defined in an Eulerian frame of reference, i.e. relative to the Eulerian unit vectors.

Assuming that the Lagrangian representation of a specific portion of matter remains the same for a period of time, the Eulerian position (x, y, z) of a specific Lagrangian point (x_0, y_0, z_0) followed in this period of time is

$$\begin{aligned} x &= x(x_0, y_0, z_0, t) \\ y &= y(x_0, y_0, z_0, t) \\ z &= z(x_0, y_0, z_0, t) \end{aligned} \tag{2.1}$$

and the Lagrangian point "occupying" a specific Eulerian position (x, y, z) at time t is

$$\begin{aligned} x_0 &= x_0(x, y, z, t) \\ y_0 &= y_0(x, y, z, t) \\ z_0 &= z_0(x, y, z, t) \end{aligned} \tag{2.2}$$

Values of any scalar quantity f, such as velocity (component-wise), pressure, gravity, density etc., may be given by functions of Eulerian as well as Lagrangian variables.

When a quantity pertains to a specific spatial position, it is Eulerian. The value of f is then given by functions where the independent variables are the Eulerian coordinates and time, as in Eq. (2.2). An Eulerian description of f may therefore be given as

$$f = f_E(x, y, z, t) = f_L[x_0(x, y, z, t), y_0(x, y, z, t), z_0(x, y, z, t), t] \tag{2.3}$$

When a quantity pertains to a specific material element, it is Lagrangian. The value of f is then given by functions where the independent variables are the Lagrangian coordinates and time, as in Eq. (2.1). A Lagrangian description of f may therefore be given as

$$f = f_L(x_0, y_0, z_0, t) = f_E[x(x_0, y_0, z_0, t), y(x_0, y_0, z_0, t), z(x_0, y_0, z_0, t), t] \tag{2.4}$$

Note that f_E is a functional expression of the variables (x, y, z, t), i.e. on Eulerian form, and f_L is a functional expression of the variables (x_0, y_0, z_0, t), i.e. on Lagrangian form. The variables in either of these functions are dependent or independent according to an additional relation from Eq. (2.1) or Eq. (2.2). An Eulerian quantity may therefore be given on Lagrangian as well as Eulerian form, and a Lagrangian quantity may be given on Eulerian as well as Lagrangian form. Eqs. (2.3) and (2.4) thus equate the values of the functions f_E and f_L in a given Eulerian or Lagrangian point at a given instant in time, not the functional expressions. No explicit distinction is made between f_L and f_E in this thesis, except for in a few cases where it is of some importance, since that would generally reduce the readability.

At one instant in time, a specific Lagrangian point corresponds to some Eulerian point. Applying the chain rule, partial derivatives with respect to spatial and material variables may then be found as

$$\frac{\partial f}{\partial x} = \frac{\partial f}{\partial x_0}\frac{\partial x_0}{\partial x} + \frac{\partial f}{\partial y_0}\frac{\partial y_0}{\partial x} + \frac{\partial f}{\partial z_0}\frac{\partial z_0}{\partial x} \tag{2.5}$$

etc.
etc.

$$\frac{\partial f}{\partial x_0} = \frac{\partial f}{\partial x}\frac{\partial x}{\partial x_0} + \frac{\partial f}{\partial y}\frac{\partial y}{\partial x_0} + \frac{\partial f}{\partial z}\frac{\partial z}{\partial x_0} \tag{2.6}$$

etc.
etc.

assuming that the partial derivatives exist at a point defined by either of Eqs. (2.1) or (2.2).

Note that when applying the chain rule on an expression of the form in Eqs. (2.3) and (2.4), an additional term in Eq. (2.5) and (2.6) including time as

$$\frac{\partial f}{\partial t}\frac{\partial t}{\partial x}$$

will not appear, because time is a variable that is independent of the spatial variables.

Gravity may be given as a vector expressed by the gradient of a scalar field $\psi_1(x, y, z) = gz$, viz.

$$\mathbf{g} = -\nabla \psi_1 = -g\,\mathbf{k} \tag{2.7}$$

where g for most practical cases is considered a constant, and

$$\nabla = \frac{\partial}{\partial x}\mathbf{i} + \frac{\partial}{\partial y}\mathbf{j} + \frac{\partial}{\partial z}\mathbf{k} \tag{2.8}$$

A complete physical understanding of material motion and its effects requires both Lagrangian and Eulerian information. The relations in Eqs. (2.1) and (2.2) must then both be known. These relations may not be possible to find on explicit analytic form, but corresponding coordinates at one instant of time may always be found numerically or by other approximate methods.

2.2 The Eulerian Equations

Motion, i.e. displacements, velocities and accelerations, is most conveniently described by vectors in an Eulerian frame of reference. The equations are therefore normally derived for an infinitesimal fixed control volume [dx, dy, dz], e.g. by the use of Reynolds' transport theorem, cf. e.g. White (1988). This means that the equations are derived in an Eulerian frame of reference. However, the conservation laws apply to specific portions of matter, and are therefore Lagrangian by nature. A slightly different approach is therefore followed here, in order to clarify the role of the so-called material derivative. Eqs. (2.12) - (2.14) below therefore form a basis also for the Lagrangian equations for conservation of momentum.

The Eulerian equation of continuity is

$$\frac{1}{\rho}\frac{d\rho}{dt} + \nabla \cdot \mathbf{V} = \frac{1}{\rho}\frac{d\rho}{dt} + \frac{\partial u}{\partial x} + \frac{\partial v}{\partial y} + \frac{\partial w}{\partial z} = 0 \tag{2.9}$$

In incompressible flow, Eq. (2.9) reduces to

$$\nabla \cdot \mathbf{V} = \frac{\partial u}{\partial x} + \frac{\partial v}{\partial y} + \frac{\partial w}{\partial z} = 0 \tag{2.10}$$

Euler's equations for conservation of linear momentum of a frictionless (i.e. inviscid) incompressible fluid are

$$\begin{aligned} a_x &= \frac{du}{dt} = G_x - \frac{1}{\rho}\frac{\partial p}{\partial x} \\ a_y &= \frac{dv}{dt} = G_y - \frac{1}{\rho}\frac{\partial p}{\partial y} \\ a_z &= \frac{dw}{dt} = G_z - \frac{1}{\rho}\frac{\partial p}{\partial z} \end{aligned} \tag{2.11}$$

where G_x, G_y, and G_z are forces per unit mass (i.e. 'body' forces, e.g. gravity) in the respective directions. In the case of gravity being the only 'body' force, the components are $G_x = 0$, $G_y = 0$ and $G_z = -g$.

Including friction and compressibility as well yields Cauchy's differential equation. This equation may be written on vector form as, cf. e.g. Aris (1989) or Lin and Segel (1988),

$$\rho \mathbf{a} = \rho \frac{d}{dt}\mathbf{V} = \rho \mathbf{G} + \nabla \cdot \mathbf{T} \tag{2.12}$$

The forces are divided into to types, **G** being a mass-dependent 'body' force as in Eq. (2.11), and **T** a stress tensor representing 'surface' forces acting on the boundaries between the material elements. The stress tensor **T** includes quantities such as thermodynamic pressure, viscosity and compressibility. Eq. (2.12) holds for any continuum no matter how the stress tensor is related to the rate of strain (Aris, 1989).

Conservation of angular momentum yields the result that the stress tensor and shear stresses are symmetric, except for in so-called 'polar fluids' (Lin and Segel, 1988, and Aris, 1989).

For a compressible Newtonian fluid, Eq. (2.12) yields Navier-Stokes equation. A Newtonian fluid is one that exhibits a linear relation between the shear stress and the rate of strain. Assuming further that the fluid is incompressible, eliminating the problem of bulk viscosity, Navier-Stokes equation takes the form (cf. White, 1991)

$$\frac{d}{dt}\mathbf{V} = \nabla\left(-\frac{p}{\rho} - \psi_1\right) + \upsilon\nabla^2\mathbf{V} \tag{2.13}$$

where ψ_1 is given by Eq. (2.7), and on component form

$$\begin{aligned}
\frac{du}{dt} &= -\frac{1}{\rho}\frac{\partial p}{\partial x} + \upsilon\left(\frac{\partial^2 u}{\partial x^2} + \frac{\partial^2 u}{\partial y^2} + \frac{\partial^2 u}{\partial z^2}\right) \\
\frac{dv}{dt} &= -\frac{1}{\rho}\frac{\partial p}{\partial y} + \upsilon\left(\frac{\partial^2 v}{\partial x^2} + \frac{\partial^2 v}{\partial y^2} + \frac{\partial^2 v}{\partial z^2}\right) \\
\frac{dw}{dt} &= -\left(\frac{1}{\rho}\frac{\partial p}{\partial z} + g\right) + \upsilon\left(\frac{\partial^2 w}{\partial x^2} + \frac{\partial^2 w}{\partial y^2} + \frac{\partial^2 w}{\partial z^2}\right)
\end{aligned} \tag{2.14}$$

No subscripts are used in the preceding equations. However, since they are Lagrangian by nature, all functions may be written on the form $f_E[x(x_0, y_0, z_0, t), y(x_0, y_0, z_0, t), z(x_0, y_0, z_0, t), t]$, cf. Eqs. (2.1) and (2.4). However, this section aims at presenting equations for Eulerian quantities on the form $f_E(x, y, z, t)$, cf. Eqs. (2.2) and (2.3). Therefore, the Eulerian form of the time derivative of the material velocity is required.

The time derivative of the material velocity may be found by differentiating the function $f_L(x_0, y_0, z_0, t)$ with time, keeping the Lagrangian variables constant. According to Eq. (2.4), this is equivalent to differentiating the function $f_E[x(x_0, y_0, z_0, t), y(x_0, y_0, z_0, t), z(x_0, y_0, z_0, t), t]$ with time, viz.

$$\begin{aligned}
\frac{df_L}{dt} &= \frac{Df_E}{Dt} = \frac{\partial f_E}{\partial t} + \frac{\partial f_E}{\partial x}\frac{dx}{dt} + \frac{\partial f_E}{\partial y}\frac{dy}{dt} + \frac{\partial f_E}{\partial z}\frac{dz}{dt} \\
&= \frac{\partial f_E}{\partial t} + u\frac{\partial f_E}{\partial x} + v\frac{\partial f_E}{\partial y} + w\frac{\partial f_E}{\partial z} = \frac{\partial f_E}{\partial t} + (\mathbf{V} \cdot \nabla) f_E
\end{aligned} \tag{2.15}$$

Invoking Eq. (2.2), i.e. keeping the Eulerian variables fixed, makes the derivative Eulerian, i.e. applying to $f_E(x, y, z, t)$. Eq. (2.15) then gives the instantaneous time rate of change of a quantity of the Lagrangian point that happens to be in this Eulerian position at this instant in time, hence the term 'material derivative', cf. e.g. Lin and Segel (1988), Kinsman (1965) or Lighthill (1989). This does, however, require that fluid is present at this instant in time in the

spatial point under consideration. This is clearly not always the case, e.g. in the splash zone of surface waves, but approximations still yield valuable solutions.

Eq. (2.15) is valid for scalar quantities only. It can be applied on any vector if the components are treated separately as scalars, cf. Kinsman (1965) and Lighthill (1989). In e.g. the velocity vector $\mathbf{V} = u\,\mathbf{i} + v\,\mathbf{j} + w\,\mathbf{k}$, we have that u, v and w are scalars.

The Eulerian equations of motion of an incompressible Newtonian fluid are therefore as given by Eqs. (2.10) and (2.14), where all functional expressions are of the form $f_E(x, y, z, t)$ and the left-hand side of Eq. (2.14) must be written according to Eq. (2.15).

2.3 The Lagrangian Equations

In some classic textbooks (e.g. Lamb, 1932), the Lagrangian coordinates are denoted by (a, b, c). However, since a is a common symbol for amplitude and acceleration, and c is a common symbol for celerity, (x_0, y_0, z_0) have been chosen to denote the Lagrangian coordinates in this thesis. They are also often referred to as 'tags', since they are used to identify specific material elements. Lamb (1932, Art. 16) states that the Lagrangian coordinates need not be restricted to mean the initial (still water) Eulerian coordinates of a particle, they may be any quantities which serve to identify a particle, and may vary continuously from one particle to another. Note therefore that the subscript '0' do not indicate an initial Eulerian position of the Lagrangian point.

2.3.1 Conservation of mass

The continuity equation on Lagrangian form (cf. Lamb, 1932, Arts. 14 and 16) may be derived from the change of variables theorem given in Eq. (2.22). For a plane area, it can be found by considering an infinitesimal area δA as in Figure 2.1.

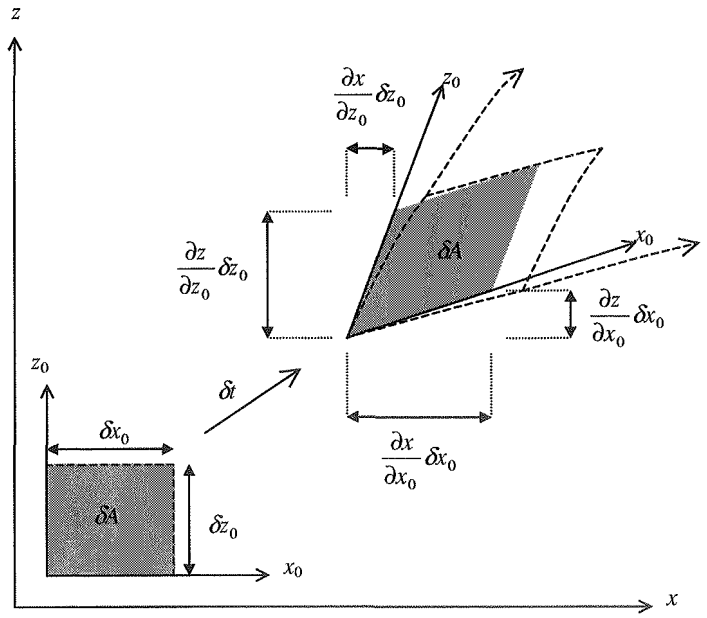

Figure 2.1 Motion and deformation of a 2D element. The approximate form is indicated by the grey shade, while the exact form is indicated by the dashed lines.

After a time increment δt, the area δA assumes, approximately, the shape of a parallelepiped (grey shade in Figure 2.1), whose area can be found by the cross product

$$\begin{aligned}\delta A\,\mathbf{j} &= \left(\frac{\partial x}{\partial x_0}\delta x_0\,\mathbf{i} + \frac{\partial z}{\partial x_0}\delta x_0\,\mathbf{k}\right)\times\left(\frac{\partial x}{\partial z_0}\delta z_0\,\mathbf{i} + \frac{\partial z}{\partial z_0}\delta z_0\,\mathbf{k}\right)\\ &= \left(\frac{\partial x}{\partial x_0}\frac{\partial z}{\partial z_0} - \frac{\partial x}{\partial z_0}\frac{\partial z}{\partial x_0}\right)\delta x_0\delta z_0\mathbf{j}\\ &= \frac{\partial(x,z)}{\partial(x_0,z_0)}\delta x_0\delta z_0\;\mathbf{j}\\ &= J\delta x_0\delta z_0\;\;\mathbf{j}\end{aligned} \tag{2.16}$$

where J is known as the Jacobi-determinant or the Jacobian. Conservation of a specific portion of matter requires, cf. Eqs. (2.3), (2.4) and (2.22),

$$\begin{aligned}&\int \rho dA = const.\\ &\Downarrow\\ \frac{d}{dt}\iint \rho_E(x,z,t)dxdz &= \frac{d}{dt}\iint \rho_E[x(x_0,z_0,t),z(x_0,z_0,t)]Jdx_0dz_0\\ &= \frac{d}{dt}\iint \rho_L(x_0,z_0,t)Jdx_0dz_0\\ &= \iint\left[\rho_L\frac{dJ}{dt}dx_0dz_0 + J\frac{d\rho_L}{dt}dx_0dz_0 + J\rho_L\frac{d(dx_0dz_0)}{dt}\right]\\ &= \iint\left(\rho_L\frac{dJ}{dt} + J\frac{d\rho_L}{dt}\right)dx_0dz_0\\ &= 0\\ &\Downarrow\\ &\frac{1}{J}\frac{dJ}{dt} = -\frac{1}{\rho_L}\frac{d\rho_L}{dt}\end{aligned} \tag{2.17}$$

since dx_0dz_0 is assumed to be constant. For incompressible flow, Eq. (2.17) yields

$$\frac{dJ}{dt} = \frac{d}{dt}\left[\frac{\partial(x,z)}{\partial(x_0,z_0)}\right] = 0 \tag{2.18}$$

i.e.

$$J = \frac{\partial(x,z)}{\partial(x_0,z_0)} = \frac{\partial x}{\partial x_0}\frac{\partial z}{\partial z_0} - \frac{\partial x}{\partial z_0}\frac{\partial z}{\partial x_0} = const. \tag{2.19}$$

Expanding Eq. (2.18) one finds

$$\frac{dJ}{dt} = \frac{d}{dt}\left[\frac{\partial(x,z)}{\partial(x_0,z_0)}\right] = \frac{d}{dt}\left[\frac{\partial x}{\partial x_0}\frac{\partial z}{\partial z_0} - \frac{\partial x}{\partial z_0}\frac{\partial z}{\partial x_0}\right]$$
$$= \frac{\partial u}{\partial x_0}\frac{\partial z}{\partial z_0} + \frac{\partial x}{\partial x_0}\frac{\partial w}{\partial z_0} - \frac{\partial u}{\partial z_0}\frac{\partial z}{\partial x_0} - \frac{\partial x}{\partial z_0}\frac{\partial w}{\partial x_0}$$
$$= \frac{\partial(u,z)}{\partial(x_0,z_0)} + \frac{\partial(x,w)}{\partial(x_0,z_0)}$$

By means of Eq. (2.28), in the 2D case, the above becomes

$$\frac{1}{J}\frac{dJ}{dt} = \nabla \cdot \mathbf{V}\,[x(x_0, z_0, t), y(x_0, z_0, t), z(x_0, z_0, t), t] \tag{2.20}$$

Combining Eqs. (2.17) and (2.20) yields

$$\frac{1}{\rho_E[x(x_0,z_0,t)]}\frac{d\rho_E[x(x_0,z_0,t)]}{dt} + \nabla \cdot \mathbf{V}_E\,[x(x_0, z_0, t), y(x_0, z_0, t), z(x_0, z_0, t), t] = 0 \tag{2.21}$$

Eqs. (2.17) - (2.21) are Lagrangian. Eq. (2.21) is equivalent to the Eulerian equation of continuity, i.e. Eqs. (2.9) and (2.10), if Eqs. (2.2), (2.3) and (2.15) are invoked, cf. Kinsman (1965, his section 2.2). The densities ρ_E and ρ_L may be set equal, e.g. constant, but they may also be kept different in order to express non-uniform density. These derivations may be shown to be correct also for the 3D case, cf. Lin and Segel (1988) and Kinsman (1965).

The true area after deformation of an incompressible area δA of finite size is the one bounded by the dashed lines in Figure 2.1. This area may be found exactly by the change of variables theorem Eq. (2.22), cf. e.g. Edwards and Penney (1990),

$$\begin{aligned}\iint F_E(x,z)\,dxdz &= \iint F_E[x(x_0,z_0),z(x_0,z_0)]\,\left|J(x_0,z_0)\right|\,dx_0dz_0 \\ &= \iint F_L(x_0,z_0)\,\left|J(x_0,z_0)\right|\,dx_0dz_0\end{aligned} \tag{2.22}$$

yielding

$$\delta A = \iint 1 \cdot dxdz = \iint 1 \cdot \left|J(x_0,z_0)\right|\,dx_0dz_0 \tag{2.23}$$

The equations in this section may be extended to 3D in a straightforward manner, considering volumes instead of areas. The 3D Jacobi-determinant is

$$\begin{aligned}J = \frac{\partial(x,y,z)}{\partial(x_0,y_0,z_0)} &= \frac{\partial x}{\partial x_0}\frac{\partial y}{\partial y_0}\frac{\partial z}{\partial z_0} + \left(\frac{\partial x}{\partial z_0}\frac{\partial y}{\partial x_0}\frac{\partial z}{\partial y_0} + \frac{\partial x}{\partial y_0}\frac{\partial y}{\partial z_0}\frac{\partial z}{\partial x_0}\right) \\ &\quad - \left(\frac{\partial x}{\partial x_0}\frac{\partial y}{\partial z_0}\frac{\partial z}{\partial y_0} + \frac{\partial x}{\partial z_0}\frac{\partial y}{\partial y_0}\frac{\partial z}{\partial x_0} + \frac{\partial x}{\partial y_0}\frac{\partial y}{\partial x_0}\frac{\partial z}{\partial z_0}\right)\end{aligned} \tag{2.24}$$

It is again emphasized that in the above equations, subscripts '0' denote Lagrangian coordinates, and not the initial Eulerian coordinates at some initial time instant. In the special case of (x_0, y_0, z_0) being the initial (still water) Eulerian coordinates, the Jacobian takes on the (constant) value 1. The difference between a Lagrangian coordinate and an initial coordinate

is further clarified in Section 4.1.1, where it is applied to Gerstner's wave theory. Note that the absolute value of the Jacobian must be greater than zero, or else it is unphysical.

2.3.2 Conservation of linear momentum

The Lagrangian form of the equations for conservation of linear momentum may be derived from Eq. (2.14). Only the incompressible case will be considered here. For inviscid flow, these equations can be found in Lamb (1932). Pierson (1962) and Monin and Yaglom (1971) present them for viscous flow also, but only for the case where the Jacobian equals 1.

The Lagrangian form of Eq. (2.14) may be found following Lamb (1932), Pierson (1962) and Moe et al. (1998). First, recall that the chain rule may be applied as follows, cf. Eq. (2.6),

$$\begin{aligned}
\frac{\partial p}{\partial x_0} &= \frac{\partial p}{\partial x}\frac{\partial x}{\partial x_0} + \frac{\partial p}{\partial y}\frac{\partial y}{\partial x_0} + \frac{\partial p}{\partial z}\frac{\partial z}{\partial x_0} \\
\frac{\partial p}{\partial y_0} &= \frac{\partial p}{\partial x}\frac{\partial x}{\partial y_0} + \frac{\partial p}{\partial y}\frac{\partial y}{\partial y_0} + \frac{\partial p}{\partial z}\frac{\partial z}{\partial y_0} \\
\frac{\partial p}{\partial z_0} &= \frac{\partial p}{\partial x}\frac{\partial x}{\partial z_0} + \frac{\partial p}{\partial y}\frac{\partial y}{\partial z_0} + \frac{\partial p}{\partial z}\frac{\partial z}{\partial z_0}
\end{aligned} \tag{2.25}$$

In order to express the pressure term of Eq. (2.14) by Lagrangian variables, the components of Eq. (2.14) are multiplied by

$$\frac{\partial x}{\partial x_0}, \frac{\partial y}{\partial x_0}, \frac{\partial z}{\partial x_0}$$

respectively, i.e.

$$\begin{aligned}
\left[\frac{du}{dt} = -\frac{1}{\rho}\frac{\partial p}{\partial x} + \upsilon\nabla^2 u\right] \cdot \frac{\partial x}{\partial x_0} \\
\left[\frac{dv}{dt} = -\frac{1}{\rho}\frac{\partial p}{\partial y} + \upsilon\nabla^2 v\right] \cdot \frac{\partial y}{\partial x_0} \\
\left[\frac{dw}{dt} + g = -\frac{1}{\rho}\frac{\partial p}{\partial z} + \upsilon\nabla^2 w\right] \cdot \frac{\partial z}{\partial x_0}
\end{aligned}$$

and then added, yielding

$$\begin{aligned}
&\left(\frac{du}{dt} - \upsilon\nabla^2 u\right)\frac{\partial x}{\partial x_0} + \left(\frac{dv}{dt} - \upsilon\nabla^2 v\right)\frac{\partial y}{\partial x_0} + \left(\frac{dw}{dt} + g - \upsilon\nabla^2 w\right)\frac{\partial z}{\partial x_0} \\
&\quad = -\frac{1}{\rho}\left(\frac{\partial p}{\partial x}\frac{\partial x}{\partial x_0} + \frac{\partial p}{\partial y}\frac{\partial y}{\partial x_0} + \frac{\partial p}{\partial z}\frac{\partial z}{\partial x_0}\right) = -\frac{1}{\rho}\frac{\partial p}{\partial x_0}
\end{aligned}$$

where the last equality is due to Eq. (2.25). Similarly, multiplying Eq. (2.14) by

$$\frac{\partial x}{\partial y_0}, \frac{\partial y}{\partial y_0}, \frac{\partial z}{\partial y_0}$$

yields

$$\left(\frac{du}{dt}-\upsilon\nabla^2 u\right)\frac{\partial x}{\partial y_0}+\left(\frac{dv}{dt}-\upsilon\nabla^2 v\right)\frac{\partial y}{\partial y_0}+\left(\frac{dw}{dt}+g-\upsilon\nabla^2 w\right)\frac{\partial z}{\partial y_0}=-\frac{1}{\rho}\frac{\partial p}{\partial y_0}$$

and multiplying Eq. (2.14) by

$$\frac{\partial x}{\partial z_0},\frac{\partial y}{\partial z_0},\frac{\partial z}{\partial z_0}$$

yields

$$\left(\frac{du}{dt}-\upsilon\nabla^2 u\right)\frac{\partial x}{\partial z_0}+\left(\frac{dv}{dt}-\upsilon\nabla^2 v\right)\frac{\partial y}{\partial z_0}+\left(\frac{dw}{dt}+g-\upsilon\nabla^2 w\right)\frac{\partial z}{\partial z_0}=-\frac{1}{\rho}\frac{\partial p}{\partial z_0}$$

In the Lagrangian frame of reference, the time derivative following the motion is simply

$$\frac{d}{dt}=\frac{\partial}{\partial t} \tag{2.26}$$

so that

$$u=\frac{\partial x}{\partial t}\text{ and }\frac{du}{dt}=\frac{\partial^2 x}{\partial t^2}$$
$$\text{etc.}$$
$$\text{etc.}$$

Hence, the Lagrangian form of Eq. (2.14) becomes

$$\begin{aligned}
&\left(\frac{\partial^2 x}{\partial t^2}-\upsilon\nabla^2 u\right)\frac{\partial x}{\partial x_0}+\left(\frac{\partial^2 y}{\partial t^2}-\upsilon\nabla^2 v\right)\frac{\partial y}{\partial x_0}+\left(\frac{\partial^2 z}{\partial t^2}+g-\upsilon\nabla^2 w\right)\frac{\partial z}{\partial x_0}=-\frac{1}{\rho}\frac{\partial p}{\partial x_0}\\
&\left(\frac{\partial^2 x}{\partial t^2}-\upsilon\nabla^2 u\right)\frac{\partial x}{\partial y_0}+\left(\frac{\partial^2 y}{\partial t^2}-\upsilon\nabla^2 v\right)\frac{\partial y}{\partial y_0}+\left(\frac{\partial^2 z}{\partial t^2}+g-\upsilon\nabla^2 w\right)\frac{\partial z}{\partial y_0}=-\frac{1}{\rho}\frac{\partial p}{\partial y_0}\\
&\left(\frac{\partial^2 x}{\partial t^2}-\upsilon\nabla^2 u\right)\frac{\partial x}{\partial z_0}+\left(\frac{\partial^2 y}{\partial t^2}-\upsilon\nabla^2 v\right)\frac{\partial y}{\partial z_0}+\left(\frac{\partial^2 z}{\partial t^2}+g-\upsilon\nabla^2 w\right)\frac{\partial z}{\partial z_0}=-\frac{1}{\rho}\frac{\partial p}{\partial z_0}
\end{aligned} \tag{2.27}$$

In Eq. (2.27), the Laplace operator is still on Eulerian form. A general procedure for transformation to Lagrangian variables is given in the following section, yielding the general Lagrangian form of the Laplacian as well as an additional Lagrangian form of the equations for conservation of linear momentum.

2.3.3 Transformation of partial derivatives (obtaining the general Lagrangian form of the Laplacian)

In general, for a scalar $f=f_L(x_0, y_0, z_0, t)=f_E[x(x_0, y_0, z_0, t), y(x_0, y_0, z_0, t), z(x_0, y_0, z_0, t), t]$, the set of equations

$$\frac{\partial f}{\partial x_0}=\frac{\partial f}{\partial x}\frac{\partial x}{\partial x_0}+\frac{\partial f}{\partial y}\frac{\partial y}{\partial x_0}+\frac{\partial f}{\partial z}\frac{\partial z}{\partial x_0}$$
$$\frac{\partial f}{\partial y_0}=\frac{\partial f}{\partial x}\frac{\partial x}{\partial y_0}+\frac{\partial f}{\partial y}\frac{\partial y}{\partial y_0}+\frac{\partial f}{\partial z}\frac{\partial z}{\partial y_0}$$

$$\frac{\partial f}{\partial z_0} = \frac{\partial f}{\partial x}\frac{\partial x}{\partial z_0} + \frac{\partial f}{\partial y}\frac{\partial y}{\partial z_0} + \frac{\partial f}{\partial z}\frac{\partial z}{\partial z_0}$$

may be solved for the partial derivatives

$$\frac{\partial f}{\partial x}, \frac{\partial f}{\partial y}, \frac{\partial f}{\partial z}$$

e.g. by Cramer's rule, yielding

$$\begin{aligned} \frac{\partial f}{\partial x} &= \frac{1}{J}\frac{\partial(f,y,z)}{\partial(x_0,y_0,z_0)} \\ \frac{\partial f}{\partial y} &= \frac{1}{J}\frac{\partial(x,f,z)}{\partial(x_0,y_0,z_0)} \\ \frac{\partial f}{\partial z} &= \frac{1}{J}\frac{\partial(x,y,f)}{\partial(x_0,y_0,z_0)} \end{aligned} \tag{2.28}$$

Applying Eq. (2.28) on the pressure, an additional Lagrangian form of Eq. (2.14) may be found as

$$\begin{aligned} \frac{\partial^2 x}{\partial t^2} &= -\frac{1}{\rho J}\frac{\partial(p,y,z)}{\partial(x_0,y_0,z_0)} + \upsilon\nabla^2 u \\ \frac{\partial^2 y}{\partial t^2} &= -\frac{1}{\rho J}\frac{\partial(x,p,z)}{\partial(x_0,y_0,z_0)} + \upsilon\nabla^2 v \\ \frac{\partial^2 z}{\partial t^2} &= -g - \frac{1}{\rho J}\frac{\partial(x,y,p)}{\partial(x_0,y_0,z_0)} + \upsilon\nabla^2 w \end{aligned} \tag{2.29}$$

cf. Gerber (1949), Corrsin (1962) and Pierson (1962).

Note that even if Eqs. (2.27) and (2.29) are equivalent, their components are not *individually* corresponding or interchangeable.

The analytic form of the inverse partial derivatives

$$\frac{\partial x_0}{\partial x}, \frac{\partial x_0}{\partial y}, \frac{\partial x_0}{\partial z}, \frac{\partial y_0}{\partial x}, \frac{\partial y_0}{\partial y}, \frac{\partial y_0}{\partial z}, \frac{\partial z_0}{\partial x}, \frac{\partial z_0}{\partial y}, \frac{\partial z_0}{\partial z}$$

may be found directly from Eq. (2.28), inserting the Lagrangian coordinates in turn as the scalar quantity f. The results are listed in Eqs. (A.13) - (A.21) in Appendix A, where the expressions have been simplified according to

$$\frac{\partial x_{i0}}{\partial x_{k0}} = \begin{cases} 1 , & i = k \\ 0 , & i \neq k \end{cases} \tag{2.30}$$

Eq. (2.28) verifies the 2D inverse partial derivatives in Eqs. (A.9) - (A.12) in Appendix A, which are derived in a different, but equivalent, manner.

The Lagrangian form of the Laplacian may now be found by differentiating f twice with respect to x, y and z, respectively, viz.

$$\frac{\partial^2 f}{\partial x^2} = \frac{\partial}{\partial x}\left(\frac{\partial f}{\partial x}\right) = \frac{\partial}{\partial x}\left(\frac{1}{J}\frac{\partial(f,y,z)}{\partial(x_0,y_0,z_0)}\right)$$

$$= \frac{\partial}{\partial x}\left(\frac{1}{J}\right)\cdot\frac{\partial(f,y,z)}{\partial(x_0,y_0,z_0)} + \frac{1}{J}\cdot\frac{\partial}{\partial x}\left(\frac{\partial(f,y,z)}{\partial(x_0,y_0,z_0)}\right)$$

$$= -\frac{1}{J^2}\cdot\frac{\partial J}{\partial x}\cdot\frac{\partial(f,y,z)}{\partial(x_0,y_0,z_0)} + \frac{1}{J^2}\cdot\frac{\partial\left(\frac{\partial(f,y,z)}{\partial(x_0,y_0,z_0)},y,z\right)}{\partial(x_0,y_0,z_0)}$$

$$= -\frac{1}{J^2}\cdot\frac{\partial(J,y,z)}{\partial(x_0,y_0,z_0)}\cdot\frac{\partial(f,y,z)}{\partial(x_0,y_0,z_0)} + \frac{1}{J^2}\cdot\frac{\partial\left(\frac{\partial(f,y,z)}{\partial(x_0,y_0,z_0)},y,z\right)}{\partial(x_0,y_0,z_0)}$$

$$= \frac{1}{J^2}\left[\frac{\partial\left(\frac{\partial(f,y,z)}{\partial(x_0,y_0,z_0)},y,z\right)}{\partial(x_0,y_0,z_0)} - \frac{\partial(J,y,z)}{\partial(x_0,y_0,z_0)}\cdot\frac{\partial(f,y,z)}{\partial(x_0,y_0,z_0)}\right]$$

and similarly

$$\frac{\partial^2 f}{\partial y^2} = \frac{1}{J^2}\left[\frac{\partial\left(x,\frac{\partial(x,f,z)}{\partial(x_0,y_0,z_0)},z\right)}{\partial(x_0,y_0,z_0)} - \frac{\partial(x,J,z)}{\partial(x_0,y_0,z_0)}\cdot\frac{\partial(x,f,z)}{\partial(x_0,y_0,z_0)}\right]$$

$$\frac{\partial^2 f}{\partial z^2} = \frac{1}{J^2}\left[\frac{\partial\left(x,y,\frac{\partial(x,y,f)}{\partial(x_0,y_0,z_0)}\right)}{\partial(x_0,y_0,z_0)} - \frac{\partial(x,y,J)}{\partial(x_0,y_0,z_0)}\cdot\frac{\partial(x,y,f)}{\partial(x_0,y_0,z_0)}\right]$$

The general Lagrangian form of the Laplacian operating on a scalar quantity may therefore be written

$$\nabla^2 f = \frac{\partial^2 f}{\partial x^2} + \frac{\partial^2 f}{\partial y^2} + \frac{\partial^2 f}{\partial z^2} \tag{2.31}$$

$$= \frac{1}{J}\left[\frac{\partial\left(\frac{1}{J}\frac{\partial(f,y,z)}{\partial(x_0,y_0,z_0)},y,z\right)}{\partial(x_0,y_0,z_0)} + \frac{\partial\left(x,\frac{1}{J}\frac{\partial(x,f,z)}{\partial(x_0,y_0,z_0)},z\right)}{\partial(x_0,y_0,z_0)} + \frac{\partial\left(x,y,\frac{1}{J}\frac{\partial(x,y,f)}{\partial(x_0,y_0,z_0)}\right)}{\partial(x_0,y_0,z_0)}\right]$$

$\Downarrow$

$$= \frac{1}{J^2}\left[\frac{\partial\left(\frac{\partial(f,y,z)}{\partial(x_0,y_0,z_0)},y,z\right)}{\partial(x_0,y_0,z_0)} + \frac{\partial\left(x,\frac{\partial(x,f,z)}{\partial(x_0,y_0,z_0)},z\right)}{\partial(x_0,y_0,z_0)} + \frac{\partial\left(x,y,\frac{\partial(x,y,f)}{\partial(x_0,y_0,z_0)}\right)}{\partial(x_0,y_0,z_0)}\right]$$

$$- \frac{1}{J^2}\left[\frac{\partial(J,y,z)}{\partial(x_0,y_0,z_0)}\cdot\frac{\partial(f,y,z)}{\partial(x_0,y_0,z_0)} + \frac{\partial(x,J,z)}{\partial(x_0,y_0,z_0)}\cdot\frac{\partial(x,f,z)}{\partial(x_0,y_0,z_0)} + \frac{\partial(x,y,J)}{\partial(x_0,y_0,z_0)}\cdot\frac{\partial(x,y,f)}{\partial(x_0,y_0,z_0)}\right]$$

In the special case of $J = 1$, the terms in the last brackets in Eq. (2.31) vanish, yielding the same expression for the Laplacian as in Pierson (1962). Pierson's presentation of the Laplacian is based on Gerber (1949) and Corrsin (1962). Gerber and Pierson both only consider the case $J = 1$, whereas Corrsin includes a Jacobian in the expression for the Laplacian. However, it seems that Corrsin applies the inverse Jacobian

$$J_{Corrsin} = J^{-1} = \frac{\partial(x_0,y_0,z_0)}{\partial(x,y,z)}$$

in his presentation.

Derivations similar to those above can be performed on equations for compressible and non-Newtonian fluid flow as well.

CHAPTER 3

VORTEX MOTION

It is customary to assume that the flow of an inviscid incompressible Newtonian fluid must be irrotational if it has only been subject to potential forces. Rotation is then defined by (half) the curl of the velocity vector. In this chapter, the available proofs of the foregoing statement, known as Lagrange's theorem, are reviewed, in order to clarify and examine the assumptions and initial conditions on which they are based. A discussion of these is given in Section 7.1, Sections 7.1.3 and 7.1.4 in particular, and a summary is given in Section 8.1.1.

3.1 Common Terms and Definitions

The relations between circulation, vorticity and rotation are normally given on Eulerian form, and may be presented as in the following, cf. e.g. Sarpkaya and Isaacson (1981).

The curl of the velocity vector **V** is defined by the cross product, cf. Eq. (2.8),

$$\text{curl } \mathbf{V} = \nabla \times \mathbf{V} \tag{3.1}$$

The components of the rotation of a fluid "particle" is commonly defined as

$$\begin{aligned} \omega_x &= \frac{1}{2}\left(\frac{\partial w}{\partial y} - \frac{\partial v}{\partial z}\right) \\ \omega_y &= \frac{1}{2}\left(\frac{\partial u}{\partial z} - \frac{\partial w}{\partial x}\right) \\ \omega_z &= \frac{1}{2}\left(\frac{\partial v}{\partial x} - \frac{\partial u}{\partial y}\right) \end{aligned} \tag{3.2}$$

which can be recognized as

$$\boldsymbol{\omega} = \frac{1}{2}\text{curl } \mathbf{V} \tag{3.3}$$

Note that Eq. (3.3) is also how the rotation (angular velocity) of a rigid body is defined.

The curl of the velocity at a Lagrangian point is quite essential in this thesis. Making use of Eqs. (A.9) - (A.12) in Appendix A, this may be found for the 2D case as

$$\begin{aligned}\frac{\partial u}{\partial z}-\frac{\partial w}{\partial x}&=\frac{\partial u}{\partial x_0}\frac{\partial x_0}{\partial z}+\frac{\partial u}{\partial z_0}\frac{\partial z_0}{\partial z}-\frac{\partial w}{\partial x_0}\frac{\partial x_0}{\partial x}-\frac{\partial w}{\partial z_0}\frac{\partial z_0}{\partial x}\\&=\frac{1}{J}\left(-\frac{\partial u}{\partial x_0}\frac{\partial x}{\partial z_0}+\frac{\partial u}{\partial z_0}\frac{\partial x}{\partial x_0}-\frac{\partial w}{\partial x_0}\frac{\partial z}{\partial z_0}+\frac{\partial w}{\partial z_0}\frac{\partial z}{\partial x_0}\right)\end{aligned} \tag{3.4}$$

The circulation Γ is defined as the line integral of the velocity vector taken around a closed curve s enclosing a surface S, viz.

$$\Gamma=\oint_s \mathbf{V}\cdot ds\,\mathbf{e}_s=\oint_s (u\,dx+v\,dy+w\,dz) \tag{3.5}$$

which after applying Stokes' theorem

$$\iint_S \operatorname{curl}\mathbf{V}\cdot dS\,\mathbf{e}_S=\oint_s \mathbf{V}\cdot ds\,\mathbf{e}_s \tag{3.6}$$

and making use of Eq. (3.3) becomes

$$\Gamma=\oint(u\,dx+v\,dy+w\,dz)=\iint_S \operatorname{curl}\mathbf{V}\cdot dS\,\mathbf{e}_S=2\iint_S \boldsymbol{\omega}\cdot dS\,\mathbf{e}_S \tag{3.7}$$

and on component form

$$\Gamma=\iint 2\omega_x\,dydz+\iint 2\omega_y\,dzdx+\iint 2\omega_z\,dxdy \tag{3.8}$$

In the above, $\mathbf{e}_s$ is the unit tangential vector of ds, and $\mathbf{e}_S$ is the unit normal vector of dS.

The vorticity $\boldsymbol{\zeta}$ is then often introduced as twice the rotation defined by Eq. (3.3), viz.

$$\boldsymbol{\zeta}=2\boldsymbol{\omega} \tag{3.9}$$

Vorticity may also be defined directly as the curl of the velocity vector in Eq. (3.1), viz.

$$\boldsymbol{\zeta}=\operatorname{curl}\mathbf{V}=\nabla\times\mathbf{V} \tag{3.10}$$

Eq. (3.10) is a definition more consistent with that of circulation in Eq. (3.5) since it defines vorticity as a pure mathematical quantity, whereas Eq. (3.9) defines it as twice the *assumed* physical rotation of a material fluid "particle".

If the curl in Eq. (3.1) is zero, an exact differential and independence of path is established, and a velocity potential exists. In the Eulerian description the velocity may then be written as

$$\begin{aligned}\mathbf{V}(x,y,z,t)&=u(x,y,z,t)\,\mathbf{i}+v(x,y,z,t)\,\mathbf{j}+w(x,y,z,t)\,\mathbf{k}\\&=\frac{\partial\varphi(x,y,z,t)}{\partial x}\mathbf{i}+\frac{\partial\varphi(x,y,z,t)}{\partial y}\mathbf{j}+\frac{\partial\varphi(x,y,z,t)}{\partial z}\mathbf{k}\\&=\nabla\varphi(x,y,z,t)\end{aligned} \tag{3.11}$$

where φ is an Eulerian velocity potential. A potential function is a scalar function whose gradient is a vector function. Further, if the fluid is incompressible, i.e. Eq. (2.10) applies, the velocity potential satisfies Laplace's equation, viz.

$$\nabla^2\varphi(x,y,z,t) = \frac{\partial\varphi^2(x,y,z,t)}{\partial x^2} + \frac{\partial\varphi^2(x,y,z,t)}{\partial y^2} + \frac{\partial\varphi^2(x,y,z,t)}{\partial z^2} = 0 \qquad (3.12)$$

Solutions of Laplace's equation are called harmonic functions, assuming they have continuous 2nd order partial derivatives. The theory of solutions of Laplace's equation is called potential theory. However, recall that potential theory does not apply to the velocity potential unless the fluid is also incompressible, cf. Glossary also.

3.2 Rotationality

3.2.1 Lagrange's theorem on the existence of a velocity potential

Lagrange's theorem (Lagrange, 1781), cf. e.g. Kochin et al. (1964), states that if an inviscid fluid is subject to potential forces only, and the density is a function of the pressure only, then a part of the fluid which at an initial instant in time contained no vorticity, did not contain any vorticity in the past, and will not contain any vorticity in the future. This is equivalent to stating that if a velocity potential exists for a part of the fluid at one instant in time, it will always exist for this part of the fluid (given the same assumptions as above).

The available proofs of Lagrange's theorem include Cauchy's vorticity equations (cf. Lamb, 1932, footnotes to Art. 17, and Stokes, 1845), Weber's transformation and the theorems of Helmholtz and Kelvin. In light of Stokes' theorem, relating vorticity and circulation (cf. Section 3.2.7), these are different derivations of the same quantity. However, Cauchy's vorticity equations and Weber's transformation consider an existing motion as compared to a state of rest, while the theorems of Helmholtz and Kelvin strictly speaking only consider an existing motion. Also, Cauchy's equations and Weber's transformation invokes Lagrangian variables, while the theorems of Helmholtz and Kelvin are normally given on Eulerian form only. Kelvin's theorem is here derived using Lagrangian variables.

Inviscid incompressible flow of a Newtonian fluid is assumed for all cases.

3.2.2 Cauchy's vorticity equations

Cauchy's vorticity equations (Cauchy, 1827) may be found in Goldstein (1960, his section 4.2), Lamb (1932, footnotes to Art. 146) and Batchelor (1967, his section 5.3).

The integral of the vorticity over a surface may be written, cf. Goldstein (1960),

$$\begin{aligned}\iint_S \zeta\cdot dS\,\mathbf{e}_S &= \iint_s (\zeta_x\,dydz + \zeta_y\,dzdx + \zeta_z\,dxdy)\\ &= \iint_s \Bigg\{ \zeta_x\left[\frac{\partial(y,z)}{\partial(x_0,y_0)}dx_0dy_0 + \frac{\partial(y,z)}{\partial(y_0,z_0)}dy_0dz_0 + \frac{\partial(y,z)}{\partial(z_0,x_0)}dz_0dx_0\right]\\ &\quad + \zeta_y\left[\frac{\partial(z,x)}{\partial(x_0,y_0)}dx_0dy_0 + \frac{\partial(z,x)}{\partial(y_0,z_0)}dy_0dz_0 + \frac{\partial(z,x)}{\partial(z_0,x_0)}dz_0dx_0\right]\\ &\quad + \zeta_z\left[\frac{\partial(x,y)}{\partial(x_0,y_0)}dx_0dy_0 + \frac{\partial(x,y)}{\partial(y_0,z_0)}dy_0dz_0 + \frac{\partial(x,y)}{\partial(z_0,x_0)}dz_0dx_0\right]\Bigg\}\end{aligned}$$

$$= \iint_S \Bigg\{ \left[\zeta_x \frac{\partial(y,z)}{\partial(x_0,y_0)} + \zeta_y \frac{\partial(z,x)}{\partial(x_0,y_0)} + \zeta_z \frac{\partial(x,y)}{\partial(x_0,y_0)} \right] dx_0 dy_0$$
$$+ \left[\zeta_x \frac{\partial(y,z)}{\partial(y_0,z_0)} + \zeta_y \frac{\partial(z,x)}{\partial(y_0,z_0)} + \zeta_z \frac{\partial(x,y)}{\partial(y_0,z_0)} \right] dy_0 dz_0 \qquad (3.13)$$
$$+ \left[\zeta_x \frac{\partial(y,z)}{\partial(z_0,x_0)} + \zeta_y \frac{\partial(z,x)}{\partial(z_0,x_0)} + \zeta_z \frac{\partial(x,y)}{\partial(z_0,x_0)} \right] dz_0 dx_0 \Bigg\}$$

where ζ_i are the components of the vorticity vector. If the initial conditions are set to

$$\frac{\partial x_i}{\partial x_{k0}} = \begin{cases} 1 , & i = k \\ 0 , & i \neq k \end{cases}$$

Eq. (3.13) may be written (for $t = 0$)

$$\iint_S \boldsymbol{\zeta} \cdot d\mathbf{S}\, \mathbf{e}_S = \iint_s \left(\zeta_z \, dx_0 dy_0 + \zeta_x \, dy_0 dz_0 + \zeta_y \, dz_0 dx_0 \right) \qquad (3.14)$$

Following Goldstein, assuming that the total value of Eq. (3.13) is constant and that the Lagrangian coordinates are fixed, and accounting for variations in density according to Eq. (2.17), one may equate Eqs. (3.13) and (3.14) and solve for ζ_x, ζ_y and ζ_z, viz.

$$\frac{1}{\rho}\zeta_x = \left(\frac{1}{\rho}\zeta_x\right)_{t=0} \frac{\partial x}{\partial x_0} + \left(\frac{1}{\rho}\zeta_y\right)_{t=0} \frac{\partial x}{\partial y_0} + \left(\frac{1}{\rho}\zeta_z\right)_{t=0} \frac{\partial x}{\partial z_0}$$
$$\frac{1}{\rho}\zeta_y = \left(\frac{1}{\rho}\zeta_x\right)_{t=0} \frac{\partial y}{\partial x_0} + \left(\frac{1}{\rho}\zeta_y\right)_{t=0} \frac{\partial y}{\partial y_0} + \left(\frac{1}{\rho}\zeta_z\right)_{t=0} \frac{\partial y}{\partial z_0} \qquad (3.15)$$
$$\frac{1}{\rho}\zeta_z = \left(\frac{1}{\rho}\zeta_x\right)_{t=0} \frac{\partial z}{\partial x_0} + \left(\frac{1}{\rho}\zeta_y\right)_{t=0} \frac{\partial z}{\partial y_0} + \left(\frac{1}{\rho}\zeta_z\right)_{t=0} \frac{\partial z}{\partial z_0}$$

Eq. (3.15) are Cauchy's vorticity equations.

The preceding presentation, based on Goldstein (1960), is not a proof of Lagrange's theorem, since the integrated vorticity (i.e. the circulation) is pre-assumed to be constant. Lamb (1932), in the footnote to his Art. 146, makes use of Weber's transformation in order to derive Cauchy's vorticity equations, and states that this constitutes Cauchy's proof of Lagrange's theorem. Cauchy's equations will therefore be verified by considering Weber's transformation.

3.2.3 Weber's transformation

Weber's transformation (Weber, 1868) of the inviscid form of Eq. (2.27) may be used to investigate the conservation of a velocity potential during the very initiation of the motion from a state of rest, cf. Lamb (1932, Arts. 15 and 17).

For simplicity, only the 2D case is considered, but the results may be extended to 3D in a straightforward manner. Gravity is given by the scalar ψ_1, cf. Eq. (2.7), and we may write Eq. (2.27) as

$$\begin{aligned}\frac{\partial^2 x}{\partial t^2}\frac{\partial x}{\partial x_0}+\frac{\partial^2 z}{\partial t^2}\frac{\partial z}{\partial x_0}&=-\frac{\partial \psi_1}{\partial x_0}-\frac{1}{\rho}\frac{\partial p}{\partial x_0}\\ \frac{\partial^2 x}{\partial t^2}\frac{\partial x}{\partial z_0}+\frac{\partial^2 z}{\partial t^2}\frac{\partial z}{\partial z_0}&=-\frac{\partial \psi_1}{\partial z_0}-\frac{1}{\rho}\frac{\partial p}{\partial z_0}\end{aligned} \tag{3.16}$$

Integrating the terms on the left hand side of Eq. (3.16) with respect to time from t_0 to t yields

$$\begin{aligned}\int_{t_0}^{t}\frac{\partial^2 x}{\partial t^2}\frac{\partial x}{\partial x_0}dt&=\left[\frac{\partial x}{\partial t}\frac{\partial x}{\partial x_0}\right]_{t_0}^{t}-\int_{t_0}^{t}\frac{\partial x}{\partial t}\frac{\partial}{\partial t}\left(\frac{\partial x}{\partial x_0}\right)dt=\left(u\frac{\partial x}{\partial x_0}\right)_t-\left(u\frac{\partial x}{\partial x_0}\right)_{t_0}-\frac{1}{2}\frac{\partial}{\partial x_0}\int_{t_0}^{t}\left(\frac{\partial x}{\partial t}\right)^2dt\\ \int_{t_0}^{t}\frac{\partial^2 z}{\partial t^2}\frac{\partial z}{\partial x_0}dt&=\left[\frac{\partial x}{\partial t}\frac{\partial z}{\partial x_0}\right]_{t_0}^{t}-\int_{t_0}^{t}\frac{\partial x}{\partial t}\frac{\partial}{\partial t}\left(\frac{\partial z}{\partial x_0}\right)dt=\left(w\frac{\partial z}{\partial x_0}\right)_t-\left(w\frac{\partial z}{\partial x_0}\right)_{t_0}-\frac{1}{2}\frac{\partial}{\partial x_0}\int_{t_0}^{t}\left(\frac{\partial z}{\partial t}\right)^2dt\\ \int_{t_0}^{t}\frac{\partial^2 x}{\partial t^2}\frac{\partial x}{\partial z_0}dt&=\left[\frac{\partial x}{\partial t}\frac{\partial x}{\partial z_0}\right]_{t_0}^{t}-\int_{t_0}^{t}\frac{\partial x}{\partial t}\frac{\partial}{\partial t}\left(\frac{\partial x}{\partial z_0}\right)dt=\left(u\frac{\partial x}{\partial z_0}\right)_t-\left(u\frac{\partial x}{\partial z_0}\right)_{t_0}-\frac{1}{2}\frac{\partial}{\partial z_0}\int_{t_0}^{t}\left(\frac{\partial x}{\partial t}\right)^2dt\\ \int_{t_0}^{t}\frac{\partial^2 z}{\partial t^2}\frac{\partial z}{\partial z_0}dt&=\left[\frac{\partial x}{\partial t}\frac{\partial z}{\partial z_0}\right]_{t_0}^{t}-\int_{t_0}^{t}\frac{\partial x}{\partial t}\frac{\partial}{\partial t}\left(\frac{\partial z}{\partial z_0}\right)dt=\left(w\frac{\partial z}{\partial z_0}\right)_t-\left(w\frac{\partial z}{\partial z_0}\right)_{t_0}-\frac{1}{2}\frac{\partial}{\partial z_0}\int_{t_0}^{t}\left(\frac{\partial z}{\partial t}\right)^2dt\end{aligned} \tag{3.17}$$

where the prevailing integrals have been transformed as follows

$$\int_{t_0}^{t}\frac{\partial x}{\partial t}\frac{\partial}{\partial t}\left(\frac{\partial x}{\partial x_0}\right)dt=\int_{t_0}^{t}\frac{\partial x}{\partial t}\frac{\partial}{\partial x_0}\left(\frac{\partial x}{\partial t}\right)dt=\frac{1}{2}\frac{\partial}{\partial x_0}\int_{t_0}^{t}\left(\frac{\partial x}{\partial t}\right)^2dt \tag{3.18}$$

etc.
etc.
etc.

Defining a scalar φ_t by

$$\varphi_t=\int_{t_0}^{t}\left\{\int\frac{1}{\rho}dp+\psi_1-\frac{1}{2}\left[\left(\frac{\partial x}{\partial t}\right)^2+\left(\frac{\partial z}{\partial t}\right)^2\right]\right\}dt=\int_{t_0}^{t}\left\{\int\frac{1}{\rho}dp+\psi_1-\frac{1}{2}q^2\right\}dt \tag{3.19}$$

and

$$\frac{d\varphi_t}{dt}=\int\frac{1}{\rho}dp+\psi_1-\frac{1}{2}q^2 \tag{3.20}$$

where $q^2=u^2+w^2$, the time-integrated form of Eq. (3.16) may be written

$$\begin{aligned}\left(u\frac{\partial x}{\partial x_0}+w\frac{\partial z}{\partial x_0}\right)_t-\left(u\frac{\partial x}{\partial x_0}+w\frac{\partial z}{\partial x_0}\right)_{t_0}&=-\frac{\partial \varphi_t}{\partial x_0}\\ \left(u\frac{\partial x}{\partial z_0}+w\frac{\partial z}{\partial z_0}\right)_t-\left(u\frac{\partial x}{\partial z_0}+w\frac{\partial z}{\partial z_0}\right)_{t_0}&=-\frac{\partial \varphi_t}{\partial z_0}\end{aligned} \tag{3.21}$$

The initial conditions at t_0 are set to

$$t = t_0: \qquad u = u_{t_0}, \quad w = w_{t_0}, \quad \frac{\partial x}{\partial x_0} = \frac{\partial z}{\partial z_0} = 1, \quad \frac{\partial x}{\partial z_0} = \frac{\partial z}{\partial x_0} = 0 \tag{3.22}$$

Note that Eq. (3.22) defines the Lagrangian coordinates as the Eulerian coordinates at $t = t_0$.

Invoking initial values in Eq. (3.21) according to Eq. (3.22) yields

$$\begin{aligned} u\frac{\partial x}{\partial x_0} + w\frac{\partial z}{\partial x_0} - u_{t_0} &= -\frac{\partial \varphi_t}{\partial x_0} \\ u\frac{\partial x}{\partial z_0} + w\frac{\partial z}{\partial z_0} - w_{t_0} &= -\frac{\partial \varphi_t}{\partial z_0} \end{aligned} \tag{3.23}$$

Multiplying the equations in Eq. (3.23) by dx_0 and dz_0, respectively, and adding, yields

$$\left(\begin{aligned} & u\frac{\partial x}{\partial x_0}dx_0 + w\frac{\partial z}{\partial x_0}dx_0 - u_{t_0}dx_0 = -\frac{\partial \varphi_t}{\partial x_0}dx_0 \\ & + \\ & u\frac{\partial x}{\partial z_0}dz_0 + w\frac{\partial z}{\partial z_0}dz_0 - w_{t_0}dz_0 = -\frac{\partial \varphi_t}{\partial z_0}dz_0 \end{aligned} \right)$$

$$\Downarrow$$

$$\begin{aligned} & u\left(\frac{\partial x}{\partial x_0}dx_0 + \frac{\partial x}{\partial z_0}dz_0\right) + w\left(\frac{\partial z}{\partial x_0}dx_0 + \frac{\partial z}{\partial z_0}dz_0\right) \\ & = -\left(\frac{\partial \varphi_t}{\partial x_0}dx_0 + \frac{\partial \varphi_t}{\partial z_0}dz_0\right) + \left(u_{t_0}dx_0 + w_{t_0}dz_0\right) \end{aligned}$$

$$\Downarrow$$

$$udx + wdz = -d\varphi_t + \left(u_{t_0}dx_0 + w_{t_0}dz_0\right) \tag{3.24}$$

Assuming that a velocity potential exists at $t = t_0$, i.e.

$$u_{t_0}dx_0 + w_{t_0}dz_0 = -d\varphi_{t_0} \tag{3.25}$$

we may write Eq. (3.24) as

$$udx + wdz = -d\varphi_t - d\varphi_{t_0} = d\varphi \tag{3.26}$$

meaning that a velocity potential exists also at time t.

Eq. (3.25) may be confirmed for an initial state of rest, since then

$$u_{t_0} = w_{t_0} = 0 \;\Rightarrow\; d\varphi_{t_0} = 0\,, \quad \varphi_{t_0} = const. \tag{3.27}$$

Note that Weber's transformation, and thus Cauchy's vorticity equations, rests on the initial assumptions Eqs. (3.22) and (3.27), and that the Lagrangian coordinates representing a specific portion of matter are assumed to remain the same from t_0 to t.

3.2.4 Helmholtz' theorem on the rate of change of vorticity

Helmholtz' theorem (Helmholtz, 1858) pertains to the rate of change of the vorticity. Considering Navier-Stokes equation on (Eulerian) vector form, i.e. Eq. (2.13), invoking Eq. (2.15) and making use of the vector identity

$$\mathbf{V}\times(\nabla\times\mathbf{V}) = \frac{1}{2}\nabla(\mathbf{V}\cdot\mathbf{V}) - \mathbf{V}\cdot\nabla\mathbf{V} \tag{3.28}$$

we may write

$$\frac{\partial}{\partial t}\mathbf{V} - \mathbf{V}\times\boldsymbol{\zeta} = -\nabla\left(\frac{p}{\rho}+\psi_1+\frac{1}{2}q^2\right) + \upsilon\nabla^2\mathbf{V} \tag{3.29}$$

where $\mathbf{V}\cdot\mathbf{V} = q^2$ is a scalar and the vorticity is an Eulerian vector field $\boldsymbol{\zeta} = \boldsymbol{\zeta}(x, y, z, t)$. Taking the curl of both sides of Eq. (3.29) yields

$$\frac{\partial}{\partial t}\boldsymbol{\zeta} = \nabla\times(\mathbf{V}\times\boldsymbol{\zeta}) + \upsilon\nabla^2\boldsymbol{\zeta} \tag{3.30}$$

since

$$\nabla\times(\nabla\psi_2) = 0$$

where ψ_2 is a scalar field defined by

$$\psi_2 = -\left(\frac{p}{\rho}+\psi_1+\frac{1}{2}q^2\right) \tag{3.31}$$

The first term on the right-hand side of Eq. (3.30) may be written

$$\nabla\times(\mathbf{V}\times\boldsymbol{\zeta}) = (\boldsymbol{\zeta}\cdot\nabla)\mathbf{V} - (\mathbf{V}\cdot\nabla)\boldsymbol{\zeta} + \mathbf{V}(\nabla\cdot\boldsymbol{\zeta}) - \boldsymbol{\zeta}(\nabla\cdot\mathbf{V})$$

since

$$\nabla\cdot\mathbf{V} = 0$$

$$\nabla\cdot\boldsymbol{\zeta} = \nabla\cdot(\nabla\times\mathbf{V}) = 0$$

Eq. (3.30) may therefore be simplified to

$$\frac{\partial}{\partial t}\boldsymbol{\zeta} = (\boldsymbol{\zeta}\cdot\nabla)\mathbf{V} - (\mathbf{V}\cdot\nabla)\boldsymbol{\zeta} + \upsilon\nabla^2\boldsymbol{\zeta} \tag{3.32}$$

$\mathbf{V}$ and $\boldsymbol{\zeta}$ are mutually perpendicular vectors, and the first two terms on the right-hand side of Eq. (3.32) therefore vanish in a 2D flow. Eq. (3.32) is often re-written according to Eq. (2.15), viz.

$$\frac{D}{Dt}\boldsymbol{\zeta} = (\boldsymbol{\zeta}\cdot\nabla)\mathbf{V} + \upsilon\nabla^2\boldsymbol{\zeta} \tag{3.33}$$

Eqs. (3.30), (3.32) and (3.33) all represent Helmholtz' theorem on vorticity.

3.2.5 The acceleration potential and the persistence of vorticity

The acceleration in inviscid incompressible flow of a Newtonian fluid may be expressed by a potential function. Invoking Lagrangian variables, the persistence of the curl of the Lagrangian velocity may be shown to follow directly from this acceleration potential.

Considering the inviscid form of the equations of motion Eq. (2.13), expressing gravity by the potential function ψ_1 as in Eq. (2.7), we have

$$\mathbf{a} = \frac{d}{dt}\mathbf{V} = \nabla\left(-\frac{p}{\rho} - \psi_1\right) = \nabla\varphi_{acc.} \tag{3.34}$$

where the time differentiation represents a material derivative. Taking the curl of both sides of Eq. (3.34) yields

$$\begin{gathered} \operatorname{curl}\mathbf{a} = \nabla\times(\nabla\varphi_{acc.}) = 0 \\ \Downarrow \\ \left(\frac{\partial a_z}{\partial y} - \frac{\partial a_y}{\partial z}\right) = \left(\frac{\partial a_x}{\partial z} - \frac{\partial a_z}{\partial x}\right) = \left(\frac{\partial a_y}{\partial x} - \frac{\partial a_x}{\partial y}\right) = 0 \end{gathered} \tag{3.35}$$

The following applies to the 2D case only. Invoking Lagrangian variables, we may now derive the following relation

$$\begin{aligned} \frac{d}{dt}\left(\frac{\partial u}{\partial z} - \frac{\partial w}{\partial x}\right) &= \frac{d}{dt}\left(\frac{\partial u}{\partial x_0}\frac{\partial x_0}{\partial z} + \frac{\partial u}{\partial z_0}\frac{\partial z_0}{\partial z} - \frac{\partial w}{\partial x_0}\frac{\partial x_0}{\partial x} - \frac{\partial w}{\partial z_0}\frac{\partial z_0}{\partial x}\right) \\ &= \frac{d}{dt}\left[\frac{1}{J}\left(-\frac{\partial u}{\partial x_0}\frac{\partial x}{\partial z_0} + \frac{\partial u}{\partial z_0}\frac{\partial x}{\partial x_0} - \frac{\partial w}{\partial x_0}\frac{\partial z}{\partial z_0} + \frac{\partial w}{\partial z_0}\frac{\partial z}{\partial x_0}\right)\right] \\ &= \frac{1}{J}\left(-\frac{\partial a_x}{\partial x_0}\frac{\partial x}{\partial z_0} - \frac{\partial u}{\partial x_0}\frac{\partial u}{\partial z_0} + \frac{\partial a_x}{\partial z_0}\frac{\partial x}{\partial x_0} + \frac{\partial u}{\partial z_0}\frac{\partial u}{\partial x_0}\right) \\ &+ \frac{1}{J}\left(-\frac{\partial a_z}{\partial x_0}\frac{\partial z}{\partial z_0} - \frac{\partial w}{\partial x_0}\frac{\partial w}{\partial z_0} + \frac{\partial a_z}{\partial z_0}\frac{\partial z}{\partial x_0} + \frac{\partial w}{\partial z_0}\frac{\partial w}{\partial x_0}\right) \\ &= \frac{1}{J}\left(-\frac{\partial a_x}{\partial x_0}\frac{\partial x}{\partial z_0} + \frac{\partial a_x}{\partial z_0}\frac{\partial x}{\partial x_0} - \frac{\partial a_z}{\partial x_0}\frac{\partial z}{\partial z_0} + \frac{\partial a_z}{\partial z_0}\frac{\partial z}{\partial x_0}\right) \\ &= \frac{\partial a_x}{\partial x_0}\frac{\partial x_0}{\partial z} + \frac{\partial a_x}{\partial z_0}\frac{\partial z_0}{\partial z} - \frac{\partial a_z}{\partial x_0}\frac{\partial x_0}{\partial x} - \frac{\partial a_z}{\partial z_0}\frac{\partial z_0}{\partial x} \\ &= \frac{\partial a_x}{\partial z} - \frac{\partial a_z}{\partial x} \end{aligned} \tag{3.36}$$

where use has been made of Eqs. (A.9) - (A.12) in Appendix A, and the Jacobian is assumed to be constant. Note that the time differentiation has been done while following the Lagrangian points. In light of Eq. (3.35), we may therefore write

$$\frac{d}{dt}(\operatorname{curl}\mathbf{V}) = \operatorname{curl}\mathbf{a} = \nabla\times(\nabla\varphi_{acc.}) = 0 \tag{3.37}$$

for the type of motion defined in the beginning of Section 3.2.1. Considering a fixed Lagrangian point, zero curl of the acceleration vector thus implies a constant curl of the velocity vector in 2D flow.

Differentiating Eq. (2.18) with time yields

$$\begin{aligned}
\frac{d^2J}{dt^2} &= \frac{d}{dt}\left(\frac{\partial u}{\partial x_0}\frac{\partial z}{\partial z_0}+\frac{\partial x}{\partial x_0}\frac{\partial w}{\partial z_0}-\frac{\partial u}{\partial z_0}\frac{\partial z}{\partial x_0}-\frac{\partial x}{\partial z_0}\frac{\partial w}{\partial x_0}\right)\\
&=\left(\frac{\partial a_x}{\partial x_0}\frac{\partial z}{\partial z_0}+\frac{\partial u}{\partial x_0}\frac{\partial w}{\partial z_0}\right)+\left(\frac{\partial u}{\partial x_0}\frac{\partial w}{\partial z_0}+\frac{\partial x}{\partial x_0}\frac{\partial a_z}{\partial z_0}\right)\\
&-\left(\frac{\partial a_x}{\partial z_0}\frac{\partial z}{\partial x_0}+\frac{\partial u}{\partial z_0}\frac{\partial w}{\partial x_0}\right)-\left(\frac{\partial u}{\partial z_0}\frac{\partial w}{\partial x_0}+\frac{\partial x}{\partial z_0}\frac{\partial a_z}{\partial x_0}\right)\\
&=\left(\frac{\partial a_x}{\partial x_0}\frac{\partial z}{\partial z_0}+\frac{\partial x}{\partial x_0}\frac{\partial a_z}{\partial z_0}-\frac{\partial a_x}{\partial z_0}\frac{\partial z}{\partial x_0}-\frac{\partial x}{\partial z_0}\frac{\partial a_z}{\partial x_0}\right)\\
&+\left(\frac{\partial u}{\partial x_0}\frac{\partial w}{\partial z_0}+\frac{\partial u}{\partial x_0}\frac{\partial w}{\partial z_0}-\frac{\partial u}{\partial z_0}\frac{\partial w}{\partial x_0}-\frac{\partial u}{\partial z_0}\frac{\partial w}{\partial x_0}\right)\\
&=J\left(\frac{\partial a_x}{\partial x_0}\frac{\partial x_0}{\partial x}+\frac{\partial z_0}{\partial z}\frac{\partial a_z}{\partial z_0}+\frac{\partial a_x}{\partial z_0}\frac{\partial z_0}{\partial x}+\frac{\partial x_0}{\partial z}\frac{\partial a_z}{\partial x_0}\right)+2\left(\frac{\partial u}{\partial x_0}\frac{\partial w}{\partial z_0}-\frac{\partial u}{\partial z_0}\frac{\partial w}{\partial x_0}\right)\\
&=J\left(\frac{\partial a_x}{\partial x_0}\frac{\partial x_0}{\partial x}+\frac{\partial a_x}{\partial z_0}\frac{\partial z_0}{\partial x}+\frac{\partial a_z}{\partial x_0}\frac{\partial x_0}{\partial z}+\frac{\partial a_z}{\partial z_0}\frac{\partial z_0}{\partial z}\right)+2\left(\frac{\partial u}{\partial x_0}\frac{\partial w}{\partial z_0}-\frac{\partial u}{\partial z_0}\frac{\partial w}{\partial x_0}\right)\\
&=J\left(\frac{\partial a_x}{\partial x}+\frac{\partial a_z}{\partial z}\right)+2\left(\frac{\partial u}{\partial x_0}\frac{\partial w}{\partial z_0}-\frac{\partial u}{\partial z_0}\frac{\partial w}{\partial x_0}\right)=0
\end{aligned}$$

$$\Downarrow$$

$$\nabla\cdot\mathbf{a}=-\frac{2}{J}\left(\frac{\partial u}{\partial x_0}\frac{\partial w}{\partial z_0}-\frac{\partial u}{\partial z_0}\frac{\partial w}{\partial x_0}\right)=-\frac{2}{J}\frac{\partial(u,w)}{\partial(x_0,z_0)} \tag{3.38}$$

where, again, use has been made of Eqs. (A.9) - (A.12) in Appendix A. Combining Eqs. (3.34) and (3.38) yields

$$\nabla\cdot\mathbf{a}=\nabla\cdot(\nabla\varphi_{acc.})=\nabla^2\varphi_{acc.}=-\frac{2}{J}\frac{\partial(u,w)}{\partial(x_0,z_0)} \tag{3.39}$$

Eq. (3.39) differs from Laplace's equation by the magnitude of the right-hand side. Potential theory can therefore not be used to determine this acceleration potential, unless the divergence of the acceleration can be required to be zero. Eq. (3.35) still serves as a fundamental condition on the solution of flow problems as defined in the beginning of Section 3.2.1.

3.2.6 Kelvin's theorem on the rate of change of circulation

Kelvin's theorem (1869) considers the rate of change of circulation around a closed curve. The circulation around the closed curve is defined as

$$\Gamma=\oint_s \mathbf{V}_E(x,y,z,t)\cdot ds\,\mathbf{e}_s \tag{3.40}$$

Performing a change of variables by invoking Eq. (2.1) yields

$$\begin{aligned}\Gamma &= \oint_{s_0} \mathbf{V}_E[x(x_0, y_0, z_0, t), y(x_0, y_0, z_0, t), z(x_0, y_0, z_0, t)] \cdot \frac{ds}{ds_0} ds_0\, \mathbf{e}_s \\ &= \oint_{s_0} \mathbf{V}_L(x_0, y_0, z_0, t) \cdot \frac{ds}{ds_0} ds_0\, \mathbf{e}_s\end{aligned} \tag{3.41}$$

Eqs. (3.40) and (3.41) are mathematically equivalent. Hence, the curve is always defined by the same Lagrangian points, presumably always representing the same material "particles".

Finding the time rate of change of the circulation around a curve defined by a specific set of Lagrangian coordinates is clearest if the equation is treated component-wise. The component form of the last term in Eq. (3.41) is

$$\begin{aligned}\frac{ds}{ds_0} \cdot ds_0\, \mathbf{e}_s = &\left(\frac{\partial x}{\partial x_0} dx_0 + \frac{\partial x}{\partial y_0} dy_0 + \frac{\partial x}{\partial z_0} dz_0\right) \mathbf{i} \\ &+ \left(\frac{\partial y}{\partial x_0} dx_0 + \frac{\partial y}{\partial y_0} dy_0 + \frac{\partial y}{\partial z_0} dz_0\right) \mathbf{j} \\ &+ \left(\frac{\partial z}{\partial x_0} dx_0 + \frac{\partial z}{\partial y_0} dy_0 + \frac{\partial z}{\partial z_0} dz_0\right) \mathbf{k}\end{aligned} \tag{3.42}$$

For simplicity, only the 2D case in the (x, z)-plane is considered in the following, but the results may be extended to 3D in a straightforward manner.

When following a specific Lagrangian curve, the differential ds_0 is constant. This yields

$$\begin{aligned}\frac{D}{Dt}\Gamma &= \frac{d}{dt} \oint_{s_0} \mathbf{V}_L(x_0, z_0, t) \cdot \frac{ds}{ds_0} ds_0\, \mathbf{e}_s \\ &= \frac{d}{dt} \oint_{s_0} \Big[u(x_0, z_0, t)\, \mathbf{i} \cdot \left(\frac{\partial x}{\partial x_0} dx_0 + \frac{\partial x}{\partial z_0} dz_0\right) \mathbf{i} \\ &\qquad + w(x_0, z_0, t)\, \mathbf{k} \cdot \left(\frac{\partial z}{\partial x_0} dx_0 + \frac{\partial z}{\partial z_0} dz_0\right) \mathbf{k} \Big] \\ &= \oint_{s_0} \frac{d}{dt} \left[u \left(\frac{\partial x}{\partial x_0} dx_0 + \frac{\partial x}{\partial z_0} dz_0 \right) + w \left(\frac{\partial z}{\partial x_0} dx_0 + \frac{\partial z}{\partial z_0} dz_0 \right) \right] \\ &= \oint_{s_0} \Bigg[\frac{du}{dt} \left(\frac{\partial x}{\partial x_0} dx_0 + \frac{\partial x}{\partial z_0} dz_0 \right) + \frac{dw}{dt} \left(\frac{\partial z}{\partial x_0} dx_0 + \frac{\partial z}{\partial z_0} dz_0 \right) \\ &\qquad + u \left(\frac{\partial u}{\partial x_0} dx_0 + \frac{\partial u}{\partial z_0} dz_0 \right) + w \left(\frac{\partial w}{\partial x_0} dx_0 + \frac{\partial w}{\partial z_0} dz_0 \right) \Bigg] \\ &= \oint_{s_0} \Bigg[\left(\frac{\partial x}{\partial x_0} dx_0 + \frac{\partial x}{\partial z_0} dz_0 \right) \left(-\frac{1}{\rho J} \frac{\partial (p, z)}{\partial (x_0, z_0)} + \nu \nabla^2 u \right) \\ &\qquad + \left(\frac{\partial z}{\partial x_0} dx_0 + \frac{\partial z}{\partial z_0} dz_0 \right) \left(-g - \frac{1}{\rho J} \frac{\partial (x, p)}{\partial (x_0, z_0)} + \nu \nabla^2 w \right)\end{aligned}$$

$$
\begin{aligned}
&+ udu + wdw\Big]\\
&= \oint_{s_0}\Bigg[\left(-\frac{1}{\rho J}\frac{\partial(p,z)}{\partial(x_0,z_0)}\frac{\partial x}{\partial x_0}-\frac{1}{\rho J}\frac{\partial(x,p)}{\partial(x_0,z_0)}\frac{\partial z}{\partial x_0}-g\frac{\partial z}{\partial x_0}\right)dx_0\\
&\quad+\left(-\frac{1}{\rho J}\frac{\partial(p,z)}{\partial(x_0,z_0)}\frac{\partial x}{\partial z_0}-\frac{1}{\rho J}\frac{\partial(x,p)}{\partial(x_0,z_0)}\frac{\partial z}{\partial z_0}-g\frac{\partial z}{\partial z_0}\right)dz_0\\
&\quad+\upsilon\left(\nabla^2 u\frac{\partial x}{\partial x_0}+\nabla^2 w\frac{\partial z}{\partial x_0}\right)dx_0+\upsilon\left(\nabla^2 u\frac{\partial x}{\partial z_0}+\nabla^2 w\frac{\partial z}{\partial z_0}\right)dz_0\\
&\quad+d(\tfrac{1}{2}u^2)+d(\tfrac{1}{2}w^2)\Bigg]\\
&= \oint_{s_0}\Bigg[-\frac{\partial(\frac{1}{\rho}p+gz)}{\partial x_0}dx_0-\frac{\partial(\frac{1}{\rho}p+gz)}{\partial z_0}dz_0\\
&\quad+\upsilon\left(\nabla^2 u\frac{\partial x}{\partial x_0}+\nabla^2 w\frac{\partial z}{\partial x_0}\right)dx_0+\upsilon\left(\nabla^2 u\frac{\partial x}{\partial z_0}+\nabla^2 w\frac{\partial z}{\partial z_0}\right)dz_0\\
&\quad+d(\tfrac{1}{2}u^2)+d(\tfrac{1}{2}w^2)\Bigg]\\
&= \oint_{s_0}\upsilon\left(\nabla^2 u\frac{\partial x}{\partial x_0}+\nabla^2 w\frac{\partial z}{\partial x_0}\right)dx_0+\upsilon\left(\nabla^2 u\frac{\partial x}{\partial z_0}+\nabla^2 w\frac{\partial z}{\partial z_0}\right)dz_0 \qquad (3.43)\\
&= \oint_{s}\upsilon\nabla^2\,\mathbf{V}_E\cdot\,ds\,\mathbf{e}_s
\end{aligned}
$$

where Eq. (2.29) is inserted for the time rate of change of the velocity and the Lagrangian form of the Laplacian is defined by Eq. (2.31). The last transition to the common Eulerian form is true because a Lagrangian curve at one instant in time is identical to an Eulerian curve. The determinants containing the pressure were simplified in the following manner

$$
\begin{aligned}
&\left(-\frac{1}{\rho J}\frac{\partial(p,z)}{\partial(x_0,z_0)}\frac{\partial x}{\partial x_0}-\frac{1}{\rho J}\frac{\partial(x,p)}{\partial(x_0,z_0)}\frac{\partial z}{\partial x_0}-g\frac{\partial z}{\partial x_0}\right)dx_0\\
&=\left[-\frac{1}{\rho J}\left(\frac{\partial p}{\partial x_0}\frac{\partial z}{\partial z_0}\frac{\partial x}{\partial x_0}-\frac{\partial p}{\partial z_0}\frac{\partial z}{\partial x_0}\frac{\partial x}{\partial x_0}\right)-\frac{1}{\rho J}\left(\frac{\partial x}{\partial x_0}\frac{\partial p}{\partial z_0}\frac{\partial z}{\partial x_0}-\frac{\partial x}{\partial z_0}\frac{\partial p}{\partial x_0}\frac{\partial z}{\partial x_0}\right)\right]dx_0\\
&=\left[-\frac{1}{\rho J}\left(\frac{\partial p}{\partial x_0}\frac{\partial z}{\partial z_0}\frac{\partial x}{\partial x_0}-\frac{\partial x}{\partial z_0}\frac{\partial p}{\partial x_0}\frac{\partial z}{\partial x_0}\right)-\frac{1}{\rho J}\left(-\frac{\partial p}{\partial z_0}\frac{\partial z}{\partial x_0}\frac{\partial x}{\partial x_0}+\frac{\partial x}{\partial x_0}\frac{\partial p}{\partial z_0}\frac{\partial z}{\partial x_0}\right)\right]dx_0\\
&=\left[-\frac{1}{\rho J}\left(\frac{\partial p}{\partial x_0}\frac{\partial z}{\partial z_0}\frac{\partial x}{\partial x_0}-\frac{\partial x}{\partial z_0}\frac{\partial p}{\partial x_0}\frac{\partial z}{\partial x_0}\right)\right]dx_0=\left[-\frac{1}{\rho J}\frac{\partial p}{\partial x_0}\left(\frac{\partial x}{\partial x_0}\frac{\partial z}{\partial z_0}-\frac{\partial x}{\partial z_0}\frac{\partial z}{\partial x_0}\right)\right]dx_0
\end{aligned}
$$

$$= -\frac{1}{\rho J}\frac{\partial p}{\partial x_0} J dx_0 = -\frac{1}{\rho}\frac{\partial p}{\partial x_0} dx_0 = -\frac{\partial(\frac{1}{\rho} p)}{\partial x_0}\, dx_0$$

yielding the exact differential form and therefore cancellation over the closed curve along with the gravity term and the squared velocity term.

3.2.7 Stokes' theorem relating circulation and vorticity

Circulation and vorticity are related through Stokes' theorem, cf. Eq. (3.6), viz.

$$\iint_S (\nabla \times \mathbf{V}_E) \cdot dS\, \mathbf{e}_S = \oint_s \mathbf{V}_E \cdot ds\, \mathbf{e}_s$$

$$\Downarrow$$

$$\frac{D}{Dt}\left[\iint_S (\nabla \times \mathbf{V}_E) \cdot dS\, \mathbf{e}_S\right] = \frac{D}{Dt}\left(\oint_s \mathbf{V}_E \cdot ds\, \mathbf{e}_s\right)$$

$$= \oint_s \upsilon \nabla^2 \mathbf{V}_E \cdot ds\, \mathbf{e}_s \qquad (3.44)$$

Assuming incompressible flow, Eq. (3.44) may be written

$$\frac{D}{Dt}\iint_S (\nabla \times \mathbf{V}_E) \cdot dS\, \mathbf{e}_S = -\upsilon \oint_s \nabla \times (\nabla \times \mathbf{V}_E) \cdot ds\, \mathbf{e}_s \qquad (3.45)$$

Note that Stokes' theorem is defined in an Eulerian frame of reference.

3.3 Eulerian Potential Theory and Lagrangian Variables

The continuity requirement in incompressible 2D flow, cf. Eqs. (2.10) and (2.21), may be written

$$\frac{\partial w}{\partial z} - \left(-\frac{\partial u}{\partial x}\right) = 0 \qquad (3.46)$$

meaning that an exact differential $d\psi$ exists as

$$d\psi = u dz - w dx$$

where

$$u = \frac{\partial \psi}{\partial z}, \quad w = -\frac{\partial \psi}{\partial x} \qquad (3.47)$$

The scalar function ψ (the stream function) is now defined as

$$\psi = \int_s u dz - w dx$$

where s is the curve of integration. If the curl of the velocity is zero, i.e.

$$\frac{\partial u}{\partial z} - \frac{\partial w}{\partial x} = 0 \tag{3.48}$$

an exact differential $d\varphi$ exists as

$$d\varphi = udx + wdz$$

where

$$u = \frac{\partial \varphi}{\partial x}, \quad w = \frac{\partial \varphi}{\partial z} \tag{3.49}$$

and the scalar function φ (the velocity potential) is defined as

$$\varphi = \int_s udx + wdz$$

Comparing Eqs. (3.47) and (3.49) shows that

$$\frac{d\psi}{dz} = \frac{\partial \varphi}{\partial x}, \quad -\frac{d\psi}{dx} = \frac{\partial \varphi}{\partial z} \tag{3.50}$$

These are recognizable as the Cauchy-Riemann equations, verifying the existence of a complex analytic function

$$\varphi_{complex}(Z) = \varphi(x,z) + i\psi(x,z) \tag{3.51}$$

where

$$Z = x + iz$$

Since the complex function of Eq. (3.51) is analytic, φ and ψ both satisfy Laplace's equation, cf. Eq. (3.12), and have continuous 2nd order partial derivatives, i.e. they are harmonic functions. This may be verified by combining Eqs. (3.47) and (3.48), yielding

$$\frac{\partial u}{\partial z} - \frac{\partial w}{\partial x} = \frac{\partial^2 \psi}{\partial z^2} + \frac{\partial^2 \psi}{\partial x^2} = \nabla^2 \psi = 0 \tag{3.52}$$

and combining Eqs. (3.46) and (3.49), yielding

$$\frac{\partial u}{\partial x} + \frac{\partial w}{\partial z} = \frac{\partial^2 \varphi}{\partial x^2} + \frac{\partial^2 \varphi}{\partial x^2} = \nabla^2 \varphi = 0 \tag{3.53}$$

However, as in the equations of motion, these potential functions are assumed to apply to a specific portion of matter. The potential in Eq. (3.51) must therefore exist on Lagrangian form, which imposes certain conditions on the relations between the Lagrangian and Eulerian variables. The following is based on the proof of the theorem of harmonic functions under conformal mapping, as presented in Kreyszig (1988, his section 17.2: "Use of Conformal Mapping"):

Eq. (3.51) yields

$$\begin{aligned}\varphi_{complex}(Z) &= \varphi(x,z)+i\psi(x,z)\\ &= \varphi[x(x_0,z_0),z(x_0,z_0)]+i\psi[x(x_0,z_0),z(x_0,z_0)]\\ &= \varphi_L(x_0,z_0)+i\psi_L(x_0,z_0)\\ &= \varphi_L[x_0(x,z),z_0(x,z)]+i\psi_L[x_0(x,z),z_0(x,z)] = \varphi_{L,complex}[Z_0(Z)]\end{aligned} \tag{3.54}$$

where the last line results from invoking Eq. (2.2) again, and

$$Z_0 = x_0 + iz_0$$

Due to continuity, the stream function always exists in 2D incompressible flow. Therefore, if the curl of the velocity is zero, Eq. (3.52) is satisfied. If a velocity potential also exist, Eq. (3.53) is satisfied and the complex function in Eq. (3.54) is analytic in the (x, z)-plane.

It is now claimed that the Lagrangian and the Eulerian forms of the complex potential in Eq. (3.54) must both be analytic. The relations $x_0(x, z)$ and $z_0(x, z)$ must then be analytic in a complex sense, i.e. satisfying the Cauchy-Riemann equations, viz.

$$\begin{aligned}&\frac{\partial x_0(x,z)}{\partial x} = \frac{\partial z_0(x,z)}{\partial z} \Leftrightarrow \frac{1}{J}\frac{\partial z(x_0,z_0)}{\partial z_0} = \frac{1}{J}\frac{\partial x(x_0,z_0)}{\partial x_0} \Rightarrow \frac{\partial z(x_0,z_0)}{\partial z_0} = \frac{\partial x(x_0,z_0)}{\partial x_0}\\ &\frac{\partial x_0(x,z)}{\partial z} = -\frac{\partial z_0(x,z)}{\partial x} \Leftrightarrow -\frac{1}{J}\frac{\partial x(x_0,z_0)}{\partial z_0} = \frac{1}{J}\frac{\partial z(x_0,z_0)}{\partial x_0} \Rightarrow \frac{\partial x(x_0,z_0)}{\partial z_0} = -\frac{\partial z(x_0,z_0)}{\partial x_0}\end{aligned} \tag{3.55}$$

where use has been made of Eqs. (A.9) - (A.12) in Appendix A. Note that analyticity implies that the Eulerian region defining a material element is a conformal mapping of the Lagrangian region defining the element.

Inserting Eq. (3.55) into the Jacobian, which by assumption equals 1, yields

$$\begin{aligned}J &= \frac{\partial(x,z)}{\partial(x_0,z_0)} = \frac{\partial x}{\partial x_0}\frac{\partial z}{\partial z_0} - \frac{\partial x}{\partial z_0}\frac{\partial z}{\partial x_0}\\ &= \begin{cases}\left(\dfrac{\partial x}{\partial x_0}\right)^2 + \left(\dfrac{\partial z}{\partial x_0}\right)^2 = \dfrac{|dx_0|^2}{dx_0^2} = 1\\ \left(\dfrac{\partial z}{\partial z_0}\right)^2 + \left(\dfrac{\partial x}{\partial z_0}\right)^2 = \dfrac{|dz_0|^2}{dz_0^2} = 1\end{cases}\end{aligned} \tag{3.56}$$

The area of an infinitesimal 2D element is found by a cross product, cf. Eq. (2.16), and may be written

$$dA = dxdz = Jdx_0dz_0 = dx_0dz_0 = |dx_0|\ |dz_0|\ \sin\kappa \tag{3.57}$$

where κ is the angle between two curves defined by x_0 = *const.* and z_0 = *const.* The differentials dx_0 and dz_0 may be set to 1. Comparing Eqs. (3.56) and (3.57) then shows that

$\sin\kappa$ must always be 1, i.e. that lines of constant x_0 and z_0 cross each other orthogonally in an Eulerian frame of reference, if $J = 1$ in the point where they cross. This also follows from the definition of conformal mapping. The condition $J \neq 0$ is a sufficient condition that $x(x_0, z_0) + iz(x_0, z_0)$ represents a one-to-one mapping of a Lagrangian region onto an Eulerian region. See Kreyszig (1988, his section 16.1: "Conformal Mapping") also.

If the Jacobian is everywhere and always 1, i.e. uniform and constant, requiring an Eulerian velocity potential to exist then allows very simple forms of deformation only, if any at all. However, the ability to deform into "arbitrary" and curved shapes is quite essential for a fluid. With respect to waves, a trochoidal or sine-shaped surface is not possible if lines of constant x_0 and z_0 have to cross orthogonally, cf. Figure 4.1, if there is no mass transport. Hence, a mass transport must be set up in order to restore orthogonality. Such a mass transport should follow from a potential solution, which is also the case, namely Stokes drift. Stokes drift does restore orthogonality, but only in a part of the wave and only quite instantaneously. In Section 4.3, Stokes drift and Stokes waves are considered from a Lagrangian point of view. It is there shown that this solution violates continuity after a very short period of time, and that it therefore is theoretically inconsistent in the Lagrangian frame of reference.

3.4 Physical Rotation of a Fluid Element

By rotation we normally mean how an element turns about itself, expressed e.g. by an angular velocity about its own axis if such an axis can be specified. However, rotation of a fluid element is normally defined as half the curl of the velocity vector, cf. Eqs. (3.1) - (3.3), and this is not suited to describe how a deformable fluid element turns about itself. Expressions that do describe the actual physical rotation of a deformable fluid element better may be found for a small element defined in Lagrangian coordinates, considering the rate of change of relative positions of different points on or within the element boundaries.

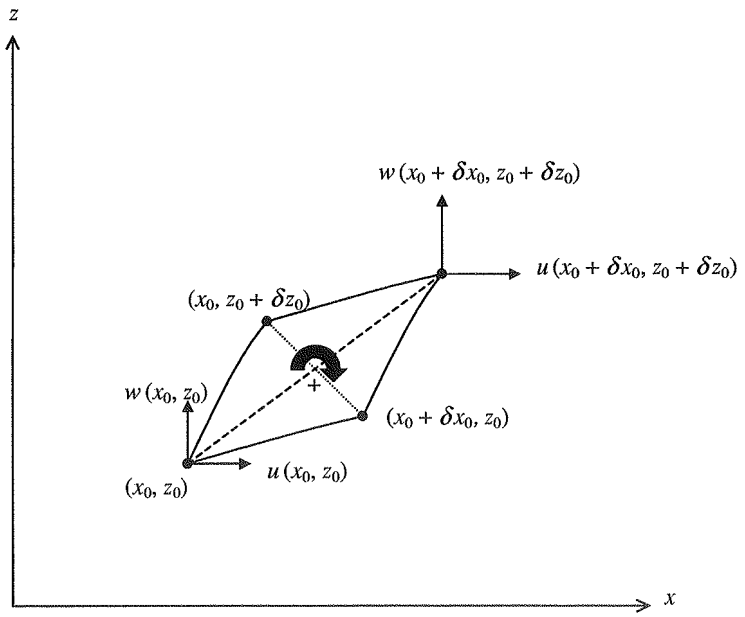

Figure 3.1 Motion of a 2D element (δx_0, δz_0). x_0 and z_0 are constant along the respective solid lines in the figure. The dashed line represents diagonal $D1$, and the dotted line represents diagonal $D2$.

As in Figure 3.1, we may consider the diagonals of a small element defined by the four "corners" (x_0, z_0), $(x_0 + \delta x_0, z_0)$, $(x_0, z_0 + \delta z_0)$ and $(x_0 + \delta x_0, z_0 + \delta z_0)$. The rotation of the diagonal $D1$ may be expressed by the difference in the velocities at the two "corners" (x_0, z_0) and $(x_0 + \delta x_0, z_0 + \delta z_0)$, viz.

$$\begin{aligned}
\delta u &= u(x_0 + \delta x_0, z_0 + \delta z_0) - u(x_0, z_0) \\
&\approx \frac{\partial u}{\partial x_0}\delta x_0 + \frac{1}{2}\frac{\partial^2 u}{\partial x_0^2}(\delta x_0)^2 + \left(\frac{\partial u}{\partial z_0} + \frac{1}{2}\frac{\partial^2 u}{\partial z_0^2}\delta z_0 + \frac{\partial\left(\frac{\partial u}{\partial z_0}\right)}{\partial x_0}\delta x_0 \right)\delta z_0 \\
&= \frac{\partial u}{\partial x_0}\delta x_0 + \frac{\partial u}{\partial z_0}\delta z_0 + \frac{1}{2}\frac{\partial^2 u}{\partial x_0^2}(\delta x_0)^2 + \frac{1}{2}\frac{\partial^2 u}{\partial z_0^2}(\delta z_0)^2 + \frac{\partial^2 u}{\partial z_0 \partial x_0}\delta x_0 \delta z_0
\end{aligned}$$

$$\begin{aligned}
\delta w &= w(x_0 + \delta x_0, z_0 + \delta z_0) - w(x_0, z_0) \\
&\approx \frac{\partial w}{\partial x_0}\delta x_0 + \frac{1}{2}\frac{\partial^2 w}{\partial x_0^2}(\delta x_0)^2 + \left(\frac{\partial w}{\partial z_0} + \frac{1}{2}\frac{\partial^2 w}{\partial z_0^2}\delta z_0 + \frac{\partial\left(\frac{\partial w}{\partial z_0}\right)}{\partial x_0}\delta x_0 \right)\delta z_0 \\
&= \frac{\partial w}{\partial x_0}\delta x_0 + \frac{\partial w}{\partial z_0}\delta z_0 + \frac{1}{2}\frac{\partial^2 w}{\partial x_0^2}(\delta x_0)^2 + \frac{1}{2}\frac{\partial^2 w}{\partial z_0^2}(\delta z_0)^2 + \frac{\partial^2 w}{\partial z_0 \partial x_0}\delta x_0 \delta z_0
\end{aligned}$$

The differentiation is done following the two lower lines in Figure 3.1, meaning that the derivative with respect to x_0 is taken at $z_0 = const.$ and the derivative with respect to z_0 is taken at $x_0 + \delta x_0 = const.$ Alternatively, differentiation may be done following the two upper lines.

If the changes in the velocity components are not symmetric, the diagonal will appear to rotate in a fixed Eulerian frame of reference. Note that the diagonal is a straight line, and will therefore not generally consist of the same Lagrangian points throughout the motion, except for the endpoints. Considering the element to be infinitesimal, i.e. δx_0 and $\delta z_0 \to 0$, and assuming that the 2nd order derivatives in the derivation above are not infinite, a *qualitative* measure of the angular velocity of this diagonal is

$$\omega_{D1} = \frac{\partial u}{\partial x_0} + \frac{\partial u}{\partial z_0} - \frac{\partial w}{\partial x_0} - \frac{\partial w}{\partial z_0} = \left(\frac{\partial u}{\partial x_0} - \frac{\partial w}{\partial z_0} \right) + \left(\frac{\partial u}{\partial z_0} - \frac{\partial w}{\partial x_0} \right) \tag{3.58}$$

where the signs are according to Figure 3.1. Quantification of the actual angular velocity must be done considering the Eulerian dimensions of an element of finite size at a given instant in time. For the other diagonal in Figure 3.1 ($D2$, dotted line) we find

$$\begin{aligned}
\delta u &= u(x_0 + \delta x_0, z_0) - u(x_0, z_0 + \delta z_0) \\
&\approx \frac{\partial u}{\partial x_0}\delta x_0 + \frac{1}{2}\frac{\partial^2 u}{\partial x_0^2}(\delta x_0)^2 - \frac{\partial u}{\partial z_0}\delta z_0 - \frac{1}{2}\frac{\partial^2 u}{\partial z_0^2}(\delta z_0)^2 \\
&= \frac{\partial u}{\partial x_0}\delta x_0 - \frac{\partial u}{\partial z_0}\delta z_0 + \frac{1}{2}\frac{\partial^2 u}{\partial x_0^2}(\delta x_0)^2 - \frac{1}{2}\frac{\partial^2 u}{\partial z_0^2}(\delta z_0)^2
\end{aligned}$$

$$\begin{aligned}\delta w &= w(x_0+\delta x_0, z_0) - w(x_0, z_0+\delta z_0)\\ &\approx \frac{\partial w}{\partial x_0}\delta x_0 + \frac{1}{2}\frac{\partial^2 w}{\partial x_0^2}(\delta x_0)^2 - \frac{\partial w}{\partial z_0}\delta z_0 - \frac{1}{2}\frac{\partial^2 w}{\partial z_0^2}(\delta z_0)^2\\ &= \frac{\partial w}{\partial x_0}\delta x_0 - \frac{\partial w}{\partial z_0}\delta z_0 + \frac{1}{2}\frac{\partial^2 w}{\partial x_0^2}(\delta x_0)^2 - \frac{1}{2}\frac{\partial^2 w}{\partial z_0^2}(\delta z_0)^2\end{aligned}$$

hence

$$\omega_{D2} = -\left[\frac{\partial u}{\partial x_0} - \frac{\partial u}{\partial z_0} + \frac{\partial w}{\partial x_0} - \frac{\partial w}{\partial z_0}\right] = -\left(\frac{\partial u}{\partial x_0} - \frac{\partial w}{\partial z_0}\right) + \left(\frac{\partial u}{\partial z_0} - \frac{\partial w}{\partial x_0}\right) \tag{3.59}$$

An expression for the physical rotation of an infinitesimal element may then be found as the mean of the rotation of the two diagonals, viz.

$$\omega_M = \frac{1}{2}(\omega_{D1} + \omega_{D2}) = \frac{\partial u}{\partial z_0} - \frac{\partial w}{\partial x_0} \tag{3.60}$$

Note that Eq. (3.60) describes physical rotation qualitatively rather than quantitatively.

Eq. (3.60) is identical to a definition of rotation given in Segel (1987), although it is there derived in a different manner assuming $J = 1$. It is there (Segel's section 4.1) stated explicitly that "*In many classical texts, the infinitesimal strain tensor is denoted by ε_{ik}, although each component is interpreted as if one were considering the material strain tensor*". The tensor ε_{ik} referred to is equivalent to the curl defined in Section 3.1, and the material strain tensor is equivalent to Eq. (3.60). It is further shown that the difference between these two definitions is of second order, and therefore negligible for infinitesimal strains (deformations) only.

However, it is customary to consider the two "basic" lines originating at the "corner" (x_0, z_0) in Figure 3.1. By the same reasoning as for the diagonals, we find that a qualitative mean angular velocity for these two lines is

$$\omega_{(x0,z0)} = \frac{1}{2}\left[\left(\frac{\partial u}{\partial z_0} - \frac{\partial w}{\partial z_0}\right) + \left(\frac{\partial u}{\partial x_0} - \frac{\partial w}{\partial x_0}\right)\right] = \frac{1}{2}\left[\left(\frac{\partial u}{\partial x_0} - \frac{\partial w}{\partial z_0}\right) + \left(\frac{\partial u}{\partial z_0} - \frac{\partial w}{\partial x_0}\right)\right] \tag{3.61}$$

i.e. equivalent to ω_{D1}. We may of course also consider the two lines originating in the points $(x_0, z_0 + \delta z_0)$, $(x_0 + \delta x_0, z_0)$ and $(x_0 + \delta x_0, z_0 + \delta z_0)$, respectively. These are all likely to yield expressions equivalent to ω_{D1} and ω_{D2}. Note that Eq. (3.61) is also only a qualitative measure. The difference between this equation and Eq. (3.2) does not imply that there is an error anywhere, but that they describe different quantities. However, it is clear that Eqs. (3.2) and (3.3) do not describe how a material element turns about itself very well, they do not describe the angular velocity of a material fluid "particle" unambiguously, as will be shown for the Gerstner wave in Section 4.1.3. See also Section 7.1.4 for a historical note on vorticity and its interpretation.

There is no obvious "correct" choice between the above different expressions for physical rotation of material elements. Whereas rigid body rotation is a clear and unambiguous concept, mathematically as well as physically, there are several ways of defining and describing the physical rotation of a deformable material element.

CHAPTER 4

WAVE THEORY

This chapter covers the basic Lagrangian theory of 2D regular waves in intermediate and deep water. As usual, water is considered incompressible, and viscosity is ignored. Modelling of irregular waves is treated in Chapter 5, but some simplified expressions for narrow-banded irregular waves are included in Sections 4.1.6 and 4.2.3.

The case of deep water, i.e. $h/\lambda > 0.5$, is covered by Gerstner's wave theory, and the case of intermediate water is covered by Miche's theory. Intermediate water is normally defined by the interval 0.05 - 0.1 < h/λ < 0.5. In the limit of infinite depth, Miche's theory equals Gerstner's theory. Shallow water or varying depth is not considered.

4.1 Gerstner's Wave Theory

Gerstner's wave theory (Gerstner, 1802 and 1809) is an exact analytical solution of the full nonlinear Lagrangian equations of motion. It applies to 2D motion on infinite depth. Detailed presentations of Gerstner's wave theory may be found in Lamb (1932), Milne-Thomson (1996), Wiegel (1964), Kinsman (1965), Kochin et al. (1964) and Le Méhauté (1976).

4.1.1 Kinematics and continuity

Gerstner's solution for the motion (displacement) of a Lagrangian point is

$$\begin{aligned} x &= x_0 - ae^{kz_0}\cos(\omega t - kx_0) \\ z &= z_0 + ae^{kz_0}\sin(\omega t - kx_0) \end{aligned} \tag{4.1}$$

where x and z represent the Eulerian position of the Lagrangian point (x_0, x_0). The Eulerian frame of reference is here defined by $z = 0$ a distance ½ ka^2 above the still water level, and z_0 runs from 0 to ($-h - ½\,ka^2$) where h is the depth in still water. This follows from conservation of mass, as will be shown in the following. The phase in Eq. (4.1) is a matter of definition, and may be found to be different in other presentations.

The velocities and accelerations are

$$
\begin{aligned}
u &= \frac{\partial x}{\partial t} = \omega a e^{kz_0} \sin(\omega t - kx_0) \\
w &= \frac{\partial z}{\partial t} = \omega a e^{kz_0} \cos(\omega t - kx_0) \\
a_x &= \frac{\partial^2 x}{\partial t^2} = \omega^2 a e^{kz_0} \cos(\omega t - kx_0) \\
a_z &= \frac{\partial^2 z}{\partial t^2} = -\omega^2 a e^{kz_0} \sin(\omega t - kx_0)
\end{aligned}
\tag{4.2}
$$

For reference, the expression for the partial derivatives of the displacements, velocities and accelerations are also given, viz.

$$
\begin{aligned}
\frac{\partial x}{\partial x_0} &= 1 - kae^{kz_0} \sin(\omega t - kx_0) \\
\frac{\partial x}{\partial z_0} &= -kae^{kz_0} \cos(\omega t - kx_0) \\
\frac{\partial z}{\partial x_0} &= -kae^{kz_0} \cos(\omega t - kx_0) \\
\frac{\partial z}{\partial z_0} &= 1 + kae^{kz_0} \sin(\omega t - kx_0)
\end{aligned}
\tag{4.3}
$$

$$
\begin{aligned}
\frac{\partial u}{\partial x_0} &= -\omega kae^{kz_0} \cos(\omega t - kx_0) \\
\frac{\partial u}{\partial z_0} &= \omega kae^{kz_0} \sin(\omega t - kx_0) \\
\frac{\partial w}{\partial x_0} &= \omega kae^{kz_0} \sin(\omega t - kx_0) \\
\frac{\partial w}{\partial z_0} &= \omega kae^{kz_0} \cos(\omega t - kx_0)
\end{aligned}
\tag{4.4}
$$

$$
\begin{aligned}
\frac{\partial a_x}{\partial x_0} &= \omega^2 kae^{kz_0} \sin(\omega t - kx_0) \\
\frac{\partial a_x}{\partial z_0} &= \omega^2 kae^{kz_0} \cos(\omega t - kx_0) \\
\frac{\partial a_z}{\partial x_0} &= \omega^2 kae^{kz_0} \cos(\omega t - kx_0) \\
\frac{\partial a_z}{\partial z_0} &= -\omega^2 kae^{kz_0} \sin(\omega t - kx_0)
\end{aligned}
\tag{4.5}
$$

The inverse partial derivatives of the spatial variables are, cf. Eq. (4.3) and Eqs. (A.9) - (A.12) in Appendix A,

$$\begin{aligned}
\frac{\partial x_0}{\partial x} &= \frac{1+kae^{kz_0}\sin(\omega t - kx_0)}{1-k^2a^2e^{2kz_0}} \\
\frac{\partial x_0}{\partial z} &= \frac{kae^{kz_0}\cos(\omega t - kx_0)}{1-k^2a^2e^{2kz_0}} \\
\frac{\partial z_0}{\partial x} &= \frac{kae^{kz_0}\cos(\omega t - kx_0)}{1-k^2a^2e^{2kz_0}} \\
\frac{\partial z_0}{\partial z} &= \frac{1-kae^{kz_0}\sin(\omega t - kx_0)}{1-k^2a^2e^{2kz_0}}
\end{aligned} \tag{4.6}$$

Eq. (4.1) describes a closed circular orbit, with radius decaying exponentially with depth. The wave amplitude is a, the wave circular frequency is ω, the wave number is k, and the wave celerity/phase velocity, i.e. the speed of propagation of the wave form in an Eulerian frame of reference, is c. The latter three quantities are defined as

$$\omega = 2\pi f = \frac{2\pi}{T}, \quad k = \frac{2\pi}{\lambda}, \quad c = \frac{\omega}{k} \tag{4.7}$$

where T is the wave period and λ is the wavelength.

Eq. (4.1) is a parametric representation of the motion, which makes construction of a spatial picture of Gerstner waves a bit more troublesome than by ordinary "formulas" of the surface elevation. Figure 4.1 shows a snapshot of one wavelength of a Gerstner wave. The depth included in the figure equals half a wavelength. Figure 4.1 is equivalent to Lamb's figure of the Gerstner wave (Lamb, 1932, Art. 251), and represents the limit steepness $ka = 1$, cf. Eq. (4.8). Steepnesses approaching 1 may be physically unreasonable, but considering the limit case clarifies the geometrical properties of Gerstner waves. The steepness cannot be greater than 1, since lines of constant z_0 would then cross themselves near the free surface. This would be unphysical, since two different material elements would then occupy the same Eulerian region simultaneously.

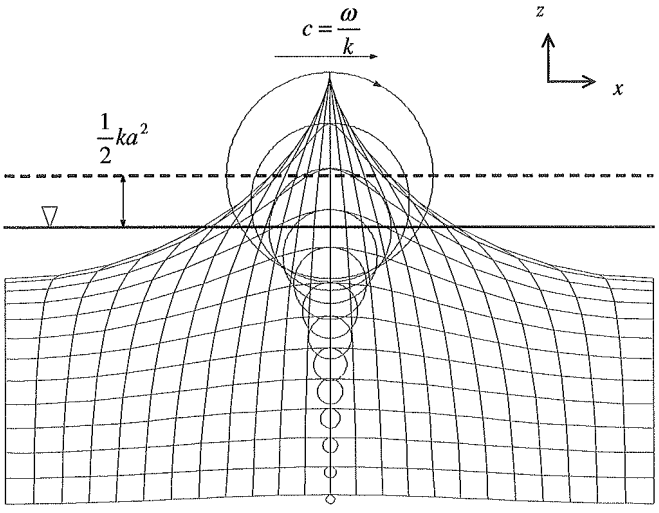

Figure 4.1 Eulerian snapshot of a Gerstner wave with the limit steepness $ka = 1$. ∇ marks the still water line, and the dashed line represents the vertical shift of a surface "particle" given by Eq. (4.13).

The wave crest propagates to the right. The longitudinal lines are lines of constant z_0, and the "standing" lines are lines of constant x_0. The circles show the orbital paths of the Lagrangian point on each of the lines of constant z_0 that are now directly beneath the crest. The direction of the orbital velocity gives the direction of wave propagation, as shown for the uppermost orbit.

The lines of constant z_0 form what is known as trochoids, cf. e.g. Le Méhauté (1976). A trochoid may be explained as the path followed by a point on a circular disk that rolls without slipping along a straight line. For the above Gerstner wave, the disk rolls with its center always on a straight horizontal line through the center of the circular orbit associated with the trochoid under consideration. Since the wavelength in a Gerstner wave is equal at all depths, all trochoids throughout the depth are formed by disks of radius $\lambda/2\pi$. The disk must therefore roll "upside-down", since the cusps are directed upwards, on a straight line that lies $\lambda/2\pi$ above the orbital centre. The distance from the center of the disk to the point followed is $a\ \exp(kz_0)$. When the point followed lies on the circumference of the disk, as for the limit case $ka = 1$ in Figure 4.1, this is the extreme shape of a trochoid; a cycloid.

The Jacobian resulting from Eq. (4.1) is

$$J_{Gerstner} = \frac{\partial(x,z)}{\partial(x_0,z_0)} = \frac{\partial x}{\partial x_0}\frac{\partial z}{\partial z_0} - \frac{\partial x}{\partial z_0}\frac{\partial z}{\partial x_0} = 1 - k^2 a^2 e^{2kz_0} \tag{4.8}$$

Since the Jacobian is constant, the Lagrangian equation of continuity in Section 2.3.1 is satisfied. Since the Jacobian must be greater than zero, the steepness must satisfy the condition $ka < 1$. The theoretical limiting steepness in Gerstner waves is therefore considerably higher than in e.g. 2nd order Stokes waves, which have a limiting steepness $ka < \pi/7$ (≈ 0.45), approximately (cf. e.g. Wiegel, 1964).

However, the Jacobian is not uniform, meaning that infinitesimal Lagrangian elements $dx_0 dz_0$ do not represent Eulerian elements of equal size throughout the depth. This is easily seen by the sub-elements of Figure 4.1. These are bounded by crossing lines of constant x_0 and z_0, respectively, and are all defined by the same values of Δx_0 and Δz_0 (both set to be $\lambda/24$ in Figure 4.1). The non-uniform Jacobian may therefore be explained as a continuous decrease in the "mesh-size" of the Lagrangian frame of reference as the free surface is approached from below, since Eulerian unit vectors are fixed.

The Jacobian alone ensures conservation of mass of infinitesimal elements. However, mass must also be conserved on a larger scale. Following Kochin et al. (1964), one may consider the integral

$$A = \int_0^{\lambda} (z - z_0)\,dx \tag{4.9}$$

Considering a "frozen" wave as in Figure 4.1, this integral represents the (Eulerian) area bounded by the trochoidal surface defined by $z_0 = const.$ and $0 \le x_0 \le \lambda$, and the straight horizontal line defined by $z = z_0$ and $0 \le x \le \lambda$. Note that the interval in x_0 equals the interval in x. If not, the terms T, ω, λ, k and c would not have the physical meaning they are normally assumed to have. From Eq. (4.3) we may write

$$dx = 1 - kae^{kz_0} \sin(\omega t - kx_0)\,dx_0 \tag{4.10}$$

since the integration is performed along a line of constant z_0. The area in Eq. (4.9) may then be found as

$$A = \int_0^\lambda (z - z_0)dx = \int_0^\lambda \left[ae^{kz_0}\sin(\omega t - kx_0)\left(1 - kae^{kz_0}\sin(\omega t - kx_0)\right)\right]dx_0$$
$$= ae^{kz_0}\int_0^\lambda \sin(\omega t - kx_0)dx_0 - ka^2e^{2kz_0}\int_0^\lambda \sin^2(\omega t - kx_0)dx_0$$
$$= -\frac{1}{2}ka^2e^{2kz_0}\lambda \qquad \textbf{(4.11)}$$

If Eq. (4.1) described symmetric waves, e.g. pure sine waves, the area in Eq. (4.11) would be zero. The negative area in Eq. (4.11) means that in there is an asymmetry in the wave profile, yielding an amount of ρA more mass below $z = z_0$ than above, pr. wavelength.

Compared to the still water situation, the mean vertical level of a Lagrangian point is therefore "shifted" upwards by

$$\Delta z_{Gerstner} = \frac{1}{2}ka^2e^{2kz_0} \qquad \textbf{(4.12)}$$

A Lagrangian point therefore moves in a circular orbit about a point that lies a distance $\Delta z_{Gerstner}$ above its still water position. The vertical shift is not uniform, but increases towards the surface in accordance with the decrease in the Jacobian.

For the Lagrangian points constituting the free surface, the vertical shift is

$$\Delta z_{Gerstner,surface} = \frac{1}{2}ka^2 \qquad \textbf{(4.13)}$$

The vertical shift is not directly apparent from Eq. (4.1). Considering Figure 4.1, the Eulerian frame of reference would "normally" be defined by $z = 0$ at the still water level (the solid line). However, the form of Eq. (4.1) requires that $z = 0$ a distance ½ ka^2 above (the dashed line), if the solution is to remain exact. Therefore, z_0 must run from 0 to ($-h - ½\ ka^2$) where h represents the depth in still water. This increase in the interval of z_0 also follows from Eq. (2.23), since the Jacobian is everywhere less than 1. It may seem that the vertical shift could be "absorbed" by the infinite depth, but that is not the case. It is a real effect that has its maximum at the free surface and vanishes towards the bottom, hence the choice of reference level for the Eulerian frame of reference and the associated interval for z_0 in Eq. (4.1). Note that this is just a change in Eulerian reference level, not in the Eulerian unit vectors.

This yields the asymmetric surface profile of Gerstner waves, with long troughs and steep crests, resembling that of higher order Stokes waves and real ocean waves. The top of the crests lie a + ½ ka^2 above the still water level, and the bottom of the troughs lie – a + ½ ka^2 below the still water level.

The still water level may be used as Eulerian zero-level, correct to 2nd order, by writing Eq. (4.1) as

$$\begin{aligned} x &= x_0 - ae^{kz_0}\cos(\omega t - kx_0) \\ z^* &= z_0 + ae^{kz_0}\sin(\omega t - kx_0) + \frac{1}{2}ka^2e^{2kz_0} \end{aligned} \qquad \textbf{(4.14)}$$

The Jacobian now equals 1 to 2nd order, but has a non-constant term at 3rd order, viz.

$$J^* = 1 - k^3 a^3 e^{3kz_0} \sin(\omega t - kx_0) \tag{4.15}$$

In this case, z_0 runs from 0 to – h. Eq. (4.14) may also be found as a perturbation solution of the linearized form of the governing equations. The Eulerian frame of reference is then by assumption defined by $z = 0$ at the still water level, and the 2nd order vertical shift appears as the 2nd order perturbation solution, cf. Pierson (1961, 1962) and Moe et al. (1998).

4.1.2 Pressure and the dispersion relation

Inserting the acceleration from Eq. (4.2) and the partial derivatives from Eq. (4.3) into the inviscid form of Eq. (2.27) yields

$$\begin{aligned}
\frac{1}{\rho}\frac{\partial p}{\partial x_0} &= -\frac{\partial^2 x}{\partial t^2}\frac{\partial x}{\partial x_0} - \left(\frac{\partial^2 z}{\partial t^2} + g\right)\frac{\partial z}{\partial x_0} = -\left(\omega^2 - gk\right)ae^{kz_0}\cos(\omega t - kx_0) \\
\frac{1}{\rho}\frac{\partial p}{\partial z_0} &= -\frac{\partial^2 x}{\partial t^2}\frac{\partial x}{\partial z_0} - \left(\frac{\partial^2 z}{\partial t^2} + g\right)\frac{\partial z}{\partial z_0} = \left(\omega^2 - gk\right)ae^{kz_0}\sin(\omega t - kx_0) - g + \omega^2 ka^2 e^{2kz_0}
\end{aligned} \tag{4.16}$$

The dynamic free surface boundary condition requires that the pressure is constant along the free surface, i.e.

$$\begin{aligned}
&\frac{1}{\rho}\frac{\partial p}{\partial x_0}\bigg|_{z_0=0} = 0 \\
&\Downarrow \\
&\omega^2 = gk
\end{aligned} \tag{4.17}$$

Eq. (4.17) is recognizable as the dispersion relation from Airy wave theory (Airy, 1845). It follows that the pressure is independent of x_0 over the entire depth. The fact that the free surface boundary conditions are exactly satisfied on the true free surface is perhaps the most important property of the Gerstner wave.

The expression for the pressure may now be found by integrating the second line of Eq. (4.16) with respect to z_0, viz.

$$\begin{aligned}
&\frac{1}{\rho}\frac{\partial p}{\partial z_0} = -g + \omega^2 ka^2 e^{2kz_0} \\
&\Downarrow \\
&\frac{p}{\rho} = -gz_0 + \frac{1}{2}\omega^2 a^2 e^{2kz_0} + C_p
\end{aligned} \tag{4.18}$$

where C_p is a constant independent of x_0. Setting the pressure on the surface to zero yields

$$C_p = -\frac{1}{2}\omega^2 a^2 = -\frac{1}{2}gka^2 \tag{4.19}$$

hence

$$\frac{p}{\rho g} = -z_0 - \frac{1}{2}ka^2\left(1 - e^{2kz_0}\right) \tag{4.20}$$

or

$$p = -\rho g z_0 - \frac{1}{2}\rho g k a^2 \left(1 - e^{2kz_0}\right) \tag{4.21}$$

Lines of constant z_0 are therefore also lines of constant pressure, and a given Lagrangian point always experiences the same pressure in a Gerstner wave.

Considering Eqs. (4.14) and (4.15) instead, the pressure is found to leave only one term to second order, viz.

$$p^* = -\rho g z_0 \tag{4.22}$$

with a periodic term at third order.

4.1.3 Vorticity, circulation and rotation

The non-zero vorticity in Gerstner waves may be found according to Eq. (3.4), viz.

$$\begin{aligned}\zeta = \frac{\partial u}{\partial z} - \frac{\partial w}{\partial x} &= \frac{1}{J}\left(-\frac{\partial u}{\partial x_0}\frac{\partial x}{\partial z_0} + \frac{\partial u}{\partial z_0}\frac{\partial x}{\partial x_0} - \frac{\partial w}{\partial x_0}\frac{\partial z}{\partial z_0} + \frac{\partial w}{\partial z_0}\frac{\partial z}{\partial x_0}\right) \\ &= \frac{-2\omega k^2 a^2 e^{2kz_0}}{1 - k^2 a^2 e^{2kz_0}}\end{aligned} \tag{4.23}$$

The vorticity is constant and negative. Interpreting it as a rigid body rotation of a "particle", it means that the direction of the angular velocity is in opposite sense to the orbital velocity in Figure 4.1. From Stokes' theorem, cf. Section 3.2.7, it follows that the circulation in Gerstner waves also is constant and negative.

However, from Eq. (4.1) it can be seen that the velocity along the vertical boundaries in Figure 4.1, considering the entire wave, is zero. Since the Lagrangian points constituting the surface move in closed orbits, there is no net flow along the free surface. Also, the velocity vanishes at the bottom. Therefore, the circulation is not a flow of mass along the boundary of an element. The negative vorticity and circulation in Gerstner waves is merely a result of an elongation of the elements in the troughs, where the horizontal velocity is negative, and a converse shortening in the crests, where the horizontal velocity is positive. The elongation and shortening is associated with the elements becoming "shallower" in the crests and "deeper" in the troughs, respectively, as apparent from the uppermost elements in Figure 4.1. The line integral defining the circulation, cf. Eq. (3.5) and Section 3.2.6, only accounts for variations in the lengths of the boundary elements, variations in the thicknesses are neglected. McClimans (1980) has shown that the elongation and shortening of elements in surface waves explains an increase in the wave generated drift velocity of Spar buoys, which have a significant penetration into the water, as compared to that of surface floats.

We may now consider a small element of a Gerstner wave, and follow it through one wave period. In Figure 4.2, a "band" of elements defined by $0 \le x_0 \le \lambda$ and $z_0 - \Delta z_0 \le z_0 \le z_0 + \Delta z_0$ is shown. Each element in this band may also be considered representing one specific element in different phases of a wave period. The behaviour of the diagonal $D1$, defined in Section 3.4, is an indication of how the element rotates.

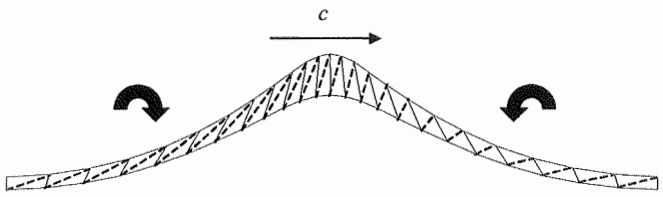

Figure 4.2 A "band" of elements from Figure 4.1 (the third from the free surface). The element boundaries are given in solid lines while the diagonals $D1$ are given in dashed lines.

The wave profile propagates to the right. Therefore, the element farthest to the right represents the element in the first phase, while the element farthest to the left represents the element one wave period (almost) later. The curved arrows indicate the direction of rotation of the diagonal before and after the element has constituted the crest.

Figure 4.2 shows that there is not a constant negative physical rotation of material elements in Gerstner waves. The rotations of the diagonals vary periodically. It can be seen that the angular velocity of the diagonal in the figure is zero in the crest and in the trough, negative (counterclockwise) as the element "moves" from the trough to the crest, and positive (clockwise) as the element "moves" from the crest to the trough. The converse diagonal $D2$ will behave conversely. The elements in Figure 4.2 are not quite "infinitesimal", but the behaviour of the diagonals is qualitatively the same no matter how small the elements are.

Eqs. (3.58) and (3.59) predict the following rotation of the respective diagonals in Gerstner waves

$$\begin{aligned}\omega_{D1} &= \left(\frac{\partial u}{\partial x_0} - \frac{\partial w}{\partial z_0}\right) + \left(\frac{\partial u}{\partial z_0} - \frac{\partial w}{\partial x_0}\right) = -2\omega k a e^{kz_0}\cos(\omega t - kx_0) \\ \omega_{D2} &= -\left[\left(\frac{\partial u}{\partial x_0} - \frac{\partial w}{\partial z_0}\right) + \left(\frac{\partial u}{\partial z_0} - \frac{\partial w}{\partial x_0}\right)\right] = 2\omega k a e^{kz_0}\cos(\omega t - kx_0)\end{aligned} \tag{4.24}$$

The rotation ω_{D1} in Eq. (4.24), which is of first order, is in opposite phase to the vertical velocity of a Lagrangian point, cf. Eq. (4.2). This is in accordance with Figure 4.2. The same agreement is found for the other diagonal.

Defining the physical rotation of an infinitesimal Gerstner element by Eq. (3.60) yields

$$\omega_M = \frac{\partial u}{\partial z_0} - \frac{\partial w}{\partial x_0} = 0 \tag{4.25}$$

The rotation of the *diagonals* should not be considered the physical rotation of the *element*, but they are to some extent observable quantities. The actual rotation of an element appears to be more adequately described by the mean rotation of both diagonals, given by Eqs. (3.60) and (4.25), but this quantity is somewhat harder to observe and confirm visually for elements of finite size. We may therefore say that there is no *physical rotation* of material elements (or "particles") in Gerstner waves, even if there is vorticity, but this is a matter of definition of the term 'rotation', cf. Section 3.4. The common definition of rotation given by Eq. (3.3), i.e. half the vorticity, does not describe the behaviour of elements in Gerstner waves very well.

Moe (2000) also points out the difference between the constant negative vorticity in Gerstner waves and the actual behaviour of fluid elements in Gerstner waves. He calculates the angular velocity of the diagonals and finds, as above, that they "wiggle" back and forth.

4.1.4 Energy

Energy is not considered to any extent in this thesis, and the expressions below, based on Kochin et al. (1964) and Milne-Thomson (1996), are included for completeness only.

The kinetic energy pr. wavelength may be found as, cf. Eqs. (4.2) and (4.8),

$$\begin{aligned} E_k &= \frac{1}{2}mq^2 = \frac{1}{2}\rho\iint_{S_0}\left(u^2+w^2\right)J dx_0 dz_0 = \frac{1}{2}\rho\iint_{S_0}\omega^2 a^2 e^{2kz_0}\left(1-k^2a^2e^{2kz_0}\right)dx_0 dz_0 \\ &= \frac{1}{2}\rho g a^2\iint_{S_0}\left(ke^{2kz_0}-k^3a^2e^{4kz_0}\right)dx_0 dz_0 = \frac{1}{2}\rho g a^2\int_0^{\lambda}\left[\frac{1}{2}e^{2kz_0}-\frac{1}{4}k^2a^2e^{4kz_0}\right]_{-\infty}^{0} dx_0 \\ &= \frac{1}{4}\rho g a^2\left(1-\frac{1}{2}k^2a^2\right)\lambda \end{aligned} \tag{4.26}$$

The potential energy pr. wavelength may be found as, cf. Eqs. (4.1), (4.8) and (4.12),

$$\begin{aligned} E_p &= mg\left[(z-z_0)+\Delta z\right] = \rho g\iint_{S_0}\left[(z-z_0)+\Delta z\right]J dx_0 dz_0 = \rho g\iint_{S_0}\Delta z J dx_0 dz_0 \\ &= \rho g\iint_{S_0}\frac{1}{2}ka^2e^{2kz_0}\left(1-k^2a^2e^{2kz_0}\right)dx_0 dz_0 = \frac{1}{2}\rho g a^2\iint_{S_0}\left[ke^{2kz_0}-k^3a^2e^{4kz_0}\right]dx_0 dz_0 \\ &= \frac{1}{2}\rho g a^2\int_0^{\lambda}\left[\frac{1}{2}e^{2kz_0}-\frac{1}{4}k^2a^2e^{4kz_0}\right]_{-\infty}^{0} dx_0 \\ &= \frac{1}{4}\rho g a^2\left(1-\frac{1}{2}k^2a^2\right)\lambda \end{aligned} \tag{4.27}$$

The contribution from $(z - z_0)$ is periodic and cancel out over a wavelength.

The kinetic and potential energies pr. wavelength are therefore equal also in Gerstner waves, and the total energy pr. wavelength is

$$E = E_k + E_p = \frac{1}{2}\rho g a^2\left(1-\frac{1}{2}k^2a^2\right)\lambda \tag{4.28}$$

There is no net flux of kinetic energy, since the elements move in closed orbits, but the potential energy moves with the wave form, i.e. with the phase velocity. The potential energy is half of the total energy, so the total energy moves with half the phase velocity, i.e. what is known as group velocity c_g. Hence, the mean flux of energy (averaged over a wavelength) is

$$P = \frac{E}{\lambda}c_g = \frac{1}{4}\rho g a^2\left(1-\frac{1}{2}k^2a^2\right)\frac{\omega}{k}, \qquad c_g = \frac{1}{2}c = \frac{1}{2}\frac{\omega}{k} \tag{4.29}$$

4.1.5 Gerstner waves on Eulerian form and mean values in fixed Eulerian points

The Eulerian form of Gerstner's wave theory may be found by Taylor-expansions of the expressions in the preceding sections, and values in fixed Eulerian points in the splash zone may be found by determining when this Eulerian point is in water. The derivations below are based on the work by Moe and Arntsen (1996), and the expressions include terms up to second order in wave amplitude.

First, it is useful to define two variables χ and ξ by

$$\begin{aligned} \chi &= x - x_0 = -ae^{kz_0}\cos(\omega t - kx_0) \\ \xi &= z - z_0 = ae^{kz_0}\sin(\omega t - kx_0) \end{aligned} \tag{4.30}$$

and introduce the following expansions, correct to first order in $k\chi$ and $k\xi$,

$$e^{kz_0} = e^{k(z-\xi)} = e^{kz}(1 - k\xi)$$

$$\begin{aligned} \sin(\omega t - kx_0) &= \sin(\omega t - k[x - \chi]) = \sin(\omega t - kx + k\chi) \\ &= \sin(\omega t - kx)\cos(k\chi) + \cos(\omega t - kx)\sin(k\chi) \\ &= \sin(\omega t - kx)\cdot 1 + \cos(\omega t - kx)\cdot k\chi \\ &= \sin(\omega t - kx) + k\chi\cos(\omega t - kx) \end{aligned}$$

$$\begin{aligned} \cos(\omega t - kx_0) &= \cos(\omega t - k[x - \chi]) = \cos(\omega t - kx + k\chi) \\ &= \cos(\omega t - kx)\cos(k\chi) - \sin(\omega t - kx)\sin(k\chi) \\ &= \cos(\omega t - kx)\cdot 1 - \sin(\omega t - kx)\cdot k\chi \\ &= \cos(\omega t - kx) - k\chi\sin(\omega t - kx) \end{aligned}$$

Eq. (4.30) may now be written as

$$\begin{aligned} \chi &= -ae^{kz}(1 - k\xi)[\cos(\omega t - kx) - k\chi\sin(\omega t - kx)] \\ \xi &= ae^{kz}(1 - k\xi)[\sin(\omega t - kx) + k\chi\cos(\omega t - kx)] \end{aligned} \tag{4.31}$$

and solved by successive approximations. The order of approximation is in the following given by superscripts. To zeroth order we have

$$\begin{aligned} \chi^0 = 0 \quad &\Rightarrow \quad x_0^0 = x \\ \xi^0 = 0 \quad &\Rightarrow \quad z_0^0 = z \end{aligned} \tag{4.32}$$

The 1st order solution is found by inserting the 0th order solution into Eq. (4.31), viz.

$$\begin{aligned} \chi^1 &= -ae^{kz}\cos(\omega t - kx) \quad \Rightarrow \quad x_0^1 = x + ae^{kz}\cos(\omega t - kx) \\ \xi^1 &= \; ae^{kz}\sin(\omega t - kx) \quad \Rightarrow \quad z_0^1 = z - ae^{kz}\sin(\omega t - kx) \end{aligned} \tag{4.33}$$

and the 2nd order solution is found by inserting the 1st order solution into Eq. (4.31), viz.

$$\begin{aligned} \chi^2 &= -ae^{kz}\left(1 - k\xi^1\right)\left[\cos(\omega t - kx) - k\chi^1\sin(\omega t - kx)\right] = -ae^{kz}\cos(\omega t - kx) \\ \xi^2 &= ae^{kz}\left(1 - k\xi^1\right)\left[\sin(\omega t - kx) + k\chi^1\cos(\omega t - kx)\right] = ae^{kz}\sin(\omega t - kx) - ka^2e^{2kz} \end{aligned} \tag{4.34}$$

and therefore

$$\begin{aligned} x_0^2 &= x + ae^{kz}\cos(\omega t - kx) \\ z_0^2 &= z - ae^{kz}\sin(\omega t - kx) + ka^2e^{2kz} \end{aligned} \tag{4.35}$$

However, since a perturbation solution assumes that $J = 1$ and that $z = 0$ at the still water level, the vertical shift in Eqs. (4.12) and (4.14) cannot be ignored. Since the shift itself is of second order, it may be included simply by adding it to the right-hand side of Eq. (4.34). It could also have been included in Eq. (4.30) and downwards, i.e. expanding Eq. (4.14) instead of Eq. (4.1).

The Lagrangian point occupying the Eulerian point (x, z) at time t, correct to second order in wave amplitude, is therefore given by

$$\begin{aligned} x_0 &= x + ae^{kz}\cos(\omega t - kx) \\ z_0 &= z - ae^{kz}\sin(\omega t - kx) + \frac{1}{2}ka^2e^{2kz} \end{aligned} \tag{4.36}$$

where $z = 0$ at the still water level.

The expressions for the velocities and accelerations, cf. Eq. (4.2), may be expanded in the same way as above, inserting χ and ξ from Eq. (4.34), yielding

$$\begin{aligned} u &= \omega a e^{kz}\sin(\omega t - kx) - \omega k a^2 e^{2kz} \\ w &= \omega a e^{kz}\cos(\omega t - kx) \\ a_x &= \omega^2 a e^{kz}\cos(\omega t - kx) \\ a_z &= -\omega^2 a e^{kz}\sin(\omega t - kx) + \omega^2 k a^2 e^{2kz} \\ \zeta &= -2\omega k^2 a^2 e^{2kz} \\ \nabla \cdot \mathbf{V} &= 0 \end{aligned} \tag{4.37}$$

The vertical shift has no significance for the expressions in Eq. (4.37), since it will only contribute at third order. The pressure is found by inserting z_0 from Eq. (4.36) into (4.22), since $z = 0$ at the still water level, yielding

$$p = \rho g\left[-\left(z + \frac{1}{2}ka^2e^{2kz}\right) + ae^{kz}\sin(\omega t - kx)\right] \tag{4.38}$$

The surface profile η may be found by setting $z_0 = 0$ in Eq. (4.1), and inserting x_0 from Eq. (4.36) with $z = \eta$, viz.

$$\begin{aligned}
\eta &= a\sin(\omega t - kx_0) = a\sin\left(\omega t - k\left[x + ae^{k\eta}\cos(\omega t - kx)\right]\right) \\
&= a\sin\left((\omega t - kx) - kae^{k\eta}\cos(\omega t - kx)\right) \\
&= a\left[\sin(\omega t - kx)\cos\left(kae^{k\eta}\cos(\omega t - kx)\right) - \cos(\omega t - kx)\sin\left(kae^{k\eta}\cos(\omega t - kx)\right)\right] \\
&= a\left[\sin(\omega t - kx)\cdot 1 - \cos(\omega t - kx)\cdot kae^{k\eta}\cos(\omega t - kx)\right] \\
&= a\sin(\omega t - kx) - ka^2\cos^2(\omega t - kx)
\end{aligned}$$

Again, the vertical shift must be accounted for if relating the surface elevation to the still water level, yielding

$$\eta = a\sin(\omega t - kx) - ka^2\cos^2(\omega t - kx) + \frac{1}{2}ka^2 \tag{4.39}$$

Inserting Eq. (4.39) into Eq. (4.38) yields to second order

$$\begin{aligned}
\frac{p}{\rho g} &= -\eta + ae^{k\eta}\sin(\omega t - kx) - \frac{1}{2}ka^2e^{2k\eta} \\
&= -a\sin(\omega t - kx) + ka^2\cos^2(\omega t - kx) - \frac{1}{2}ka^2 \\
&\quad + a\left[1 + ka\sin(\omega t - kx)\right]\sin(\omega t - kx) - \frac{1}{2}ka^2 \\
&= -a\sin(\omega t - kx) + ka^2\left[\cos^2(\omega t - kx) + \sin^2(\omega t - kx)\right] + a\sin(\omega t - kx) - ka^2 \\
&= 0
\end{aligned}$$

so that constant (zero) pressure on the free surface is satisfied. Also, inserting Eq. (4.39) into z_0 in Eq. (4.36) shows that $z_0(\eta) = 0$, i.e. that z_0 running from $-h$ to 0 defines z from $-h$ to η. This is as expected, since $z = 0$ at the still water level means that $J = 1$, and therefore that the intervals in Lagrangian coordinates equals the still water intervals in Eulerian coordinates.

Using trigonometric relations, Eq. (4.39) may be rewritten

$$\begin{aligned}
\eta &= a\sin(\omega t - kx) - ka^2\left[\cos^2(\omega t - kx) - \frac{1}{2}\right] \\
&= a\sin(\omega t - kx) - \frac{1}{2}ka^2\left[\cos^2(\omega t - kx) - \sin^2(\omega t - kx)\right] \\
&= a\sin(\omega t - kx) - \frac{1}{2}ka^2\cos[2(\omega t - kx)] \qquad (4.40) \\
&= -a\cos\left(\omega t - kx + \frac{\pi}{2}\right) + \frac{1}{2}ka^2\cos\left[2\left(\omega t - kx + \frac{\pi}{2}\right)\right] \qquad (4.41)
\end{aligned}$$

Eq. (4.41) is equivalent to an expansion of the trochoid given by Kinsman (1965, his equations 5.2:41 and 5.2:42) to second order. Kinsman's expansion is to fourth order, and he concludes that the surface profile of Gerstner waves (the trochoid) to third order is identical to the surface profile of 3rd order Stokes waves on infinite depth, with a divergence at fourth order. This result can be found in Wiegel (1964) also.

The surface profile resulting from Eqs. (4.39) - (4.41) as compared to a pure sine wave is seen in Figure 4.3.

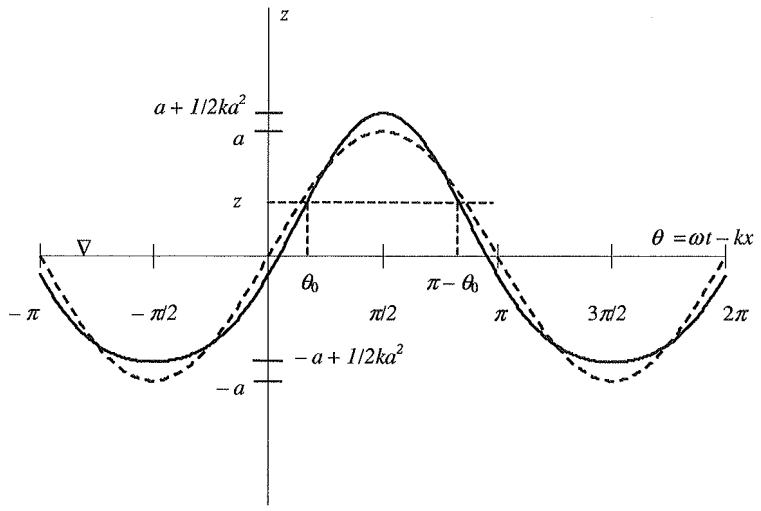

Figure 4.3 Trochoid to 2nd order (solid line) compared to a sine wave (dashed line). The horizontal axis is the still water line (marked by ∇). The figure is based on a similar figure in Moe and Arntsen (1996).

In order to find the correct timeseries and mean values in the splash zone, it is necessary to determine in which phases of a wave period a fixed Eulerian point is submerged in water, cf. Figure 4.3. A fixed Eulerian point is in water if z_0 from Eq. (4.36) is equal to or less than zero, i.e. $z_0 \leq 0$. This yields the following condition from Eq. (4.36), cf. Moe and Arntsen (1996),

$$\sin(\omega t - kx) = \sin\theta_0 \geq \frac{z + \frac{1}{2}ka^2e^{2kz}}{ae^{kz}} = \frac{z + \frac{1}{2}ka^2}{a(1+kz)} \tag{4.42}$$

If this condition is not satisfied, the Eulerian point is out of water. Velocities, accelerations, pressure etc. must then be discarded and excluded from the analysis.

From Eq. (4.37) it follows that the mean horizontal velocity below the splash zone, i.e. in Eulerian points that are always below the wave trough, is

$$\overline{u}_{submerged} = -\omega ka^2e^{2kz} \tag{4.43}$$

Eq. (4.43) is valid irrespective of how the Eulerian frame of reference is defined with respect to the still water level, since this will only make a difference at third order in this case.

The mean Eulerian horizontal velocity in the splash zone, averaged over one wave period keeping x fixed, is now found as, cf. Figure 4.3 and Moe and Arntsen (1996),

$$\begin{aligned}\overline{u} &= \frac{1}{2\pi}\int_{\theta_0}^{\pi-\theta_0}\left[\omega a e^{kz}\sin\theta - \omega k a^2 e^{2kz}\right]d\theta \\ &= \frac{1}{\pi}\int_{\theta_0}^{\pi/2}\left[\omega a e^{kz}\sin\theta - \omega k a^2 e^{2kz}\right]d\theta \\ &= \frac{\omega a}{\pi}e^{kz}\left[-\cos\theta - kae^{kz}\theta\right]_{\theta_0}^{\pi/2} \\ &= \frac{\omega a}{\pi}e^{kz}\left[\cos\theta_0 - kae^{kz}\left(\frac{\pi}{2}-\theta_0\right)\right] \end{aligned} \qquad \textbf{(4.44)}$$

where θ_0 is given by Eq. (4.42). Below the splash zone, θ_0 always equals $-\pi/2$, cf. Figure 4.3, and Eq. (4.44) then yields the same result as Eq. (4.43). The typical form of the mean horizontal velocity is shown in Figure 6.2 and Figure 6.3. These figure strictly speaking pertain to intermediate water and Miche's solution, but the form of the profile is qualitatively the same.

It may be difficult to see how a closed orbital motion produces a mean Eulerian velocity. A simple explanation is as follows: Consider a fixed Eulerian point. This point will be occupied by different fluid "particles" at different instants throughout a wave period. "Particles" that come from below, i.e. that have their orbital centres below the Eulerian point in question, will have a positive horizontal velocity in this point, while "particles" that come from above will have a negative horizontal velocity. "Particles" with orbital centres at the same vertical level as the Eulerian point in question will only have a vertical velocity component here. Since the orbital velocities decay exponentially with the depth of the orbital centres, the negative contributions from above outweigh the positive contributions from below, resulting in a mean negative Eulerian velocity in a fixed Eulerian point below the splash zone. In the splash zone, i.e. $-a + \frac{1}{2}ka^2 < z < a + \frac{1}{2}ka^2$, there will not always be water, since no "particle" has its orbital centre above $z = \frac{1}{2}ka^2$. The contributions from above will become fewer as we move upwards in the splash zone, and vanish entirely at $z = \frac{1}{2}ka^2$. All contributions from below has prevailed to this level, but these also become fewer as we move further up, and of course no contributions are found above $z = a + \frac{1}{2}ka^2$. The greatest negative mean horizontal velocity is therefore found at $z < -a + \frac{1}{2}ka^2$, i.e. at the level of the trough, and the greatest positive value is found at $z = \frac{1}{2}ka^2$, i.e. at the level of the orbital centre of the surface "particles".

It is also interesting to note that there is a mean vertical acceleration below the splash zone, directed upwards, viz.

$$\overline{a}_{z,submerged} = \omega^2 k a^2 e^{2kz} \qquad \textbf{(4.45)}$$

In the splash zone, its mean value is

$$\overline{a}_z = \frac{\omega^2 a}{\pi}e^{kz}\left[-\cos\theta_0 + kae^{kz}\left(\frac{\pi}{2}-\theta_0\right)\right] \qquad \textbf{(4.46)}$$

The mean values of the vertical velocity and horizontal accelerations are zero below the splash zone. In the splash zone, however, these will also produce mean values, viz.

$$\overline{u}_{submerged} = \overline{w}_{submerged} = 0$$

$$\overline{w} = \frac{\omega a}{\pi} e^{kz}\left[1 - \sin\theta_0\right] \qquad (4.47)$$

$$\overline{a}_x = \frac{\omega^2 a}{\pi} e^{kz}\left[1 - \sin\theta_0\right]$$

For the pressure, the mean values below and in the splash zone, respectively, are

$$\overline{p}_{submerged} = -\rho g\left(z + \frac{1}{2}ka^2 e^{2kz}\right)$$

$$\overline{p} = \frac{\rho g}{\pi}\left[ae^{kz}\cos\theta_0 - \left(z + \frac{1}{2}ka^2 e^{2kz}\right)\left(\frac{\pi}{2} - \theta_0\right)\right] \qquad (4.48)$$

where the pressure is based on Eq. (4.38).

Note that all results in this section are based on $z = 0$ at the still water level. The free surface is always defined by $z_0 = 0$, irrespective of how the reference level of the Eulerian frame of reference is defined.

4.1.6 Mean Eulerian horizontal velocity in narrow-banded Gerstner waves

It is also of interest to determine mean Eulerian values in irregular Gerstner waves. Following Moe and Arntsen (1996), it is assumed that the involved processes are ergodic and narrow-banded and that the velocities and surface elevation are Gaussian with Rayleigh distributed peaks. The latter assumptions are in conflict with the asymmetry and vertical shift associated with Gerstner waves. However, the vertical shift is of second order and appears as a nonlinear contribution in a perturbation approach, cf. Pierson (1961) and Moe et al. (1998). Including it is therefore anyhow in conflict with straightforward superposition of components.

The mean (time averaged) value of a quantity in an ergodic stochastic process may be expressed by its expectation. For the horizontal velocity, which is a function of the wave amplitude, the expectation may be written

$$\overline{u}(z) = E[u(z)] = \int_0^\infty p_a(a)E[u|a]da \qquad (4.49)$$

$$p_a = \frac{a}{\sigma_\eta^2} e^{-\frac{a^2}{2\sigma_\eta^2}}, \quad a \geq 0 \qquad (4.50)$$

where p_a is the Rayleigh distribution, σ_η is the standard deviation and σ_η^2 is the variance of the surface elevation. Since in a narrow-banded sea the waves occur sequentially rather than simultaneously, E[u|a] may be given by Eqs. (4.42) and (4.44). Also, since the surface elevation is assumed to be a Gaussian process with expectation E[η] = 0, the variance equals the 0th spectral moment of the surface elevation, i.e.

$$\sigma_\eta^2 = m_0 = \int_0^\infty S(\omega)d\omega, \quad m_i = \int_0^\infty \omega^i S(\omega)d\omega \qquad (4.51)$$

The horizontal velocity is also a function of a representative circular frequency. Moe and Arntsen (1996) apply the mean zero crossing frequency of the surface elevation as the representative frequency in the expectation of the horizontal velocity. The mean zero crossing frequency of the surface elevation is defined by

$$\omega_{20} = \sqrt{\frac{m_2}{m_0}} \tag{4.52}$$

The wave number to apply must be that associated with this frequency through the dispersion relation in Eq. (4.17). Inserting into Eq. (4.49) yields for infinite depth

$$\begin{aligned}\overline{u}(z) &= E[u] = \int_0^\infty p_a(a) E[u|a]\,da \\ &= \int_0^\infty \frac{\omega_{20} a^2}{\pi\sigma_\eta^2} e^{k_{20}z - \frac{a^2}{2\sigma_\eta^2}} \left[\cos\left(\sin^{-1}\theta_0\right) - k_{20} a e^{k_{20}z}\left(\frac{\pi}{2} - \sin^{-1}\theta_0\right)\right] da\end{aligned} \tag{4.53}$$

where θ_0 is given by Eq. (4.42) since $z = 0$ at the still water level. The 2nd order vertical shift is included in the expression for θ_0. This is not strictly consistent in the irregular case, but it is included since the analysis is done on a wave by wave basis. The dependency on z in Eq. (4.42) is kept on exponential form, in order to avoid the denominator ever being zero. Eq. (4.53) must be solved numerically for each value of z. Although Eq. (4.53) is derived for the splash zone, it is applicable throughout the entire depth by ensuring that θ_0 always equal $-\pi/2$ below the splash zone, cf. Eq. (4.44) and related comments. In MATLAB, this may be handled by considering the real part of $\sin^{-1}(\theta_0)$. Since the wave amplitudes are Rayleigh distributed, we also have that

$$\sigma_\eta = H_{m0}/4 \tag{4.54}$$

where H_{m0} is the significant wave height in a Gaussian sea.

A simple expression for the mean horizontal velocity *below the splash zone* may now be found by inserting Eq. (4.43) instead of Eq. (4.44) into Eq. (4.49), and integrate analytically by integration by parts. Making use of Eqs. (4.17) and (4.54) also, this yields

$$\overline{u}(z)_{submerged} = -2\omega_{20} k_{20} e^{2k_{20}z}\sigma_\eta^2 = -\frac{\omega_{20}^3 H_{m0}^2}{8g} e^{\frac{2\omega_{20}^2}{g}z} \tag{4.55}$$

Further, ω_{20} may be given approximately e.g. by the peak frequency in Pierson-Moskowitz (P-M) type spectra and JONSWAP spectra, cf. e.g. Faltinsen (1990, pp. 23-31), viz.

$$\begin{aligned}\omega_{20} &\approx 1.4\omega_p \quad Pierson-Moskowitz \\ \omega_{20} &\approx 1.3\omega_p \quad JONSWAP\end{aligned} \tag{4.56}$$

A coarse estimate of the mean horizontal velocity below the splash zone in narrow-banded irregular Gerstner waves, assuming Pierson-Moskowitz type spectra and JONSWAP spectra, respectively, is then

$$\overline{u}(z)_{submerged} \approx \begin{cases} -9\dfrac{H_{m0}^2}{T_p^3} e^{\frac{16}{T_p^2}z} \ [m/s], & Pierson-Moskowitz \\ -7\dfrac{H_{m0}^2}{T_p^3} e^{\frac{14}{T_p^2}z} \ [m/s], & JONSWAP \end{cases} \tag{4.57}$$

It is not obvious that the chosen representative frequency is the most appropriate, and it must be kept in mind that the components attenuate differently with depth. The spectral mean- and peak frequencies, with corresponding wave numbers, may turn out to be equally good choices in some cases, and may be inserted into Eqs. (4.53) and (4.55) instead of ω_{20} and k_{20}. For points always submerged, assuming that we have a ratio C_ω between the representative frequency and the peak frequency, a more general form of Eq. (4.57) is

$$\overline{u}(z)_{submerged} \approx -C_\omega^3 \frac{\pi^3 H_{m0}^2}{gT_p^3} e^{C_\omega^2 \frac{8\pi^2}{gT_p^2} z} \quad [m/s] \ , \ C_\omega = \frac{\omega_{representative}}{\omega_p} \ , \ z < -\frac{3}{4} H_{m0} \qquad \textbf{(4.58)}$$

The region of validity given at the end of Eq. (4.58) is based on Figure 6.35 and is only approximate. Considering profiles of $\overline{u}(z)$ over the entire depth as in Figure 6.35, and making use of the knowledge of the solution below the splash zone given by Eq. (4.58), it should be possible to construct simple approximate "formulas" for the splash zone also. Mean values for other quantities than the horizontal velocity may be determined in the same manner as above.

4.2 Miche's Solution

There are several works on waves on finite depth based on Lagrangian frames of reference. Miche's solution for uniform depth is presented here, but Miche also considered the effect of a gradually shoaling bottom. Biesel (1952) extended Miche's results for shoaling bottoms, and according to Neumann and Pierson (1966) this was probably the most realistic solution for waves normal to a sloping beach. Carrier and Greenspan (1958) have also treated waves on a sloping beach from a Lagrangian point of view. Dubreil-Jacotin (1934) worked on Gerstner waves and similar waves on finite depth, cf. Wehausen and Laitone (1960). She has also shown that a wave motion may be superposed upon a steady current having an arbitrary velocity distribution, and that mass transport may then take any desired value (Longuet-Higgins, 1953). However, in light of Section 4.3 at the end of this chapter, the latter statements may be questionable.

4.2.1 Miche's 2nd order solution for finite and uniform depth

Miche (1944) derived a 2nd order solution for finite and uniform depth by perturbation. The perturbation procedure is also described in Moe et al. (1998). A phase-shift of $-\pi/2$ is introduced as compared to Miche's original publication, in order to have the expression on the same form as Gerstner's theory in Section 4.1.

In the limit of infinite depth, Miche's solution is equivalent to Gerstner's. However, Miche added a 2nd order Stokes-like drift in order to make the solution irrotational. The effect of adding such a drift is considered in Section 4.3 (for the case of infinite depth only).

Miche's solution is

$$\begin{aligned} x &= x_0 - a\frac{\cosh k(z_0+h)}{\sinh kh}\cos(\omega t - kx_0) + ka^2 \frac{\sin 2(\omega t - kx_0)}{4\sinh^2 kh}\left[1 - \frac{3}{2}\frac{\cosh 2k(z_0+h)}{\sinh^2 kh}\right] \\ &\quad + a^2 U(z_0)\cdot t \\ z &= z_0 + a\frac{\sinh k(z_0+h)}{\sinh kh}\sin(\omega t - kx_0) + ka^2 \frac{\sinh 2k(z_0+h)}{4\sinh^2 kh}\left[1 - \frac{3}{2}\frac{\cos 2(\omega t - kx_0)}{\sinh^2 kh}\right] \end{aligned} \qquad \textbf{(4.59)}$$

Eq. (4.59) satisfies $J = 1$ to second order. The Eulerian frame of reference is here defined by $z = 0$ at the still water level, and z_0 runs from 0 to $-h$. This follows from the perturbation approach, as for Eqs. (4.14) and (4.15).

The "particle"-orbits in Miche's solution are ellipses to 1st order. An example of the orbital path described by Eq. (4.59) is shown in Figure 4.4, where it is assumed that $U(z_0) = 0$ and therefore the equation describes a closed orbit over a wave period.

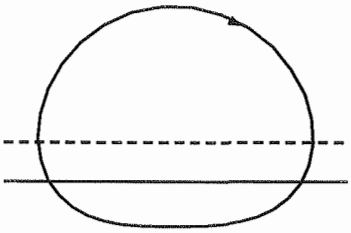

Figure 4.4 Orbital path of a surface "particle" in a 2nd order Miche wave with $ka \approx 0.6$, $h/\lambda \approx 0.2$. The solid horizontal line represents the still water line, and the dashed horizontal line shows the vertical shift for a surface "particle", i.e. its mean vertical position, cf. Eq. (4.61).

The steepness is chosen quite high in Figure 4.4, and the depth to wavelength ratio relatively small, in order to visualize the effects of the periodic 2nd order terms. They can be seen to make the "particle"-orbits more circular above the mean vertical position, and more flattened below the mean vertical position. Thus, their effect is to sharpen the crests and flatten the troughs, cf. Moe et al. (1998).

A 2nd order constant vertical shift is directly apparent from Eq. (4.59), viz.

$$\Delta z_{Miche} = ka^2 \frac{\sinh 2k(z_0+h)}{4\sinh^2 kh} = \frac{1}{2}ka^2 \frac{\cosh k(z_0+h)\sinh k(z_0+h)}{\sinh^2 kh} \tag{4.60}$$

which in the limit of infinite depth equals Eq. (4.12). The points constituting the free surface get the following shift in mean vertical position

$$\Delta z_{Miche,surface} = \frac{1}{2}ka^2 \frac{\cosh kh}{\sinh kh} \tag{4.61}$$

If in Eq. (4.59) $U(z_0) = 0$, the solution has a constant 2nd order negative vorticity, viz.

$$\zeta = -2\omega k^2 a^2 \frac{\cosh k(z_0+h)\sinh k(z_0+h)}{\sinh^2 kh} \tag{4.62}$$

The solution is (initially) irrotational if $U(z_0)$ equals

$$U(z_0) = \omega k \frac{1}{2\sinh^2 kh}\left[\cosh 2k(z_0+h) - \frac{\sinh 2kh}{2kh}\right] \tag{4.63}$$

However, re-inserting Eq. (4.59) with the 2nd order current as given by Eq. (4.63) into the governing equations, yields a 3rd order term growing in time in the Jacobian as well as in the vorticity. In Section 4.3, it is shown that this term is of second order in magnitude after less than one wave period.

The velocities and accelerations in Miche's solution are

$$\begin{aligned}
u &= \omega a \frac{\cosh k(z_0+h)}{\sinh kh}\sin(\omega t - kx_0) + \omega k a^2 \frac{\cos 2(\omega t - kx_0)}{2\sinh^2 kh}\left[1 - \frac{3}{2}\frac{\cosh 2k(z_0+h)}{\sinh^2 kh}\right] \\
&\quad + a^2 U(z_0) \\
w &= \omega a \frac{\sinh k(z_0+h)}{\sinh kh}\cos(\omega t - kx_0) + \omega k a^2 \frac{3}{4}\frac{\sinh 2k(z_0+h)\sin 2(\omega t - kx_0)}{\sinh^4 kh} \\
a_x &= \omega^2 a \frac{\cosh k(z_0+h)}{\sinh kh}\cos(\omega t - kx_0) - \omega^2 k a^2 \frac{\sin 2(\omega t - kx_0)}{\sinh^2 kh}\left[1 - \frac{3}{2}\frac{\cosh 2k(z_0+h)}{\sinh^2 kh}\right] \\
a_z &= -\omega^2 a \frac{\sinh k(z_0+h)}{\sinh kh}\sin(\omega t - kx_0) + \omega^2 k a^2 \frac{3}{2}\frac{\sinh 2k(z_0+h)\cos 2(\omega t - kx_0)}{\sinh^4 kh}
\end{aligned} \tag{4.64}$$

and the pressure is

$$\begin{aligned}
\frac{p}{\rho g} &= -z_0 - a\frac{\sinh kz_0}{\sinh kh \cosh kh}\sin(\omega t - kx_0) \\
&\quad + ka^2 \frac{\sinh kz_0}{4\sinh^2 kh}\left\{3\cos 2(\omega t - kx_0)\left[\frac{\cosh kz_0}{\sinh^2 kh} - \frac{2\cosh k(z_0+h)}{\cosh kh}\right] - \frac{2\cosh k(z_0+h)}{\cosh kh}\right\}
\end{aligned} \tag{4.65}$$

The pressure can be seen to equal that of Eq. (4.22), and not that of Eq. (4.21), in the case of infinite depth, since the perturbation is based on $z = 0$ at the still water level.

The dispersion relation is the same to second as well as to first order, equivalent to that of 2nd order Stokes waves, viz.

$$\omega^2 = kg\tanh kh \tag{4.66}$$

It will often be sufficient to consider only the 1st order terms combined with the constant 2nd order vertical shift of Miche's solution. The first order terms yields the following Jacobian

$$J_{Miche,\ 1st} = 1 - \frac{k^2 a^2\left[\cosh^2 k(z_0+h) - \cos^2(\omega t - kx_0)\right]}{\sinh^2 kh} \tag{4.67}$$

Including only the constant vertical shift of the 2nd order terms yields

$$J_{Miche,\ 1st+\Delta z} = 1 - \frac{k^2 a^2\left[\frac{1}{2} - \cos^2(\omega t - kx_0)\right]}{\sinh^2 kh} = 1 + \frac{1}{2}\frac{k^2 a^2}{\sinh^2 kh}\cos 2(\omega t - kx_0) \tag{4.68}$$

The vorticities in these two cases have comparable 2nd order periodic terms. The last term on the right-hand side of Eq. (4.68) is of third order or less if

$$\frac{k^2a^2}{2\sinh^2 kh} \le k^3a^3 \quad \Rightarrow \quad \frac{1}{\sinh kh} \le \sqrt{2ka} \tag{4.69}$$

For a steepness of e.g. $ka = 0.01$, Eq. (4.69) yields $h/\lambda > 0.42$, for $ka = 0.1$ it yields $h/\lambda > 0.25$, for $ka = 0.2$ it yields $h/\lambda > 0.20$, and for $ka = 0.5$ it yields $h/\lambda > 0.14$. Miche's 1st order solution, combined with the constant 2nd order vertical shift, is therefore a reasonable approximation also to second order in the deeper range of intermediate water, since the vertical shift is then the only 2nd order term that prevails. The applicability of this simplified approach is seen to increase with increasing steepness, and is only of practical interest if $ka \ge O(0.01)$.

4.2.2 Miche's solution on Eulerian form and mean values in fixed Eulerian points

By the same procedure as in Section 4.1.5, one may find the Eulerian form of Miche's solution to second order, with $z = 0$ at the still water level, viz.

$$x_0 = x + a\frac{\cosh k(z+h)}{\sinh kh}\cos(\omega t - kx) + ka^2\frac{\sin 2(\omega t - kx)}{4\sinh^2 kh}\left[1 + \frac{3}{2}\frac{\cosh 2k(z+h)}{\sinh^2 kh}\right]$$

$$z_0 = z - a\frac{\sinh k(z+h)}{\sinh kh}\sin(\omega t - kx) + ka^2\frac{\sinh 2k(z+h)}{4\sinh^2 kh}\left[1 + \frac{3}{2}\frac{\cos 2(\omega t - kx)}{\sinh^2 kh}\right]$$

$$u = \omega a\frac{\cosh k(z+h)}{\sinh kh}\sin(\omega t - kx) - \omega ka^2\frac{\cosh 2k(z+h)}{2\sinh^2 kh}\left[1 + \frac{3}{2}\frac{\cos 2(\omega t - kx)}{\sinh^2 kh}\right]$$

$$w = \omega a\frac{\sinh k(z+h)}{\sinh kh}\cos(\omega t - kx) + \omega ka^2\frac{3}{4}\frac{\sinh 2k(z+h)\sin 2(\omega t - kx)}{\sinh^4 kh}$$

$$a_x = \omega^2 a\frac{\cosh k(z+h)}{\sinh kh}\cos(\omega t - kx) - \omega^2 ka^2\frac{\sin 2(\omega t - kx)}{2\sinh^2 kh}\left[1 - \frac{3\cosh 2k(z+h)}{\sinh^2 kh}\right] \tag{4.70}$$

$$a_z = -\omega^2 a\frac{\sinh k(z+h)}{\sinh kh}\sin(\omega t - kx) + \omega^2 ka^2\frac{\sinh 2k(z+h)}{2\sinh^2 kh}\left[1 + \frac{3}{2}\frac{\cos 2(\omega t - kx)}{\sinh^2 kh}\right]$$

$$\begin{aligned}\frac{p}{\rho g} = -z + a\left[-\frac{\sinh kz}{\sinh kh\cosh kh} + \frac{\sinh k(z+h)}{\sinh kh}\right]\sin(\omega t - kx) \\ + \frac{ka^2}{\sinh^2 kh}\left\{-\frac{1}{2}\sinh k(z+h)\cosh k(z+h) - \frac{\sinh kz\cosh k(z+h)}{2\cosh kh}\right. \\ \left. + \frac{3}{4}\left[-\frac{\sinh 2k(z+h)}{2\sinh^2 kh} + \frac{\sinh kz\cosh kz}{\sinh^2 kh} - \frac{2\sinh kz\cosh k(z+h)}{\cosh kh}\right]\cos 2(\omega t - kx)\right\}\end{aligned}$$

$$\eta = a\sin(\omega t - kx) - ka^2\frac{\cosh kh}{\sinh kh}\left[\cos^2(\omega t - kx) + \frac{1}{2} - \frac{3}{2}\frac{1}{\sinh^2 kh}\cos 2(\omega t - kx)\right]$$

In the limit of infinite depth, the above expressions equal those of Gerstner' theory in Section 4.1.5. It is easily verified that the Eulerian velocities satisfy continuity and give the expected vorticity to second order, viz.

$$\nabla \cdot \mathbf{V} = 0$$

$$\zeta = -2\omega k^2 a^2 \frac{\cosh k(z+h)\sinh k(z+h)}{\sinh^2 kh}$$

The mean values to second order in fixed Eulerian points that are always submerged are

$$\begin{aligned}
\overline{u}_{submerged} &= -\omega k a^2 \frac{\cosh 2k(z+h)}{2\sinh^2 kh} \\
\overline{w}_{submerged} &= 0 \\
\overline{a}_{x,submerged} &= 0 \\
\overline{a}_{z,submerged} &= \omega^2 k a^2 \frac{\sinh 2k(z+h)}{2\sinh^2 kh} \\
\frac{\overline{p}_{submerged}}{\rho g} &= -z + \frac{ka^2}{\sinh^2 kh}\left[-\frac{1}{2}\sinh k(z+h)\cosh k(z+h) - \frac{\sinh kz \cosh k(z+h)}{2\cosh kh}\right]
\end{aligned} \tag{4.71}$$

The condition on the phase for points to be submerged in the splash zone, cf. Eq. (4.42), is found for the 2nd order case by requiring $z_0 \leq 0$ in Eq. (4.70), yielding

$$z - a\frac{\sinh k(z+h)}{\sinh kh}\sin(\omega t - kx) + ka^2 \frac{\sinh 2k(z+h)}{4\sinh^2 kh}\left[1 + \frac{3}{2}\frac{\cos 2(\omega t - kx)}{\sinh^2 kh}\right] = 0$$

$$\Downarrow$$

$$z - a\frac{\sinh k(z+h)}{\sinh kh}\sin(\omega t - kx) + ka^2 \frac{\sinh 2k(z+h)}{4\sinh^2 kh} + \frac{3}{8}\frac{ka^2 \sinh 2k(z+h)}{\sinh^4 kh}\cos 2(\omega t - kx) = 0$$

$$\Downarrow$$

$$z - a\frac{\sinh k(z+h)}{\sinh kh}\sin(\omega t - kx) + ka^2 \frac{\sinh 2k(z+h)}{4\sinh^2 kh} + \frac{3}{8}\frac{ka^2 \sinh 2k(z+h)}{\sinh^4 kh}\left[1 - 2\sin^2(\omega t - kx)\right] = 0$$

$$\Downarrow$$

$$\frac{3}{4}\frac{ka^2 \sinh 2k(z+h)}{\sinh^4 kh}\sin^2(\omega t - kx) + a\frac{\sinh k(z+h)}{\sinh kh}\sin(\omega t - kx) - \left[z + ka^2 \frac{\sinh 2k(z+h)}{4\sinh^2 kh} + \frac{3}{8}\frac{ka^2 \sinh 2k(z+h)}{\sinh^4 kh}\right] = 0$$

$$\Downarrow$$

$$\sin\theta_0 = \frac{-B+\sqrt{B^2-4AC}}{2A} \tag{4.72}$$

where

$$\begin{aligned} A &= \frac{3}{4}\frac{ka^2\sinh 2k(z+h)}{\sinh^4 kh} \\ B &= a\frac{\sinh k(z+h)}{\sinh kh} \\ C &= -\left[z + ka^2\frac{\sinh 2k(z+h)}{4\sinh^2 kh} + \frac{3}{8}\frac{ka^2\sinh 2k(z+h)}{\sinh^4 kh}\right] \end{aligned} \tag{4.73}$$

In Eq. (4.72), the plus sign in front of the square root turns out to be the appropriate. A minus sign will always return $\theta_0 = -\pi/2$, also for points in the splash zone.

The mean values in the splash zone are found in the same way as in Section 4.1.5, yielding to second order

$$\overline{u} = \frac{\omega a}{\pi}\frac{\cosh k(z+h)}{\sinh kh}\cos\theta_0 - \frac{\omega ka^2}{\pi}\frac{\cosh 2k(z+h)}{2\sinh^2 kh}\left[\left(\frac{\pi}{2}-\theta_0\right) - \frac{3}{4\sinh^2 kh}\sin 2\theta_0\right]$$

$$\overline{w} = \frac{\omega a}{\pi}\frac{\sinh k(z+h)}{\sinh kh}[1-\sin\theta_0] + \frac{\omega ka^2}{\pi}\frac{3\sinh 2k(z+h)}{8\sinh^4 kh}[1+\cos 2\theta_0]$$

$$\overline{a}_x = \frac{\omega^2 a}{\pi}\frac{\cosh k(z+h)}{\sinh kh}[1-\sin\theta_0] - \frac{\omega^2 ka^2}{\pi}\frac{[1+\cos 2\theta_0]}{4\sinh^2 kh}\left[1 - \frac{3\cosh 2k(z+h)}{\sinh^2 kh}\right]$$

$$\overline{a}_z = -\frac{\omega^2 a}{\pi}\frac{\sinh k(z+h)}{\sinh kh}\cos\theta_0 + \frac{\omega^2 ka^2}{\pi}\frac{\sinh 2k(z+h)}{2\sinh^2 kh}\left[\left(\frac{\pi}{2}-\theta_0\right) - \frac{3}{4\sinh^2 kh}\sin 2\theta_0\right] \tag{4.74}$$

$$\begin{aligned} \frac{\overline{p}}{\rho g} = \frac{a}{\pi}&\left[-\frac{\sinh kz}{\sinh kh\cosh kh} + \frac{\sinh k(z+h)}{\sinh kh}\right]\cos\theta_0 \\ &-\frac{1}{\pi}\left[z + \frac{ka^2}{2\sinh^2 kh}\sinh k(z+h)\cosh k(z+h) + \frac{\sinh kz\cosh k(z+h)}{2\cosh kh}\right]\left(\frac{\pi}{2}-\theta_0\right) \\ &-\frac{1}{\pi}\frac{3ka^2}{8\sinh^2 kh}\left[-\frac{\sinh 2k(z+h)}{2\sinh^2 kh} + \frac{\sinh kz\cosh kz}{\sinh^2 kh} - \frac{2\sinh kz\cosh k(z+h)}{\cosh kh}\right]\sin 2\theta_0 \end{aligned}$$

The expressions for the simplified form suggested at the end of Section 4.2.1 are

$$
\begin{aligned}
x_0 &= x + a\frac{\cosh k(z+h)}{\sinh kh}\cos(\omega t - kx) \\
z_0 &= z - a\frac{\sinh k(z+h)}{\sinh kh}\sin(\omega t - kx) + ka^2\frac{\sinh k(z+h)\cosh k(z+h)}{2\sinh^2 kh} \\
u &= \omega a\frac{\cosh k(z+h)}{\sinh kh}\sin(\omega t - kx) - \omega ka^2\frac{\cosh 2k(z+h)}{2\sinh^2 kh} \\
w &= \omega a\frac{\sinh k(z+h)}{\sinh kh}\cos(\omega t - kx) \\
a_x &= \omega^2 a\frac{\cosh k(z+h)}{\sinh kh}\cos(\omega t - kx) \\
a_z &= -\omega^2 a\frac{\sinh k(z+h)}{\sinh kh}\sin(\omega t - kx) + \omega^2 ka^2\frac{\sinh 2k(z+h)}{2\sinh^2 kh} \\
\frac{p}{\rho g} &= -z + a\frac{\sinh k(z+h)}{\sinh kh}\sin(\omega t - kx) - \frac{1}{2}ka^2\frac{\sinh k(z+h)\cosh k(z+h)}{\sinh^2 kh} \\
\eta &= a\sin(\omega t - kx) - ka^2\frac{\cosh kh}{\sinh kh}\left[\cos^2(\omega t - kx) + \frac{1}{2}\right]
\end{aligned}
\tag{4.75}
$$

The resemblance to the Eulerian form of Gerstner waves is obvious from Eq. (4.75).

The mean values for point always submerged are the same as given by Eq. (4.71), except for the mean pressure that now becomes

$$
\frac{\overline{p}_{submerged}}{\rho g} = -z - \frac{1}{2}ka^2\frac{\sinh k(z+h)\cosh k(z+h)}{\sinh^2 kh} \tag{4.76}
$$

The "splash zone condition" θ_0 is now found by requiring $z_0 \le 0$ in Eq. (4.75), yielding

$$
\sin\theta_0 = \frac{z\sinh kh + \frac{1}{2}ka^2\sinh k(z+h)\frac{\cosh k(z+h)}{\sinh kh}}{a\sinh k(z+h)} \tag{4.77}
$$

which in the limit of infinite depth equals Eq. (4.42).

The mean values in the splash zone according to the simplified form are found to be

$$\overline{u} = \frac{\omega a}{\pi}\frac{\cosh k(z+h)}{\sinh kh}\cos\theta_0 - \frac{\omega k a^2}{\pi}\frac{\cosh 2k(z+h)}{2\sinh^2 kh}\left(\frac{\pi}{2}-\theta_0\right)$$

$$\overline{w} = \frac{\omega a}{\pi}\frac{\sinh k(z+h)}{\sinh kh}[1-\sin\theta_0]$$

$$\overline{a}_x = \frac{\omega^2 a}{\pi}\frac{\cosh k(z+h)}{\sinh kh}[1-\sin\theta_0] \tag{4.78}$$

$$\overline{a}_z = -\frac{\omega^2 a}{\pi}\frac{\sinh k(z+h)}{\sinh kh}\cos\theta_0 + \frac{\omega^2 k a^2}{\pi}\frac{\sinh 2k(z+h)}{2\sinh^2 kh}\left(\frac{\pi}{2}-\theta_0\right)$$

$$\frac{\overline{p}}{\rho g} = \frac{a}{\pi}\frac{\sinh k(z+h)}{\sinh kh}\cos\theta_0 - \frac{1}{\pi}\left[z+\frac{1}{2}ka^2\frac{\sinh k(z+h)\cosh k(z+h)}{\sinh^2 kh}\right]\left(\frac{\pi}{2}-\theta_0\right)$$

The typical form of the mean Eulerian horizontal velocity is similar to that of Gerstner waves, and is shown in Figure 6.2 and Figure 6.3.

Note that the simplified form of Miche's 2nd order solution referred to in this section is based on a Taylor-expansion of the "full" 2nd order Lagrangian expressions in Eqs. (4.59), (4.64) and (4.65). Taylor-expansion of the 1st order terms only, plus the vertical shift, will yield 2nd order terms that are different from those in the simplified Eulerian form presented above. This means that one must distinguish between a simplified Lagrangian form and a simplified Eulerian form. Recall also that all expressions in this section are based on $z = 0$ at the still water level.

4.2.3 Mean Eulerian horizontal velocity in narrow-banded Miche waves

Expressions equivalent to those in Section 4.1.6 may also be found for Miche waves. As for Gerstner waves, 2nd order terms are included in the narrow band analysis. This yields

$$\overline{u}(z) = \int_0^\infty \frac{\omega_{20}a^2}{\pi\sigma_\eta^2} e^{-\frac{a^2}{2\sigma_\eta^2}} \left\{ \frac{\cosh k_{20}(z+h)}{\sinh k_{20}h}\cos\theta_0 - k_{20}a\frac{\cosh 2k_{20}(z+h)}{2\sinh^2 k_{20}h}\left[\left(\frac{\pi}{2}-\theta_0\right) - \frac{3}{4\sinh^2 k_{20}h}\sin 2\theta_0\right]\right\} da \tag{4.79}$$

where θ_0 is given by Eqs. (4.72) and (4.73). The relation between ω_{20} and k_{20} is now given by the dispersion relation for finite depth, i.e. Eq. (4.66).

For the simplified form, where θ_0 is given by Eq. (4.77), we get

$$\overline{u}(z) = \int_0^\infty \frac{\omega_{20}a^2}{\pi\sigma_\eta^2} e^{-\frac{a^2}{2\sigma_\eta^2}} \left[\frac{\cosh k_{20}(z+h)}{\sinh k_{20}h}\cos\theta_0 - k_{20}a\frac{\cosh 2k_{20}(z+h)}{2\sinh^2 k_{20}h}\left(\frac{\pi}{2}-\theta_0\right)\right] da \tag{4.80}$$

As in Section 4.1.6, ω_{20} and k_{20} may be replaced by other representative values.

We may also find estimates for the mean horizontal velocity in points always submerged, corresponding to those in Eq. (4.57), viz.

$$\overline{u}(z)_{submerged} \approx \begin{cases} -9\dfrac{H_{m0}^2}{T_p^3}\dfrac{\cosh\left[16T_p^{-2}(z+h)\right]}{2\sinh^2\left(8T_p^{-2}h\right)} \ [m/s], & Pierson-Moskowitz \\ -7\dfrac{H_{m0}^2}{T_p^3}\dfrac{\cosh\left[14T_p^{-2}(z+h)\right]}{2\sinh^2\left(7T_p^{-2}h\right)} \ [m/s], & JONSWAP \end{cases} \tag{4.81}$$

and more generally, corresponding to Eq. (4.58), we have

$$\overline{u}(z)_{submerged} \approx -C_\omega^3 \frac{\pi^3 H_{m0}^2}{gT_p^3} \frac{\cosh\left[C_\omega^2 \dfrac{8\pi^2}{gT_p^2}(z+h)\right]}{2\sinh^2\left(C_\omega^2 \dfrac{4\pi^2}{gT_p^2}h\right)} \ [m/s] \ , \ z < -\frac{3}{4}H_{m0} \tag{4.82}$$

Eqs. (4.81) and (4.82) apply to the "full" 2nd order case as well as to the simplified approach, because the higher order periodic terms cancel out.

4.3 Stokes Waves from a Lagrangian Point of View

In light of Section 3.3, and the result of Dubreil-Jacotin referred to in the introduction to Section 4.2, it is of interest to consider a potential solution including a non-uniform drift in a Lagrangian frame of reference. Since Miche made his solution irrotational by adding a Stokes-like drift, cf. Section 4.2.1, it is reasonable to start out by considering this solution. It is then simplest to consider the limit case of infinite depth, where the drift is identical to Stokes drift and Miche's solution without drift is identical to Gerstner's solution. In the limit of infinite depth, Miche's solution including Stokes drift is identical to the Lagrangian form of 2nd order Stokes waves.

The Lagrangian form of 2nd order Stokes waves may be found by Taylor expansions, cf. e.g. Newman (1977) or Dean and Dalrymple (1991). The "particle"-paths are then found to be (open) circular orbits with a net forward drift; Stokes drift. The expression for Stokes drift in intermediate water is (cf. e.g. Dean and Dalrymple, 1991)

$$u_{Stokes\ drift} = \frac{gk^2a^2}{\omega}\frac{\cosh 2k(z_0+h)}{\sinh 2kh} \tag{4.83}$$

Note that Eq. (4.83) is often given as a function of the Eulerian variable z in textbooks, which by itself may be a source of confusion. The expression is however best given on Lagrangian form, e.g. as for infinite depth in Faltinsen (1990). Then the Lagrangian form of 2nd order Stokes waves becomes

$$\begin{aligned} x &= x_0 - ae^{kz_0}\cos(\omega t - kx_0) + \omega k a^2 e^{2kz_0} t \\ z &= z_0 + ae^{kz_0}\sin(\omega t - kx_0) \end{aligned} \tag{4.84}$$

which is easily recognized as Gerstner's theory with Stokes drift added.

An expression for the mean Eulerian horizontal velocity in 2nd order Stokes waves, including Stokes drift, may be found in the same manner as in Eq. (4.44), yielding

$$\overline{u} = \frac{\omega a}{\pi} e^{kz} \cos\theta_0 \tag{4.85}$$

where θ_0 is given by Eq. (4.42). For finite depth, the corresponding expression is

$$\overline{u} = \frac{\omega a}{\pi} \frac{\cosh k(z+h)}{\sinh kh} \cos\theta_0 \tag{4.86}$$

where θ_0 is now given by Eq. (4.77). The typical form of Eqs. (4.85) and (4.86) is compared to that of Miche (and Gerstner) waves in Figure 6.2 and Figure 6.3. Note that the mean horizontal velocity according to Eqs. (4.85) and (4.86) is zero below the splash zone.

The limit of validity of Stokes' 2nd order wave theory (Stokes, 1847 and 1880) in deep water is approximately (cf. e.g. Wiegel, 1964, or LeBlond and Mysak, 1978, also)

$$ka < \frac{\pi}{7} \approx 0.142\pi \approx 0.45 \tag{4.87}$$

The Jacobian resulting from Eq. (4.84) is

$$J = \frac{\partial x}{\partial x_0}\frac{\partial z}{\partial z_0} - \frac{\partial x}{\partial z_0}\frac{\partial z}{\partial x_0} = 1 - k^2 a^2 e^{2kz_0} + 2\omega k^3 a^3 e^{3kz_0} t \cos(\omega t - kx_0) \tag{4.88}$$

which has a constant deviation from 1 of 2nd order and a term initially of 3rd order growing in time. The corresponding vorticity also includes an initial 3rd order term growing in time, viz.

$$\zeta = 2\frac{\omega k^3 a^3 e^{3kz_0}\left[\omega t \cos(\omega t - kx_0) - \sin(\omega t - kx_0)\right]}{1 - k^2 a^2 e^{2kz_0} + 2\omega k^3 a^3 e^{3kz_0} t \cos(\omega t - kx_0)} \tag{4.89}$$

The amplitude of the increasing term in the Jacobian is

$$2\omega k^3 a^3 e^{3kz_0} t \tag{4.90}$$

The length of time until this term is of order n may be found as

$$(ka)^n e^{nkz_0} = 2\omega k^3 a^3 e^{3kz_0} t = 4\pi k^3 a^3 e^{3kz_0} \frac{t}{T}$$

$$\Downarrow$$

$$\frac{t}{T} = \frac{(ka)^n e^{nkz_0}}{4\pi k^3 a^3 e^{3kz_0}} \tag{4.91}$$

where T is the wave period. This gives for the respective orders

$$\begin{aligned} 0^{\text{th}}\text{ order:}\quad & \frac{t}{T} = \frac{1}{4\pi k^3 a^3 e^{3kz_0}} \\ 1^{\text{st}}\text{ order:}\quad & \frac{t}{T} = \frac{1}{4\pi k^2 a^2 e^{2kz_0}} \\ 2^{\text{nd}}\text{ order:}\quad & \frac{t}{T} = \frac{1}{4\pi k a e^{kz_0}} \end{aligned} \tag{4.92}$$

The time t/T, which may be called a relative length of time until breakdown at the given order, is also dependent on the vertical coordinate. Some example values will therefore be given for each order, for different values of ka and kz_0. The ka-values are chosen to be 0.1, 0.2 and the assumed approximate limit value $\pi/7$, cf. Eq. (4.87). The kz_0-values are chosen to be 0, $-0.5ka$ and $-ka$, since this thesis emphasize on the splash zone conditions. The results are given in Table 4-1, Table 4-2 and Table 4-3. Plots of 2nd order Stokes waves at different instants in time are also included below, in order to visualize the "breakdown".

Table 4-1 t/T to 2nd order

	$kz_0 = 0$	$kz_0 = -0.5ka$	$kz_0 = -ka$
$ka = 0.1$	0.80	0.84	0.88
$ka = 0.2$	0.40	0.44	0.49
$ka = \pi/7$	0.18	0.22	0.28

Table 4-2 t/T to 1st order

	$kz_0 = 0$	$kz_0 = -0.5ka$	$kz_0 = -ka$
$ka = 0.1$	7.96	8.79	9.72
$ka = 0.2$	1.99	2.43	2.97
$ka = \pi/7$	0.39	0.62	0.97

Table 4-3 t/T to 0th order

	$kz_0 = 0$	$kz_0 = -0.5ka$	$kz_0 = -ka$
$ka = 0.1$	79.58	92.46	107.42
$ka = 0.2$	9.95	13.43	18.12
$ka = \pi/7$	0.87	1.72	3.37

The plots below are based on Eq. (4.84). The longitudinal lines are lines of constant z_0, and these were horizontal in the still water situation. The "standing" lines are lines of constant x_0, and these were vertical in the still water situation, cf. Figure 4.1 also. Note that the scales are not the same in the different plots. It is assumed that at time $t = 0$, Stokes waves exists in which Stokes drift has not yet "acted". The plots are based on the assumed steepest possible waves, i.e. $ka = \pi/7$, but the effects are qualitatively the same for lower steepnesses. The waves propagate to the right.

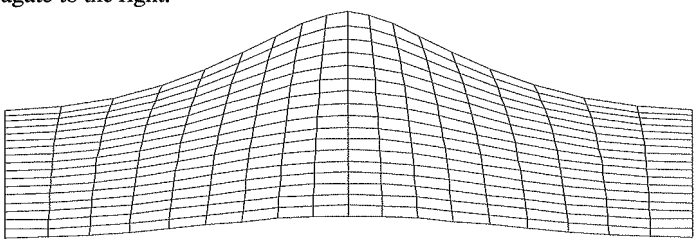

Figure 4.5 Stokes wave, $ka = \pi/7$, $t = 0$.

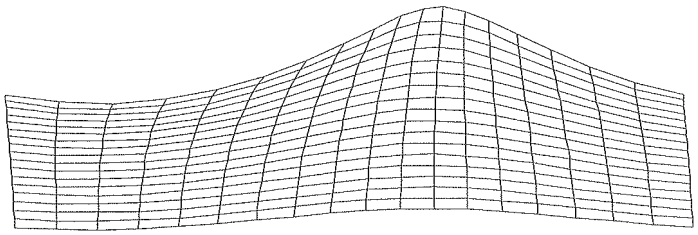

Figure 4.6 Stokes wave, $ka = \pi/7$, $t = 0.1T$.

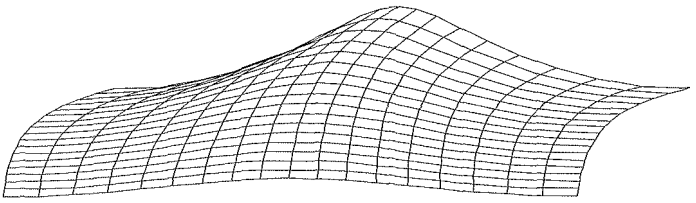

Figure 4.7 Stokes wave, $ka = \pi/7$, $t = T$.

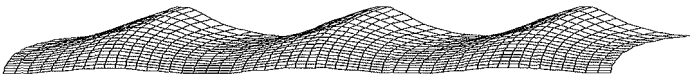

Figure 4.8 Stokes waves, $ka = \pi/7$, $t = 2T$.

Figure 4.6, Figure 4.7 and Figure 4.8 show that the inclusion of Stokes drift to a certain degree restores the orthogonality of element boundaries in front of the wave crest, as conformal mapping would require (cf. Section 3.3). It can also be seen that the elements in front of the crest are "enlarged", while the elements behind the crest are "reduced". This periodic variation, which is growing in amplitude with time, is the one described by the 3rd order term in Eq. (4.88).

Figure 4.8 includes three wave crests, showing that a regular wave profile of the surface is apparently maintained even if continuity is eventually violated to the leading order. The amplitude is also maintained. However, after a few wave periods the profile of these waves eventually resemble that of a spilling breaker. For lower values of the steepness ka, the regular wave profile is maintained for a longer period of time.

From the above tables and figures the following conclusions may be drawn for the conditions in the splash zone:

- 2nd order Stokes waves of steepness $ka \geq 0.1$ break down at 2nd order well within one wave period, practically immediately, and are therefore theoretically inconsistent in the Lagrangian frame of reference.
- 2nd order Stokes waves of steepness $ka \geq 0.1$ break down at 1st order within a few wave periods.
- 2nd order Stokes waves of steepness $ka \approx \pi/7$, i.e. the assumed limit steepness, break down at 0th order within a couple of wave periods.
- The dependency on depth is practically insignificant in the surface region.

The increasing and periodic variation of the size of the elements is unphysical. The elements cannot "grow" in one part of the wave and "vanish" in another.

For Stokes' wave theory to be theoretically consistent in this Lagrangian sense to 2nd order for at least 10 to 20 wave periods for $-a < z_0 < 0$, i.e. within the splash zone, the maximum allowable ka-values can be found from Eq. (4.92) to be approximately 0.005.

- Therefore, for 2nd order Stokes waves to be theoretically consistent in the Lagrangian frame of reference also in the splash zone for more than a couple of wave periods, the steepness ka can at most be of the order $O(0.01)$. For the theory to be consistent over "many" wave periods, the limit steepness is of the order $O(0.001)$ or less.

As stated above, Eq. (4.84) may be considered a superposition of regular orbital motion and a non-uniform Lagrangian current, both individually satisfying the nonlinear equations of motion exactly. Note in particular that Stokes drift alone, which may be considered a simple shear current, does satisfy $J = 1$, meaning that it is the combination of a shear current with waves that causes the analytical inconsistencies in the Lagrangian frame of reference. The imposed combination of nonlinearity and superposition is itself also an indication of inconsistency to second order. However, Gerstner's solution *is* a solution of the governing equations for the wave problem, satisfying the boundary conditions at the true boundary, suggesting that imposing irrotationality is incorrect.

Also, the initial value of J in Eq. (4.88), i.e. at $t = 0$, has a 2^{nd} order deviation from 1. Hence, Eq. (4.88) does not satisfy the initial conditions in Cauchy's equations and Weber's transformation, cf. Sections 3.2.2 and 3.2.3 and Eq. (3.22), which are there necessary for an initial velocity potential to exist. This supports the findings in Section 3.3, namely that there appears to be a fundamental conflict between satisfying continuity and requiring irrotationality, if the motion and deformation of fluid elements is not (at best) very simple. However, it is unclear how to best "choose" the length of time Stokes drift has acted. In Table 4-1 - Table 4-3 and Figure 4.5 - Figure 4.8, it is assumed that Stokes drift "starts" at an instant in time where regular waves without mass transport already exist. This choice may itself be quite questionable, but including Stokes drift from the very initiation of the waves will only make Stokes waves even more inconsistent in the Lagrangian frame of reference.

Hence, vertically non-uniform Lagrangian currents and waves occurring simultaneously must seemingly eventually lead to some sort of breaking of the waves, since the situations shown in Figure 4.6 - Figure 4.8 are unphysical. By breaking is then meant violation of continuity and impenetrability, i.e. that a small element of fluid is split up and penetrated by other small fluid elements. This means that a small fluid element does not remain a material entity in time, and that it therefore cannot be considered an *identifiable* continuum element in time. This is not unphysical, but it expresses a limitation of the continuum model with respect to interpretation of material (Lagrangian) quantities in time. Some may prefer to speak of material "point-particles" instead of small elements, and claim that such particles cannot be penetrated or split up. However, it must then be recalled that the Jacobian, e.g. as in Eq. (4.88), applies to a single Lagrangian point. The inconsistency of Stokes waves therefore remains the same, irrespective of whether we speak of "point-particles" or small elements.

Note that it is here not concluded that waves, even regular, and non-uniform mass transport cannot exist simultaneously. The main objective of this section has been to show that one such solution *resulting* from the assumption of irrotational flow, namely Stokes waves, is inconsistent if interpreted literally in the Lagrangian frame of reference. Therefore, the results of this section do question the foundation for speaking of *identifiable material particles* in a continuum, and for how long and under which circumstances it may be relevant to do so. Hence, they also question the general applicability of the assumption of irrotational flow, and thus the correctness of Stokes waves as a basic solution for regular waves.

CHAPTER 5

WAVE MODELLING

Irregular waves are here modelled as a sum of linear regular Lagrangian wave components, according to the superposition principle. However, adding linear components in the Lagrangian frame of reference is seen to exhibit so-called nonlinear interactions when the surface elevation is plotted parametrically in an Eulerian frame of reference, e.g. as when shorter waves ride on longer waves. This is shown in Section 5.1.

A Lagrangian description alone has a limited practical value, and a method for transforming the Lagrangian solution to an Eulerian frame of reference is needed. One such method, applicable for broad-banded irregular waves as well as regular waves, is presented in Section 5.3. Producing timeseries of the surface elevation at a fixed Eulerian x-position from the Lagrangian solution requires a specific method, which is presented in Section 5.4.

Analysis of irregular waves in a Lagrangian frame of reference requires that the Lagrangian orbital amplitude spectrum is known. In experiments, the surface elevation is often measured by fixed gages, and a spectrum based on such measurements is not identical to the Lagrangian orbital amplitude spectrum. Section 5.4 therefore also includes a short discussion on the relation between these two types of spectra.

5.1 Superposition of Lagrangian Components

Eq. (4.1) is an exact solution of the nonlinear Lagrangian equations of motion. Eq. (4.14) is a perturbation solution of the same equations, and the first order terms of Eq. (4.14) is the solution of the linearized Lagrangian equations of motion. The first order terms of Eq. (4.14) look identical to Eq. (4.1), but there is a difference at second order in the definition of the vertical Eulerian variable z in these two equations. Therefore, Eq. (4.1) is strictly speaking not linear and superposing must be based on linear terms as in Eq. (4.14), i.e. with $z = 0$ at the still water level. The vertical shift in Eq. (4.14), which is equivalent to that in Eq. (4.12), is of second order, i.e. nonlinear, and therefore not included in the superposing.

Only Gerstner waves is considered in the following, but irregular Miche waves may be modelled in the same manner by superposing components given by the first order terms in Eq. (4.59).

Irregular Gerstner waves as a sum of N linear components may therefore be written

$$x = x_0 - \sum_{n=1}^{N} a_n e^{k_n z_0} \cos(\omega_n t - k_n x_0 + \varepsilon_n)$$
$$z = z_0 + \sum_{n=1}^{N} a_n e^{k_n z_0} \sin(\omega_n t - k_n x_0 + \varepsilon_n) \tag{5.1}$$

where, when related to an amplitude spectrum,

$$a_n = \sqrt{2S(\omega_n)\Delta\omega_n} \tag{5.2}$$

and ε_n are constant relative phases. When generating a synthetic wave spectrum, each component should be assigned a value of ε_n from a probability distribution $p_\varepsilon(\varepsilon)$ uniform over $0 \leq \varepsilon \leq 2\pi$, if they are all considered free wave components.

The velocity, acceleration and pressure of a Lagrangian point in irregular Gerstner waves are then found as a sum of the component velocities, accelerations and pressures, respectively, viz.

$$u = \sum_{n=1}^{N} \omega_n a_n e^{k_n z_0} \sin(\omega_n t - k_n x_0 + \varepsilon_n)$$
$$w = \sum_{n=1}^{N} \omega_n a_n e^{k_n z_0} \cos(\omega_n t - k_n x_0 + \varepsilon_n)$$
$$a_x = \sum_{n=1}^{N} \omega_n^2 a_n e^{k_n z_0} \cos(\omega_n t - k_n x_0 + \varepsilon_n) \tag{5.3}$$
$$a_z = -\sum_{n=1}^{N} \omega_n^2 a_n e^{k_n z_0} \sin(\omega_n t - k_n x_0 + \varepsilon_n)$$
$$p = -\rho g z_0$$

cf. Eqs. (4.2), (4.21) and (4.22) and recall that $z = 0$ is now at the still water level. The kinematics and pressure in irregular Miche waves are found in a similar manner from the first order terms of Eqs. (4.64) and (4.65). Note that there is a first order term in the pressure in Eq. (4.65) that should be included or excluded according to Eq. (4.69).

It is straightforward to construct a spatial picture ('snapshot') $\eta(x)$ of the surface from the parametric representation Eq. (5.1), including as many components as desired, by keeping t fixed, setting $z_0 = 0$ and letting x_0 run over some interval. Spatial snapshots of specific volumes (areas) of water in irregular waves may also be constructed, as in Figure 4.1, by letting z_0 run over an interval as well.

The common Eulerian model of irregular waves is a sum of sine waves added in the Eulerian frame of reference, viz.

$$\eta = \sum_{n=1}^{N} a_n \sin(\omega_n t - k_n x + \varepsilon_n) \tag{5.4}$$

Applying the same values for a_n, ω_n, k_n and ε_n, and comparing a surface based on Eq. (5.1) with one based on Eq. (5.4), the ability of the Lagrangian representation to automatically include so-called nonlinear interactions among the wave components is seen. In Figure 5.1 is shown the interaction between a short wave riding on a longer wave, based on a parametric

plot of Eq. (5.1). Figure 5.2 shows the superposition of the same two components according to Eq. (5.4). Only one crest of the longer wave is included.

Figure 5.1 Eulerian spatial snapshot of the surface $\eta(x)$ in two-component waves according to Eq. (5.1). $\lambda_{long}/\lambda_{short} \approx 8$, $ka_{long} \approx 0.2$, $ka_{short} \approx 0.4$.

Figure 5.2 Eulerian spatial snapshot of the surface $\eta(x)$ in two-component waves according to Eq. (5.4), with the same component parameters as in Figure 5.1.

Figure 5.3 shows the superposition of two components defined by either of Eqs. (4.39) - (4.41). These equations are equivalent to Eq. (5.4) plus a 2nd order higher harmonic from each component. The component parameters are as in Figure 5.1 and Figure 5.2.

Figure 5.3 Eulerian spatial snapshot of the surface $\eta(x)$ in two-component waves according to Eq. (4.39), with the same component parameters as in Figure 5.1 and Figure 5.2.

In Figure 5.4 is shown the interaction between two components of more comparable wavelengths.

Figure 5.4 Eulerian spatial snapshot of the surface $\eta(x)$ in two-component waves. $\lambda_{long}/\lambda_{short} \approx 3$, $ka_{long} = ka_{short} \approx 0.4$. The solid line represents the parametric form equivalent to the case in Figure 5.1, the dotted line is equivalent to the case in Figure 5.2, and the dashed line is equivalent to the case in Figure 5.3.

It can be seen that superposition in the Lagrangian frame of reference and parametric plotting produces physically reasonable interactions directly. The shorter wave is seen to be shortened in the crest and elongated in the trough of the longer wave, i.e. what would be called 'nonlinear interactions' from a purely Eulerian point of view. Modelling such interactions requires quite complex models in an Eulerian approach, if feasible to model adequately there at all.

One may argue whether or not the constant vertical shift should be included when adding components based on Eq. (4.39). It is included in Figure 5.3 and Figure 5.4, but the result is anyway seen to be closer to the added sine waves than the parametrically plotted surface elevation. Also, if the constant vertical shift is not included, it is not consistent to include the other 2nd order term either, leaving only the first order sine component as in Eq. (5.4). This underlines the importance of performing the superposition in the Lagrangian system if we want to take full advantage of the Lagrangian approach also in irregular waves.

The steepnesses of the components in the above figures are relatively high, but not unrealistic. In a way similar to Pierson (1961), we may find a condition on the combined *ka*-values in a sea state. If $x(x_0)$ in Eq. (5.1) is not monotonically increasing, $\eta(x)$ will be (at least) triple valued at some value(s) of x. The surface is then either forming a loop (which is unphysical), being vertical, or forming a "tongue" similar to a plunging breaker.

A condition for the combined *ka*-values in irregular Gerstner waves is therefore

$$\frac{dx}{dx_0} = 1 - \sum_{n=1}^{N} k_n a_n e^{k_n z_0} \sin(\omega_n t - k_n x_0 + \varepsilon_n) \geq 0$$

$$\Downarrow$$

$$\sum_{n=1}^{N} k_n a_n e^{k_n z_0} \sin(\omega_n t - k_n x_0 + \varepsilon_n) < 1 \tag{5.5}$$

which must hold for any value of z_0, not just the free surface. The "equal to" part of the inequality is excluded in the last expression above, since Eq. (5.5) must hold for a single regular component as well. The steepness *ka* must then be less than 1 for the Jacobian to exist, cf. Eq. (4.8). This means that the surface cannot be vertical or forming a "tongue" anywhere either, if the model is to remain valid with respect to continuity. A part of the surface being vertical and/or forming a "tongue" is not unphysical, since this occur in real seas. However, it is hard to see how such effects can be formed by superposition of circular orbits on uniform depth alone, and how the wave can be restored without breaking. It seems that such surface profiles can only be formed by an actual breaking event, e.g. due to depth variations or the presence of a non-uniform current (cf. Section 4.3).

A condition equivalent to Eq. (5.5) for (1st order) Miche waves is

$$\frac{dx}{dx_0} = 1 - \sum_{n=1}^{N} k_n a_n \frac{\cosh k_n(z_0 + h)}{\sinh k_n h} \sin(\omega_n t - k_n x_0 + \varepsilon_n) \geq 0$$

$$\Downarrow$$

$$\sum_{n=1}^{N} k_n a_n \frac{\cosh k_n(z_0 + h)}{\sinh k_n h} \sin(\omega_n t - k_n x_0 + \varepsilon_n) < 1 \tag{5.6}$$

Eqs. (5.5) and (5.6) may be considered effective steepnesses of irregular waves.

5.2 Wheeler's Method

Besides comparing the Lagrangian theories with measurements, it is also useful to include comparisons with standard methods for calculations of irregular wave kinematics. Due to its widespread use, Wheeler's method (Wheeler, 1970) is found appropriate for this purpose. See Gudmestad (1993) for a review of applied methods for calculating wave kinematics. Wheeler's method is a modification of linear Eulerian wave theory, developed to give a better description of the kinematics in the surface zone of irregular waves than linear Eulerian

theory is capable of. In Wheeler's method, the vertical coordinate is stretched in such a way that it is always effectively zero at the free surface, viz.

$$z_{Wheeler} = \frac{h(z-\eta)}{h+\eta} \tag{5.7}$$

Wheeler's method therefore has some resemblance to the Lagrangian models. However, it must be remembered that as a consequence of the stretching of coordinates, the expression in Wheeler's method does not satisfy the basic equations of motion properly. In deep water Eq. (5.7) simplifies to

$$z_{Wheeler} = z - \eta \tag{5.8}$$

The horizontal velocity according to Wheeler's method is then given by

$$\begin{aligned} u &= \sum_{n=1}^{N} \omega_n a_n \frac{\cosh k_n (z_{Wheeler} + h)}{\sinh k_n h} \sin(\omega_n t - k_n x + \varepsilon_n) \\ u &= \sum_{n=1}^{N} \omega_n a_n e^{k_n z_{Wheeler}} \sin(\omega_n t - k_n x + \varepsilon_n) \end{aligned} \tag{5.9}$$

for intermediate and deep water, respectively. Corresponding expressions may also be found for the vertical velocity, although Wheeler's method is strictly speaking only given for the horizontal velocity.

The highest values of the horizontal velocity occur beneath crests, and many published comparisons of theory with measurements therefore focus on this situation. Even if the results from these comparisons are not unambiguous, there is a tendency that Wheeler's method agrees reasonably well with measurements close to the free surface, while it gives to low values further down in the fluid. The underprediction is typically highest near the still water level, cf. e.g. Gudmestad (1993), Stansberg and Gudmestad (1996) and Trulsen et al. (1998). This type of deficiency is also to be expected from a theoretical point of view, cf. Figure 6.20.

Based on analysis of the irregular wave data from the experiments in Skjelbreia et al. (1991), i.e. the same experiments that are considered in Chapter 6, Gudmestad and Haver (1993) suggested that Eq. (5.9) be multiplied by the factor

$$\begin{aligned} w_f &= 1.2\left[1 + 0.16\left(\frac{z}{h}\right)\right] && -h < z < 0 \\ w_f &= 1.2\left[1 - 0.16\left(\frac{z}{\eta_{crest}}\right)\right] && 0 < z < \eta_{crest} \end{aligned} \tag{5.10}$$

where η_{crest} is the surface elevation at the very crest. Eq. (5.10) represents a 20 % increase at the still water level, reducing to 0.8 % at the crest and at the bottom. These modifications are based on values beneath crests in irregular waves, and include "*...proper corrections due to the return flow in the wave tank...*" (Gudmestad and Haver, 1993). Since this thesis questions the existence of such a return flow, calculations according to Wheeler's method are not modified according to Eq. (5.10). Note that all these considerations pertain to the horizontal velocity beneath crests only. Note also that Wheeler's method was developed to calculate kinematics from measured non-linear timeseries of the surface elevation. Using Wheeler's method to calculate kinematics from synthetic timeseries of linear irregular waves is expected to underpredict the velocities in the crests (Gudmestad, 1993).

5.3 Transforming the Lagrangian Solutions to an Eulerian Frame of Reference by Iteration

In order to determine Eulerian quantities from a Lagrangian solution, we need to determine the relations $x_0(x, z, t)$ and $z_0(x, z, t)$. Analytical approximate forms may then be attempted, such as Eqs. (4.36), (4.70) and (4.75) obtained by Taylor-expansions. However, these are not satisfactory when irregular waves are concerned, since superposition of components should be performed in the Lagrangian frame of reference, cf. Section 5.1. The implicit form of Eq. (5.1) therefore suggests that the relations $x_0(x, z, t)$ and $z_0(x, z, t)$ be found numerically by iteration.

One such iteration method is developed as a part of this thesis work. The basic idea is to take advantage of the periodicity of a regular wave, and is thoroughly explained for Gerstner waves in Sections 5.3.1 and 5.3.2. The procedure is then expanded to the irregular case in Section 5.3.3, and to regular and irregular Miche waves in Section 5.3.4. Only the 2D case in the (x, z)-plane is considered.

The method described in the following sections applies to Eulerian points in the splash zone as well as points that are always submerged in water. However, when describing the method it is convenient to assume that the point in question is always submerged. Points in the splash zone are addressed in Section 5.3.5.

5.3.1 Regular Gerstner waves

The Eulerian position of a Lagrangian point at time t is

$$\begin{aligned} x &= x_0 - ae^{kz_0}\cos(\omega t - kx_0) \\ z &= z_0 + ae^{kz_0}\sin(\omega t - kx_0) \end{aligned} \tag{5.11}$$

It is here assumed, without loss of generality, that the relative phase ε is 0. The constant vertical shift is not included in Eq. (5.11). It must still be accounted for when comparing results from the procedure outlined below with experimental measurements, if the results are to be correct to at least second order. Depending on how we define the Eulerian frame of reference, the method applies to the exact solution in Eq. (4.1) as well as the 2nd order solution in Eq. (4.14). Eq. (5.11) may be considered identical to Eq. (4.1), i.e. with $z = 0$ a distance $\frac{1}{2}ka^2$ above the still water level. Eulerian quantities may therefore be found exactly for regular Gerstner waves, whereas 3rd order errors will always exist for Miche waves.

We now seek the Lagrangian point (x_{0t}, z_{0t}) that occupies the specific Eulerian point (x_t, z_t) at a fixed time instant t. Subscript t is thus used to denote the Eulerian point (x_t, z_t) under consideration and the sought solution (x_{0t}, z_{0t}), since other points (x_0, z_0) and (x, z) will also be involved. The unknowns are therefore the Lagrangian coordinates x_{0t} and z_{0t}, while the Eulerian coordinates x_t and z_t, as well as the time t and the wave parameters a, k, and ω, are known.

Use will also be made of the position of a Lagrangian point half a wave period after t, cf. Figure 5.5, which may be written

$$\begin{aligned} x^* &= x_0 - ae^{kz_0}\cos(\omega t - kx_0 + \pi) \\ z^* &= z_0 + ae^{kz_0}\sin(\omega t - kx_0 + \pi) \end{aligned} \tag{5.12}$$

For convenience, the notations $\theta_t = \omega t - kx_t + \varepsilon$ and $\theta = \omega t - kx_0 + \varepsilon$ are introduced. Note that since t and x_t are fixed, so is θ_t. In the figures below, it is assumed that $\theta_t = 0$, but the

method is independent of the value of θ_t. Numbers after the commas in the sub- and superscripts denote the number of iterations performed.

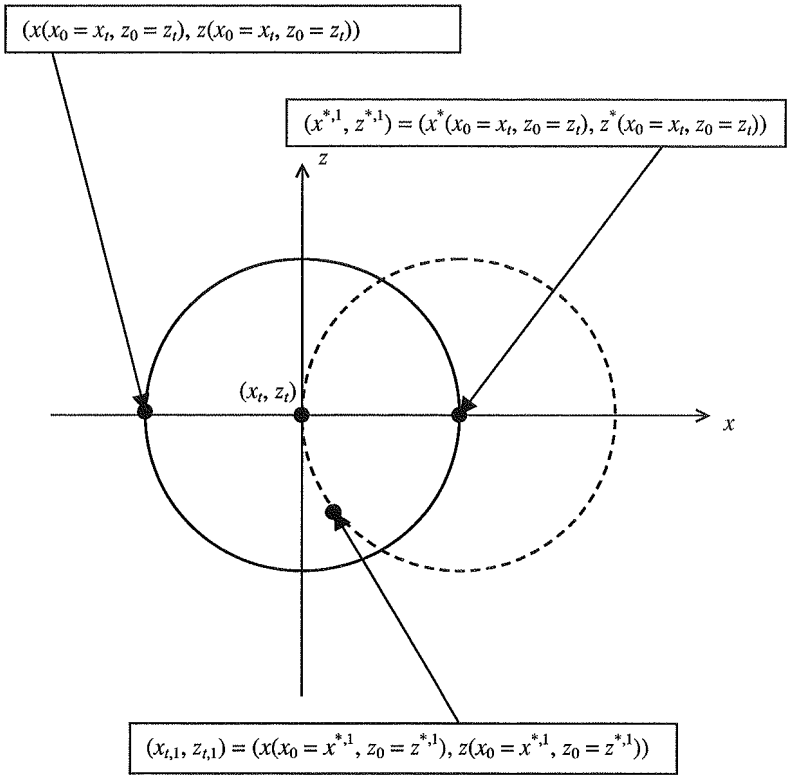

Figure 5.5 The solid circle represents the path traversed by the "particle" $(x_0 = x_t, z_0 = z_t)$ over one wave period. The dashed circle represents the path traversed by the "particle" $(x_0 = x^{*,1}, z_0 = z^{*,1})$ over one wave period.

From Figure 5.5, a reasonable first approximation of (x_{0t}, z_{0t}) is

$$\begin{aligned} x_{0t,1} &= x^*(x_0 = x_t, z_0 = z_t) = x^{*,1} \\ z_{0t,1} &= z^*(x_0 = x_t, z_0 = z_t) = z^{*,1} \end{aligned} \tag{5.13}$$

Inserting Eq. (5.13) into Eq. (5.11) yields $(x_{t,1}, z_{t,1})$. This first approximation of (x_t, z_t) will generally not be satisfactory, cf. Figure 5.5. The second approximation $(x_{0t,2}, z_{0t,2})$ is then obtained according to Figure 5.6, viz.

$$\begin{aligned} x^{*,2} &= x_{0t,1} - ae^{kz_{0t,1}} \cos(\omega t - kx_{0t,1} + \pi) \\ z^{*,2} &= z_{0t,1} + ae^{kz_{0t,1}} \sin(\omega t - kx_{0t,1} + \pi) \end{aligned} \tag{5.14}$$

$$\begin{aligned} x_{0t,2} &= x_t - ae^{kz_{0t,1}} \cos(\omega t - kx_{0t,1} + \pi) \\ z_{0t,2} &= z_t + ae^{kz_{0t,1}} \sin(\omega t - kx_{0t,1} + \pi) \end{aligned} \tag{5.15}$$

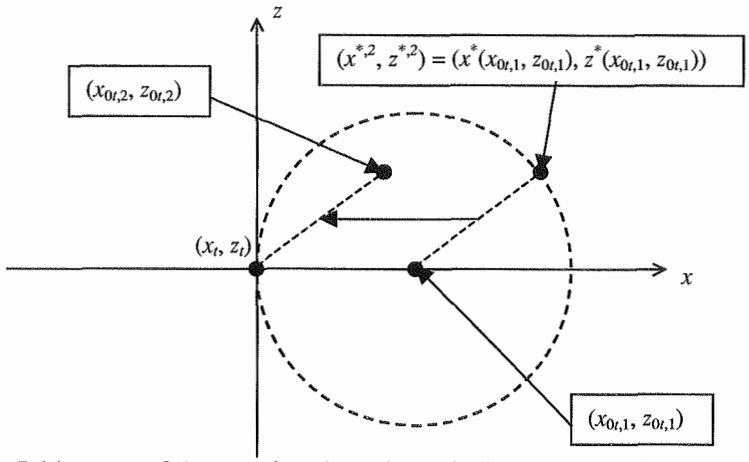

Figure 5.6 Step two of the procedure determining the Lagrangian tag (x_{0t}, z_{0t}) occupying the Eulerian position (x_t, z_t) at time t, yielding the second approximation $(x_{0t,2}, z_{0t,2})$. The dashed circle is identical to the dashed circle in Figure 5.5.

When reinserted into Eq. (5.11), Eq. (5.15) yields the second approximation of (x_t, z_t)

$$\begin{aligned} x_{t,2} &= x_{0t,2} - ae^{kz_{0t,2}} \cos(\omega t - kx_{0t,2}) \\ z_{t,2} &= z_{0t,2} + ae^{kz_{0t,2}} \sin(\omega t - kx_{0t,2}) \end{aligned} \tag{5.16}$$

If Eq. (5.16) do still not approximate (x_t, z_t) satisfactorily, we proceed in an iterative manner. We may now actually simplify the procedure, since the variables (x^*, z^*) turn out to be superfluous. They were only useful in order to establish the first approximation in Eq. (5.13) and explain the basic idea. The additional relative phase ε may also be included, given any constant value. The iteration scheme is therefore simply

$$\begin{aligned} x_{0t,m+1} &= x_t - ae^{kz_{0t,m}} \cos(\omega t - kx_{0t,m} + \varepsilon + \pi) \\ z_{0t,m+1} &= z_t + ae^{kz_{0t,m}} \sin(\omega t - kx_{0t,m} + \varepsilon + \pi) \end{aligned} \tag{5.17}$$

with initial values

$$x_{0t,0} = x_t, \quad z_{0t,0} = z_t \tag{5.18}$$

Note that the first term on the right-hand sides of Eq. (5.17) always are the fixed values (x_t, z_t), respectively. The new approximations of (x_t, z_t) are

$$\begin{aligned} x_{t,m} &= x_{0t,m} - ae^{kz_{0t,m}} \cos(\omega t - kx_{0t,m} + \varepsilon) \\ z_{t,m} &= z_{0t,m} + ae^{kz_{0t,m}} \sin(\omega t - kx_{0t,m} + \varepsilon) \end{aligned} \tag{5.19}$$

and the procedure is repeated until $(x_{t,m}, z_{t,m})$ are close enough to (x_t, z_t). How to determine what is "close enough" is discussed in the next section.

Applying the latest available approximation of x_{0t}, assuming it is an improved approximation, might be expected to speed up the iteration, viz.

$$x_{0t,m+1} = x_t - ae^{kz_{0t,m}} \cos(\omega t - kx_{0t,m} + \varepsilon + \pi)$$
$$z_{0t,m+1} = z_t + ae^{kz_{0t,m}} \sin(\omega t - kx_{0t,m+1} + \varepsilon + \pi) \quad (5.20)$$

Alternatively, one may change the order of calculation to

$$z_{0t,m+1} = z_t + ae^{kz_{0t,m}} \sin(\omega t - kx_{0t,m} + \varepsilon + \pi)$$
$$x_{0t,m+1} = x_t - ae^{kz_{0t,m+1}} \cos(\omega t - kx_{0t,m} + \varepsilon + \pi) \quad (5.21)$$

However, no significant reduction in necessary number of iterations is found by using Eqs. (5.20) or (5.21) instead of Eq. (5.17).

5.3.2 Convergence of the iteration and accuracy of the solution

An error e_m in the approximation of (x_t, z_t) after m iterations may be defined as the highest value of

$$e_{x,m} = |x_t - x_{t,m}|$$
$$e_{z,m} = |z_t - z_{t,m}| \quad (5.22)$$

where $x_{t,m}$ and $z_{t,m}$ are given by Eq. (5.19). We may assume that sufficient accuracy is obtained when $e_m < e$, where e is a pre-defined tolerance. e_m is easily controllable, since the correct values of (x_t, z_t) are known. However, there is no guarantee that the accuracy of the Lagrangian point, which is the solution we seek, is equally accurate. This is exemplified in Figure 5.7, where two different phases are considered; the crest and the trough. It is seen that even if the error $e_{z,m}$ in $(x_{t,m}, z_{t,m})$ is small in the trough, the error e_{0m} in $(x_{0t,m}, z_{0t,m})$ may be considerably greater. This effect will not be a problem in the crest. In Figure 5.7 it is assumed that there is an error in z_0 only.

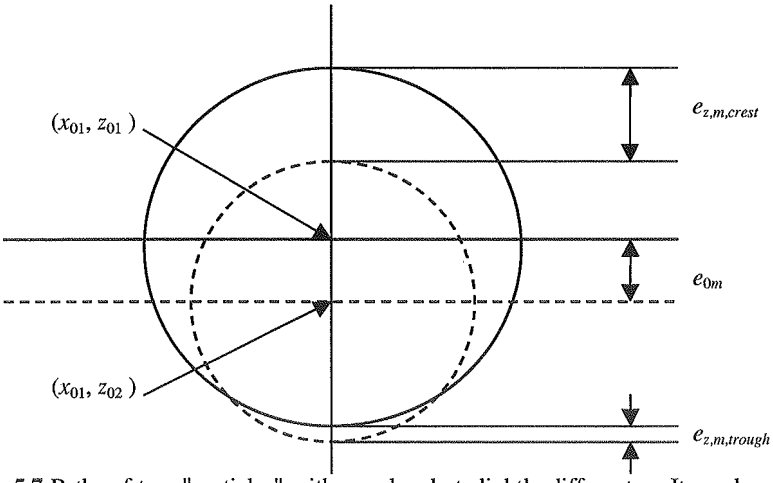

Figure 5.7 Paths of two "particles" with equal x_0 but slightly different z_0. It can be seen that e_{0m} is greater than the vertical distance between the "particles" in the trough, $e_{z,m,trough}$, while it is less than the corresponding distance in the crest $e_{z,m,crest}$. The dimensions are not quantitatively correct.

The problem is therefore to determine a suitable value of e ensuring an accuracy of e_0 in the obtained approximation $(x_{0t,m}, z_{0t,m})$ of the unknown (x_{0t}, z_{0t}). This may be done, at least for

most values of the steepness ka in regular waves that are of practical interest, by expressing e_m as a function of e_{0m}. We should then consider the general case, with possible errors in x_0 as well as in z_0. The error in x_0 is named $e_{x0,m}$, and the error in z_0 is named $e_{z0,m}$. This yields for $e_{z,m}$ (absolute values are ignored for now), cf. Figure 5.7,

$$
\begin{aligned}
e_{z,m} &= \left[z_{01} - ae^{kz_{01}}\sin(\omega t - kx_{01})\right] - \left[z_{02} - ae^{kz_{02}}\sin(\omega t - kx_{02})\right] \\
&= (z_{01} - z_{02}) - a\left[e^{kz_{01}}\sin(\omega t - kx_{01}) - e^{k[z_{01}-(z_{01}-z_{02})]}\sin(\omega t - k[x_{01} - (x_{01} - x_{02})])\right] \\
&= e_{z0,m} - a\left[e^{kz_{01}}\sin(\omega t - kx_{01}) - e^{k[z_{01}-e_{z0,m}]}\sin(\omega t - k[x_{01} - e_{x0,m}])\right] \\
&= e_{z0,m} - ae^{kz_{01}}\left[\sin(\omega t - kx_{01}) - e^{-ke_{z0,m}}\sin(\omega t - kx_{01} + ke_{x0,m})\right] \\
&= e_{z0,m} - ae^{kz_{01}}\left\{\sin(\omega t - kx_{01}) - e^{-ke_{z0,m}}\left[\sin(\omega t - kx_{01}) + ke_{x0,m}\cos(\omega t - kx_{01})\right]\right\} \\
&= e_{z0,m} - ae^{kz_{01}}\sin(\omega t - kx_{01})\left(1 - e^{-ke_{z0,m}}\right) + kae^{kz_{01}}e^{-ke_{z0,m}}e_{x0,m}\cos(\omega t - kx_{01}) \\
&= e_{z0,m} - ae^{kz_{01}}\sin(\omega t - kx_{01})\left[1 - (1 - ke_{z0,m})\right] \\
&\quad + kae^{kz_{01}}(1 - ke_{z0,m})e_{x0,m}\cos(\omega t - kx_{01}) \\
&= e_{z0,m} - \left[kae^{kz_{01}}\sin(\omega t - kx_{01})\right]e_{z0,m} \\
&\quad + \left[kae^{kz_{01}}\cos(\omega t - kx_{01}) - k^2ae^{kz_{01}}e_{z0,m}\cos(\omega t - kx_{01})\right]e_{x0,m} \\
&= e_{z0,m} - \left[kae^{kz_{01}}\sin(\omega t - kx_{01})\right]e_{z0,m} + \left[kae^{kz_{01}}\cos(\omega t - kx_{01})\right]e_{x0,m} \\
&\quad - \left[k^2ae^{kz_{01}}\cos(\omega t - kx_{01})\right]e_{x0,m}e_{z0,m} \\
&\approx e_{0m} - kae_{0m}\left\{e^{kz_{01}}\left[\sin(\omega t - kx_{01}) - \cos(\omega t - kx_{01})\right]\right\} + O\left(k^2e_{0m}^2\right) \\
&< \left(1 - \sqrt{2}ka\right)e_{0m}
\end{aligned}
\tag{5.23}
$$

where it has been assumed that

$$
O(ke_{z0,m}) = O(ke_{x0,m}) = O(ke_{0m}) << 1 \tag{5.24}
$$

The minus-sign in the parenthesis in Eq. (5.23) is the appropriate one, since in the case

$$
e_{m,z} < \left(1 + \sqrt{2}ka\right)e_{0m} \tag{5.25}
$$

the error in the Lagrangian coordinates is less than the error in the Eulerian coordinates, e.g. as for the crest in Figure 5.7, and therefore not a problem. Eq. (5.25) may be applied if performing too many iterations is a concern. The additional constant phase term ε was excluded from the above derivation, but may be included, as in Eq. (5.17), without additional complications.

We may derive an expression for the error $e_{x,m}$ in a similar manner, yielding

$$\begin{aligned} e_{x,m} &= \left[x_{01} + ae^{kz_{01}}\cos(\omega t - kx_{01})\right] - \left[x_{02} + ae^{kz_{02}}\cos(\omega t - kx_{02})\right] \\ &\approx e_{0m} + kae_{0m}\left\{e^{kz_{01}}\left[\cos(\omega t - kx_{01}) - \sin(\omega t - kx_{01})\right]\right\} + O\left(k^2 e_{0m}^2\right) \\ &\approx e_{0m} - kae_{0m}\left\{e^{kz_{01}}\left[\sin(\omega t - kx_{01}) - \cos(\omega t - kx_{01})\right]\right\} + O\left(k^2 e_{0m}^2\right) \\ &< \left(1 - \sqrt{2}ka\right)e_{0m} \end{aligned} \tag{5.26}$$

i.e. equivalent to $e_{m,z}$.

If we want an accuracy in the approximation of Lagrangian coordinates of e_0, we must therefore iterate until

$$e_m < \left(1 - \sqrt{2}ka\right)e_0 \tag{5.27}$$

i.e. the appropriate tolerance for the error in the iteration procedure is

$$e = \left(1 - \sqrt{2}ka\right)e_0 \tag{5.28}$$

Eq. (5.28) is only applicable, for all values of x_0 and z_0, if the term in the parenthesis is positive and less than 1. This imposes the following condition on the steepness

$$ka < \frac{1}{\sqrt{2}} \cong 0.707 \tag{5.29}$$

However, making use also of the exponential term in the second last lines of Eqs. (5.23) and (5.26), we find that the tolerance

$$e = (1 - ka)e_0 \tag{5.30}$$

is applicable if

$$e^{kz_0} < \frac{1}{\sqrt{2}} \quad \Rightarrow \quad z_0 < \frac{\ln\left(\frac{1}{\sqrt{2}}\right)}{k} = \frac{1}{2\pi}\ln\left(\frac{1}{\sqrt{2}}\right)\lambda \cong -\frac{\lambda}{18} \tag{5.31}$$

Eq. (5.30) is applicable for all theoretically allowable values of ka, i.e. $0 \le ka < 1$. Making use of $k = 2\pi/\lambda$ in Eq. (5.31) yields the following conditions on z_0 for the limits of the interval in ka not covered by Eqs. (5.28) and (5.29)

$$\begin{aligned} ka = 1 \quad &\Rightarrow \quad -a = -\frac{1}{2\pi}\lambda \cong -\frac{\lambda}{6} \quad &\Rightarrow \quad z_0 < -\frac{a}{3} \\ ka = \frac{1}{\sqrt{2}} \quad &\Rightarrow \quad -a = -\frac{1}{2\sqrt{2}\pi}\lambda \cong -\frac{\lambda}{9} \quad &\Rightarrow \quad z_0 < -\frac{a}{2} \end{aligned} \tag{5.32}$$

Therefore, Eq. (5.30) will always ensure that an accuracy of e_0 is obtained for $0 \le ka < 1$ and $z_0 < -a/2$. However, the correct value of z_0 is still unknown. Inserting z_0 from Eq. (5.32) into Eq. (5.11) yields for the worst case $\theta = 3\pi/2$ (trough)

$$ka = 1 \quad \Rightarrow \quad z = -\frac{a}{3} - ae^{-k\left(\frac{a}{3}\right)} \approx -1.05a$$

$$ka = \frac{1}{\sqrt{2}} \quad \Rightarrow \quad z = -\frac{a}{2} - ae^{-k\left(\frac{a}{2}\right)} \approx -1.21a \tag{5.33}$$

Therefore, Eq. (5.30) may be used for cases where $0 \le ka < 1$ and $z < -5/4a$ (approximately). Cases where both $0.707 \le ka < 1$ and $z > -5/4a$ may therefore require special attention with respect to the accuracy of the obtained values. Recall that $z = 0$ a distance $\frac{1}{2}ka^2$ above the still water level in this case.

Eqs. (5.28) - (5.33) show that it is not possible to ensure a certain accuracy of $(x_{0t,m}, z_{0t,m})$ for all values of ka and (x_t, z_t), based on the easily controllable accuracy of $(x_{t,m}, z_{t,m})$ alone. Also, Eq. (5.24) assumes that the method actually converges. A formal argument why this method will converge has not been found, but one may easily be convinced of its convergence (when the point is in water) by studying the above scheme and considering some examples. In principle, it is possible to find accurate values at any point for any steepness by performing enough iterations.

Some examples of the necessary number of iterations are given in the tables below. $\theta = (\omega t - kx_0 + \varepsilon)$ is the phase of the Lagrangian point occupying the Eulerian point. The examples are all chosen to yield $x_0 = z_0 = 0$, i.e. surface "particles", making the accuracy easily controllable. This is convenient in order to ensure that the desired accuracy is obtained also for the last five rows of Table 5-3 and Table 5-4, as well as the last row of Table 5-1 and Table 5-2. These are cases where neither Eq. (5.28) nor Eq. (5.30) are applicable, since $ka > 0.707$ and $z_0 = 0$. For the other cases, i.e. $ka = 0.1$ and $ka = 0.5$, Eqs. (5.28) and (5.29) are applied.

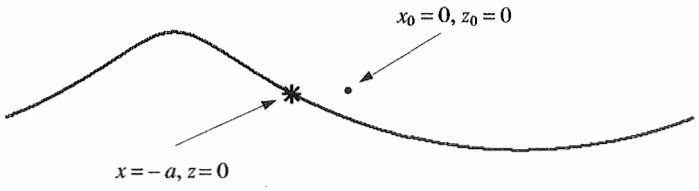

Figure 5.8 Spatial plot $\eta(x)$ of the surface. The dot represents the orbital centre of the path of the Lagrangian point ("particle") occupying the Eulerian point represented by the star, at $\theta = 0$.

Table 5-1 Necessary number of iterations (m) for the case in Figure 5.8.

	$e_0 = 10^{-6}\,a$	$e_0 = 10^{-3}\,a$	$e_0 = 10^{-2}\,a$
$ka = 0.1$	6	3	2
$ka = 0.5$	21	11	7
$ka = 0.9$	116	50	29

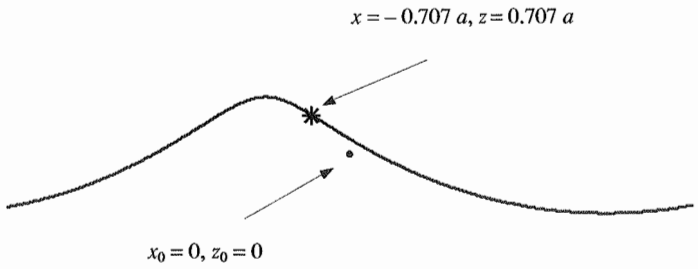

Figure 5.9 As Figure 5.8, but with $\theta = \pi/4$.

Table 5-2 Necessary number of iterations (m) for the case in Figure 5.9.

	$e_0 = 10^{-6}\ a$	$e_0 = 10^{-3}\ a$	$e_0 = 10^{-2}\ a$
$ka = 0.1$	5	3	1
$ka = 0.5$	21	11	8
$ka = 0.9$	120	56	34

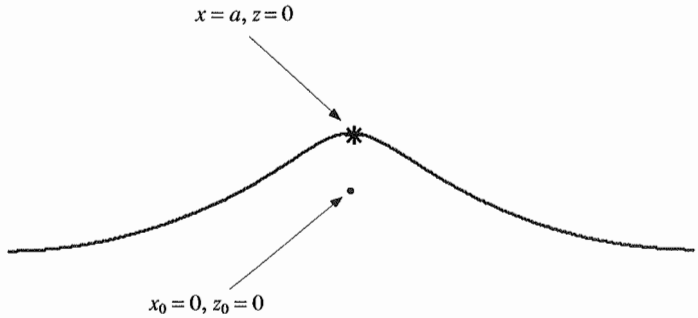

Figure 5.10 As Figure 5.8, but with $\theta = \pi/2$.

Table 5-3 Necessary number of iterations (m) for the case in Figure 5.10.

	$e_0 = 10^{-6}\ a$	$e_0 = 10^{-3}\ a$	$e_0 = 10^{-2}\ a$
$ka = 0.1$	6	3	2
$ka = 0.5$	22	12	9
$ka = 0.9$	129	64	42
$ka = 0.95$	261	127	82
$ka = 0.98$	645	303	189
$ka = 0.99$	1.265	578	349
$ka = 0.999$	11.593	4.689	2.389

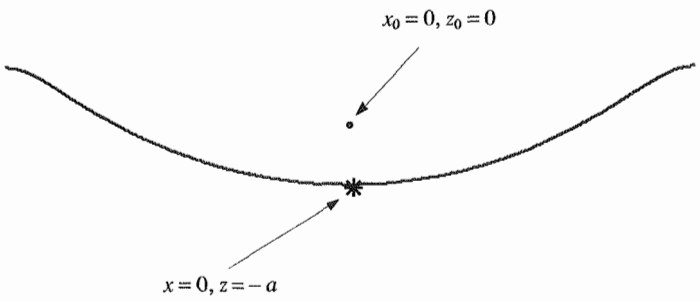

Figure 5.11 As Figure 5.8, but with $\theta = 3\pi/2$.

Table 5-4 Necessary number of iterations (m) for the case in Figure 5.11.

	$e_0 = 10^{-6}\,a$	$e_0 = 10^{-3}\,a$	$e_0 = 10^{-2}\,a$
$ka = 0.1$	5	2	1
$ka = 0.5$	20	10	6
$ka = 0.9$	114	49	27
$ka = 0.95$	222	88	45
$ka = 0.98$	522	182	77
$ka = 0.99$	983	300	107
$ka = 0.999$	7.594	1.094	178

It can be seen that the method converges very fast for all practically interesting cases in regular waves. It was also found that it is possible to find accurate solutions even as $(1 - ka)$ is close to 0 by letting the number of iterations approach infinity.

5.3.3 Irregular Gerstner waves

As stated in the beginning of Section 5.1, it is not theoretically consistent to include the vertical shifts in Gerstner's (or Miche's) solution when modelling irregular waves. The shifts are therefore ignored for the irregular case for now, and we return to an Eulerian frame of reference with $z = 0$ at the still water level. The calculations are therefore not exact as solutions of the problem, as the case was for regular Gerstner waves in Section 5.3.1. However, the iteration ensures that all spectral components may be included in an *equally* consistent manner anywhere in the fluid. Thus, the common problem of overprediction of high-frequency contributions near and above the still water level is eliminated. Appropriate spectral cut-off frequencies may then be based solely on considerations on e.g. component energies in the spectrum as well as on the range of validity of the dispersion relation.

In this section it is assumed that the Lagrangian amplitude spectrum, as well as the phases ε_n, are known.

It may not be obvious that the reasoning in Section 5.3.1 applies to the irregular case as well, but it turns out that

$$\begin{aligned} x^* &= x_0 - \sum_{n=1}^{N} a_n e^{k_n z_0} \cos(\omega_n t - k_n x_0 + \varepsilon_n + \pi) \\ z^* &= z_0 + \sum_{n=1}^{N} a_n e^{k_n z_0} \sin(\omega_n t - k_n x_0 + \varepsilon_n + \pi) \end{aligned} \tag{5.34}$$

mirror the image of

$$x = x_0 - \sum_{n=1}^{N} a_n e^{k_n z_0} \cos(\omega_n t - k_n x_0 + \varepsilon_n)$$
$$z = z_0 + \sum_{n=1}^{N} a_n e^{k_n z_0} \sin(\omega_n t - k_n x_0 + \varepsilon_n) \tag{5.35}$$

about (x_t, z_t), just as for the regular case which was shown in Figure 5.5. The method is therefore equally applicable for the irregular case, assuming that Eq. (5.5) is satisfied (Eq. (5.6) for Miche waves).

The iteration scheme for irregular Gerstner waves is

$$x_{0t,m+1} = x_t - \sum_{n=1}^{N} a_n e^{k_n z_{0t,m}} \cos(\omega_n t - k_n x_{0t,m} + \varepsilon_n + \pi)$$
$$z_{0t,m+1} = z_t + \sum_{n=1}^{N} a_n e^{k_n z_{0t,m}} \sin(\omega_n t - k_n x_{0t,m} + \varepsilon_n + \pi) \tag{5.36}$$

with initial values

$$x_{0t,0} = x_t, \quad z_{0t,0} = z_t \tag{5.37}$$

The new approximate values of (x_t, z_t) are

$$x_{t,m+1} = x_{0t,m} - \sum_{n=1}^{N} a_n e^{k_n z_{0t,m}} \cos(\omega_n t - k_n x_{0t,m} + \varepsilon_n)$$
$$z_{t,m+1} = z_{0t,m} + \sum_{n=1}^{N} a_n e^{k_n z_{0t,m}} \sin(\omega_n t - k_n x_{0t,m} + \varepsilon_n) \tag{5.38}$$

According to Eq. (5.28), an appropriate tolerance may be

$$e = \left|1 - \sqrt{2} f_{S(\omega),Gerstner}(k,a,\theta)\right| \varepsilon_0 \tag{5.39}$$

where the tolerances are defined as in Section 5.3.2, and

$$f_{S(\omega),Gerstner}(k,a,\theta) = \max\left[\sum_{n=1}^{N} k_n a_n \sin[\theta_n(x_0,t,\varepsilon_n)]\right] < 1 \tag{5.40}$$

is the maximum effective steepness based on Eq. (5.5) with $z_0 = 0$. θ_n are the phases of the spectral (Fourier) components. As in Eq. (5.29), Eq. (5.39) is then expected to be valid for

$$f_{S(\omega),Gerstner}(k,a,\theta) < \frac{1}{\sqrt{2}} \tag{5.41}$$

5.3.4 Regular and irregular Miche waves

Only the first order terms of Miche's solution are considered. According to Eq. (4.69) and related comments, we may assume that excluding the 2nd order terms in regular waves is correct when e.g. $ka > 0.2$ and $h/\lambda > 0.2$. For the irregular case it will anyhow be inconsistent

to include 2nd order terms. As for Gerstner waves, the constant vertical shift must be accounted for when comparing with experimental measurements for regular waves.

The scheme for regular (1st order) Miche waves is

$$\begin{aligned} x_{0t,m+1} &= x_t - a\frac{\cosh k(z_{0t,m}+h)}{\sinh kh}\cos(\omega t - kx_{0t,m} + \varepsilon + \pi) \\ z_{0t,m+1} &= z_t + a\frac{\sinh k(z_{0t,m}+h)}{\sinh kh}\sin(\omega t - kx_{0t,m} + \varepsilon + \pi) \end{aligned} \tag{5.42}$$

with initial values

$$x_{0t,0} = x_t, \quad z_{0t,0} = z_t \tag{5.43}$$

and new approximate values of (x_t, z_t)

$$\begin{aligned} x_{t,m} &= x_{0t,m} - a\frac{\cosh k(z_{0t,m}+h)}{\sinh kh}\cos(\omega t - kx_{0t,m} + \varepsilon) \\ z_{t,m} &= z_{0t,m} + a\frac{\sinh k(z_{0t,m}+h)}{\sinh kh}\sin(\omega t - kx_{0t,m} + \varepsilon) \end{aligned} \tag{5.44}$$

The appropriate tolerance corresponding to Eq. (5.28) is

$$e = \left(1 - \sqrt{2}ka\frac{\cosh kh}{\sinh kh}\right) e_0 \tag{5.45}$$

which for some limiting values of h/λ requires (approximately)

$$\begin{aligned} h/\lambda > 0.2 \quad &\Rightarrow \quad e = \left(1 - \frac{5}{3}ka\right) e_0 \quad \Rightarrow \quad 0.2 < ka < 0.6 \\ h/\lambda > 0.1 \quad &\Rightarrow \quad e = \left(1 - \frac{5}{2}ka\right) e_0 \quad \Rightarrow \quad 0.25 < ka < 0.4 \\ h/\lambda > 0.05 \quad &\Rightarrow \quad e = (1 - 5ka)\, e_0 \quad \Rightarrow \quad 0.3 < ka < 0.2 \end{aligned} \tag{5.46}$$

The lower limits of ka in Eq. (5.46) are determined by Eq. (4.69). The upper limits are determined by requiring that the term in the parenthesis in Eq. (5.45) is positive and less than 1. It can be seen that the requirement on ka for $h/\lambda = 0.05$ is illegal. Eq. (5.45) can therefore only be used for $h/\lambda > 0.1$ (approximately). Note that the 2nd order vertical shift is not included in Eqs. (5.42) and (5.44), meaning that the vertical Eulerian coordinate is here defined by $z = 0$ a distance $\frac{1}{2}ka^2\cosh kh/\sinh kh$ above the still water level, cf. Eq. (4.61). This is not quite in accordance with the definition of the Eulerian frame of reference form Miche's solution, but it simplifies the iteration scheme and has no effect on the results of the iteration to second order.

For irregular (1st order) Miche waves, where $z = 0$ at the still water level, the iteration scheme is

$$x_{0t,m+1} = x_t - \sum_{n=1}^{N} a_n \frac{\cosh k_n(z_{0t,m}+h)}{\sinh k_n h}\cos(\omega_n t - k_n x_{0t,m} + \varepsilon_n + \pi)$$
$$z_{0t,m+1} = z_t + \sum_{n=1}^{N} a_n \frac{\sinh k_n(z_{0t,m}+h)}{\sinh k_n h}\sin(\omega_n t - k_n x_{0t,m} + \varepsilon_n + \pi) \quad (5.47)$$

with initial values

$$x_{0t,0} = x_t, \quad z_{0t,0} = z_t \quad (5.48)$$

and new approximate values of (x_t, z_t)

$$x_{t,m+1} = x_{0t,m} - \sum_{n=1}^{N} a_n \frac{\cosh k_n(z_{0t,m}+h)}{\sinh k_n h}\cos(\omega_n t - k_n x_{0t,m} + \varepsilon_n)$$
$$z_{t,m+1} = z_{0t,m} + \sum_{n=1}^{N} a_n \frac{\sinh k_n(z_{0t,m}+h)}{\sinh k_n h}\sin(\omega_n t - k_n x_{0t,m} + \varepsilon_n) \quad (5.49)$$

A tolerance corresponding to Eq. (5.45) is

$$e = \left|1 - \sqrt{2} f_{S(\omega),Miche}(k,a,\theta)\right| e_0 \quad (5.50)$$

where

$$f_{S(\omega),Miche}(k,a,\theta) = \max\left[\sum_{n=1}^{N} k_n a_n \frac{\cosh k_n h}{\sinh k_n h}\sin[\theta_n(x_0,t,\varepsilon_n)]\right] < 1 \quad (5.51)$$

cf. Eqs. (5.6) and (5.40). Eq. (5.50) is thus expected to be valid for

$$f_{S(\omega),Miche}(k,a,\theta) < \frac{1}{\sqrt{2}} \quad (5.52)$$

5.3.5 Points in the splash zone

When the Eulerian point in question is out of water, the method will either return converged values with $z_0 > (0 + e_0)$, which is unphysical, or simply not converge. The first alternative is easily checked and dealt with. If the method does not converge, the tables in Section 5.3.2 show that one may conclude that the point is out of water if the desired accuracy is not obtained after a specific number of iterations. MATLAB, which is the numerical tool applied in this work, may also return values as *NaN* ('not a number') or $\pm$ *inf* ('infinity') when the exponential terms grow beyond the numerical limits, and allows such values to be treated in a very simple manner.

Convergence to a specific accuracy for regular waves may be ensured e.g. by iteration until the error e in $(x_{t,m}, z_{t,m})$ satisfies Eqs. (5.28) and (5.29) for Gerstner waves and Eqs. (5.45) and (5.46) for Miche waves. However, the corresponding conditions for irregular Gerstner and Miche waves, as given by Eqs. (5.39) - (5.41) and Eqs. (5.50) - (5.52), respectively, have not been derived or verified properly. For practical purposes, it is therefore found preferable to choose a quite high accuracy, e.g. $e = 10^{-4}\, a$, and terminate the iteration if convergence it s not obtained after a maximum number of iterations, e.g. 100, for the regular as well as the

irregular case. The iteration itself is then practically "exact". However, for irregular waves, this is still the solution of the linearized governing equations only.

Therefore, a point may be concluded to be out of water if

- the method converges but returns $z_0 > (0 + e_0)$
- convergence has not been obtained after e.g. 100 iterations
- returned values of x_0 and/or z_0 are *NaN* or $\pm inf$ (in MATLAB)

If the point is found to be out of water, one may in MATLAB e.g. set $z_0 = -inf$. Kinematics and pressure are thus assigned the value 0 when the point is out of water.

In addition to the tests on $(x_{t,m}, z_{t,m})$ described in Section 5.3.2, one may also check how the differences $(x_{0m+1} - x_{0m})$ and $(z_{0m+1} - z_{0m})$ behave, and stop the iteration when these are both less than e.g. e_0. However, choosing a specific accuracy e and a specific maximum number of iterations is still believed to be preferable and sufficient.

The iteration method described above may possibly be extended to the 3D case, although the increase in computational effort, especially for the irregular case, may be considerable.

A non-uniform mass transport, i.e. a Lagrangian current such as Stokes drift, may in principle also be included. However, this has not been done for two reasons; there is no obvious choice for the period of time the drift has acted, and the considerations in Section 4.3 suggests that superposing a non-uniform current on the wave solution may be theoretically inconsistent.

5.4 Wave Spectra and Timeseries of the Surface Elevation

As stated in the introduction to this chapter, we do not know the exact theoretical relation between the spectrum of the Lagrangian orbital motion of a specific "particle" and the spectrum of the surface elevation at a fixed Eulerian x-position. Since comparisons of theory with measurements are often based on the latter, it is of some importance to find whether there is a significant difference between these two types of spectra.

It is then reasonable to start with a timeseries of the surface elevation at a fixed x-position. A Fourier analysis of the timeseries, cf. Section 6.1.2, gives a set of components with amplitude a_n, circular frequency ω_n, wave number k_n and relative phase ε_n. We may then attempt to reproduce the timeseries of the surface elevation by considering the same spectrum as the Lagrangian orbital amplitude spectrum. This requires an iteration procedure similar to that presented in Section 5.3.

In Section 5.3, the unknowns were the Lagrangian coordinates (x_0, z_0) as functions of the known Eulerian coordinates (x, z). However, now the unknowns are x_0 and z, while z_0 and x are known. Since we consider the surface, we have that $z_0 = 0$ by definition. We may choose any value of x, and it is most convenient to consider $x = 0$. The relations between the different coordinates are still as given by Eq. (5.1), and inserting the present values of z_0 and x gives the following implicit problem

$$x_0(t) = \sum_{n=1}^{N} a_n \cos(\omega_n t - k_n x_0(t) + \varepsilon_n) \tag{5.53}$$

This may be formulated as an iteration scheme, viz.

$$x_{0,m+1}(t) = \sum_{n=1}^{N} a_n \cos(\omega_n t - k_n x_{0,m}(t) + \varepsilon_n) \tag{5.54}$$

where the initial values may be set as $x_{0,0}(t) = 0$ and iteration is performed e.g. until $|x_{0,m+1}(t) - x_{0,m}(t)| <$ 'a given tolerance'. For Miche waves we get

$$x_{0,m+1}(t) = \sum_{n=1}^{N} a_n \frac{\cosh k_n h}{\sinh k_n h} \cos(\omega_n t - k_n x_{0,m}(t) + \varepsilon_n) \tag{5.55}$$

Solving Eq. (5.54)/(5.55) for each discrete t yields a vector x_0, which inserted into the expression for z in Eq. (5.1), still with $z_0 = 0$, yields the timeseries of the surface elevation $\eta(t)$ at x as

$$\eta(t) = \sum_{n=1}^{N} a_n \sin(\omega_n t - k_n x_0(t) + \varepsilon_n) \tag{5.56}$$

Eq. (5.56) is identical for Miche and Gerstner waves. The timeseries of Eq. (5.56) may now be compared with the original measured timeseries. We may also perform a Fourier analysis of the new timeseries in Eq. (5.56) in order to obtain the 'output' spectrum and phases of this process, and compare this with the 'input' spectrum and phases.

Figure 5.12 shows the measured surface elevation spectrum of Case 5 (run I18_23), cf. Table 6-1.

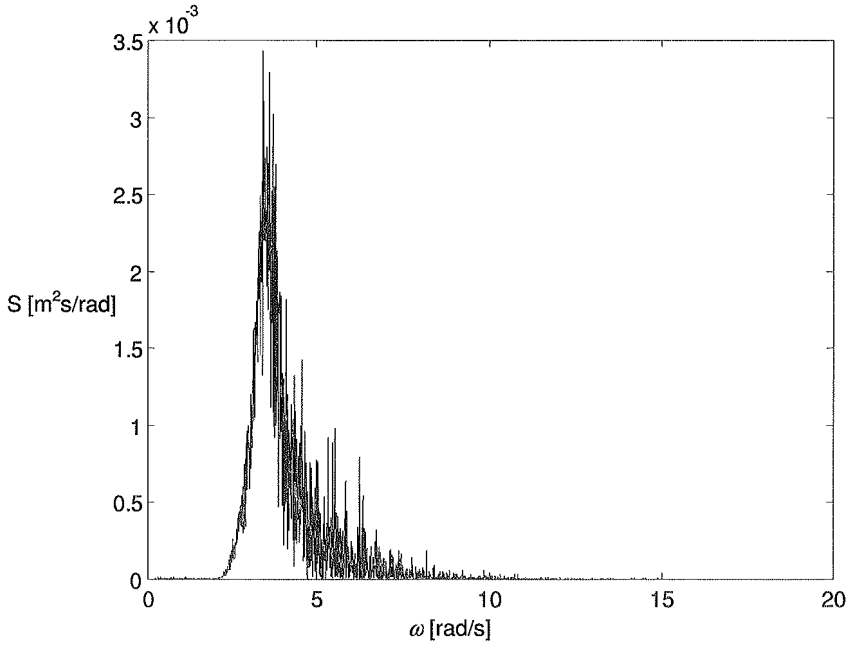

Figure 5.12 Raw spectrum of surface elevation, Case 5 (run I18_23), $T_p = 1.8$ s.

The highest value of the surface elevation in this experimental run, i.e. the highest crest, was found to lie at $t \approx 553.5$ s (the record has a total duration of 819.2 s). In Figure 5.13 is shown

a 20 second interval including this highest wave, while Figure 5.14 includes only the highest wave and the preceding and following waves.

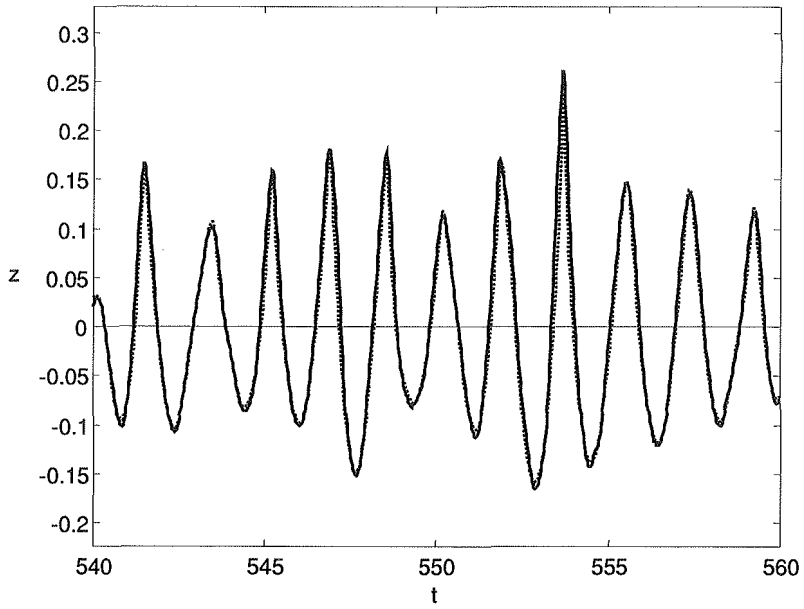

Figure 5.13 Measured timeseries in solid line, timeseries reproduced by Eqs. (5.54) and (5.56) in dotted line. Case 5 (run I18_23).

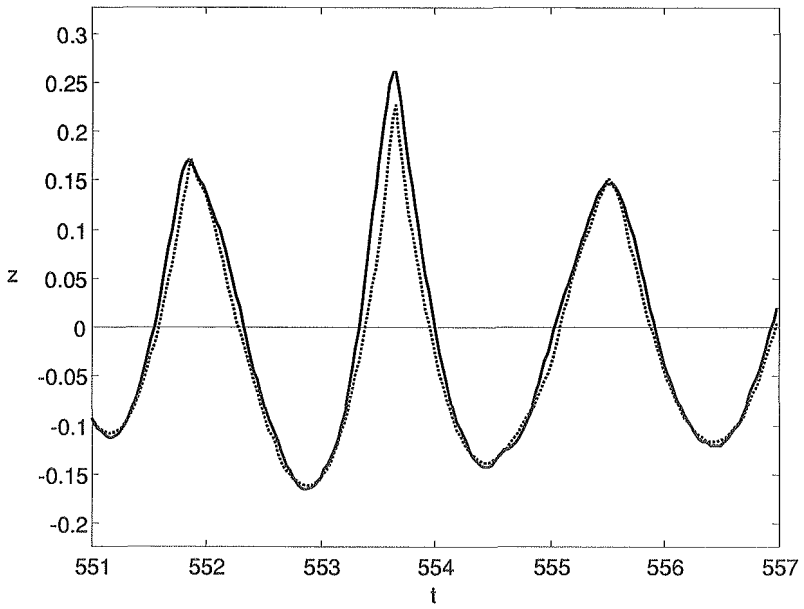

Figure 5.14 Excerpt from Figure 5.13, showing the highest crest of the timeseries.

It can be seen that the original timeseries is reproduced quite well, but not perfectly. The highest peak is clearly underestimated, while the other peaks are reproduced quite accurately. This is also evident from Figure 5.13 where several peaks are included. All frequency components are included in the example, from 0 to the Nyquist frequency. A considerably narrower frequency range is of course sufficient and physically more correct for practical purposes, and the results will only be slightly different from Figure 5.13 and Figure 5.14. Adding all components as Eulerian components, i.e. according to Eq. (5.4) with $x = 0$, reproduces the discrete points of the timeseries exactly.

The *timeseries* in the above figures is seen to qualitatively exhibit the same difference in steepening of crests and flattening of troughs as the *spatial snapshots* in Section 5.1. Hence, the difference between a Lagrangian and Eulerian description is apparent in the time domain as well as in the spatial domain. Simulations based on a synthetic spectrum reveal that this difference prevails even if the spectrum is divided into more frequency components with smaller amplitudes. Figure 5.1 - Figure 5.3 show that these differences stem from the interactions between components, and comparing Eq. (5.56) with Eq. (5.4) shows that they are governed by the phase, i.e. x vs. x_0.

Therefore, the "true" Lagrangian orbital amplitude spectrum differs somewhat from the Eulerian surface elevation spectrum, and it seems to be a very complex task to obtain one from the other, if possible at all. Still, the measured Eulerian spectrum is found to be a reasonable approximation to the Lagrangian input spectrum, as seen in the above figures, and is therefore applied as such in the calculations presented in Section 6.3. Peak values of quantities that are in phase with the surface elevation should then be reproduced quite well, e.g. the horizontal velocity. Ways of modifying the experimentally measured spectrum in order to get something closer to the "true" Lagrangian spectrum has therefore not been considered here. The results for irregular waves in Chapter 6 must be interpreted and discussed with this in mind.

However, ocean waves are often measured by buoys, and wave spectra based on such measurements may be considered more Lagrangian than Eulerian, and typical design spectra are anyhow subject to uncertainties. Hence, even if perfect agreement between Eulerian measurements and calculations based on Lagrangian expressions may be difficult to obtain, the Lagrangian approach should be very well suited for simulations and practical design purposes.

CHAPTER 6

COMPARISONS OF THEORY WITH MEASUREMENTS

6.1 Experiments, Analysis and Calculations

6.1.1 The experiments

The measurements used for the comparisons are from the extensive experiments carried out by Skjelbreia et al. (1991), where water particle velocities were measured using a laser doppler velocimeter (LDV). A more detailed description of the experiments may be found in Skjelbreia (1991), only a summary is given here.

The experiments were carried out in a wave tank at the Norwegian Hydrotechnical Laboratory (NHL, now SINTEF Civil and Environmental Engineering, Department of Coastal and Ocean Engineering) in Trondheim, cf. Figure 6.1.

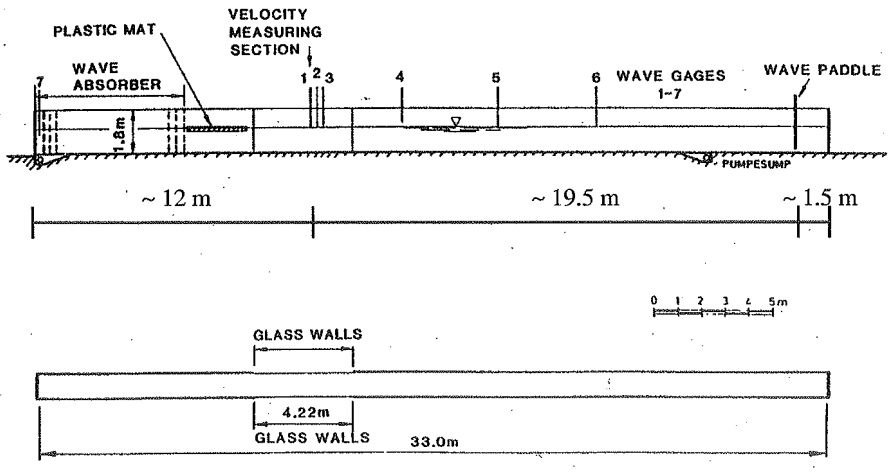

Figure 6.1 The wave tank at NHL (from Skjelbreia et al., 1991).

The tank is 33 m long, 1.02 m wide and 1.8 m deep. It is constructed of concrete with a glass section 4.22 m long, located approximately 10 m from the end of the tank, that allows viewing over the entire depth. The wavemaker is hydraulically driven, and can be discretely varied from a pure hinge mode to a pure piston mode. The wave absorber at the end of the tank consists of a series of vertical perforated steel plates, having a reflection coefficient of approximately 5% for the frequency range containing significant energy in these experiments. In addition, a floating plastic mat 2.5 m long was placed in front of the wave absorber, in order to reduce high frequency reflections from the absorber as well as cross waves.

The surface elevation was measured with standard resistive gages having streamlined supports to minimize disturbances. 7 wave gages were employed, cf. Figure 6.1. Wave gage 1 was placed at the longitudinal position of the LDV-station, but displaced 0.34 m from the centerline to avoid disturbances near the LDV measurement point. The wave gages 2, 3, 4, 5, 6 were placed to decompose incoming and reflected waves. Wave gage 7 was placed near the end of the tank to monitor the performance of the wave absorber.

Velocity measurements could be made in one point only for each experimental run. They were all made at the longitudinal position of wave gage 1, in a point on the centerline of the tank, whereas the vertical position of the measurement point could be varied from one run to another. The positioning of the LDV was accurate to ± 0.1 mm. The LDV measured the two velocity components u and w in a plane parallel to the side-walls of the tank. The LDV allowed measurements as close as 1-2 mm from the free surface, and the measurement volume had a cross-section diameter of approximately 100 μm. The accuracy of the velocity measurements were estimated to $\pm$ 0.005 m/s with better than 95% confidence. However, there are occasions when a lack of sufficient matter in the measurement volume, or possibly oversized particles passing through the measurement volume, results in erroneous measurements (Skjelbreia, 1991). These may be recognized e.g. as clearly deviating spikes in the timeseries. See Skjelbreia (1991) for further details on the technical and functional aspects of the LDV.

The surface elevation and LDV-data were sampled at a rate of 40 Hz without any filtering.

The test program consisted of nine wave conditions (cases), cf. Table 6-1. Six were irregular wave cases, two were regular wave cases and one case considered two-component waves. Approximately 30 runs were recorded for each case, yielding a total of 269 runs, with velocity measurements at several vertical levels for each case. The input control signal to the wavemaker was constructed from a JONSWAP spectrum using $\gamma = 3.0$. The spectrum was divided into 1000 frequency components, each assigned a random phase. The water level was maintained for each run to within $\pm$ 1 mm, and a period of 20-30 minutes elapsed between consecutive runs to maintain reproducibility of the runs. The latter is of importance when constructing a snapshot of the flow throughout the depth, since measurements of the velocities could only be performed in one point for each run. The water depth h was 1.3 m, except for in two cases where it was 0.6 m. The bottom in the tank is horizontal. Each run had a duration of 819.2 s, yielding $32.768 = 2^{15}$ sample points.

The velocity measurements were made at vertical levels in the region $-1.105 < z < 0.22$ for the cases where $h = 1.3$ m, and $-0.40 < z < 0.125$ for the two cases where $h = 0.6$ m ($z = 0$ at the still water level and $z = -h$ at the bottom).

Based on the peak period, all cases may be classified as 'intermediate water' cases. Cases 1, 2 and 8 are relatively close to the 'deep water' limit, while Cases 4, 6 and 7 are closer to the 'shallow water' limit.

Runs from Cases 2, 5, 6, 8 and 9 were available for the comparisons in this thesis.

Table 6-1 Test program in Skjelbreia et al. (1991). The identifyer of each case in the first column is as given by Skjelbreia. For Cases 7, 8 & 9; $T_p = T$. For Cases 8 & 9; $H_S = H$. The last two columns indicate the region of applicability of different wave theories according to Dean (1970).

Case	Wave conditions	T_p [s] (input values)	H_S [m] (measured values)	h [m]	$\frac{H_S}{gT_p^2}$	$\frac{h}{gT_p^2}$
1: I12	Irregular	1.2	0.11	1.3	0.0078	0.092
2: I14	Irregular	1.4	0.16	1.3	0.0082	0.068
3: I165	Irregular	1.65	0.17	1.3	0.0064	0.049
4: SI165	Irregular	1.65	0.17	0.6	0.0064	0.022
5: I18	Irregular	1.8	0.21	1.3	0.0066	0.041
6: I24	Irregular	2.4	0.25	1.3	0.0044	0.023
7: I2124	Two-component	2.1 & 2.4	0.18	1.3	0.0036 (average)	0.026 (average)
8: R15B	Regular	1.5	0.26	1.3	0.0118	0.059
9: SR15	Regular	1.5	0.23	0.6	0.0104	0.027

With reference to Section 6.1.2 below, Table 6-2 shows the characteristics of the original timeseries recorded by Skjelbreia et al. (1991).

Table 6-2 Characteristics of the original timeseries in Skjelbreia et al. (1991)

N	$N/2$	T_N	Δt	f_{Sample}	$f_{Nyquist}$	$\omega_{Nyquist}$
$32.768 = 2^{15}$	$16.384 = 2^{14}$	819.2 s	0.025 s	40 Hz	20 Hz	127.5 rad/s

We may of course choose to analyze only excerpts of the measured timeseries. N, $N/2$ and T_N must then be based on the excerpt, while Δt, f_{Sample}, $f_{Nyquist}$ and $\omega_{Nyquist}$ remain as in Table 6-2.

6.1.2 Obtaining component wave parameters by Fourier analysis of measured timeseries

The measured timeseries are analyzed in MATLAB using the FFT-function on the sampled timeseries. If the number of sample points is a power of 2, this function performs a fast Fourier-transform. If the number of sample points is not a power of 2, the function performs a discrete Fourier-transform. Further details on the MATLAB-functions may be found e.g. by typing '*help FFT*' in the *MATLAB Command Window*.

The Fourier-transform of the timeseries $x(m)$ of length N is found by the FFT function as

$$F_x(n) = \sum_{m=1}^{N} x(m)\, e^{[-i2\pi(n-1)(m-1)/N]} \qquad 1 \le n \le N \tag{6.1}$$

The inverse Fourier transform is found in MATLAB by the function IFFT as

$$x(m) = \frac{1}{N} \sum_{n=1}^{N} F_x(n)\, e^{[i2\pi(n-1)(m-1)/N]} \qquad 1 \le m \le N \tag{6.2}$$

The timeseries is characterized by a number of sample points N, a total duration T_N, a temporal spacing between each sample Δt and a sampling frequency f_{Sample}, viz.

$$\Delta t = \frac{1}{f_{Sample}} = \frac{T_N}{N} \tag{6.3}$$

One objective here is to find (an estimate of) the amplitude spectrum of the process $x(m)$ as a function of the circular frequency, based on the Fourier-transform of the measured timeseries. Following Newland (1993), this spectrum $S(\omega_n)$ may be obtained as

$$S(\omega_n) = 2\frac{T_N}{2\pi}\left\langle \left\{\frac{\mathrm{Re}[F_x(n)]}{N}\right\}^2 + \left\{\frac{\mathrm{Im}[F_x(n)]}{N}\right\}^2 \right\rangle \qquad 1 \le n \le \frac{N}{2}+1 \tag{6.4}$$

where the arguments ω_n are given by

$$\omega_n = \frac{2\pi(n-1)}{T_N} = \frac{2\pi(n-1)}{N\Delta t} = \frac{2\pi f(n-1)}{N} \qquad 1 \le n \le \frac{N}{2}+1 \tag{6.5}$$

The factor 2 in Eq. (6.4) appears because the spectrum is the one-sided spectrum, i.e. with positive arguments ω_n only. The maximum number of components is then $N/2 + 1$, hence the limits of n in Eqs. (6.4) and (6.5).

The Nyquist frequency is the maximum frequency that can be detected from a timeseries sampled at the rate f_{Sample}, and is found as

$$f_{Nyquist} = \frac{f_{Sample}}{2} \tag{6.6}$$

The circular Nyquist frequency is found as

$$\omega_{Nyquist} = 2\pi\frac{f_{Sample}}{2} = 2\pi\frac{1}{2\Delta t} = 2\pi\frac{N}{2T_N} = \frac{2\pi}{T_N}\frac{N}{2} \tag{6.7}$$

confirming the limits of n in the preceding equations This is irrespective of whether N and T_N represents the whole timeseries or only excerpts of it, as long as Δt is fixed.

The component amplitudes may now be found as

$$a_n = \sqrt{2S(\omega_n)\Delta\omega} \qquad 1 \le n \le \frac{N}{2}+1 \tag{6.8}$$

where $\Delta\omega$ is given by

$$\Delta\omega = \frac{2\pi}{T_N} \tag{6.9}$$

and is equal for all components.

Common Eulerian analysis normally make use of transfer-functions and inverse Fourier-transforms, meaning that it is not necessary to find the relative phases between the different components explicitly. However, the Lagrangian analysis require explicit knowledge of the relative phases ε_n. Whereas phase-information cannot be found from the spectrum alone, the

relative phases may still be found based on the form of a Fourier-series and knowledge of the Fourier-transforms. The Fourier-series representing the surface elevation, i.e. equivalent to Eq. (6.2) with $\eta(m)$ instead of $x(m)$, is

$$\eta(m)= a_1 + \sum_{n=2}^{N/2} A_n \cos\left[\frac{2\pi(n-1)\ t}{T_N}\right] + B_n \sin\left[\frac{2\pi(n-1)\ t}{T_N}\right] \qquad 1 \le m \le N \qquad \textbf{(6.10)}$$

where a_1, A_n and B_n are related to the Fourier-transform in Eq. (6.1) as

$$a_1 = \frac{F_\eta(1)}{N}, \quad A_n = 2\frac{\mathrm{Re}[F_\eta(n)]}{N}, \quad B_n = -2\frac{\mathrm{Im}[F_\eta(n)]}{N} \qquad \textbf{(6.11)}$$

Eq. (6.10) may also be written

$$\eta(m)= a_1 + \sum_{n=2}^{N/2} a_n \sin\left[\frac{2\pi(n-1)\ t}{T_N} + \varepsilon_n\right] \qquad 1 \le m \le N \qquad \textbf{(6.12)}$$

where a_n are the component amplitudes of Eq. (6.8) and a_1 is the mean value of the timeseries.

The relative phases are now found as

$$\varepsilon_n = \tan^{-1}\left\{\frac{\mathrm{Im}[F_x(n)]}{\mathrm{Re}[F_x(n)]}\right\} - sign\{\mathrm{Im}[F_x(n)]\} \cdot \langle 1 - sign\{\mathrm{Re}[F_x(n)]\}\rangle \cdot \pi + \frac{\pi}{2} \qquad 2 \le n \le \frac{N}{2}+1 \qquad \textbf{(6.13)}$$

where *sign* returns the sign of the term in the brackets, i.e. +1 or –1. The last term $\pi/2$ on the right-hand side of Eq. (6.13) is due to the use of *sin* in Eq. (6.12), since the real part is given by *cos*. The *sin*-form is chosen because this is how the phase of vertical displacement, and thus the leading order term of the surface elevation, is defined in this thesis.

The wave numbers k_n are found from the dispersion relation, given by Eq. (4.17) for Gerstner components and Eq. (4.66) for Miche components, viz.

$$\begin{aligned} &\text{Gerstner:} \quad k_n = \frac{\omega_n^2}{g} \qquad 1 \le n \le \frac{N}{2}+1 \\ &\text{Miche:} \quad k_n = \frac{\omega_n^2}{g}\tanh k_n h \qquad 1 \le n \le \frac{N}{2}+1 \end{aligned} \qquad \textbf{(6.14)}$$

The wavelengths and wave periods of the components may also be found as usual, viz.

$$\lambda_n = \frac{2\pi}{k_n}, \quad T_n = \frac{2\pi}{\omega_n} \qquad 1 \le n \le \frac{N}{2}+1 \qquad \textbf{(6.15)}$$

Note that Eqs. (6.14) and (6.15) are not physically correct for the very highest frequencies, i.e. $\omega_n > 60$ rad/s, since the surface tension is then also of significance (capillary waves). The use of the dispersion relation is also questionable for the very lowest frequencies, since these waves cannot be assumed to be free gravity waves, at least not in a closed basin such as a wave flume. Skjelbreia (1991) found that the dispersion relation holds for the energetic parts of the spectra in the experiments in Skjelbreia et al. (1991).

6.1.3 Calculations for comparison of theory with measurements

The required component parameters a_n, ω_n, k_n and ε_n are now known from the analysis described in the previous section, determined by Eqs. (6.8), (6.5), (6.14) and (6.13), respectively. The appropriate discrete time instants t_m to apply are

$$t_m = (m-1)\Delta t = \frac{(m-1)}{f} \qquad 1 \le m \le N \tag{6.16}$$

By the method in Section 5.4 we may then determine which Lagrangian point constitutes the surface at a given Eulerian x-position at a given instant in time, as well as the actual value of the surface elevation, and thus reproduce a timeseries of the surface elevation.

By the iteration method in Section 5.3 we may further determine which Lagrangian point occupies a specific Eulerian position at a specific instant in time. The value of any quantity in this Eulerian position at this instant in time may then be found by inserting these Lagrangian coordinates into e.g. Eq. (5.3) for Gerstner waves, or into the corresponding equations for Miche waves. In this way it is possible to construct timeseries of the velocity, acceleration and pressure in any fixed Eulerian position, even in the splash zone, from the Lagrangian expressions, and compare with the measured timeseries. Similarly it is possible to determine e.g. instantaneous velocity profiles beneath crests and troughs. Quantities such as the mean horizontal velocity in a vertical cross-section may be found by producing timeseries and averaging over a chosen timeseries-interval. However, this would require a lot of computation. The mean horizontal velocity is therefore assumed to be adequately described by the approximations in Sections 4.1.5, 4.1.6, 4.2.2 and 4.2.3.

In the implementation of the iteration methods in Sections 6.2 and 6.3, the tolerance e_0 is set to 10^{-4} m. The procedures are terminated after 100 iterations if convergence has not been achieved.

It is believed that the conditions in a wave flume change continuously, from an initial state where waves are being generated to a situation where bound waves, reflections etc. are present. When studying instantaneous values, it therefore seems more informative to investigate individual incidents and how these develop in time, rather than to collect results from several incidents over longer timeseries-intervals. Also, mean values of quantities should be studied in a short-term sense as well as in a long-term sense. Cieslikiewicz and Gudmestad (1993, 1994a, 1994b, 1995, 1996) have performed extensive statistical analysis of the data from the experiments by Skjelbreia et al. (1991).

The comparisons in this thesis focus on the mean horizontal velocity, since this is of special importance with respect to the underlying theory, and on the instantaneous horizontal velocity beneath crests and troughs, since this may be of particular interest with respect to applied kinematics models such as Wheeler's method, cf. Section 5.2. These quantities are also those least subject to the differences between Eulerian measurements and calculations according to Lagrangian expressions, cf. Section 5.4, and therefore best suited for such comparisons.

Any other type of comparison is of course also possible, only limited by the computational effort in iterations and calculations.

6.2 Results for Regular Waves

This section presents the results for regular waves. The results are discussed in Section 7.3. The results pertain to the two regular wave cases in Table 6-1; Cases 8 and 9. In Case 8, the wave steepness ka is 0.24, the wavelength λ is 3.45 m and the depth-to-wavelength ratio h/λ

is 0.3. In Case 9, the wave steepness ka is also 0.24, the wavelength λ is 3.00 m and the depth-to-wavelength ratio h/λ is 0.20. Both cases pertain to intermediate water, and calculations are therefore performed according to Miche's theory. These values of ka and h/λ also allow use of the so-called simplified form of Miche's solution, cf. Eq. (4.69) and related comments and the introduction to Section 5.3.4.

Some quantities for the regular waves may be useful to have at hand:

The values of the vertical shifts are, cf. Eq. (4.61),

$$\begin{aligned} &\text{Case 8:} \quad \Delta z_{Miche,surface} = 0.0157\,\text{m} \\ &\text{Case 9:} \quad \Delta z_{Miche,surface} = 0.0163\,\text{m} \end{aligned} \tag{6.17}$$

the regular wave celerities are

$$\begin{aligned} &\text{Case 8:} \quad c = \frac{\omega}{k} = 2.3 \text{ m/s} \\ &\text{Case 9:} \quad c = \frac{\omega}{k} = 2.0 \text{ m/s} \end{aligned} \tag{6.18}$$

and the values of the assumed Stokes drift are, cf. Eq. (4.83),

$$\begin{aligned} &\text{Case 8:} \quad u_{Stokes\ drift} = 0.131 \frac{\cosh 2k(z_0 + h)}{\sinh 2kh} \quad \text{[m/s]} \\ &\text{Case 9:} \quad u_{Stokes\ drift} = 0.137 \frac{\cosh 2k(z_0 + h)}{\sinh 2kh} \quad \text{[m/s]} \end{aligned} \tag{6.19}$$

When comparing theory with wave flume measurements of kinematics, describing and interpreting the mean horizontal velocity in the flume correctly is of the utmost importance. The development of this mean velocity in regular waves is therefore given special attention in Section 6.2.1.

Instantaneous vertical profiles of the horizontal velocity beneath crests and troughs are presented in Section 6.2.2.

Finally, some measured and computed timeseries for fixed Eulerian points are compared in Section 6.2.3.

The measurements considered are all made at the longitudinal position of wave gage 1, cf. Figure 6.1, approximately 19.5 m from the wavemaker and 12 m from the end of the flume.

6.2.1 Mean horizontal velocity in a vertical cross-section

The purpose of this section is to show how the mean Eulerian horizontal velocity in the flume develops and changes nature as the experiments evolve.

The mean horizontal velocity in Miche waves is calculated according to Eqs. (4.77) and (4.78). It is also interesting to compare with the mean velocity predicted by Stokes waves, including Stokes drift, as given by Eqs. (4.77) and (4.86). This is done for Case 8 in Figure 6.2 and for Case 9 in Figure 6.3. Only calculations according to Miche are included in the comparisons with measurements, but the relation to Stokes waves is always as given by Figure 6.2 and Figure 6.3.

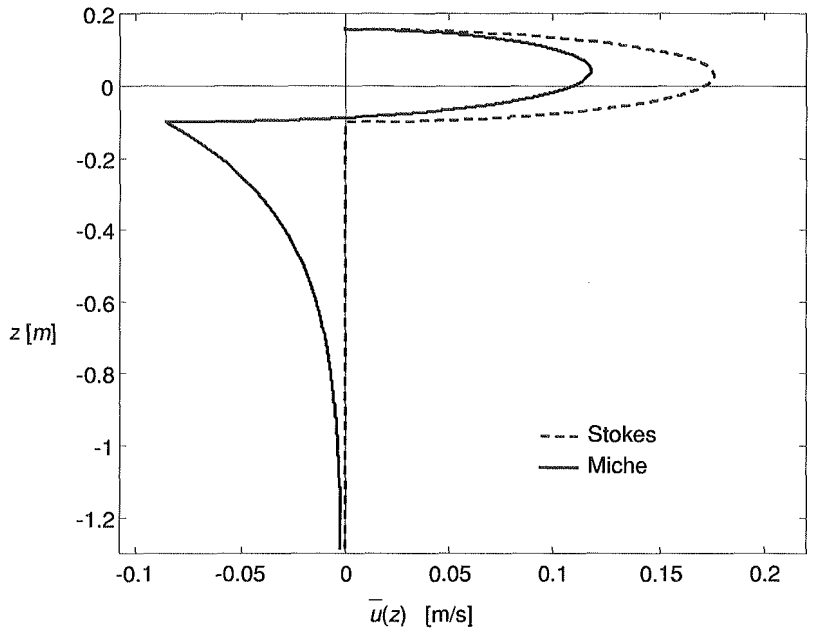

Figure 6.2 Mean Eulerian horizontal velocity in Case 8 according to Miche (–) and 2nd order Stokes waves including Stokes drift (- - -).

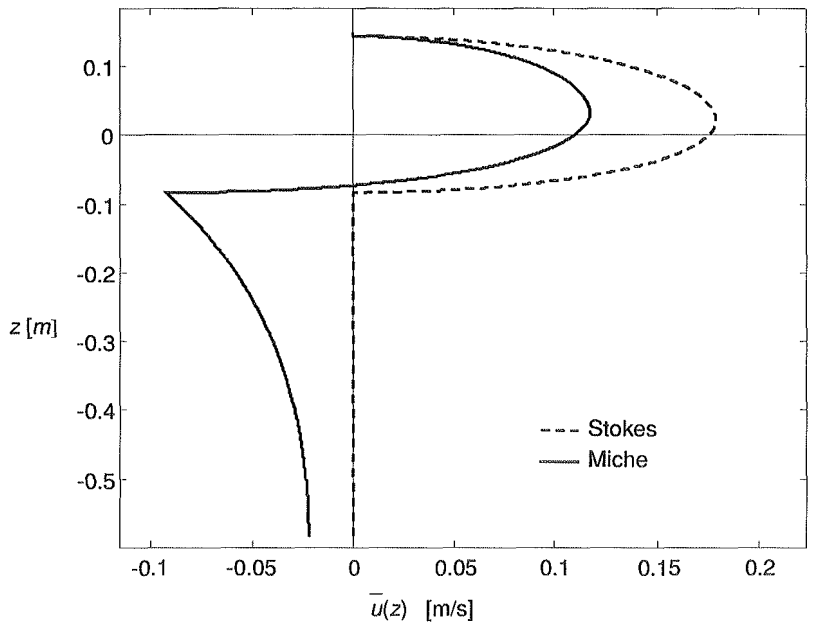

Figure 6.3 Mean Eulerian horizontal velocity in Case 9 according to Miche (–) and 2nd order Stokes waves including Stokes drift (- - -).

The averaging of velocity measurements is done over one wave period for the early parts of the records, and over ten wave periods later on. This makes it possible to identify the distinct changes in the early parts, and it gives a relatively detailed picture of the development later on while still smoothing out the most local variations. Presenting these results requires numerous plots, and these are therefore given in Appendix B. Case 8 (R15B) is there covered by Figure B.1 - Figure B.23, and Case 9 (SR15) is covered by Figure B.24 - Figure B.43. Only a few plots are included in this section, the actual timeseries-interval being given in each figure, and the reader is referred to Appendix B for a more detailed picture of the temporal development.

The typical initial part (first 60 seconds) of the surface elevation measurements in Case 8 is shown in Figure 6.4. It can be seen that the first disturbances arrive at gage 1, cf. Figure 6.1, after approximately 5-6 seconds, the wave front arrives after approximately 17-18 seconds, and a quite regular wave situation is apparently established after approximately 30 seconds.

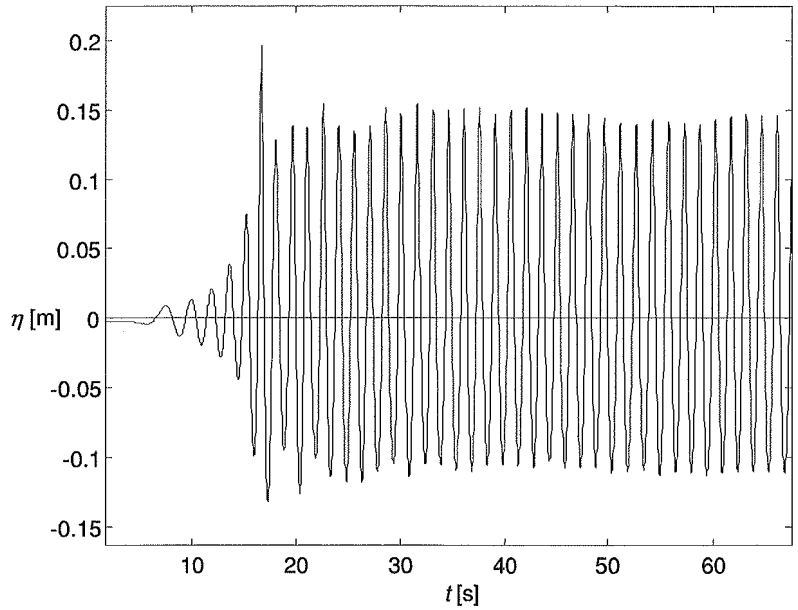

Figure 6.4 Typical first 60 seconds of the surface elevation measurements at wave gage 1 in Case 8 (figure based on run R15B_2).

The mean velocity is initially zero everywhere. No change is detected until the first disturbances in the surface elevation arrive, i.e. after approximately 5-6 seconds, cf. Figure 6.5. A distinct vertically uniform and positive (forward) mean velocity is then seen to appear. This positive mean velocity generally persists until the wave front passes, i.e. until after approximately 17-18 seconds. A distinct transition then takes place below the splash zone, cf. Figure 6.6. The mean velocity is now negative, but still practically vertically uniform, in this region. In the splash zone, the mean velocity profile is seen to take on a form similar to that predicted by Stokes waves, cf. Figure 6.2. The type of transition shown in Figure 6.6 is also reported by Johnsen (1987) and Gudmestad et al. (1988) for other regular wave experiments, and will from here on be referred to as "the first transition". The rather high negative value just above $z = 0$ in Figure 6.6 is invalid, and stems from spurious individual spikes that occur from time to time in the LDV-measurements in the splash zone, cf. Section 6.1.1. Investigation of the timeseries-interval yielding this specific mean value shows that this part of the measured signal is clearly invalid.

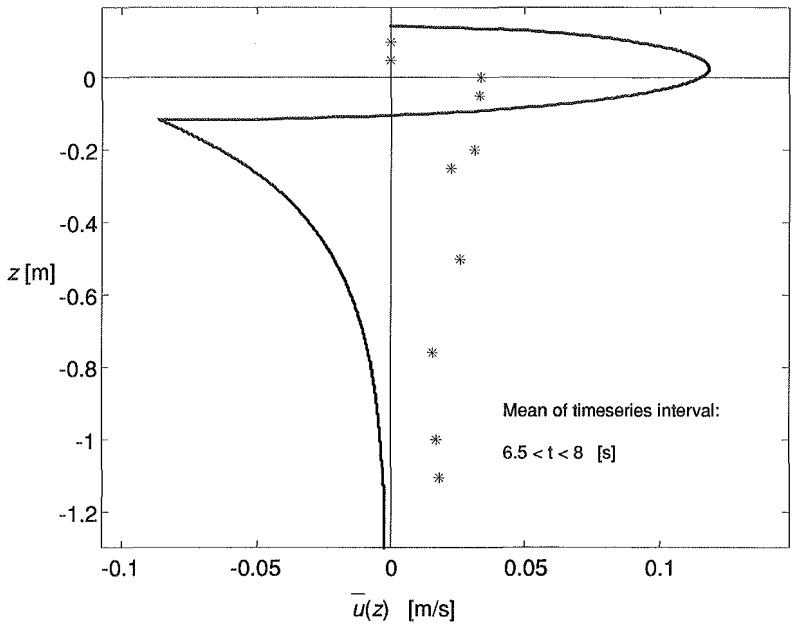

Figure 6.5 Measured (*) and calculated (–) mean horizontal velocity at wave gage 1, Case 8 (R15B), $6.5 < t < 8$ s.

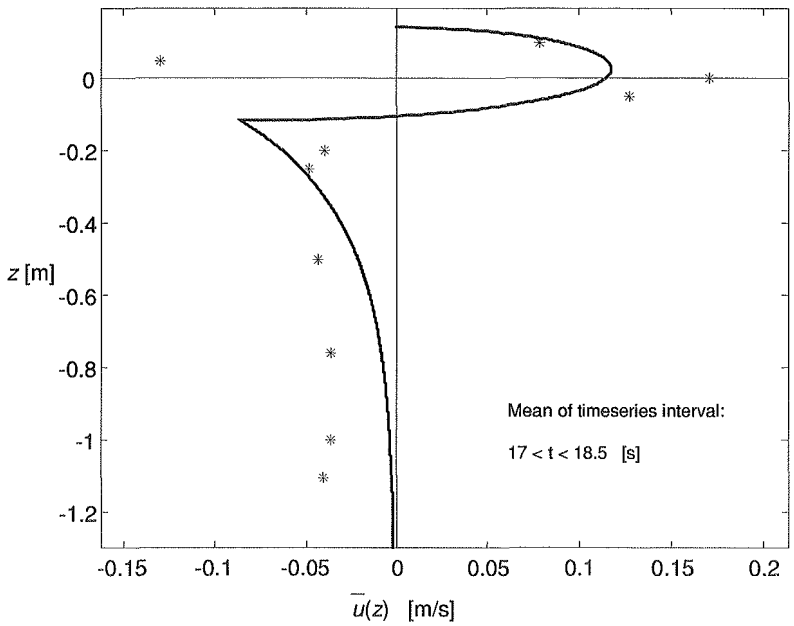

Figure 6.6 Measured (*) and calculated (–) mean horizontal velocity at wave gage 1, Case 8 (R15B), $17 < t < 18.5$ s.

When investigating the rest of the typical surface elevation measurements for Case 8, it is found that the waves generally appear to be quite regular, cf. Figure 6.7 and Figure 6.8. Some of the runs do however exhibit less regularity, while others are even more regular.

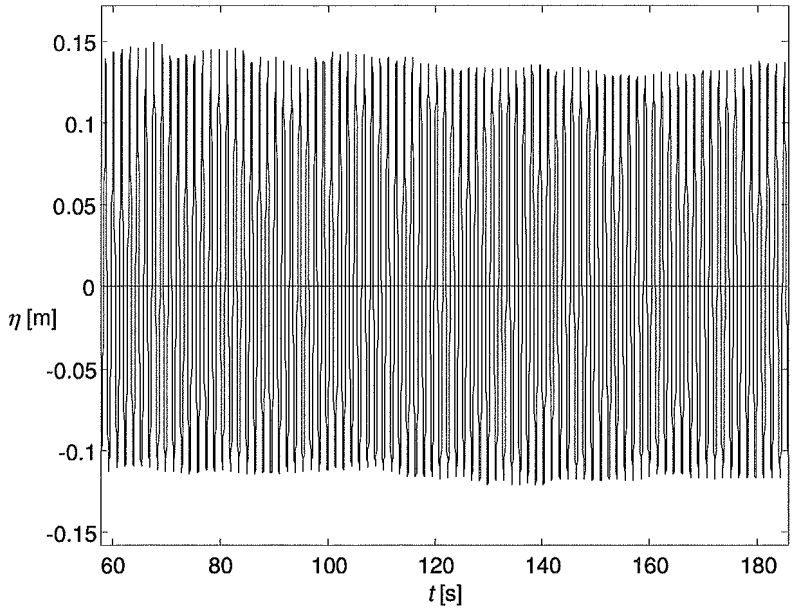

Figure 6.7 Typical surface elevation measurement at wave gage 1 for $60 < t < 180$ s in Case 8 (figure based on run R15B_2).

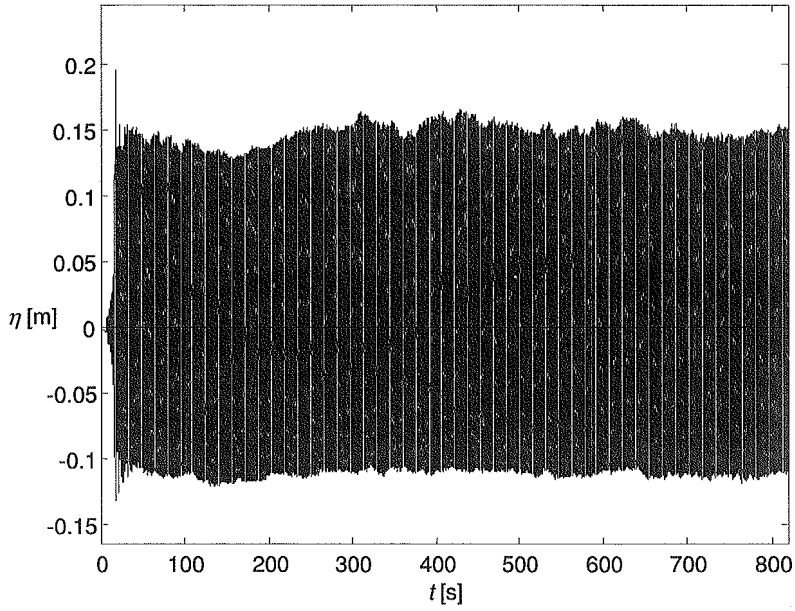

Figure 6.8 The whole surface elevation timeseries at wave gage 1, Case 8, run R15B_2.

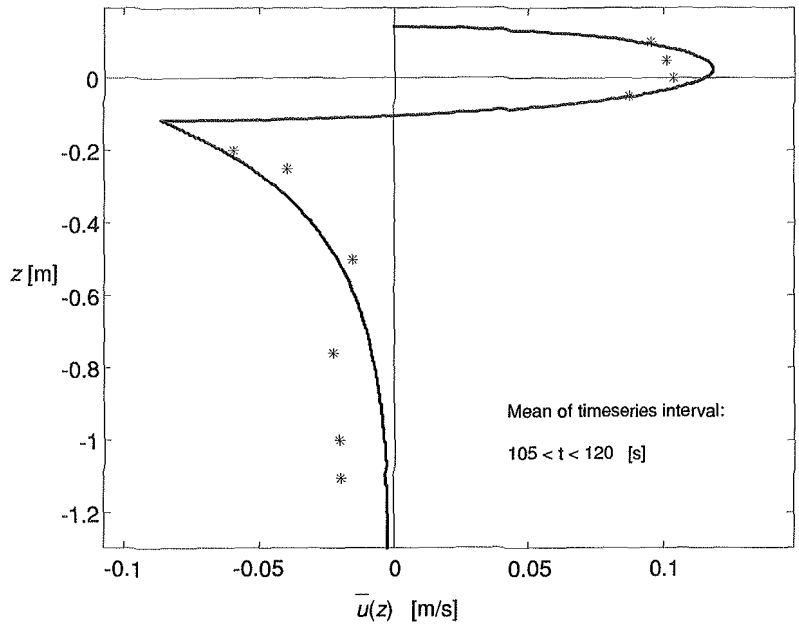

Figure 6.9 Measured (*) and calculated (–) mean horizontal velocity at wave gage 1, Case 8 (R15B), $105 < t < 120$ s.

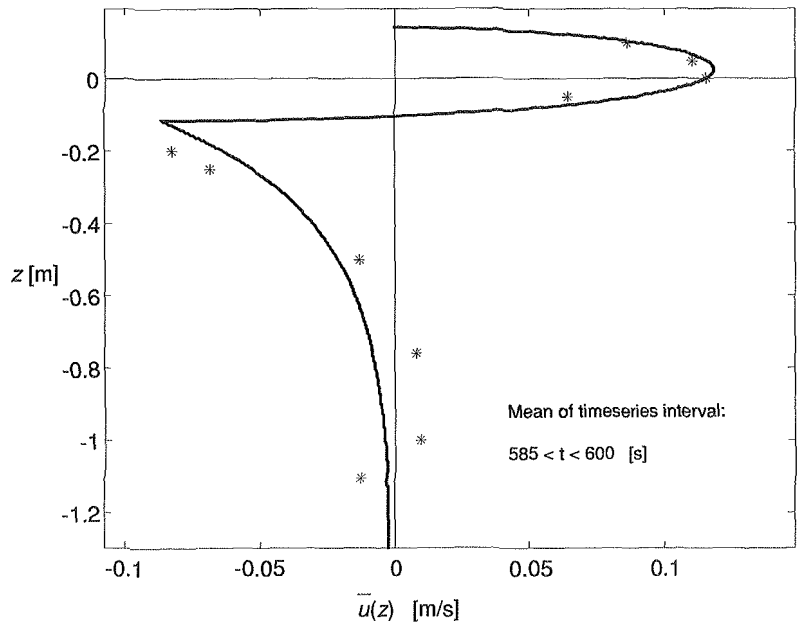

Figure 6.10 Measured (*) and calculated (–) mean horizontal velocity at wave gage 1, Case 8 (R15B), $585 < t < 600$ s.

As reported by Skjelbreia (1991), another quite distinct transition in the mean horizontal velocity takes place when roughly 50 waves have passed wave gage 1, yielding a mean velocity profile as in Figure 6.9. This will from here on be referred to as "the second transition". This transition actually takes place over some period of time, starting near the surface at $t \sim 75$ - 90 s and developing throughout depth until $t \sim 120$ - 135 s, cf. Appendix B. The mean horizontal velocity then appears to reach a steady state, except for near the bottom. A forward 'creeping flow' will eventually develop at the bottom due to viscosity, cf. Mei (1989, his Section 9.6), which may explain the change towards a positive mean velocity for the lower measurements points in Figure 6.10. It takes some time before such a creeping flow can be detected by the recordings, since the lowest measurement points are 19.5 cm above the bottom. However, the creeping flow is present at the bottom also prior to the timeseries-interval in Figure 6.10. Reproduction and video-filming of an experimental run as in Case 8, in the same flume and under the same conditions as the original experiments, reveals that the creeping flow "starts" at the bottom after approximately 105 seconds. The situation remains more or less as in Figure 6.10 for the rest of the records.

The typical initial part of the surface elevation measurements in Case 9 is shown in Figure 6.11.

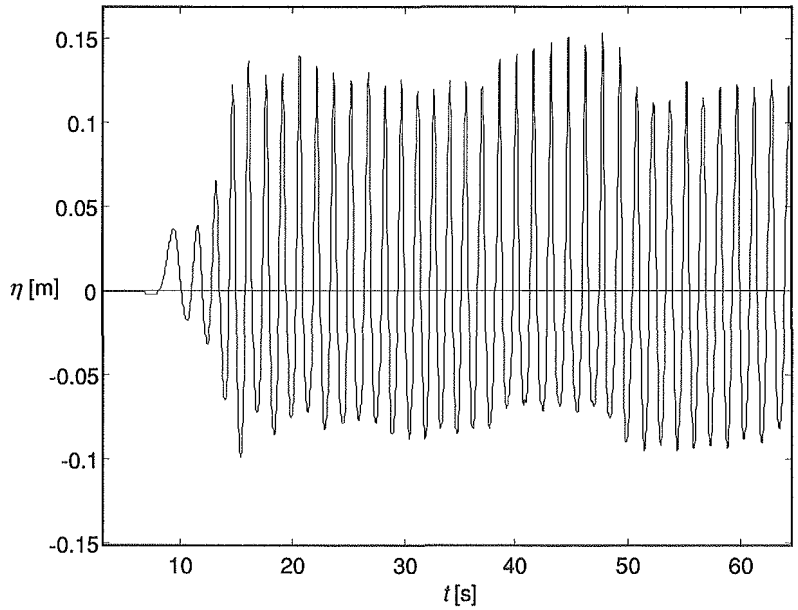

Figure 6.11 Typical first 60 seconds of the surface elevation measurements at wave gage 1 in Case 9 (SR15).

In Figure 6.11, the first disturbance arrives after 7-8 seconds, i.e. later than in Case 8, and a distinct wave front arrives after approximately 15 seconds, i.e. earlier than in Case 8. The surface elevation is clearly "non-regular" for this first minute of the record.

The evolution of the mean velocity now generally follows the pattern in Case 8. No mean horizontal velocity is registered until after approximately 7-8 seconds, i.e. as the first disturbances in the surface elevation arrive, but the magnitude of this first positive mean velocity is significantly higher than in Case 8, cf. Figure 6.12. In Figure 6.13 it is seen that the first transition takes place earlier in Case 9 than in Case 8, even if the wave celerity is now lower, suggesting that it is indeed associated with the wave front. The second transition also

takes place earlier in Case 9 than in Case 8, cf. Figure 6.14. The situation appears to remain as in Figure 6.14 for the rest of the records.

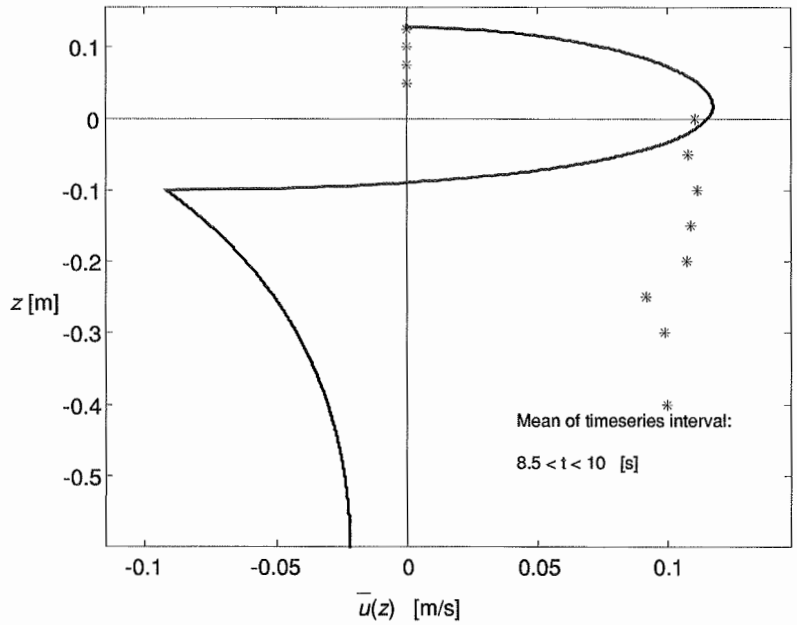

Figure 6.12 Measured (*) and calculated (–) mean horizontal velocity at wave gage 1, Case 9 (SR15), $8.5 < t < 10$ s.

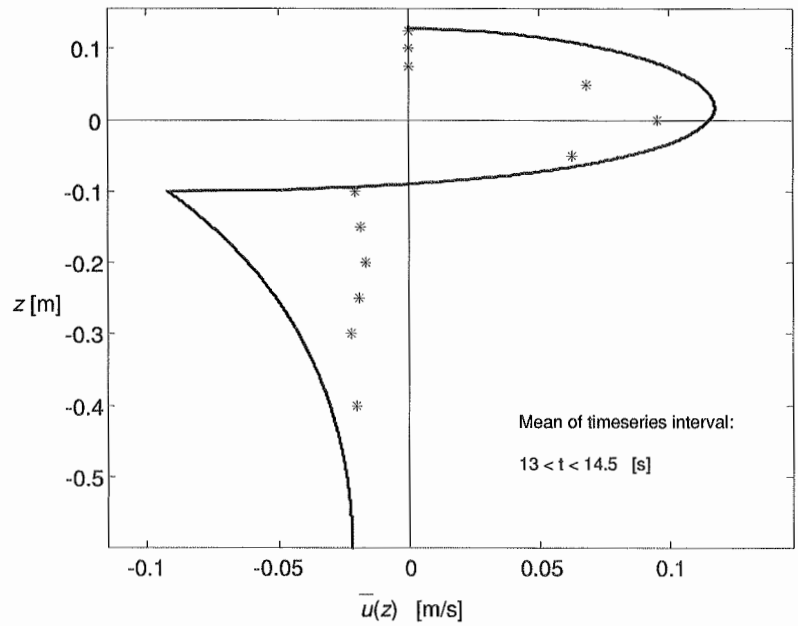

Figure 6.13 Measured (*) and calculated (–) mean horizontal velocity at wave gage 1, Case 9 (SR15), $13 < t < 14.5$ s.

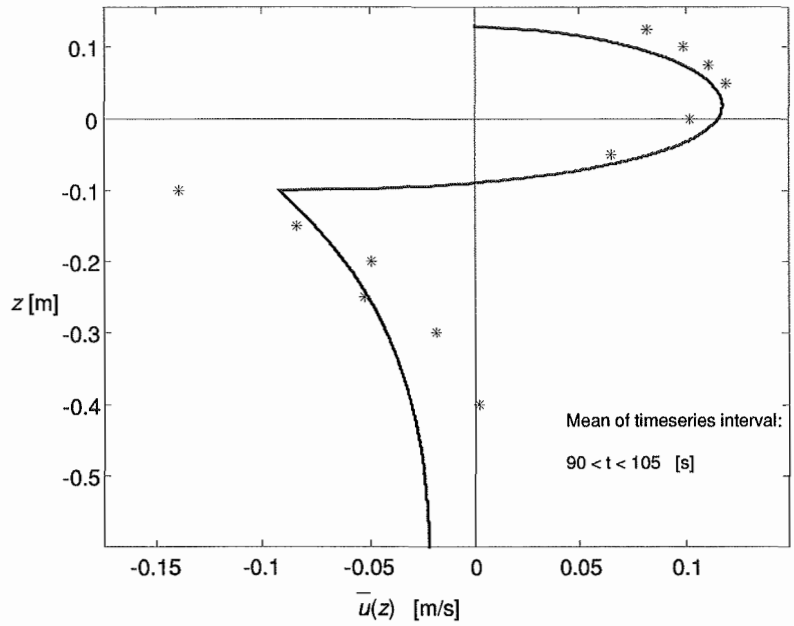

Figure 6.14 Measured (*) and calculated (–) mean horizontal velocity at wave gage 1, Case 9 (SR15), $90 < t < 105$ s.

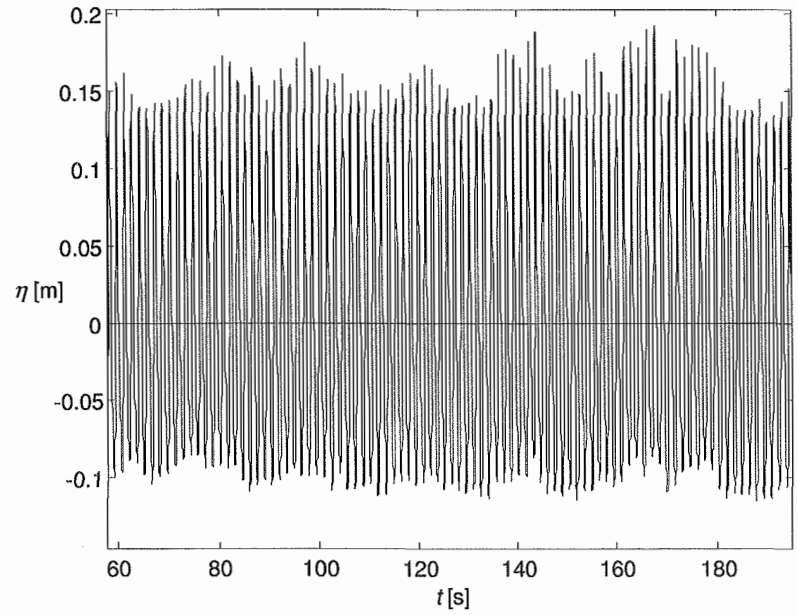

Figure 6.15 Typical surface elevation at wave gage 1 for $60 < t < 180$ s in Case 9 (SR15).

Figure 6.15 shows the typical surface elevation for $60 < t < 180$ s in Case 9. The "non-regularity" is still quite pronounced, and it remains so for the rest of the timeseries.

6.2.2 Instantaneous horizontal velocity in a vertical cross-section beneath individual crests and troughs

Large errors are introduced if the instantaneous horizontal velocity is calculated according to the approximate Eulerian form of Miche waves found by Taylor-expansion in Section 4.2.2, since the wave steepnesses in the present wave cases are not infinitesimal. These errors are significant also below the still water level. Figure 6.16 - Figure 6.19 show the difference between performing calculations according to the iteration method for regular Miche waves described in Section 5.3.4, and using the approximate Eulerian expressions for u in Eq. (4.75) to 1st and 2nd order, respectively. The surface profiles in the figures are not plotted in the correct longitudinal spatial scale, and are only meant to show the amplitudes of the crests and troughs. These figures emphasize the importance of applying the iteration method when investigating higher order quantities. For the horizontal velocity just below the crests in very steep waves, the 1st order approximation will yield positive values several times higher than that found by iteration, while the 2nd order approximation will yield negative values of magnitude comparable to the 1st order approximation.

The calculations used for the comparisons with measurements in this section are therefore made according to the iteration method for regular Miche waves described in Section 5.3.4. Comparisons are made for a crest and a trough at $t \approx 45$ s and $t \approx 150$ s for both regular wave cases. This covers the two most important situations identified in the previous section, namely after the first transition, associated with the passing of the initial wave front, and after the second transition after roughly 75-135 seconds.

It is also interesting to compare the iteration method for regular Miche waves with Wheeler's method applied to regular waves, the latter given by Eq. (5.9) (finite depth). This is done for Case 8 in Figure 6.20 and Figure 6.21.

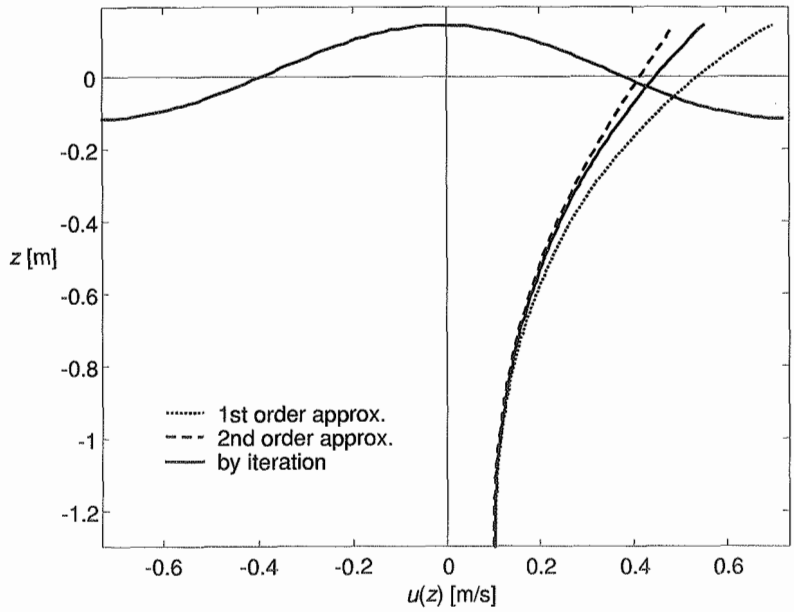

Figure 6.16 Calculations of the horizontal velocity beneath the crests in regular Miche waves corresponding to Case 8 ($H = 0.26$ m, $T = 1.5$ s, $h = 1.3$ m).

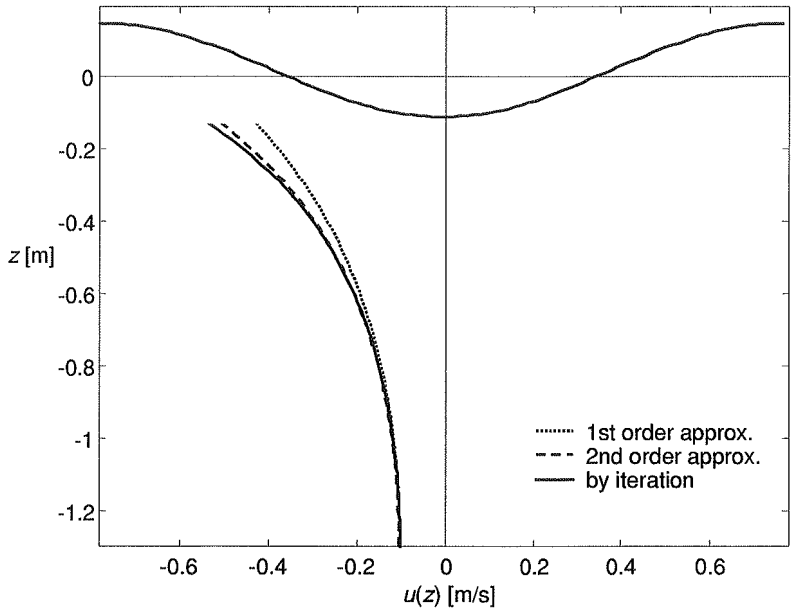

Figure 6.17 Calculations of the horizontal velocity beneath the troughs in regular Miche waves corresponding to Case 8 ($H = 0.26$ m, $T = 1.5$ s, $h = 1.3$ m).

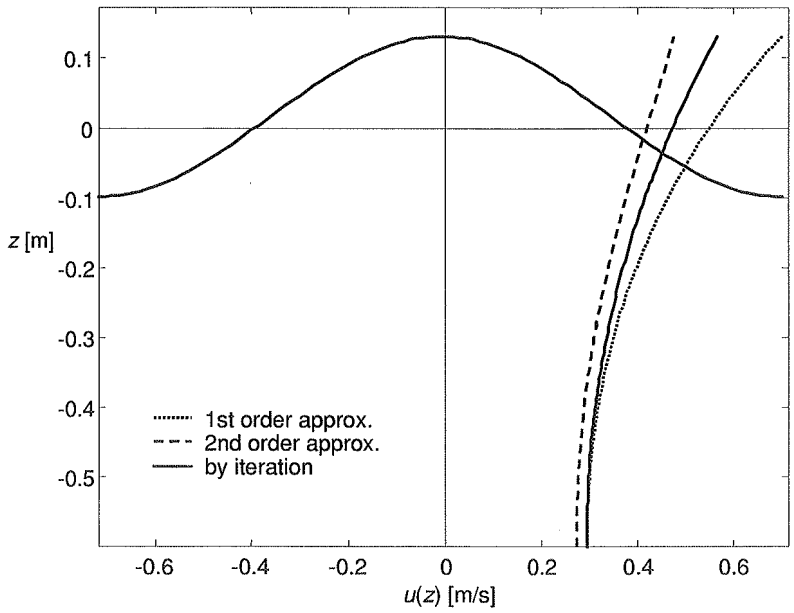

Figure 6.18 Calculations of the horizontal velocity beneath the crests in regular Miche waves corresponding to Case 9 ($H = 0.23$ m, $T = 1.5$ s, $h = 0.6$ m).

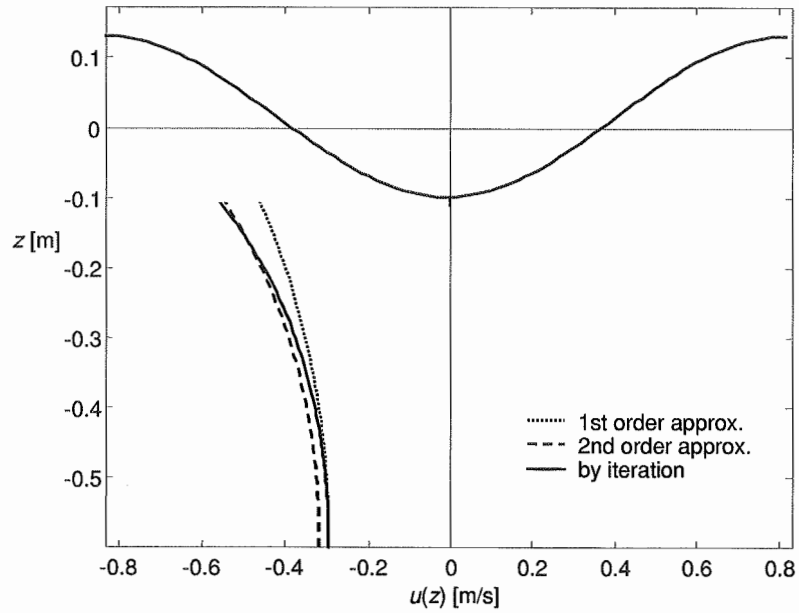

Figure 6.19 Calculations of the horizontal velocity beneath the troughs in regular Miche waves corresponding to Case 9 ($H = 0.23$ m, $T = 1.5$ s, $h = 0.6$ m).

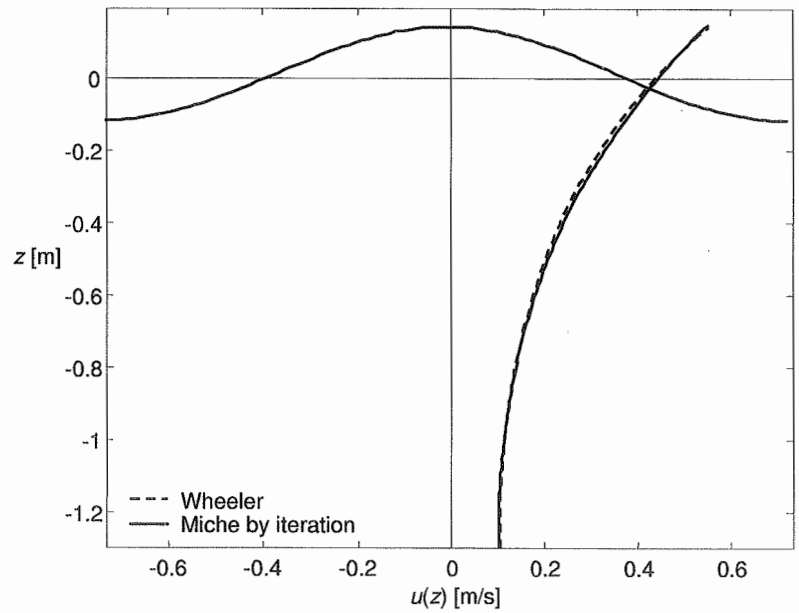

Figure 6.20 Comparison of Miche's theory (by iteration) and Wheeler's method for the horizontal velocity beneath a crest in regular waves corresponding to Case 8 ($H = 0.26$ m, $T = 1.5$ s, $h = 1.3$ m).

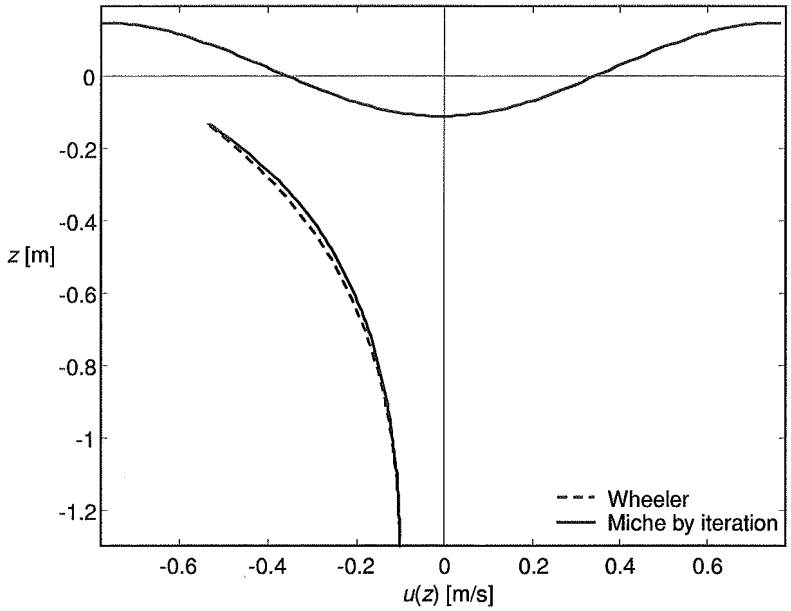

Figure 6.21 Comparison of Miche's theory (by iteration) and Wheeler's method for the horizontal velocity beneath a trough in regular waves corresponding to Case 8 (H = 0.26 m, T = 1.5 s, h = 1.3 m).

Figure 6.20 and Figure 6.21 show that Wheeler's method and Miche's solution yield identical values at the surface and at the bottom, as they should for regular waves, and the differences in the region in-between are qualitatively as expected due to the stretching of coordinates in Wheeler's method, cf. Sections 5.2 and 7.3.2 also.

When calculating regular wave kinematics, the regular wave amplitude is required as input in addition to the wave period. While the wave period in the experiments turn out to be practically constant, there are significant variations in the measured amplitudes, and these may also differ from the assumed regular wave amplitudes listed in Table 6-1. The "non-regularities" found in the surface elevation for Case 9 in Section 6.2.1 is one effect that makes it difficult to determine a representative regular wave amplitude. In addition to calculations based on the assumed amplitudes in Table 6-1, calculations are therefore also performed with amplitudes determined by the crest/trough associated with the velocity measurements at each vertical level. However, using the measured value of the surface elevation at the crests and troughs as amplitudes is not satisfactory, due to the asymmetry about the horizontal axis. A better estimate may be found solving for a in Eq. (6.20), viz.

$$\begin{aligned} &\text{Crest:} \quad a+\frac{1}{2}ka^2\frac{\cosh kh}{\sinh kh}=\eta_{measured,crest} \\ &\text{Trough:} \quad -a+\frac{1}{2}ka^2\frac{\cosh kh}{\sinh kh}=\eta_{measured,trough} \end{aligned} \tag{6.20}$$

i.e. accounting for the vertical shift in Eq. (4.61). Alternatively, the "real" amplitude may be defined as half the measured vertical distance between neighbouring crests and troughs (i.e. the local wave height), viz.

$$a = \frac{H}{2} \qquad H = \eta_{measured,crest} - \eta_{measured,trough} \tag{6.21}$$

Eq. (6.21) is more reliable than Eq. (6.20), since the former may be more influenced by bound long waves.

There may be small time lags between the experimental runs required to construct a vertical profile, cf. Section 6.1.1. The chosen value of the velocity at each vertical level is therefore that measured simultaneously with the maximum/minimum value of the surface elevation in an timeseries-interval enclosing only the crest/trough under consideration. The experiments turn out to be quite well reproduced, the time lag between the runs being typically less than $T/20$. Therefore, this approach does find and compare the crest or trough for e.g. "wave number 100" of all experimental runs of each case.

The measured profiles of the crests or troughs under consideration are included in the plots, in order to show the differences in the measured surface profiles of the different runs. The crests and troughs are focused at the vertical line $u(z) = 0$, although small offsets may occur due to the actual plotting procedure (note that the longitudinal scale of the wave profiles is not correct with respect to the vertical scale). The velocity measurements in the plots are anyhow those associated with the peak values of the surface elevation, as stated above. The thicker horizontal lines show the level of the trough and crest as predicted by Miche's theory, cf. Eq. (6.17). The thinner horizontal line represents the still water level. The value of the horizontal velocity is set equal to zero if the Eulerian point in question is found to be out of water, as can be seen from the figures pertaining to troughs.

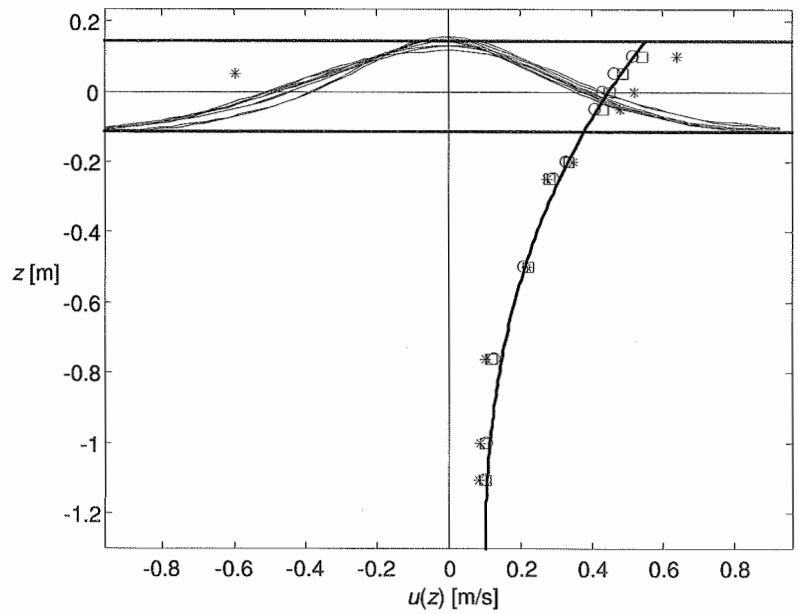

Figure 6.22 Crest at $t \approx 45$ s, Case 8 (R15B). (*): measurements, solid line: iteration using a = 0.13 m, circles: iteration using a from Eq. (6.21), squares: iteration using a from Eq. (6.20).

As in Figure 6.6, the clearly deviating value at $z = 0.05$ should be discarded.

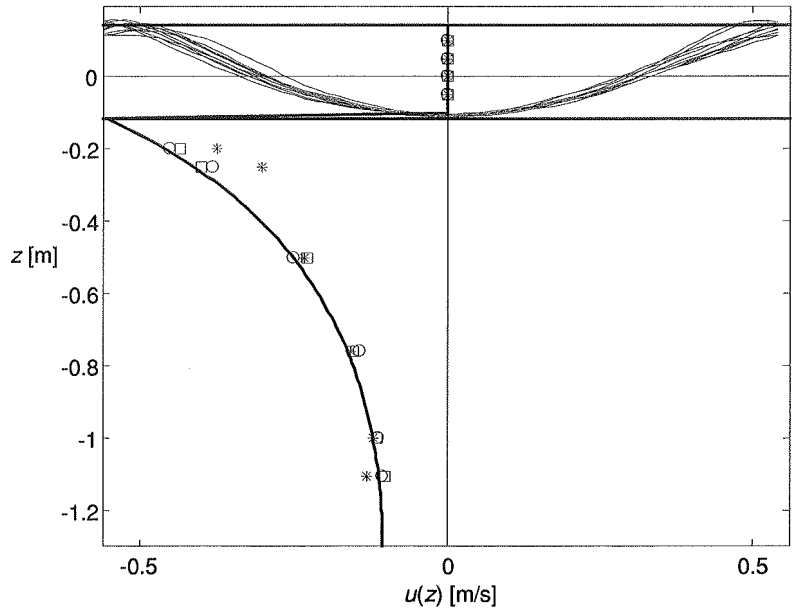

Figure 6.23 Trough at $t \approx 45$ s, Case 8 (R15B). (*): measurements, solid line: iteration using $a = 0.13$ m, circles: iteration using a from Eq. (6.21), squares: iteration using a from Eq. (6.20).

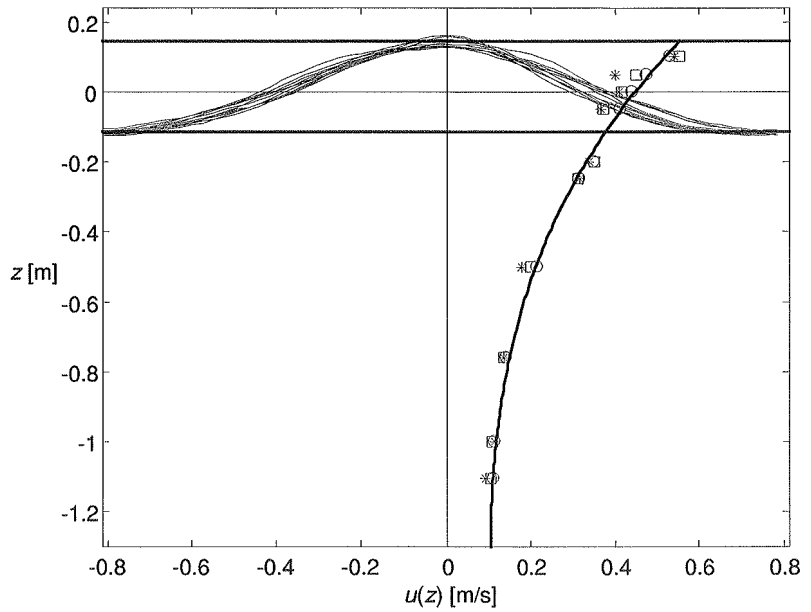

Figure 6.24 Crest at $t \approx 150$ s, Case 8 (R15B). (*): measurements, solid line: iteration using $a = 0.13$ m, circles: iteration using a from Eq. (6.21), squares: iteration using a from Eq. (6.20).

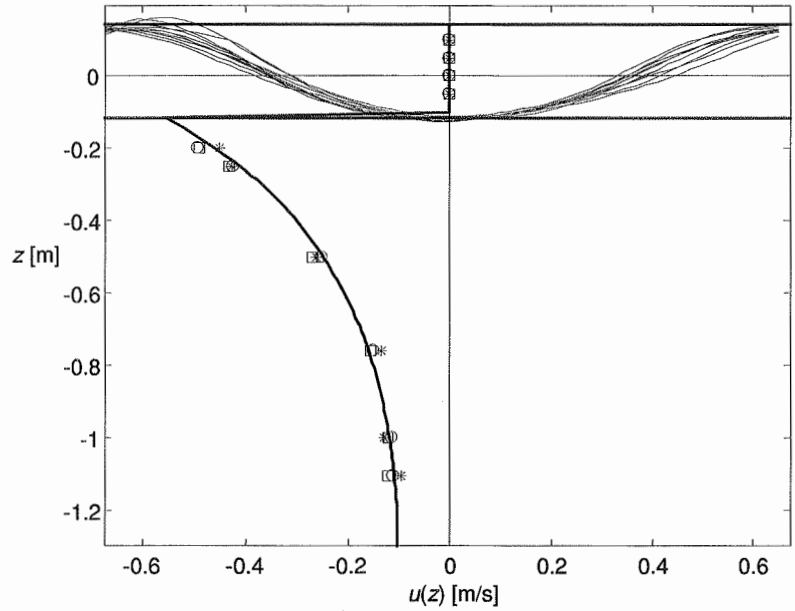

Figure 6.25 Trough at $t \approx 150$ s, Case 8 (R15B). (*): measurements, solid line: iteration using $a = 0.13$ m, circles: iteration using a from Eq. (6.21), squares: iteration using a from Eq. (6.20).

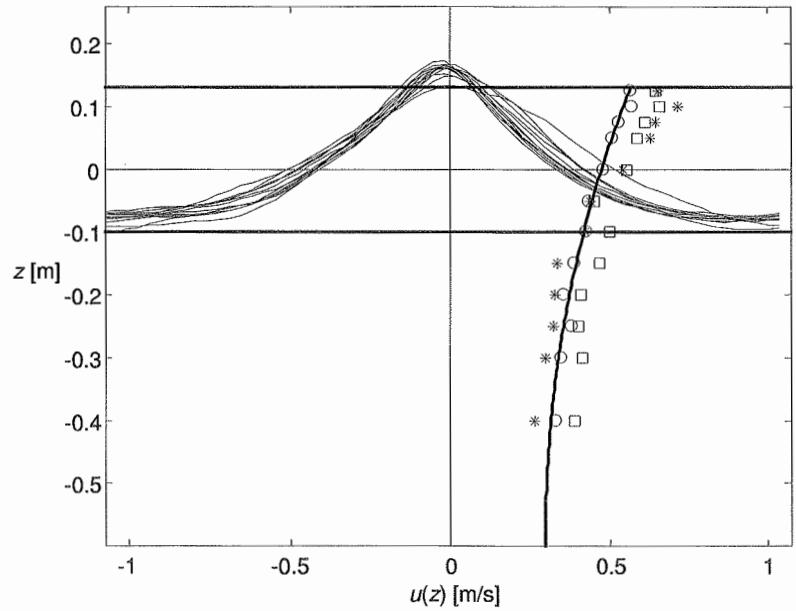

Figure 6.26 Crest at $t \approx 45$ s, Case 9 (SR15). (*): measurements, solid line: iteration using $a = 0.115$ m, circles: iteration using a from Eq. (6.21), squares: iteration using a from Eq. (6.20).

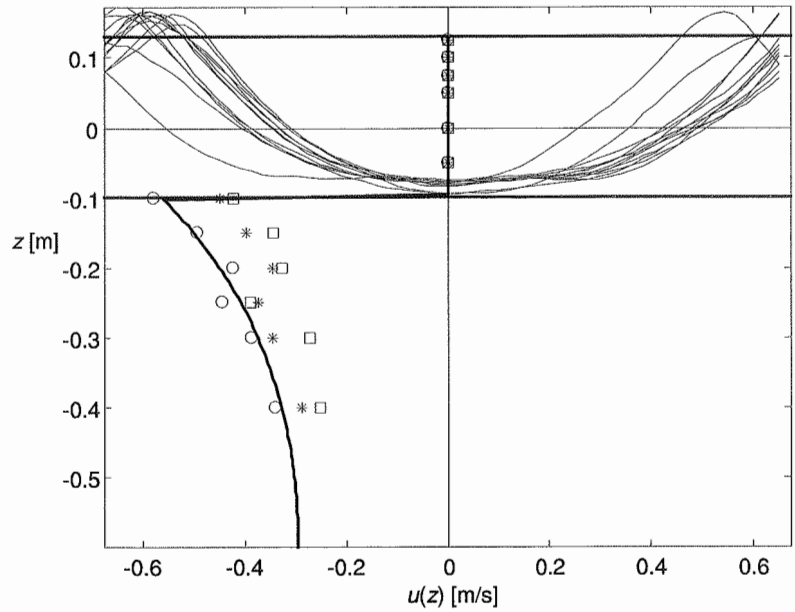

Figure 6.27 Trough at $t \approx 45$ s, Case 9 (SR15). (*): measurements, solid line: iteration using $a = 0.115$ m, circles: iteration using a from Eq. (6.21), squares: iteration using a from Eq. (6.20).

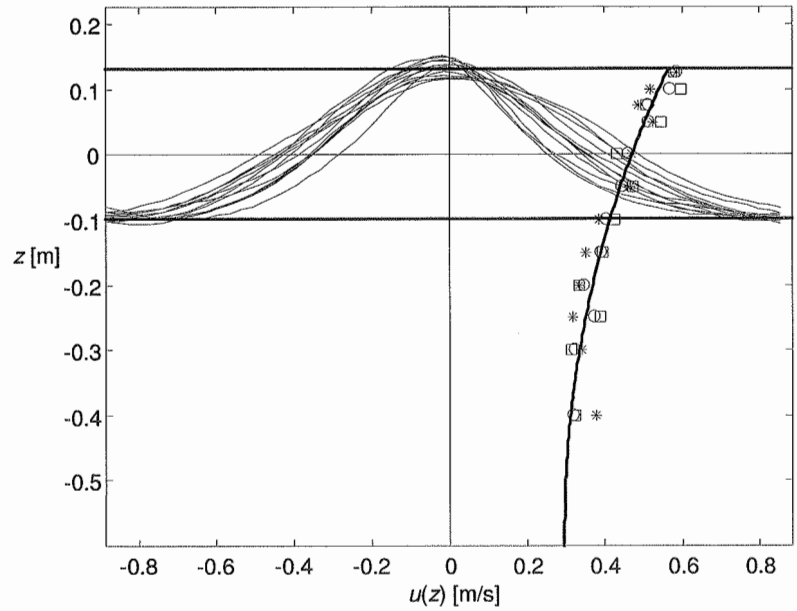

Figure 6.28 Crest at $t \approx 150$ s, Case 9 (SR15). (*): measurements, solid line: iteration using $a = 0.115$ m, circles: iteration using a from Eq. (6.21), squares: iteration using a from Eq. (6.20).

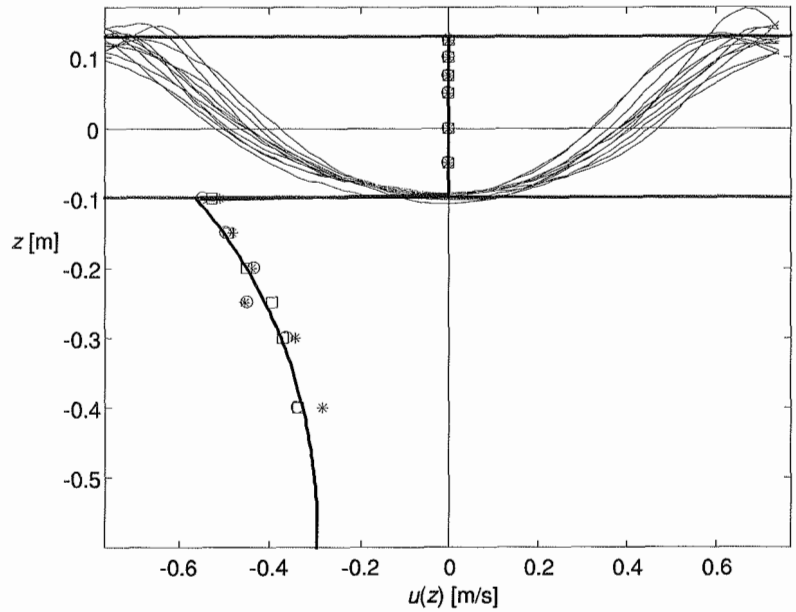

Figure 6.29 Trough at $t \approx 150$ s, Case 9 (SR15). (*): measurements, solid line: iteration using $a = 0.115$ m, circles: iteration using a from Eq. (6.21), squares: iteration using a from Eq. (6.20).

Miche's theory is seen to yield too low values beneath crests and too high values beneath troughs at $t \approx 45$ s, while it compares very well with the measurements at $t \approx 150$ s. This is in accordance with the findings for the mean velocity in the previous section. It can also be seen that the level of the crests and troughs predicted by Miche's theory is in good agreement with the measured surface elevations, except for in Figure 6.26 and Figure 6.27. These are also the figures where the difference between applying a from Table 6-1, Eq. (6.20) or (6.21), respectively, is most significant. Hence, there is a clear discrepancy between theory and measurements in the period after the first transition, and an overall agreement, also in the splash zone, after the second transition. These results have been confirmed for other time instants also.

6.2.3 Timeseries of the surface elevation and velocities in fixed spatial points

As in the previous section, the velocities in this section are calculated according to the iteration method for regular Miche waves described in Section 5.3.4. The surface elevation is calculated according to the method described in Section 5.4. Only Case 8 is considered here, for the two timeseries-intervals $43 < t < 47$ s and $148 < t < 152$ s. These intervals include the waves considered in the previous section (at $t \approx 45$ and $t \approx 150$), as well as the preceding and following waves. The amplitude used in the calculations is as given by Table 6-1, i.e. $a = 0.13$ m. Comparisons are made for the surface elevation as well as the horizontal and vertical velocity at two vertical levels; one near the crest and one below the trough. As the measurement point comes out of water, the LDV "freezes" at the last recorded value. Recall that invalid spikes are likely to occur just as the point comes into or goes out of water, cf. Figure 6.31. Calculated velocities are included only for the intervals when the Eulerian point in question is found to be in water theoretically. The phase is defined by the crest of the measured waves. The measured wave crests are slightly asymmetrical about a vertical axis, meaning that the calculations and measurements may be slightly out of phase in other parts of the wave (e.g. at troughs and zero crossings).

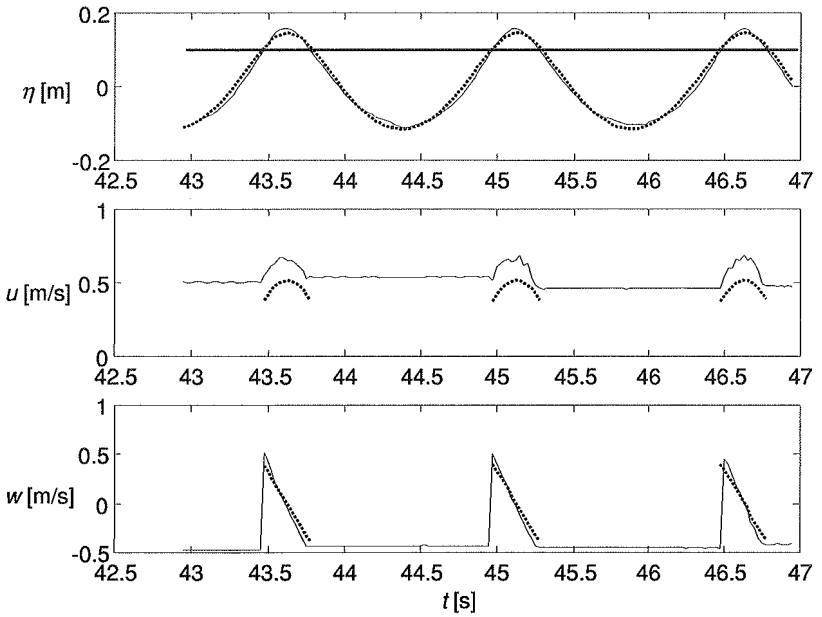

Figure 6.30 Timeseries of the surface elevation and velocities at $z = 0.10$ (horizontal line in plot of η), $43 < t$ 47 s, Case 8 (run R15B_8). The measured timeseries are given by solid lines, while calculations according to Miche are given by dotted lines.

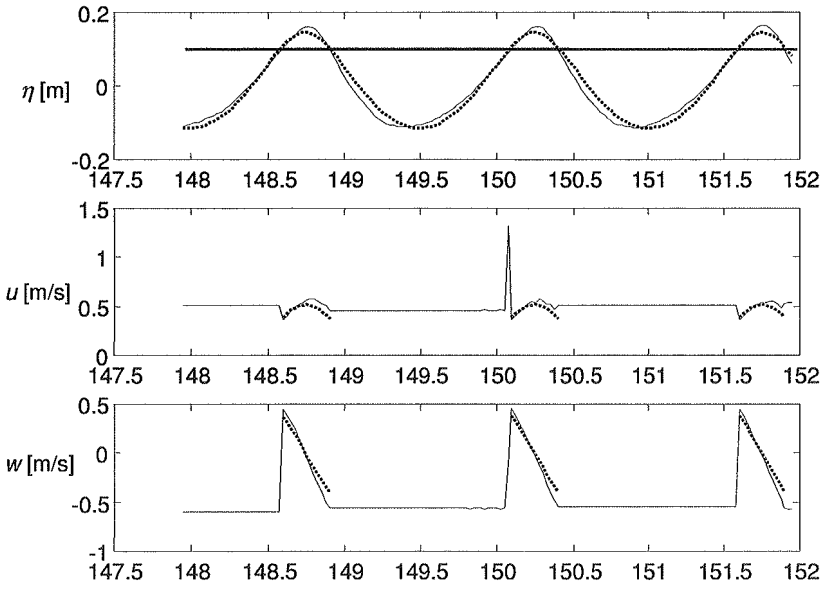

Figure 6.31 Timeseries of the surface elevation and velocities at $z = 0.10$ (horizontal line in plot of η), $148 < t < 152$ s, Case 8 (run R15B_8). The measured timeseries are given by solid lines, while calculations according to Miche are given by dotted lines.

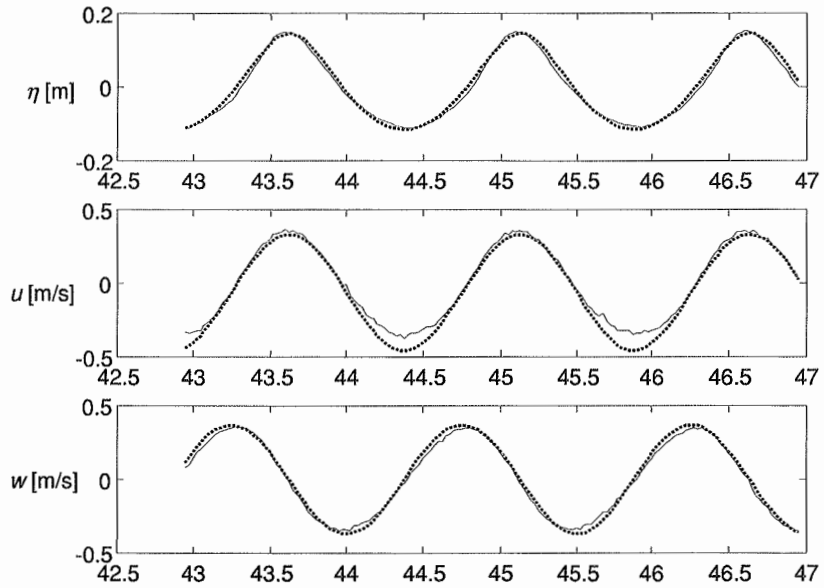

Figure 6.32 Timeseries of the surface elevation and velocities at $z = -0.20$, $43 < t < 47$ s, Case 8 (run R15B_4). The measured timeseries are given by solid lines, while calculations according to Miche are given by dotted lines.

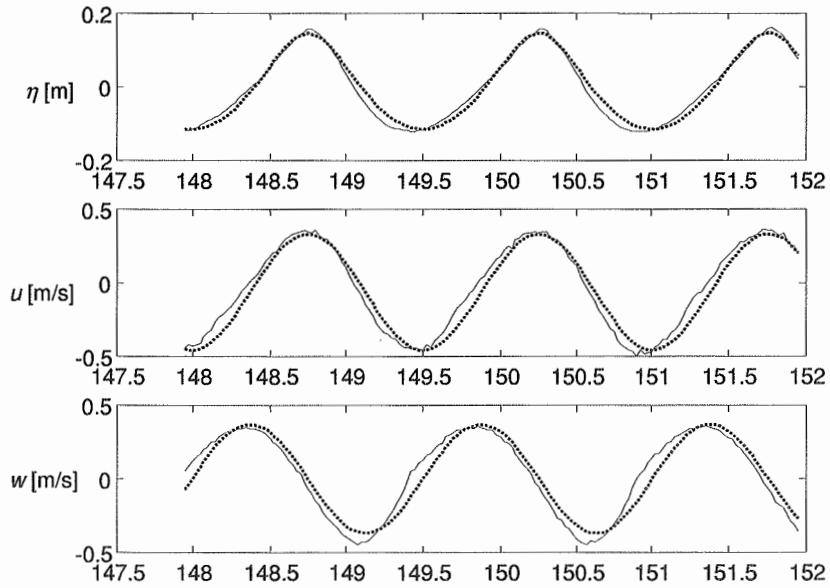

Figure 6.33 Timeseries of the surface elevation and velocities at $z = -0.20$, $148 < t < 152$ s, Case 8 (run R15B_4). The measured timeseries are given by solid lines, while calculations according to Miche are given by dotted lines.

As in the previous sections, clear discrepancies between the calculated and measured horizontal velocities are found for $t \sim 45$ s, while they compare better for $t \sim 150$ s. The discrepancies in the vertical velocity in Figure 6.33 are found to stem from quite local variations, cf. Section 7.3.4.

6.3 Results for Irregular Waves

This section presents the results for irregular waves. The results are discussed in Section 7.4. The same types of comparisons are made for irregular waves as for regular waves. In order to reduce the influence of finite depth, and reduce the number of figures, most comparisons are made for Case 2 (I14) cf. Table 6-1. The peak period of this wave case corresponds to a depth-to-wavelength ratio $h/\lambda = 0.43$. The peak period of Case 5 (I18) corresponds to $h/\lambda = 0.27$, and the peak period of Case 6 (I24) corresponds to $h/\lambda = 0.18$.

The component parameters are found by Fourier analysis of the entire record of the measured surface elevation, i.e. $N = 32.768$ and $T_N = 819.2$ s, cf. Sections 6.1.2 and 6.1.3. The component steepnesses are found to lie in the range $0.002 < k_n a_n < 0.013$, and the component amplitudes are found to lie in the range $0 < a_n < 6$ mm, cf. Figure 6.34. These values are typical values for all runs in all cases in the irregular wave experiments. The typical form of the amplitude spectrum for Case 2 is shown in Figure 6.48.

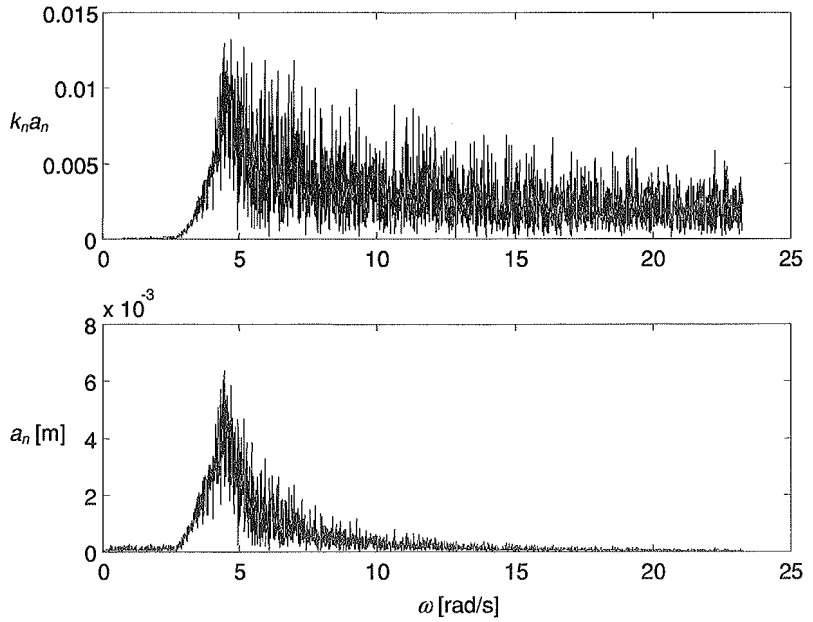

Figure 6.34 Typical plot of component steepnesses and amplitudes. This plot is based on run I14_1, and includes components in the frequency range $0 < \omega < 3\omega_{20}$.

6.3.1 Mean horizontal velocity in a vertical cross-section

The mean Eulerian horizontal velocity in irregular waves is calculated according to Eqs. (4.77) and (4.80).

Figure 6.35 shows the measured and calculated mean horizontal velocity for Case 2, the measured values being averaged over the entire timeseries. In Eq. (4.80), the mean velocity is

based on the mean zero crossing frequency ω_{20} (~ 5.15 rad/s). However, Figure 6.35 also include calculations using the spectral peak frequency ω_p (~ 4.49 rad/s) and the spectral mean frequency ω_{10} (~ 4.90 rad/s), respectively, as the representative narrow band frequency in Eq. (4.80). It can be seen that the calculations are quite insensitive to which frequency is considered representative, except for in the lower part of the splash zone, and the calculations are in good agreement with the measurements. Figure 6.35 also include calculations based on Eq. (4.82). It would here seem reasonable to consider a JONSWAP spectrum, and use Eq. (4.81) instead of Eq. (4.82), since the control signal to the wavemaker was constructed from a JONSWAP spectrum. However, from timeseries analysis, the ratio between ω_{20} and ω_p is found to be 1.15 for Case 2, which differs somewhat from Eq. (4.56). Therefore, Eq. (4.82) with $C_\omega = 1.15$ is used in Figure 6.35. It can be seen that below the splash zone this yields the same result as Eq. (4.80) using ω_{20}, as expected. The rest of the figures in this section are based on ω_{20} as the representative narrow band frequency.

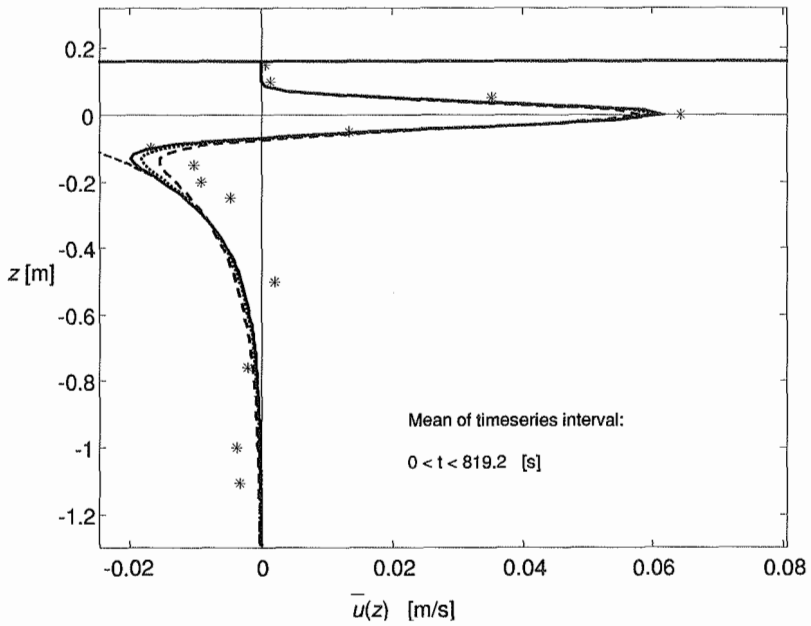

Figure 6.35 Measured (*) and calculated mean horizontal velocity at wave gage 1, Case 2 (I14), $0 < t < 819.2$ s. The solid line pertains to ω_{20}, the dotted line to ω_{10}, and the thicker dashed line to ω_p. The thinner dashed line also pertains to ω_{20}, and is based on Eq. (4.82) with $C_\omega = 1.15$. The upper horizontal line represents the significant wave height.

In irregular waves, the mean horizontal velocity must be expected to vary somewhat from wave to wave. In order to investigate the development of the mean velocity in the irregular case, we should therefore consider relatively long timeseries-intervals. Design sea states often have a peak period of approximately 15 s and ocean measurements typically have a duration of 20 minutes or more, corresponding to roughly 80 peak periods or more. An interval corresponding to 80-100 peak periods is therefore found appropriate for these comparisons.

For Case 2, it is found that during the first ~ 2-3 minutes there is a positive mean velocity in the splash zone and a nearly vertically uniform negative mean velocity below the splash zone, cf. Figure 6.36. A transition similar to that found for regular waves then appears to take place, yielding a mean velocity profile as shown in Figure 6.37. The profile is there seen to be quite similar to that predicted by the narrow band assumption, although there is a marked

underprediction at the typical vertical level of the troughs. Similar results are found for Case 5 (I18) and Case 6 (I24) also, cf. Figure 6.38 and Figure 6.39. The transition takes place earlier in these cases than in Case 2, typically within ~ 2 minutes.

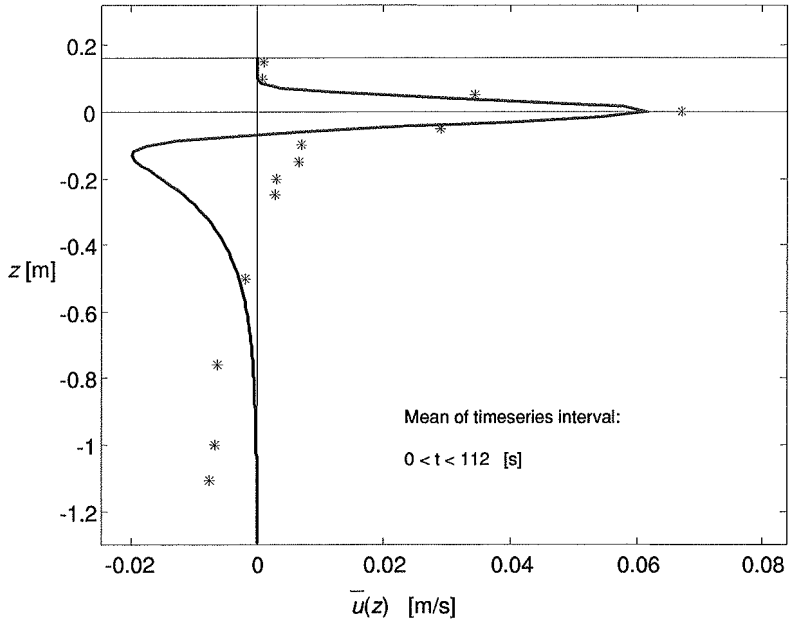

Figure 6.36 Measured (*) and calculated (–) mean horizontal velocity at wave gage 1, Case 2 (I14), $0 < t < 112$ s (80 T_p).

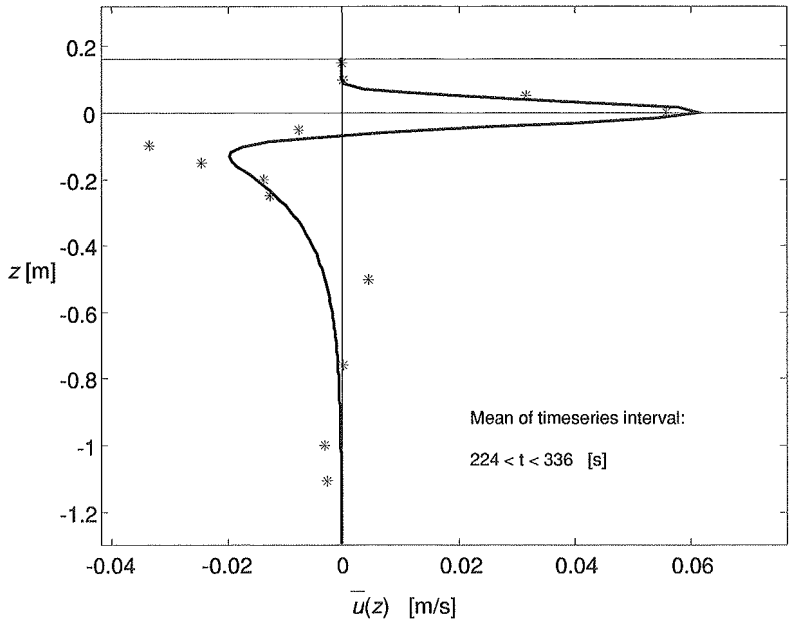

Figure 6.37 Measured (*) and calculated (–) mean horizontal velocity at wave gage 1, Case 2 (I14), $224 < t < 336$ s (80 T_p).

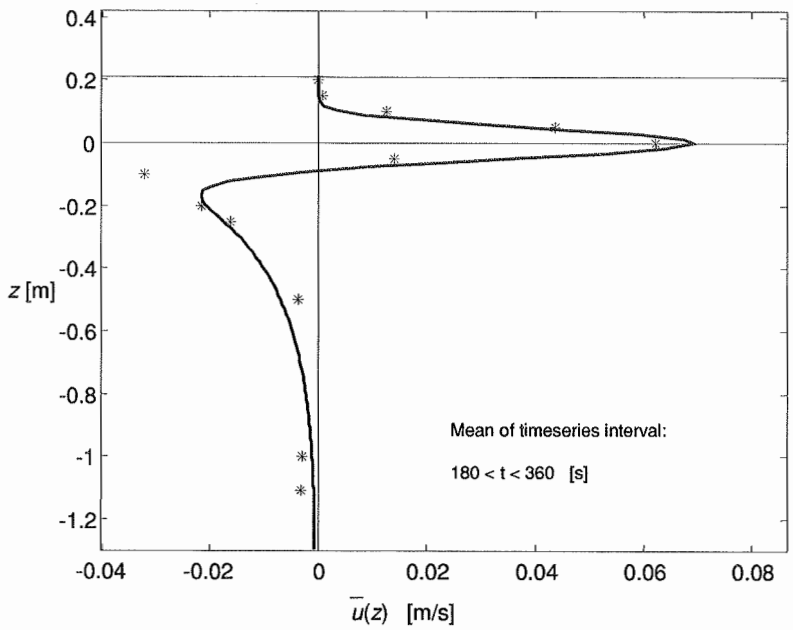

Figure 6.38 Measured (*) and calculated (–) mean horizontal velocity at wave gage 1, Case 5 (I18), $180 < t < 360$ s ($100\ T_p$).

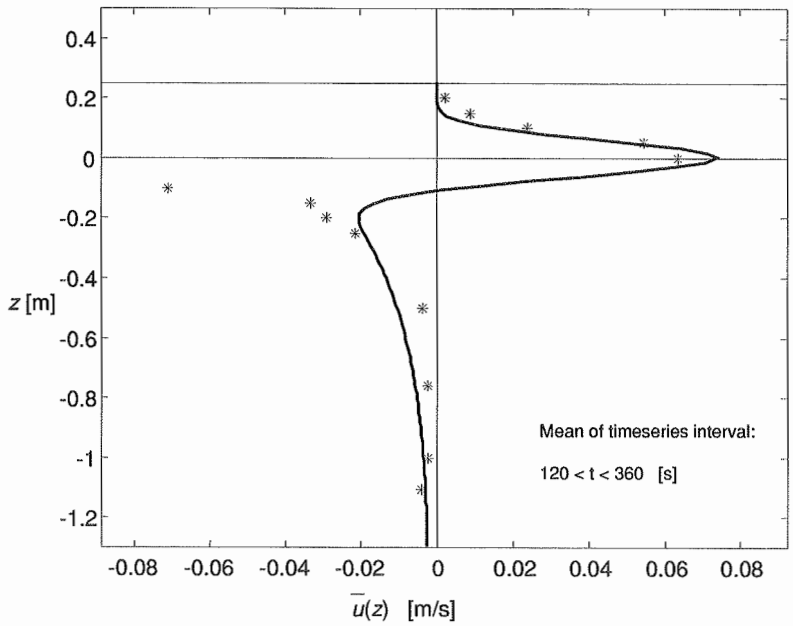

Figure 6.39 Measured (*) and calculated (–) mean horizontal velocity at wave gage 1, Case 6 (I24), $120 < t < 360$ s ($100\ T_p$).

It is also of interest to investigate short-term variations in the mean horizontal velocity, e.g. the variation from wave to wave. Three successive individual waves in Case 2 have been chosen for this purpose, including one of the highest waves of Case 2, namely those with crests at $t \approx 554.5$, 556 and 557.5 s, respectively, in Figure 6.40.

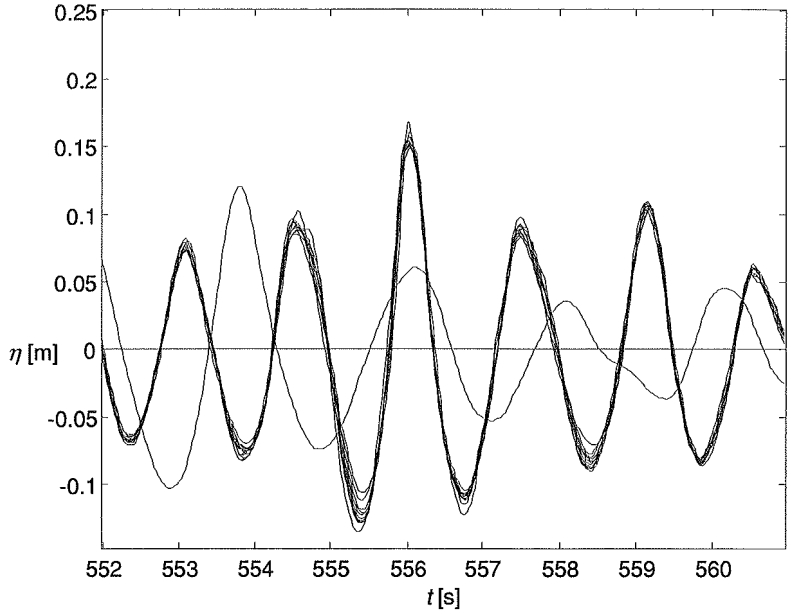

Figure 6.40 Excerpt of surface elevation at wave gage 1, $552 < t < 561$ s. All available runs of Case 2 are included.

Recall that the LDV measurements at each vertical level required one designated experimental run, cf. Section 6.1.1. The irregular waves were generated by the same input signal to the wavemaker, and from a theoretical point of view this should result in the exact same surface elevation records. Such perfect reproduction of experimental runs is of course not possible, but Figure 6.40 shows that the runs of Case 2 were still very well reproduced. There is however one run that clearly deviates from the others. Timeseries analysis of this run (I14_15), which is associated with the velocity measurements at $z = 0.10$, yields a peak period of 2.5 s. This means that this specific run is not comparable to the others of Case 2 at all. The measured velocities at this vertical level should therefore be discarded, and are left out of the rest of the comparisons.

Figure 6.41 - Figure 6.43 show the horizontal velocity averaged over 1.5 s for the three individual waves under consideration. An interval of 1.5 s is chosen because this appears to be an appropriate mean period for all the waves included in Figure 6.40. The calculated "narrow band profile" is the same in all three figures below. This profile cannot be expected to compare well with short-term values, and is only included as a reference curve. A marked increase in the mean velocity below as well as above the still water level can be seen for the highest wave in Figure 6.42, as compared to the preceding and following smaller waves in Figure 6.41 and Figure 6.43, respectively.

The same type of comparison is made for three waves in Case 5 (I18) also, cf. Figure 6.45 - Figure 6.47. The waves considered there are those with crests at $t \approx 165.8$, 167.7 and 169.3 s, respectively, in Figure 6.44. The different runs are seen to be nearly perfectly reproduced in Case 5 also. The measured velocities are now averaged over a period of 1.8 s. A short-term

variation similar to that in Figure 6.41 - Figure 6.43 is seen in Figure 6.45 - Figure 6.47 as well, although less pronounced.

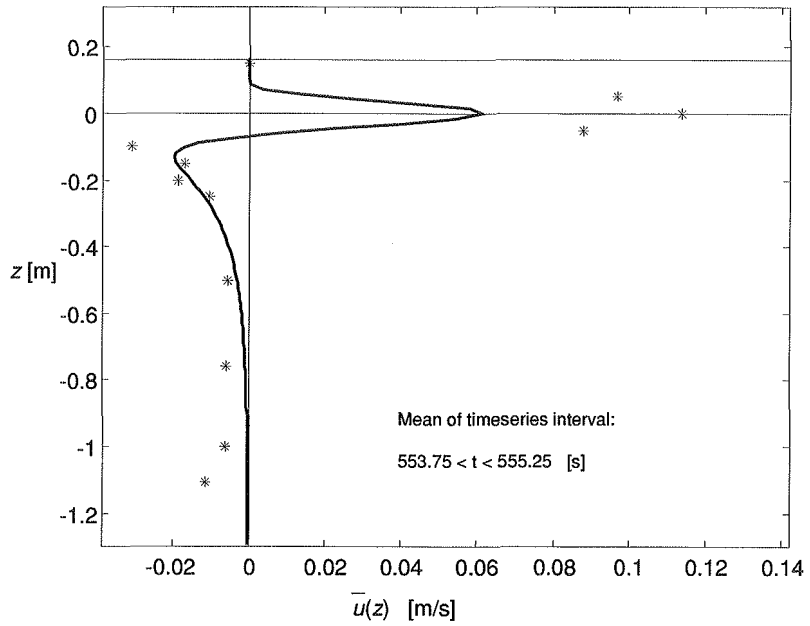

Figure 6.41 Measured (*) and calculated (–) mean horizontal velocity at wave gage 1, Case 2 (I14), 553.75 < t < 555.25 s.

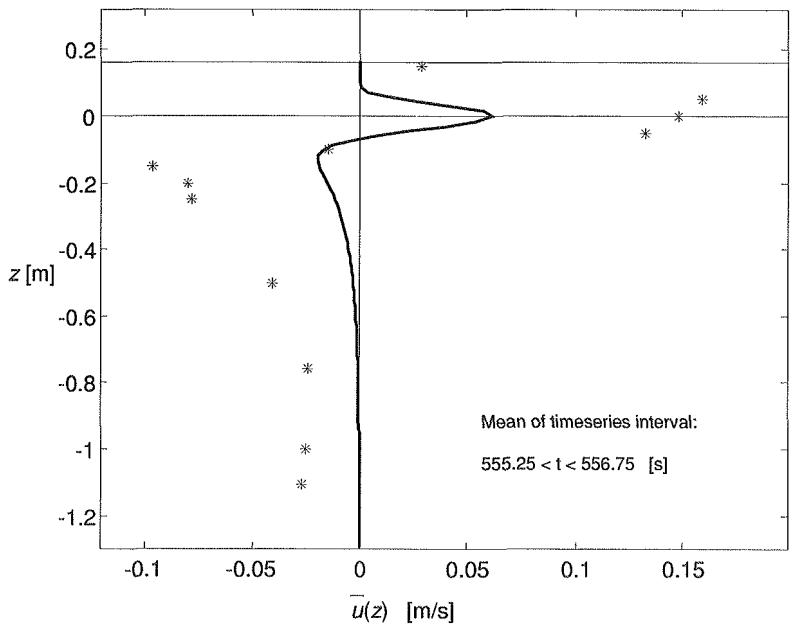

Figure 6.42 Measured (*) and calculated (–) mean horizontal velocity at wave gage 1, Case 2 (I14), 555.25 < t < 556.75 s.

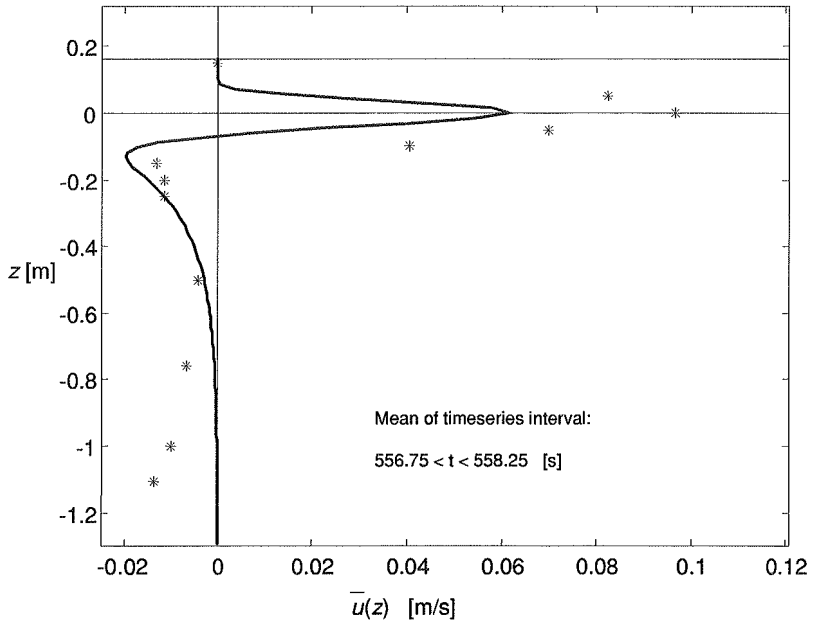

Figure 6.43 Measured (*) and calculated (–) mean horizontal velocity at wave gage 1, Case 2 (I14), $556.75 < t < 558.25$ s.

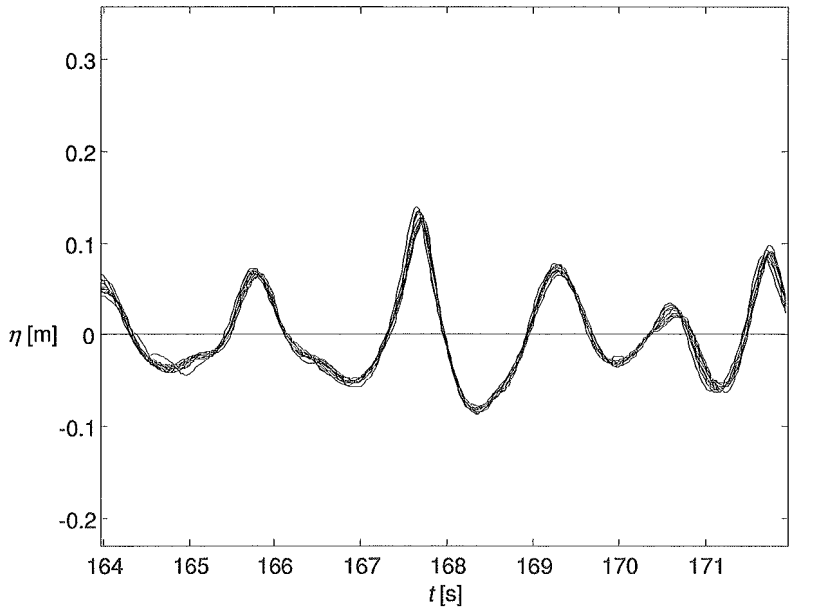

Figure 6.44 Excerpt of surface elevation at wave gage 1, $164 < t < 172$ s. All available runs of Case 5 are included.

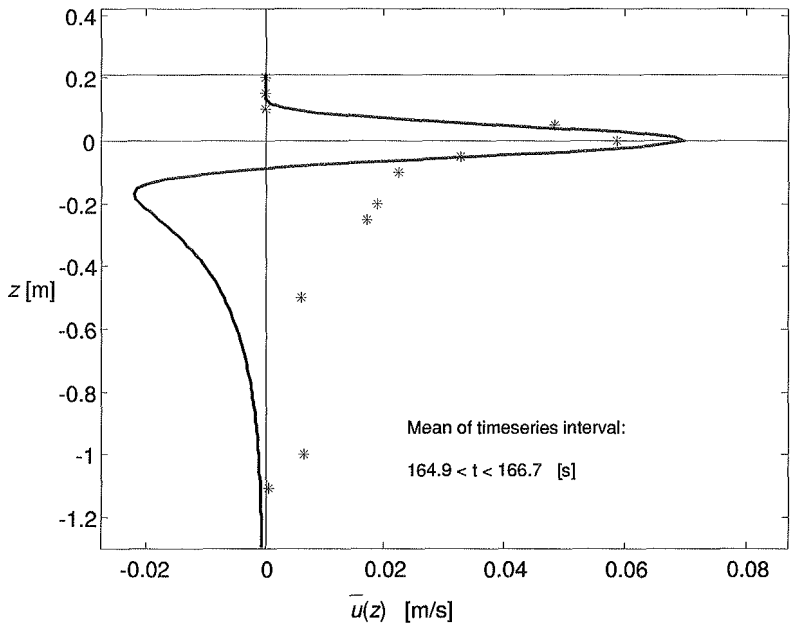

Figure 6.45 Measured (*) and calculated (–) mean horizontal velocity at wave gage 1, Case 5 (I18), $164.9 < t < 166.7$ s.

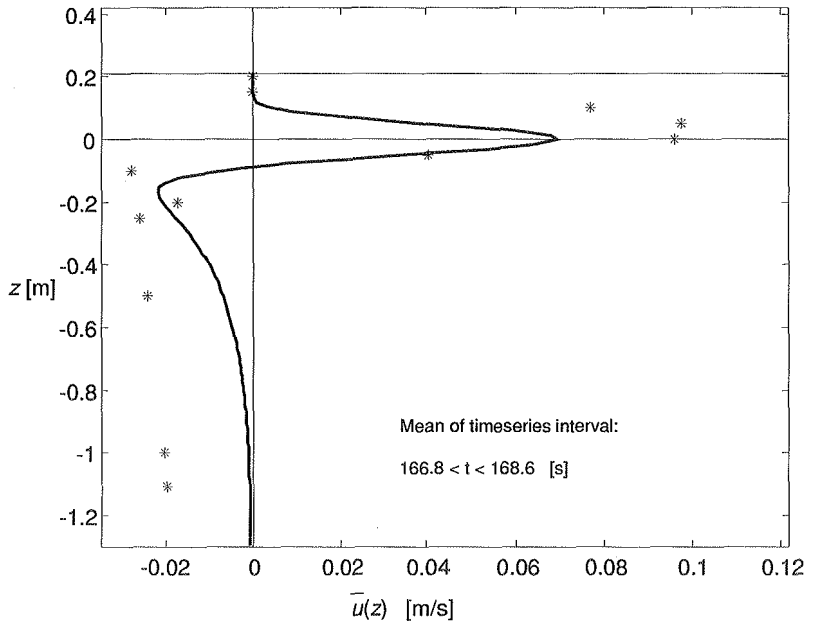

Figure 6.46 Measured (*) and calculated (–) mean horizontal velocity at wave gage 1, Case 5 (I18), $166.8 < t < 168.6$ s.

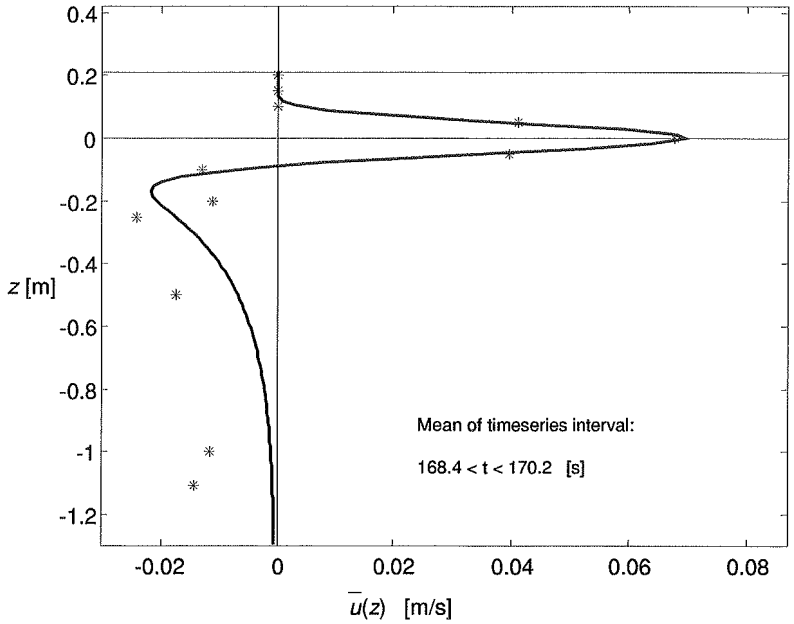

Figure 6.47 Measured (*) and calculated (–) mean horizontal velocity at wave gage 1, Case 5 (I18), $168.4 < t < 170.2$ s.

The results in Figure 6.41 - Figure 6.43 and Figure 6.44 - Figure 6.47 may be of particular interest and importance, since they suggest that the mean velocity is indeed a result of closed orbital "particle"-paths. A higher individual wave is clearly associated with higher positive *and negative* values in the mean velocity profile, as predicted by Gerstner and Miche. A return-current, i.e. a real backward mass flow independent of the instantaneous wave, should not exhibit short-term variations of this nature or magnitude, cf. Section 7.4.1 also.

Reproduction and video-filming of an experimental run as in Case 5, in the same flume and under the same conditions as the original experiments, shows that a weak creeping flow appears be set up after 5-6 minutes. No creeping flow is observed for Case 2, while it may be more significant in Case 6.

6.3.2 Instantaneous horizontal velocity in a vertical cross-section beneath individual crests and troughs

The results for the horizontal velocity in this section include calculations according the iteration method for irregular Miche waves described in Sections 5.3.4, and calculations according to Wheeler's method for finite depth, cf. Section 5.2. The surface elevation is calculated according to the iteration method described in Section 5.4.

In Figure 6.48 is shown the measured (raw) spectrum of the surface elevation of run I14_1. This spectrum is representative for all runs of Case 2, except of course run I14_15, cf. Figure 6.40. Most of the energy is seen to be included in the frequency range $\frac{1}{2}\omega_{20} < \omega < 2\omega_{20}$, and practically all energy is included within $0 < \omega < 3\omega_{20}$ ($\omega_{20} \approx 5.15$ rad/s).

In Figure 6.49 - Figure 6.64 is shown the instantaneous horizontal velocity beneath some chosen individual crests and associated troughs in Case 2. These are the crest at $t \approx 100$ s, which is the highest individual wave in Case 2, the crest at $t \approx 556$ s, which is the highest

individual wave in the interval $120 < t < 780$ s, and a moderate crest at $t \approx 373$ s. Note that calculations according to Miche may conclude that the Eulerian point in question is out of water even if it actually was in water in the experiments, and set the velocity at this level to zero. This is not the case for the calculations according to Wheeler's method, since these are based on the measured surface elevation.

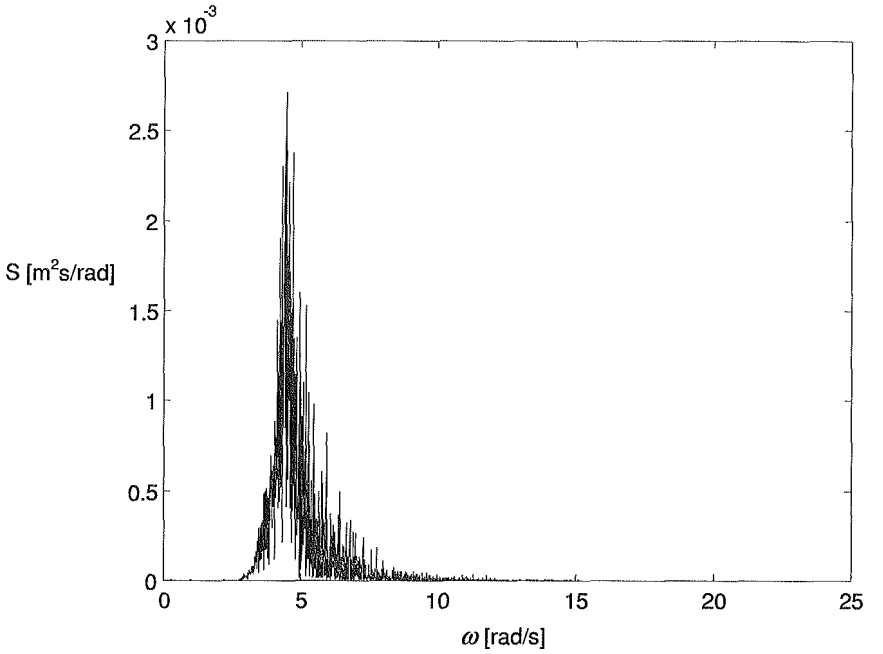

Figure 6.48 Surface elevation amplitude spectrum measured at wave gage 1, Case 2, run I14_1.

The highest crest at $t \approx 100.3$ s is considered in Figure 6.49 - Figure 6.55. Figure 6.49 - Figure 6.52 show the effect of including/excluding frequency components higher than $2\omega_{20}$ in the calculations. The high frequency contributions are seen to be quite significant for Wheeler's method near the free surface for this highest crest. The significance of the highest frequency components seems to be less in the calculations according to Miche. Even if the actual comparisons appear to be better when including the higher frequencies, this does not mean that it is physically correct to include them. Nor is it physically correct to include the lowest frequency components in this way. However, all frequency components are significant for the surface elevation and thus for the iteration methods in Sections 5.3 and 5.4. Therefore, since we do not know what the most appropriate frequency range is, different frequency ranges are applied in the comparisons. The horizontal velocity beneath the other crests and troughs in Figure 6.51 is shown in Figure 6.53 - Figure 6.55.

The measured and calculated surface elevation near the moderate wave at $t \approx 373$ is shown in Figure 6.56, and the horizontal velocity beneath the neighbouring crest and troughs is shown in Figure 6.57 - Figure 6.59. The measured and calculated surface elevation near the high wave at $t \approx 556$ is shown in Figure 6.60, and the horizontal velocity beneath the neighbouring crests and troughs is shown in Figure 6.60 - Figure 6.64. There is an odd 'kink' at the top of the velocity profile calculated according to Miche in Figure 6.61, which is found to stem from the very lowest frequency components, i.e. $0 < \omega << \omega_{20}$, cf. Figure 6.62. The reason for this is that the iteration method for irregular Miche waves is sensitive to low frequency contributions. This is described in more detail in Section 7.2.2.

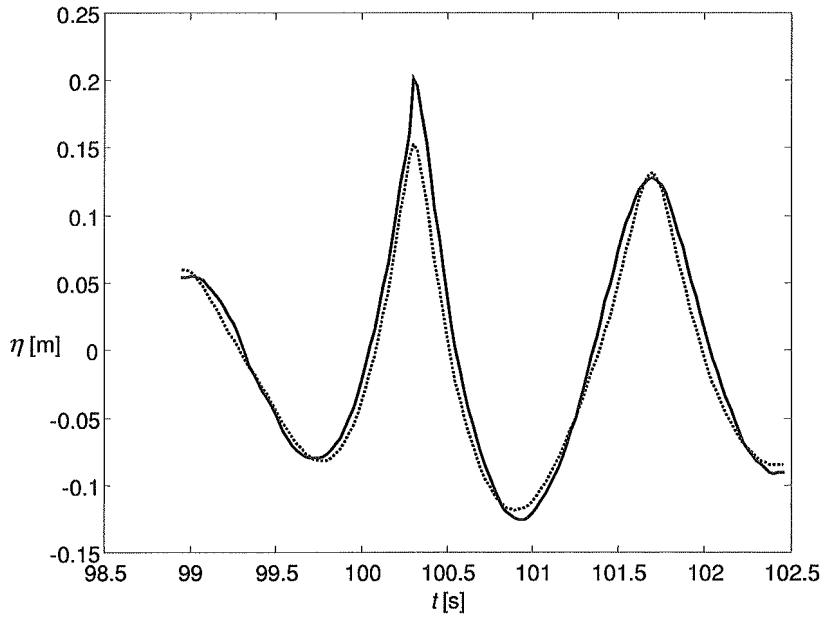

Figure 6.49 Excerpt of measured (–) and calculated (...) surface elevation at wave gage 1, Case 2 (run I14_1), $99 < t < 102.5$. Spectral frequency range: $\frac{1}{2}\omega_{20} < \omega < 2\omega_{20}$.

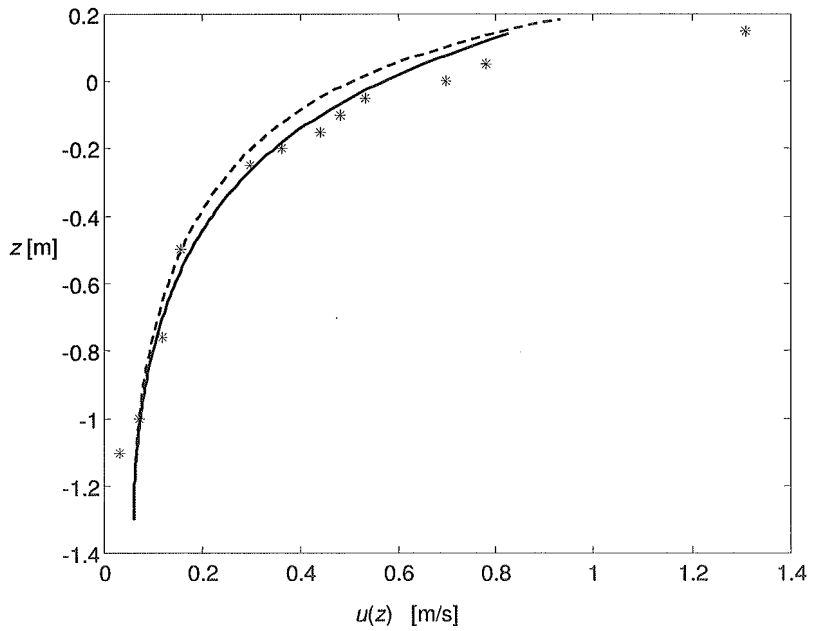

Figure 6.50 Horizontal velocity beneath crest at $t \approx 100.3$ s in Figure 6.49; (*) measured values, (–) calculations according to Miche, (- - -) calculations according to Wheeler. Spectral frequency range: $\frac{1}{2}\omega_{20} < \omega < 2\omega_{20}$.

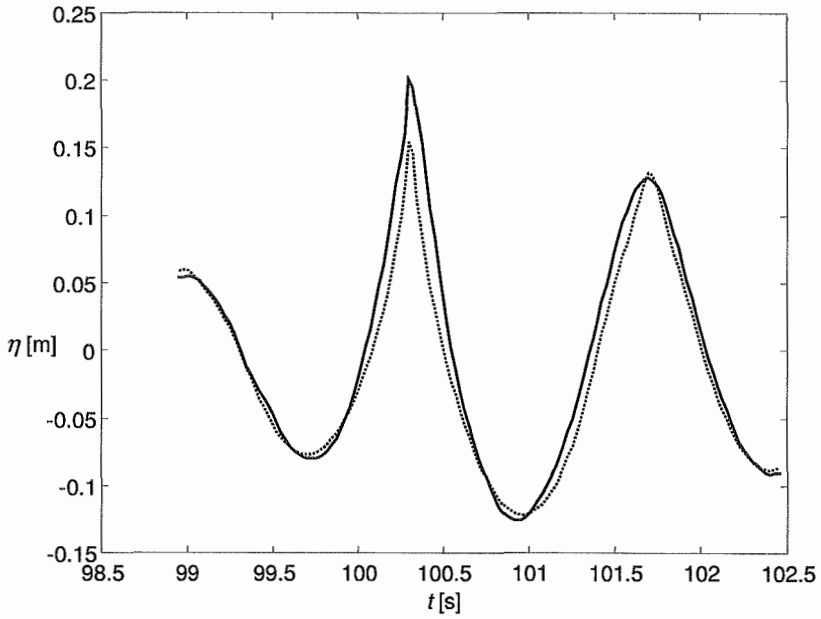

Figure 6.51 Excerpt of measured (–) and calculated (...) surface elevation at wave gage 1, Case 2 (run I14_1), $99 < t < 102.5$. Spectral frequency range: $0 < \omega < 3\omega_{20}$.

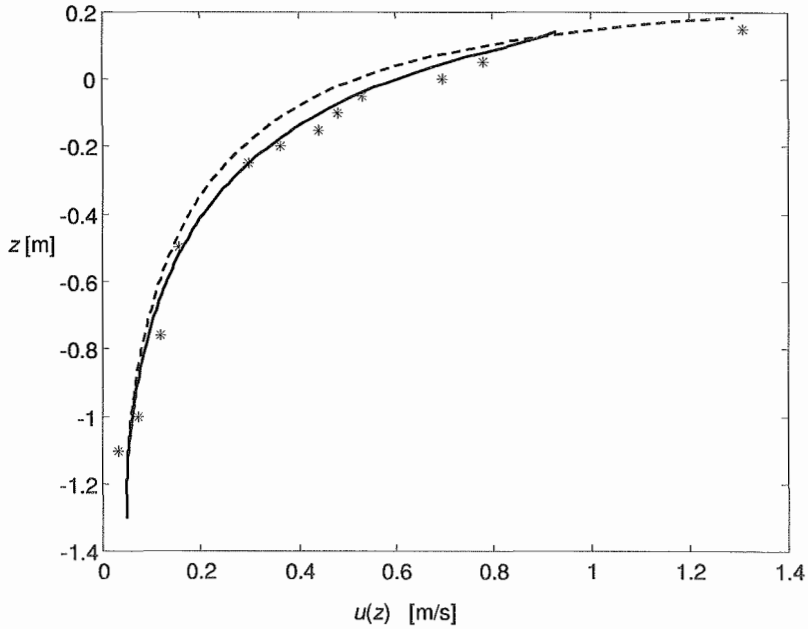

Figure 6.52 Horizontal velocity beneath crest at $t \approx 100.3$ s in Figure 6.51; (*) measured values, (–) calculations according to Miche, (- - -) calculations according to Wheeler. Spectral frequency range: $0 < \omega < 3\omega_{20}$.

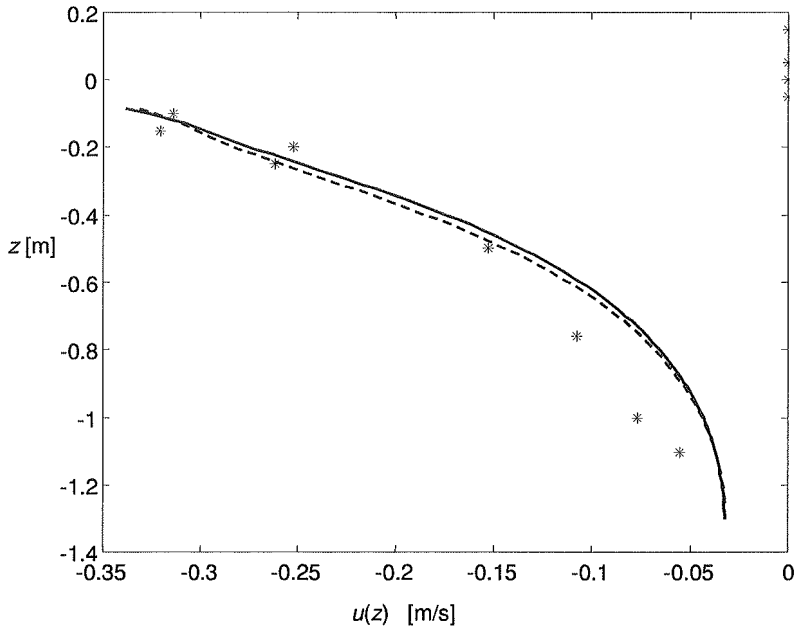

Figure 6.53 Horizontal velocity beneath trough at $t \approx 99.7$ s in Figure 6.51; (*) measured values, (–) calculations according to Miche, (- - -) calculations according to Wheeler. Spectral frequency range: $0 < \omega < 3\omega_{20}$.

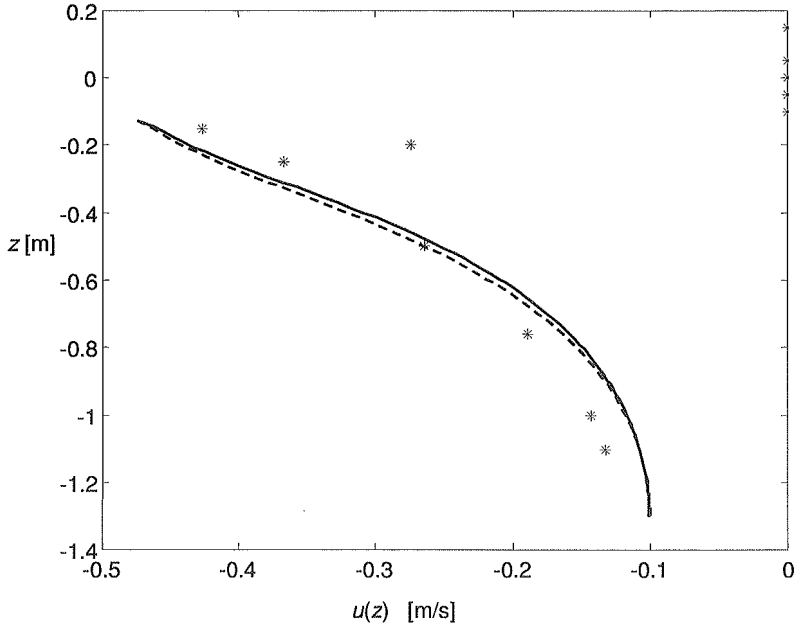

Figure 6.54 Horizontal velocity beneath trough at $t \approx 101$ s in Figure 6.51; (*) measured values, (–) calculations according to Miche, (- - -) calculations according to Wheeler. Spectral frequency range: $0 < \omega < 3\omega_{20}$.

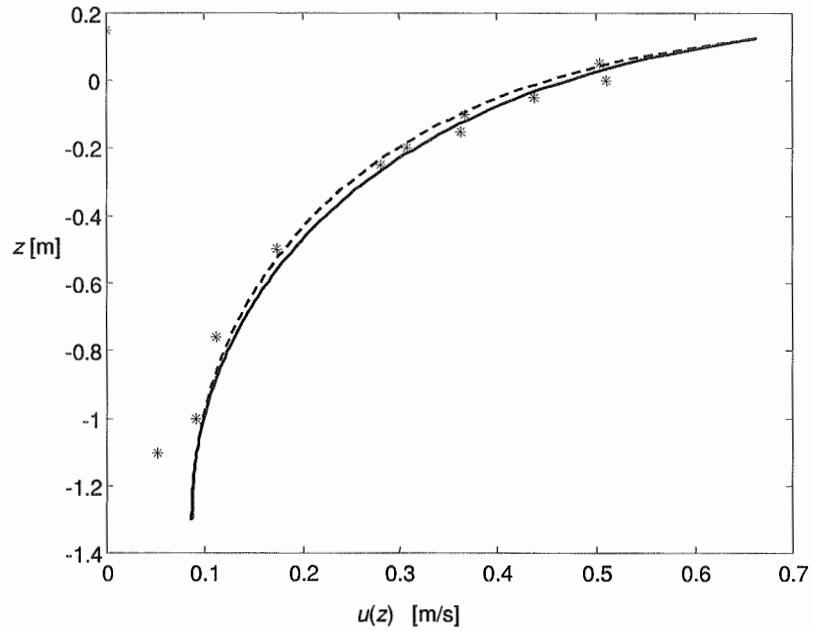

Figure 6.55 Horizontal velocity beneath crest at $t \approx 101.7$ s in Figure 6.51; (*) measured values, (–) calculations according to Miche, (- - -) calculations according to Wheeler. Spectral frequency range: $0 < \omega < 3\omega_{20}$.

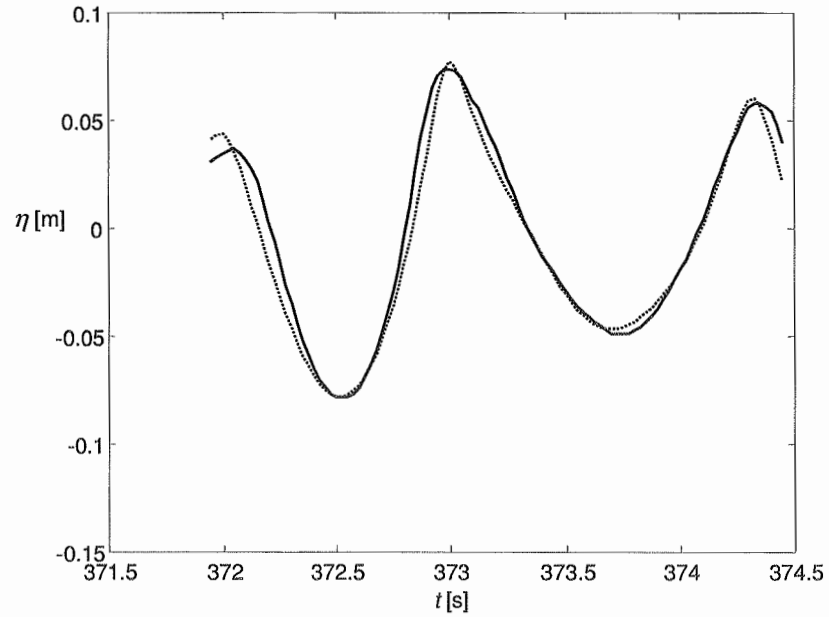

Figure 6.56 Excerpt of measured (–) and calculated (...) surface elevation at wave gage 1, Case 2 (run I14_1), $372 < t < 374.5$. Spectral frequency range: $0 < \omega < 3\omega_{20}$.

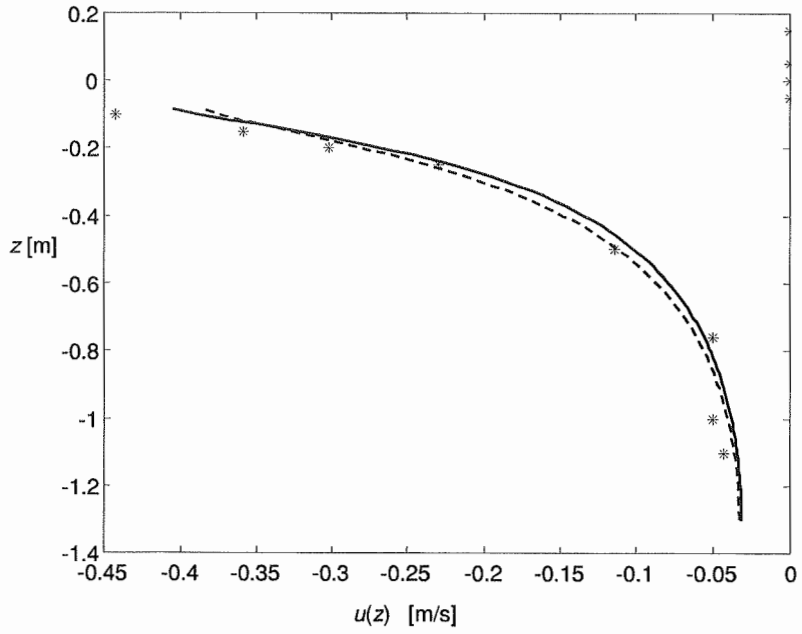

Figure 6.57 Horizontal velocity beneath trough at $t \approx 372.5$ s in Figure 6.56; (*) measured values, (–) calculations according to Miche, (- - -) calculations according to Wheeler. Spectral frequency range: $0 < \omega < 3\omega_{20}$.

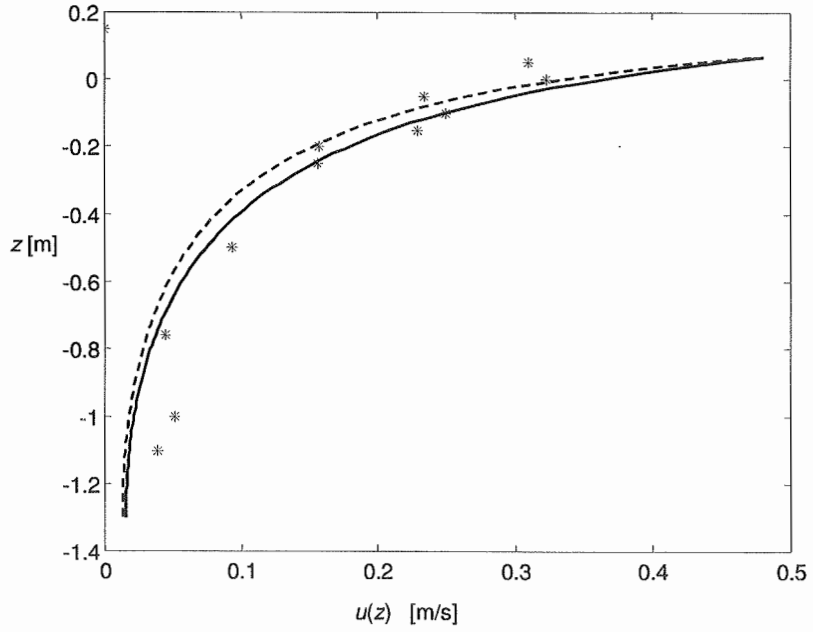

Figure 6.58 Horizontal velocity beneath crest at $t \approx 373$ s in Figure 6.56; (*) measured values, (–) calculations according to Miche, (- - -) calculations according to Wheeler. Spectral frequency range: $0 < \omega < 3\omega_{20}$.

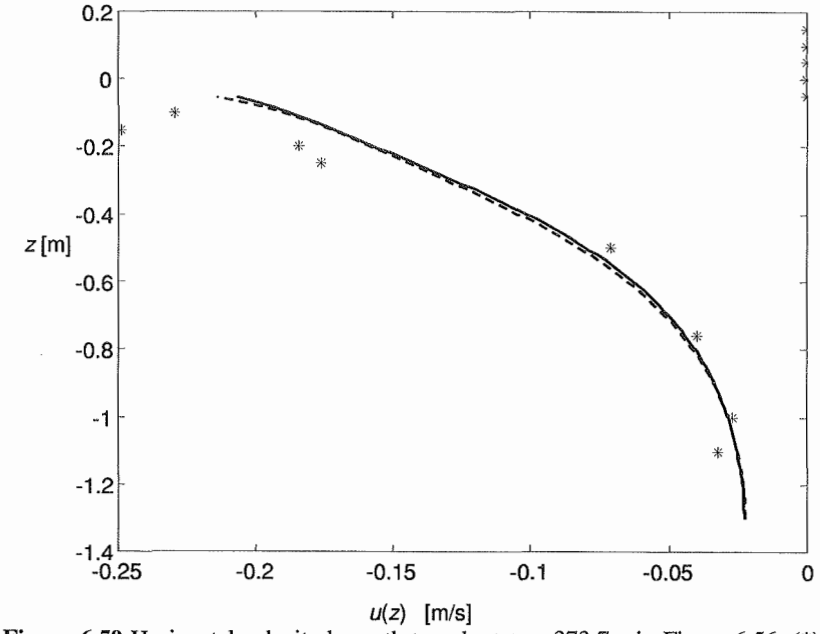

Figure 6.59 Horizontal velocity beneath trough at $t \approx 373.7$ s in Figure 6.56; (*) measured values, (–) calculations according to Miche, (- - -) calculations according to Wheeler. Spectral frequency range: $0 < \omega < 3\omega_{20}$.

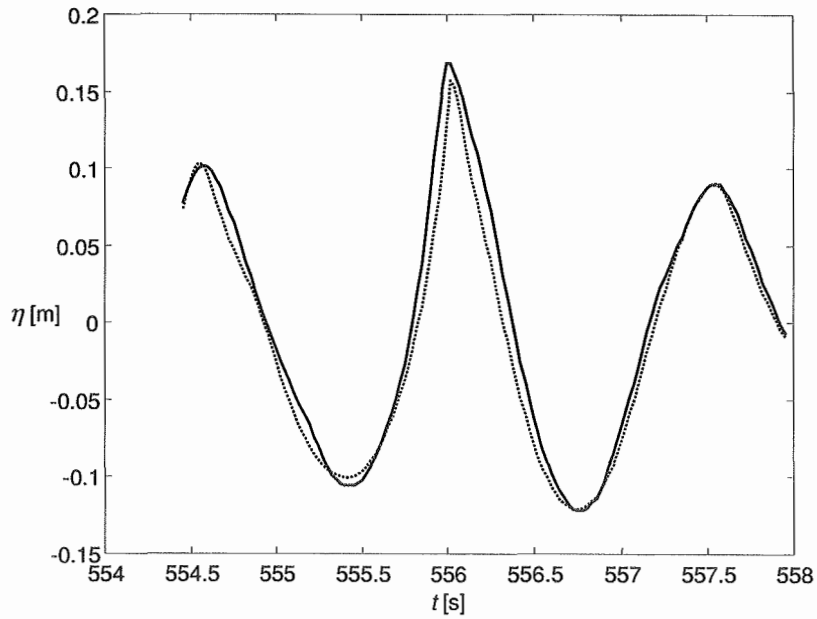

Figure 6.60 Excerpt of measured (—) and calculated (...) surface elevation at wave gage 1, Case 2 (run I14_1), $554.5 < t < 558$. Spectral frequency range: $0 < \omega < 3\omega_{20}$.

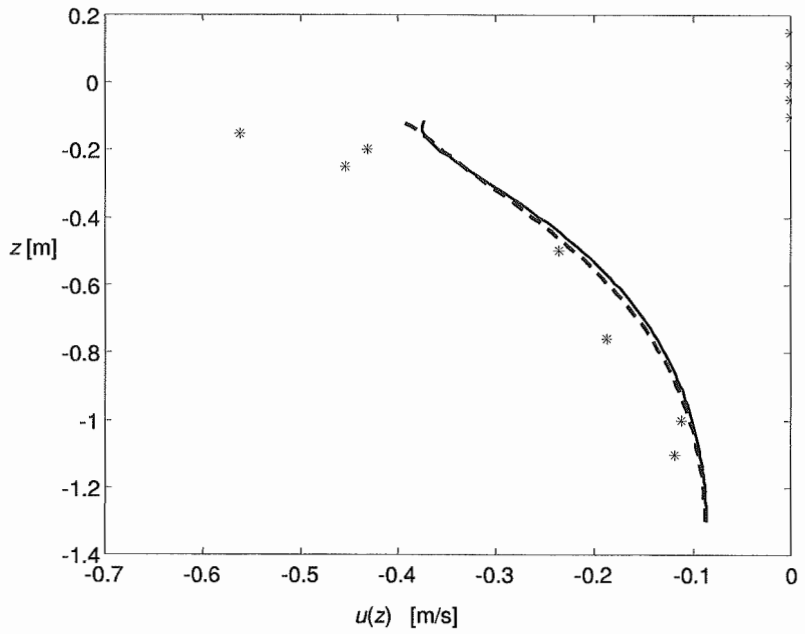

Figure 6.61 Horizontal velocity beneath trough at $t \approx 555.5$ s in Figure 6.60; (*) measured values, (–) calculations according to Miche, (- - -) calculations according to Wheeler. Spectral frequency range: $0 < \omega < 3\omega_{20}$.

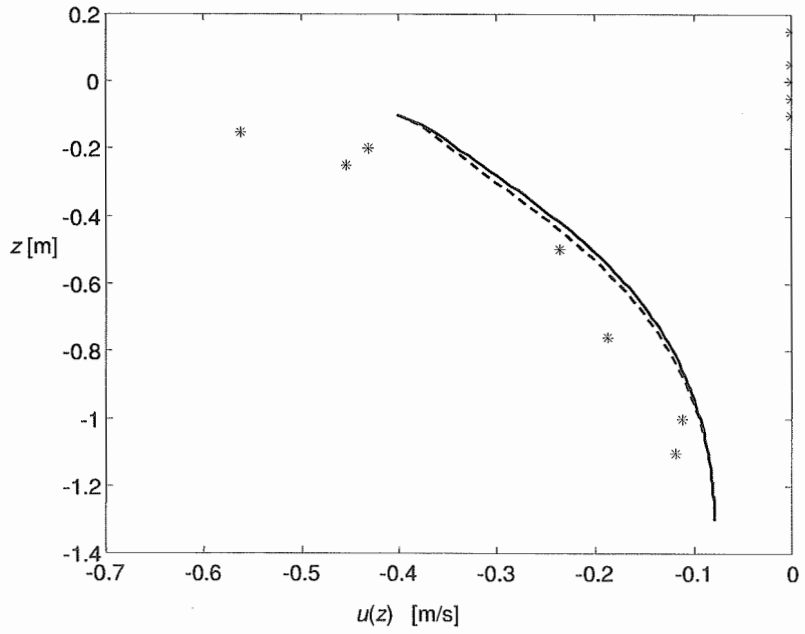

Figure 6.62 Horizontal velocity beneath trough at $t \approx 555.5$ s in Figure 6.60; (*) measured values, (–) calculations according to Miche, (- - -) calculations according to Wheeler. Spectral frequency range: $0.1\,\omega_{20} < \omega < 3\omega_{20}$.

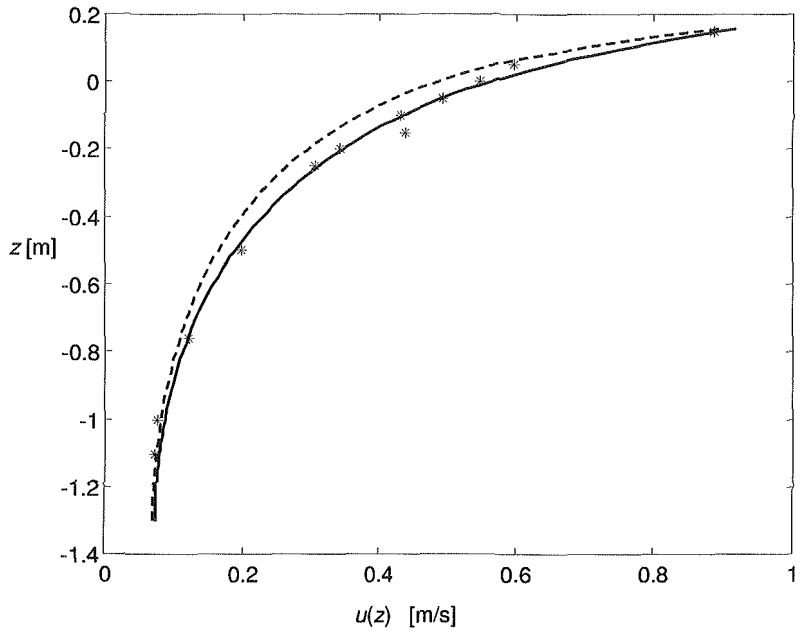

Figure 6.63 Horizontal velocity beneath crest at $t \approx 556$ s in Figure 6.60; (*) measured values, (–) calculations according to Miche, (- - -) calculations according to Wheeler. Spectral frequency range: $0 < \omega < 3\omega_{20}$.

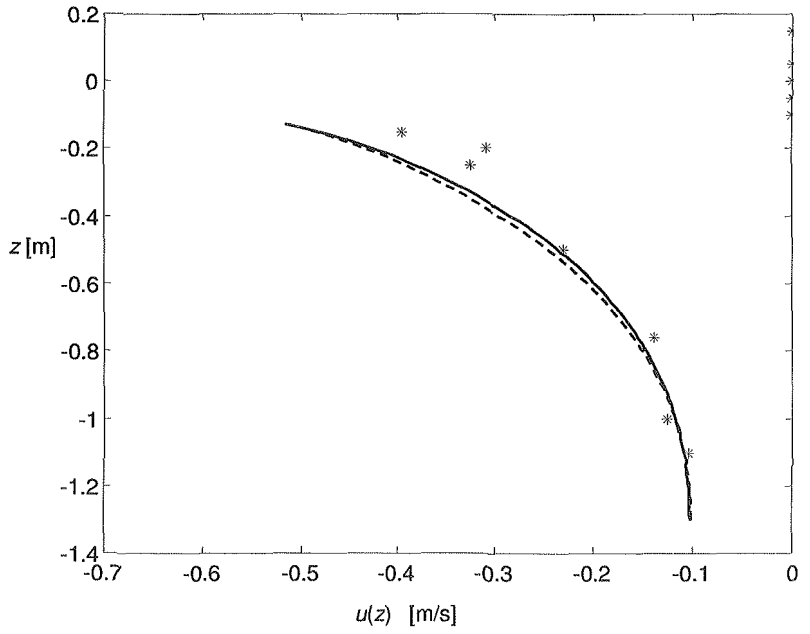

Figure 6.64 Horizontal velocity beneath trough at $t \approx 556.7$ s in Figure 6.60; (*) measured values, (–) calculations according to Miche, (- - -) calculations according to Wheeler. Spectral frequency range: $0 < \omega < 3\omega_{20}$.

Some results are included for the highest crest in Case 5 as well, cf. Figure 6.65 - Figure 6.69.

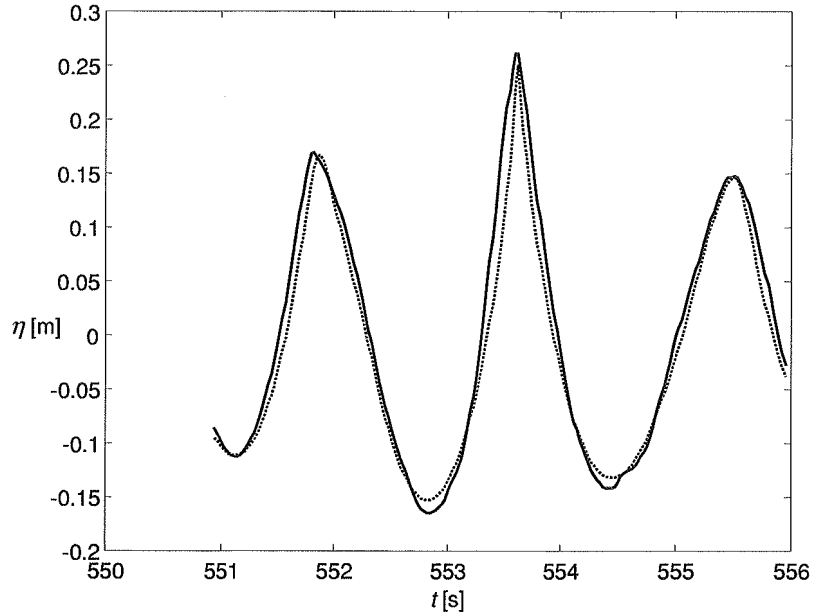

Figure 6.65 Excerpt of measured (–) and calculated (...) surface elevation at wave gage 1, Case 5 (run I18_23), $551.5 < t < 556$. Spectral frequency range: $\frac{1}{2}\omega_{20} < \omega < 3\omega_{20}$.

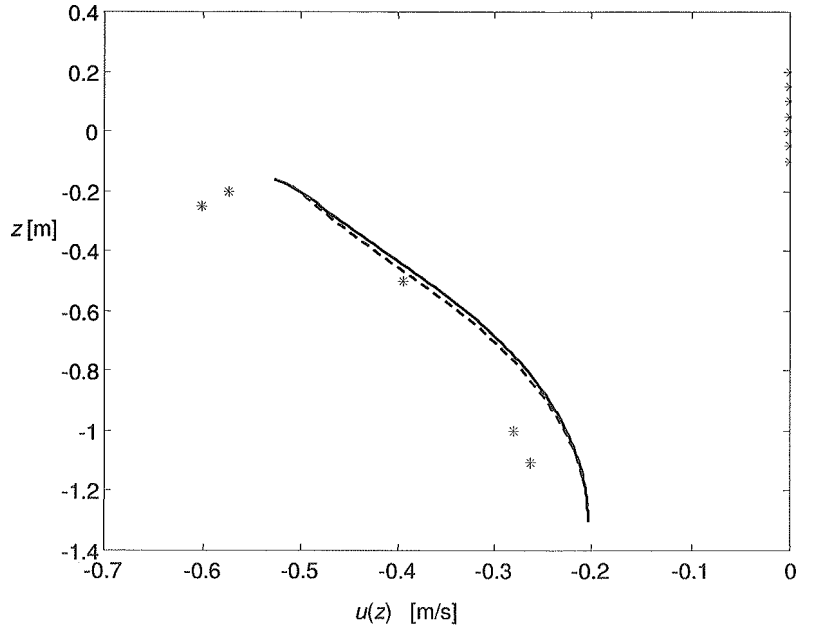

Figure 6.66 Horizontal velocity beneath trough at $t \approx 552.8$ s in Figure 6.65; (*) measured values, (–) calculations according to Miche, (- - -) calculations according to Wheeler. Spectral frequency range: $\frac{1}{2}\omega_{20} < \omega < 3\omega_{20}$.

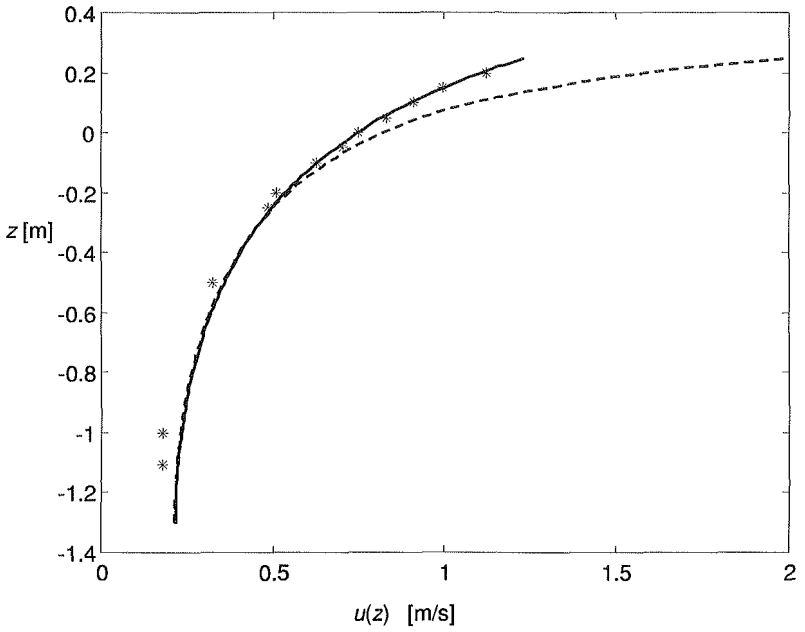

Figure 6.67 Horizontal velocity beneath crest at $t \approx 553.5$ s in Figure 6.65; (*) measured values, (–) calculations according to Miche, (- - -) calculations according to Wheeler. Spectral frequency range: $\frac{1}{2}\omega_{20} < \omega < 3\omega_{20}$.

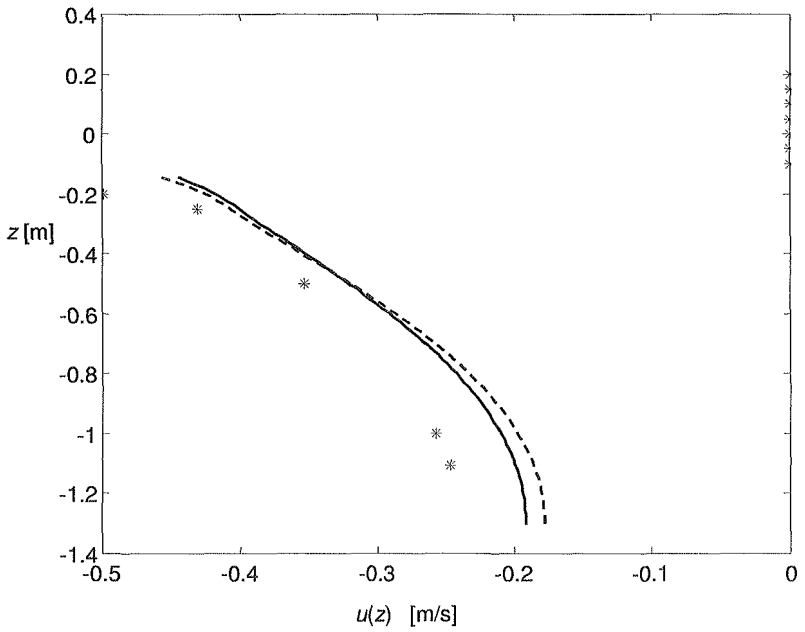

Figure 6.68 Horizontal velocity beneath trough at $t \approx 554.5$ s in Figure 6.65; (*) measured values, (–) calculations according to Miche, (- - -) calculations according to Wheeler. Spectral frequency range: $\frac{1}{2}\omega_{20} < \omega < 3\omega_{20}$.

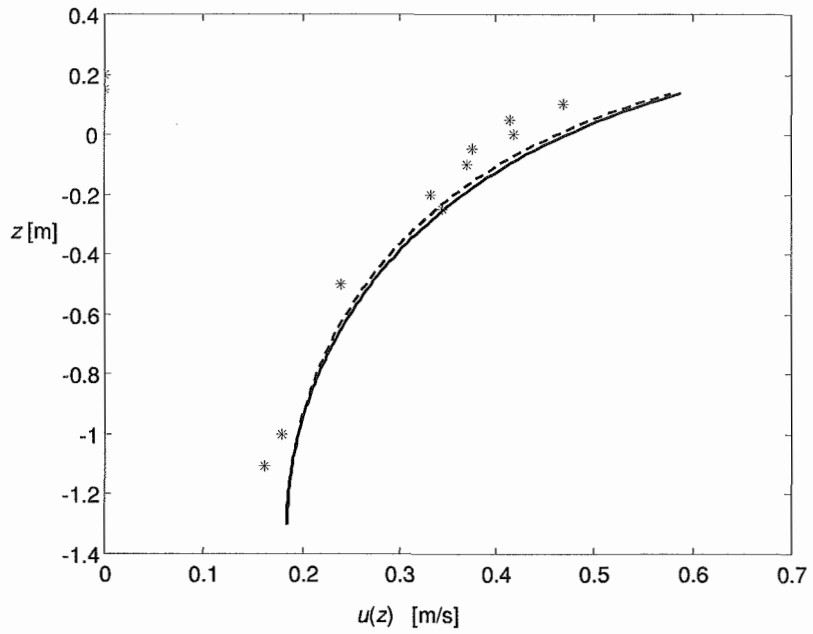

Figure 6.69 Horizontal velocity beneath crest at $t \approx 555.5$ s in Figure 6.65; (*) measured values, (–) calculations according to Miche, (- - -) calculations according to Wheeler. Spectral frequency range: $\frac{1}{2}\omega_{20} < \omega < 3\omega_{20}$.

Calculations according to Miche fail to reproduce the surface elevation perfectly, as expected due to the difference between Lagrangian and Eulerian spectra, but still appears to predict the horizontal velocity profile beneath crests and troughs better than Wheeler's method does. The velocities are still clearly overpredicted in some cases and clearly underpredicted in others, and calculations compare better with measurements beneath crests than troughs.

6.3.3 Timeseries of the surface elevation, effective steepness and velocities in fixed spatial points

The calculations in this section are performed according to the iteration method for irregular Miche waves described in Sections 5.3.4 and 5.4. Wheeler's method is not included below, since the relation between it and calculations according to Miche is assumed to be adequately covered in Section 6.3.2. Do however note that timeseries according to Wheeler's method are generally more "in phase" with timeseries measured in fixed Eulerian positions, since they are not subject to the difference between an Eulerian and a Lagrangian spectrum. The figures below are based on a spectral frequency range $0 < \omega < 3\omega_{20}$.

In Sections 5.4 and 6.3.2 it is shown that there will be differences between measured and calculated timeseries. Therefore, only a few examples are included her. As in Section 6.2.3, the vertical level under consideration is shown by a horizontal line in the surface elevation plot. The measured values are "frozen" at the last recorded value as the point comes out of water. Calculated values are included only for the intervals when the point in question is found to be in water theoretically. In addition to the surface elevation and horizontal and vertical velocities, plots of the effective steepness given by Eq. (5.6) are also included. For the surface, this is found in the same way as the surface elevation, i.e. according to Section 5.4. For a fixed z-position, it is found in the same way as the velocities, i.e. according to Section 5.3.4.

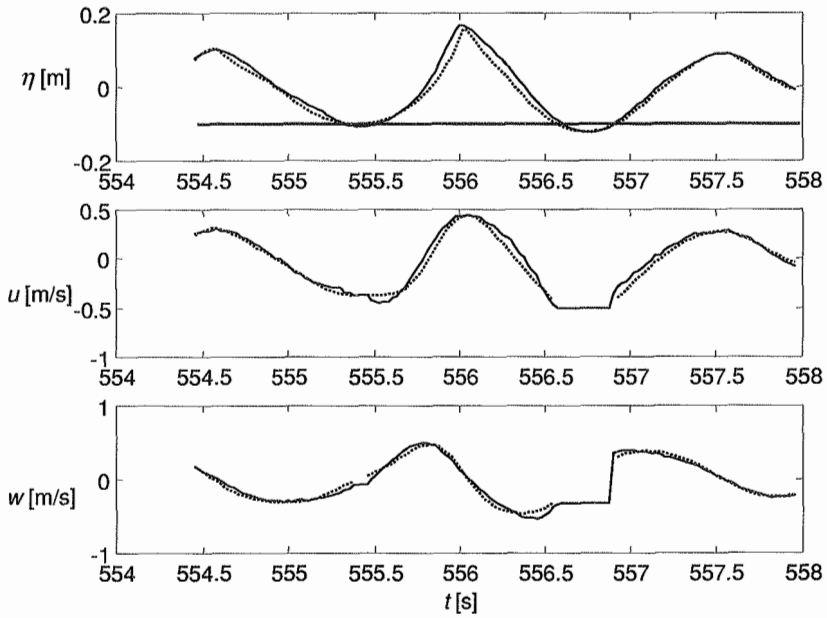

Figure 6.70 Excerpt of timeseries of the surface elevation and horizontal and vertical velocity at $z = -0.10$, $554.5 < t < 558$ s, Case 2 (run I14_1). The measured timeseries are given by solid lines, while calculations according to Miche are given by dotted lines.

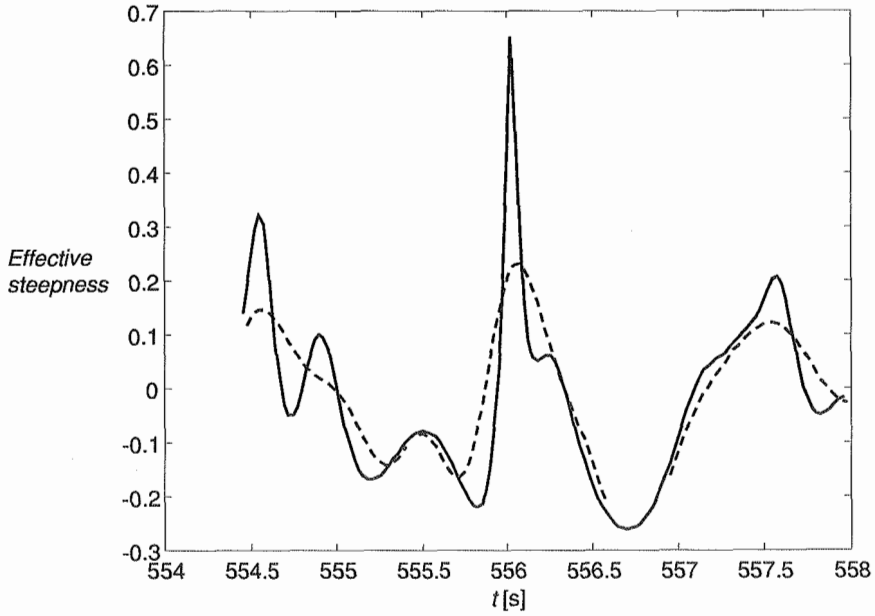

Figure 6.71 Effective steepness for the waves in Figure 6.70, calculated according to Eq. (5.6). The solid line represents the value at the surface, while the dashed line represents the value at $z = -0.10$, both at $x = 0$.

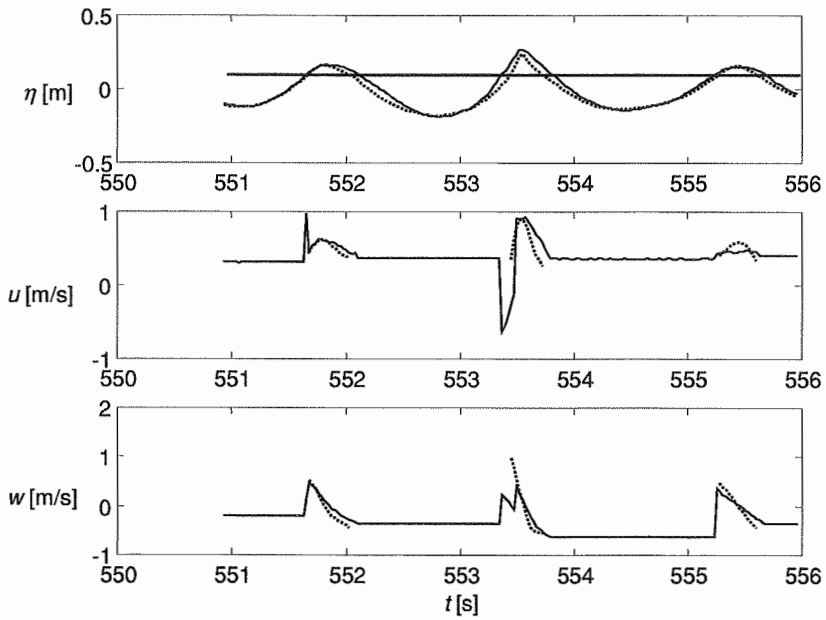

Figure 6.72 Excerpt of timeseries of the surface elevation and horizontal and vertical velocity at $z = 0.10$, $551 < t < 556$ s, Case 5 (run I18_15). The measured timeseries are given by solid lines, while calculations according to Miche are given by dotted lines.

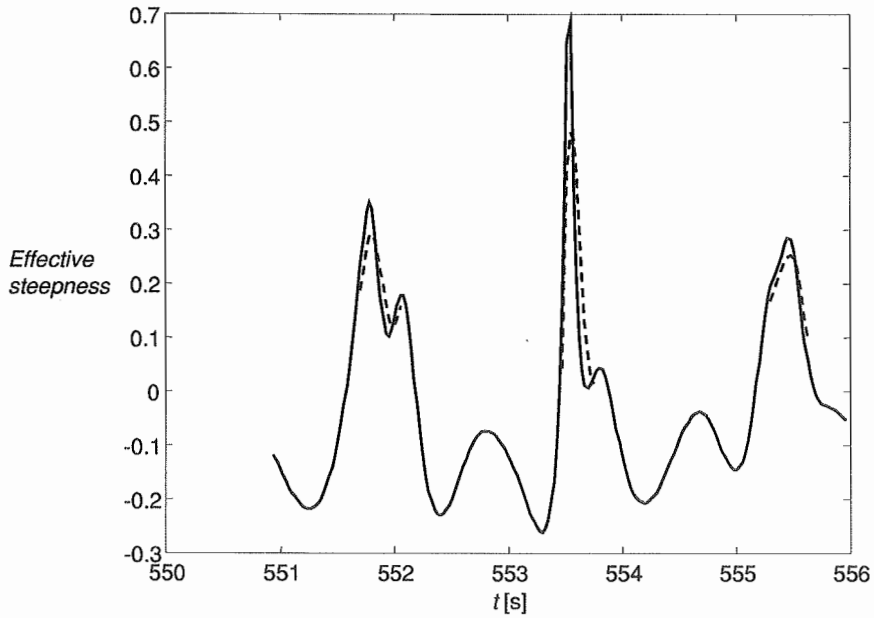

Figure 6.73 Effective steepness for the waves in Figure 6.72, calculated according to Eq. (5.6). The solid line represents the value at the surface, while the dashed line represents the value at $z = -0.10$, both at $x = 0$.

It is seen that the differences between the measured and calculated velocities correspond to the differences in surface elevation. A difference in the slope of the vertical velocity similar to that found for regular waves in Section 6.2.3 is seen in Figure 6.72 also. The measured values of w at $t \approx 553.5$ s in Figure 6.72 are clearly erroneous, and invalid spikes can also be observed for u in the same figure.

The effective steepness can be seen to reach values close to 0.7. The steepnesses are found to be practically unaffected by applying Eq. (5.5) and Eq. (4.17) instead of Eqs. (5.6) and (4.66).

Even if this has not been studied in detail, the horizontal velocity at all depths seems to be in phase with the surface elevation, cf. Figure 6.70. This seems to be the case in regular as well as irregular waves, in the early part of the timeseries as well as later on.

CHAPTER 7

DISCUSSION

7.1 The Basic Equations of Motion and Vortex Motion

7.1.1 The continuum model, the Jacobian and the Lagrangian frame of reference

In a continuum, the relations in Eqs. (2.1) and (2.2) must exist and be single-valued, cf. e.g. Truesdell and Toupin (1960). These relations may be found as solutions of the equations of motion. Also, a Lagrangian form of an Eulerian solution, and vice versa, may be found for any instant, e.g. by Taylor-expansions or iteration. A Jacobian may therefore always be determined, from an Eulerian as well as a Lagrangian solution.

The Jacobian and the Lagrangian frame of reference are closely related to the concept of continuity as well as to each other. For simplicity, only the 2D case will be discussed here, and the density is assumed to be uniform and constant. Conservation of mass is then ensured by conservation of area, as illustrated in Figure 2.1. Considering an infinitesimal area, which in still water was defined by $\delta A = dxdz$, Eq. (2.16) yields the following condition for the Jacobian and the Lagrangian frame of reference

$$Jdx_0dz_0 = const. \tag{7.1}$$

Continuity must apply to an element of finite size as well, yielding an integral relation as in Eq. (2.23), viz.

$$\iint Jdx_0dz_0 = const. \tag{7.2}$$

As stated in Section 2.2, the conservation laws apply to specific portions of matter, not to regions of space, and are therefore Lagrangian by nature. Although the material and the spatial descriptions are both due to Euler, it was Lagrange who introduced the Lagrangian coordinates as we know them, cf. Lamb (1932), Tokaty (1994) and Levi (1995). Hence the term 'Lagrangian' for the material description.

According to Lagrange, the material (i.e. Lagrangian) coordinates defining a specific material element at any time can be set equal to the Eulerian coordinates defining the element in a state

of rest. With reference to Eq. (7.1), this means that $dx_0 = dx$ and $dz_0 = dz$ at all times. The continuity requirement according to Lagrange must therefore be $J = 1$.

However, the solution of the equations of motion may result in a Jacobian different from 1. This is the case for Gerstner waves, cf. Eq. (4.8), viz.

$$J_{Gerstner} = 1 - k^2 a^2 e^{2kz_0} \tag{7.3}$$

Recall that Gerstner's solution is an *exact analytical solution* of the *nonlinear* equations of motion and boundary conditions. Perturbation solutions based on $ka << 1$ and $J = 1$ are physically equivalent to Gerstner's exact solution, cf. Eqs. (4.14) and (4.15) and related comments, only less accurate.

Lamb (1932, Art. 16) states that the Lagrangian coordinates need not be restricted to mean the initial (still water) Eulerian coordinates of a particle, they may be any quantities which serve to identify a particle, and may vary continuously from one particle to another. According to Lamb, the condition $J = const.$ therefore suffices to ensure continuity, as found in Section 2.3.1, and Eq. (7.3) thus satisfies continuity.

Hence, Lagrange and Lamb both *start* by assuming that the "meaning" of the Lagrangian coordinates remain the same at all times, i.e. that a Lagrangian point always represents the same material "particle". It then *follows* that the Jacobian must be constant, viz.

$$J = \frac{const.}{dx_0 dz_0} = const. \tag{7.4}$$

However, Eq. (7.3) leaves a physical problem with respect to Eq. (7.4). Even if the Jacobian in Eq. (7.3) is not explicitly a function time, it is a function of the wave amplitude and wavelength. A wave must somehow be generated over a finite period of time, and the wave amplitude and wavelength changes during generation. The Jacobian in Eq. (7.3) is therefore only constant as long as the wave amplitude and wavelength is constant, or in other words, as long as the state of deformation is constant. If the wave amplitude or wavelength changes, the Jacobian changes, and the Lagrangian frame of reference must be redefined according to Eqs. (2.23) and (7.2). Note that even if an element in a regular Gerstner wave deforms continuously during a wave period, its state of deformation is still uniquely determined by the wave amplitude and wavelength. The *redefinition of the Lagrangian frame of reference* is explained for the exact form of Gerstner waves in Section 4.1.1, in particular in the text between Eq. (4.9) and Eq. (4.14). The interval dz_0 defining a material element in existing waves is there found to be different from the interval dz defining it in still water, since z runs from 0 to $-h$ and z_0 runs from 0 to $(-h - \frac{1}{2}ka^2)$, where h is the water depth in still water. The intervals dx_0 and dx are equal. In the approximate form of Gerstner's solution, i.e. Eqs. (4.14) and (4.15), the intervals dz_0 and dx_0 are both equal to dz and dx, respectively, by *assumption*.

One may therefore say that in a perturbation approach, the inconvenience of redefining the Lagrangian frame of reference is avoided at the cost of reduced accuracy, while an exact solution may be found at the cost of a less convenient Lagrangian frame of reference. The former is of course a perfectly reasonable way of *obtaining an approximate solution*. However, Eqs. (7.3) and (7.4) are not only of importance with respect to waves and Gerstner's solution, they also have fundamental theoretical implications. They show that a Lagrangian frame of reference exists which is superior to that associated with $J = 1$. Therefore, it is argued here that it is incorrect to *impose general conditions on the solution* based on $J = 1$, e.g. as done in Eq. (3.22).

It is then appropriate to ask why Lagrange and Lamb, and others, claim that the "meaning" of the Lagrangian points have to be constant; what is the argument for putting a 'tag' on a specific fluid "particle"? Why must J, x_0 and dz_0 be constant individually, when it should be sufficient that the product (or integral of) Jdx_0dz_0 is constant? In order to address these questions it is necessary to consider the assumptions made with respect to physics as well as mathematics.

Continuity in a mathematical sense means that for surface (volume) integrals, the area (volume) of integration is reducible to a single point, cf. e.g. Batchelor (1967, his section 2.6). Conditions on the integral itself then also applies to the integrand, meaning that the dimensions $dxdz$ and dx_0dz_0 of the infinitesimal continuum element in Eqs. (7.1) and (7.2) are neglected.

Note then that e.g. Kinsman (1965, cf. his Eq. 2.2:9 and related comments) is not categorical about reducibility; he states that reducibility applies in his example because *no restrictions were made with respect to the area (volume) of integration.* In general, an entire infinitesimal area Jdx_0dz_0 must be considered in order to speak of a portion of matter. For reducibility to apply to the integral of Jdx_0dz_0, it is therefore necessary to invoke the restriction that the Lagrangian region dx_0dz_0 defining a specific portion of matter is constant in time. However, neither the continuum model nor mathematics requires that the Lagrangian frame of reference itself must be defined in a constant manner in time, yielding identifiable "point-particles". The latter would in fact be in conflict with the continuum model; a continuum-particle is a contradiction in terms. The typical dimension of a water element must be of the order 10^{-9} m or greater for the continuum hypothesis to make sense (Lin and Segel, 1988). There is still room for infinitely many points within such a small element, and even within the size of an atom for that matter, and there is no argument for requiring the physical "meaning" of the individual Lagrangian points to be constant.

Hence, reducibility from e.g. a curve to a point is not unambiguous; the mass (matter) associated with a point depends on the value of the Jacobian in this point. A single Lagrangian point can then only be considered a specific material "particle" in time *if* the Jacobian and the "meaning" of the Lagrangian points are constant separately, but these *need not be* constant separately; it is sufficient that they together satisfy Eqs. (7.1) and (7.2) (assuming constant and uniform density). It must then be concluded that requiring reducibility to "point-particles" identifiable in time is not generally correct, and that a curve cannot be said to represent the same portion of matter at all times by means of reducibility alone.

With respect to the continuum hypothesis and continuous motion, it is then sufficient that the relations in Eqs. (2.1) and (2.2) exist and are single-valued *at any instant*, and that any change in the Jacobian in time is continuous and physically reasonable. The Lagrangian frame of reference should be considered the instantaneously appropriate change of variables between a material and spatial description of a material element of some size, rather than a set of identifiable "point-particles". Hence, the Jacobian and the Lagrangian frame of reference follow from the motion rather than determine and restrain it. Interchanging of the terms 'material' and 'Lagrangian' must be done with care.

7.1.2 The material derivative and the basic equations of motion

As stated in the beginning of Section 2.2, the Eulerian equations of motion may be derived for an infinitesimal fixed control area (volume). The basic Eulerian equations are not influenced by the definition of the Lagrangian frame of reference, and therefore yield correct descriptions of *Eulerian* quantities.

If the Jacobian is not constant in time, the "meaning" of a Lagrangian point is not constant in time either. The Lagrangian points would then have to be functions of time in order to represent the same material "particles" at all times. A derivation similar to that leading to Eq.

(2.15) would then yield a material derivative different from that actually given in Eq. (2.15). However, that would be unphysical. Eq. (2.15) is still the proper form of the material derivative, but it must generally be associated with at least an infinitesimal area $dxdz = Jdx_0dz_0$ to pertain to a specific material element (in the 2D case). Care must therefore be taken when deriving secondary conditions and equations based on a material intepretation of the basic Eulerian equations, cf. Section 7.1.3.

The Lagrangian equations for linear momentum, i.e. Eqs. (2.27) and (2.29), are also unaffected, since the chain rule may be applied for any instant. However, these equations on differential form must be interpreted as applying to *some* portion of matter at a given instant in time, but we may not be able to identify *which* portion of matter unless we consider a Lagrangian region $Jdx_0dy_0dz_0$.

Further, based on Section 7.1.1, the Lagrangian equations of continuity in Section 2.3.1 must in general include the differential dimensions, i.e. as in Eq. (2.16) and in the derivation prior to Eq. (2.17). Eq. (2.17) itself must be considered applicable only for the special case when it can be assumed that $dx_0dz_0 = const.$ for a specific portion of matter. For the 2D incompressible case, the Lagrangian equation of continuity is then $Jdx_0dz_0 = const.$ For the general case, the equation of continuity is

$$dm = \rho(x_0, y_0, z_0, t) \cdot J(x_0, y_0, z_0, t) \cdot dx_0 dy_0 dz_0 = const. \tag{7.5}$$

$$m = \iiint_{V_0(t)} \rho(x_0, y_0, z_0, t) \cdot J(x_0, y_0, z_0, t) \cdot dx_0 dy_0 dz_0 = const. \tag{7.6}$$

where m represents mass and $V_0(t)$ is the Lagrangian region defining this portion of matter. V_0 varies in time according to the Jacobian, so that m is constant. Note that the Lagrangian frame of reference should be redefined according to the integral relations in Eqs. (2.23), (7.2) and (7.6) rather than according to the differential expressions in Eqs. (2.16), (7.1) and (7.5), since the Jacobian is a *function* of the Lagrangian variables. Hence, the Jacobian should be determined first, as a solution of the equations of motion and given boundary conditions, and the Lagrangian frame of reference should then be (re)defined to yield conservation of mass.

This could possibly offer an alternative method for finding higher order solutions of flow problems, e.g. as suggested for Miche waves in Section 7.2.1 and more generally in Section 7.2.3. However, any change in the Jacobian and redefinition of the Lagrangian frame of reference must be reasonable with respect to the problem under consideration, and the general applicability and practical value of such an approach has not been studied further.

7.1.3 Rotation and Lagrange's theorem

In Section 3.4 is shown that there is a difference between the rotation of a deformable infinitesimal element and rigid body rotation. This is exemplified in Section 4.1.3, where it is shown that elements in Gerstner waves do not have a net physical rotation about themselves, and that the circulation is not a net transport of mass along element boundaries. Gerstner waves may therefore be said to be without (physical) rotation, but, as stated at the end of Section 3.4, this is a matter of definition of the term 'rotation' (cf. Glossary also). Anyhow, vorticity is still present in Gerstner's solution, meaning that it violates Lagrange's theorem (which requires potential flow for this particular problem).

However, according to Sections 3.3 and 4.3, requiring an Eulerian velocity potential to exist precludes the deformation necessary to form waves, if the Jacobian is everywhere and always 1. Note that is is not uncommon to neglect deformation of small elements. In Monin and Yaglom (1971), it is stated that the infinitesimal fluid elements under consideration are *"...considered moving "as a whole", that is, without noticeable deformation. In other words, a*

"fluid particle" is an identifiable "point" of the volume of fluid which is moving within this volume according to the equations of fluid mechanics...". Batchelor (1967, his section 2.1) and Lighthill (1989) are somewhat less explicit with respect to neglecting deformation, and state instead that the dimensions of the infinitesimal element are *"...not involved..."* or *"...negligible...".* However, the dimensions must be involved, because the continuum hypothesis itself requires that we consider at least small 'lumps' of fluid. Also, the deformation of a larger element is the integrated effect of the deformations of the differential elements. If a larger element deforms, the boundary of this element deforms, hence the material elements constituting the boundary must deform. This can only happen if they have a size.

To be proofs of Lagrange's theorem, the derivations in Sections 3.2.2 - 3.2.6 must pertain to the same portions of matter at all times. This is presumably ensured by following specific Lagrangian points (x_0, z_0) or specific Lagrangian curve segments dx_0 and dz_0, assuming that a Lagrangian point always have the same physical "meaning" and that the Jacobian is constant. It must then also be generally correct to set the Jacobian equal to 1, which is also customary to do. However, according to the above and Sections 7.1.1 and 7.1.2, it is necessary to consider an area Jdx_0dz_0 in order to follow a specific portion of matter, and the Jacobian and the Lagrangian region defining a material element may vary individually, as long as the product Jdx_0dz_0 is constant in time.

To be more specific, the closed boundary curve in Kelvin's theorem does not necessarily represent the same portion of matter as the bounded element deforms. The material boundary of an element of finite size is shown in grey in Figure 7.1, where the circulation is indicated by the arrows. In order to be material, this boundary must have a thickness. At any instant in time, we may consider the limit as the thickness of this grey area approaches zero, yielding a curve (the outer line), and we may associate this curve with a specific portion of matter. However, this limit must generally be taken at every instant. Assuming that the bounded area in Figure 7.1 is deforming, the limit (the boundary curve) taken at two different instants in time cannot generally be associated with *the same* portion of matter, cf. Section 4.1.3 also.

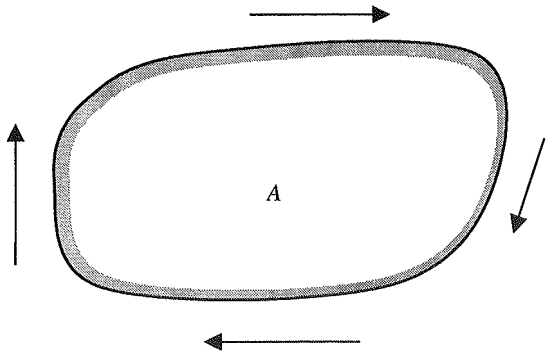

Figure 7.1 The material boundary (in grey) of an element of finite size (A). The outer line represents the limit as the thickness of the grey ring approaches zero. The arrows indicate the circulation along this limit curve.

Note that even if the closed curve in Kelvin's theorem encloses a finite area, cf. Section 3.2.6, this area is not in any way included in Kelvin's theorem itself; Kelvin's theorem only considers a line integral along a curve and thus only the curve itself. A line integral may also exist for a curve that is not closed, and it is then obvious that the curve cannot be associated with a specific area. However, since the curve considered in Kelvin's theorem is closed, the enclosed area *may* be included by invoking Stokes' theorem, cf. Section 3.2.7. However, by

invoking Stokes' theorem we no longer have a line integral under consideration, but a surface integral of the curl. Helmholtz' theorem applies to the curl (i.e. vorticity), but only as a point value. It can therefore only verify Kelvin's theorem as a proof of Lagrange's theorem *if* the area is negligible, which leaves us where we started.

Therefore, assuming that J need not be constant as the state of deformation changes, Weber's transformation, Caucy's equations and the theorems of Kelvin and Helmholtz cannot be said to consider the same portion of matter at all times, and it will not be physically relevant to impose conditions on them as if they did. Hence, they cannot be considered proofs of Lagrange's theorem as given in Section 3.2.1.

Also, according to the initial conditions in Weber's transformation and Cauchy's equations, given by Eq. (3.22), the existence of an initial velocity potential requires that $J = 1$. This means that $J = const.$ is not sufficient to ensure continuity in potential flow; the constant value must be 1. There is then a conflict between accepting that Eq. (7.3) satisfies continuity and requiring zero vorticity. If the former is accepted it is not relevant to require zero vorticity. Conversely, if zero vorticity is required, Eq. (7.3) cannot be said to satisfy continuity. However, while it is generally accepted that Gerstner's theory and Eq. (7.3) does satisfy continuity, the theory is still normally discarded since it is has vorticity. This is clearly inconsistent, if the initial conditions in Weber's transformation are necessary for an initial velocity potential to exist. However, it is not reasonable to compromize with regard to the continuity requirement, which is the most fundamental of the basic requirements in the continuum model, in order to satisfy such secondary conditions on vorticity. The initial condition given by Eq. (3.22) then satisfies continuity only approximately, and cannot be used as an argument to require potential flow to higher orders. This is in accordance with the findings in Sections 3.3 and 4.3.

The equations governing vortex motion is then Eqs. (3.32) and (3.35), where the former is only to be interpreted in Eulerian sense. Eq. (3.33) is only interpretable in a Lagrangian sense *while* the Jacobian is constant, meaning that vorticity and circulation can only be required to be constant as long as the state of deformation, e.g. given by the wave amplitude and wavelength when waves are concerned, does not change. Further, also in light of the initial condition Eq. (3.22) in Weber's transformation, vorticity and circulation must be allowed and expected to be of the same order of magnitude as the Jacobian's deviation from 1. The concepts of vortex lines and vortex tubes should therefore be reconsidered, since curves cannot generally be assumed to always consist of the same matter.

Requiring potential flow is then only correct to the same order as the Jacobian equals 1, which, according to the statements so far in Sections 7.1.1, 7.1.2 and the present section, is true to any order in special cases only, e.g. in uniform flow. The assumed existence of an Eulerian velocity potential in inviscid flow, and thus the use of potential theory and conformal mapping, should therefore also be reconsidered. This may also be of interest with respect to D'Alembert's paradox, which yields zero net force on a body in steady potential flow. When flowing around a body, fluid elements must deform near the body, which according to the above renders potential flow invalid in this region. D'Alembert's paradox, yielding zero net force, is however a reasonable approximation if the velocities, and thus the deformations, are very small, i.e. when the Jacobian is indeed close to 1.

Finally, it is not unusual that higher order perturbation solutions are found applicable even for cases where the perturbation parameter is not as small as originally assumed. This is the case for 2nd order Stokes waves. These waves are originally based on a perturbation assuming $ka \ll 1$, while at the end of the analysis it is found that $ka < 0.45$, approximately, is sufficient for convergence (cf. Eq. (4.87)). However, Section 4.3 shows that the latter limit is only valid quite instantaneously, and that Stokes waves of finite height violate the basic equations after less than a wave period. In the same section is shown that Stokes' wave theory, which is a

potential solution, may only be applied for a significant period of time if the wave amplitude is very small. Again, this is reasonable, since the Jacobian is then again very close to 1.

7.1.4 Some remarks on vorticity with respect to the physics of fluid motion

It is often stated that vorticity (in 2D incompressible flow) needs to be generated by velocity gradients at the boundaries, and that it is then somehow diffused, by conduction or convection, throughout the fluid. However, it has been shown that vorticity does not unambiguously express how a fluid element turns about itself, cf. Sections 3.4 and 4.1.3, i.e. it is not equivalent to a physical 'spin' of material fluid elements. Also, the material derivative must be associated with a region of some size, which appears to be of particular importance for a tensor such as the curl. It is therefore hard to see what is traditionally meant by generation and diffusion of vorticity.

Vorticity is "generated" when a deformation is generated, e.g. when non-uniform mass transport is generated, or when elements are deformed without mass transport, e.g. as in Gerstner waves, cf. Figure 4.1. The extension of a region of deformation may then itself be considered a "diffusion of vorticity". As a parallel, recall that the mean Eulerian velocity in Gerstner waves is not a "generated" current (in the sense of mass transport) in any way, it is merely the Eulerian result of the orbital Lagrangian motion, and it only exists where the waves themselves exist.

It is also of interest to note that the term 'vorticity' was apparently introduced by Lamb in his *Hydrodynamics* in an attempt to resolve a "*...heated public controversy between Helmholtz and Bertrand...*" over the interpretation of the term 'rotation' (Levi, 1995, p. 297). Bertrand, a French mathematician, insisted that Helmholtz results were incorrect, while Helmholtz accused Bertrand for distorting his concepts. Bertrand considered an example (simplified to 2D here) where $u = z$ and $w = 0$, which in Bertrand's opinion represents motion in a straight line without any physical rotation or 'spin'. Nevertheless, this motion yields curl $\mathbf{V} = 1$ and thus a 'rotation' according to Helmholtz. Levi (1995) still concludes that "*...The truth is that the existence of the velocity curl in a flow field only implies that the particles spin about themselves; an effect caused by viscosity, for instance, in the flow region near a wall...*". Kinsman (1965, his section 2.5) also includes a discussion on vorticity, but is less explicit and more cautious about how to interpret and identify it.

7.2 Wave Theory and Modelling

7.2.1 The wave theories of Gerstner and Miche

In Section 7.1, the common assumption that motion generated by potential forces has to result in a potential flow is questioned. It is there argued that the Jacobian must be allowed to deviate from 1, and a vorticity of the same order of magnitude as the Jacobian's deviation from 1 must be allowed and expected.

Gerstner's theory is then a physically correct solution for regular waves on infinite depth, in the limit of negligible viscosity. The fact that Gerstner's solution is an exact analytical solution is primarily due to the regularity and the assumption of infinite depth. This makes a constant Jacobian and a constant definition of the Lagrangian frame of reference possible.

In intermediate water Miche's solution applies. The fact that Miche's 1st order solution does not yield a constant Jacobian to second order, need perhaps not be interpreted just as a violation of continuity at second order. It can also be an indication that such waves may not be regular to second order on finite depth. In Figure 6.11 and Figure 6.15 is seen that a "non-regularity", apparently of second order when comparing to the magnitude of the vertical shift

given by Eq. (6.17), is present from the very first waves and for the rest of the records. This is not the case in Figure 6.4 and Figure 6.7, at least not very pronounced, which pertain to deeper water. The physical relevancy of seeking a regular solution to second order for such waves on finite depth, as in the 2nd order part of Miche's solution, may therefore be questioned. With reference to Section 7.1.2, the 2nd order solution for such waves on finite depth could possibly be found by determining a time-varying Lagrangian frame of reference compensating for the time-varying Jacobian resulting from the 1st order solution, i.e. Eq. (4.67), so that Eq. (7.2) is always satisfied. This may e.g. result in a time-varying vertical shift, cf. Eqs. (4.60) and (4.61), and effects such as bound waves etc. may be inherent in the solution. It is also unclear if and how e.g. radiation stress should be included in a Lagrangian analysis. However, these issues could not be verified or investigated any further within the limited time frame of this thesis work.

In Section 4.3 it is shown that Stokes waves violate the assumed continuity requirement $J = const.$ at second order within less than a wave period. Since it has been suggested that a non-constant Jacobian may be accounted for by a corresponding redefinition of the Lagrangian frame of reference, it seems that this could apply to Stokes waves as well. However, the growth of the Jacobian in Stokes waves is fundamentally different from the 2nd order periodic variation of the Jacobian in e.g. Miche waves, cf. Eqs. (4.67) and (4.68). In Stokes waves, the Jacobian grows very rapidly in time and is eventually of the leading order, cf. Table 4-1 - Table 4-3. This growth cannot be compensated for by a corresponding redefinition of the Lagrangian frame of reference in a physically reasonable manner, cf. Section 7.1.2.

Some may argue that Stokes drift is not to be interpreted as "literally" as in Section 4.3, but that a "redistribution" of mass must be allowed. That may be physically correct. However, requiring the vorticity in an existing wave to be zero also requires that the Jacobian and the vorticity are interpretable "literally" for at least the period of time required to generate the wave. If not, one cannot compare an existing wave situation with a still water situation in this respect. Also, any type of redistribution of mass necessary due to Stokes drift would be nothing but a violation of continuity and the principle of impenetrability of matter (which is inherent in the continuity requirement), in which case we cannot speak of identifiable material particles in Stokes waves. However, Stokes waves is a result of the assumption of irrotational motion, which is based on the assumption of identifiable material particles. Therefore, it is hard to see how Gerstner's theory can be discarded if Stokes waves are not discarded, i.e. if Eqs. (4.88) - (4.92) and Table 4-1 are ignored. This supports Gerstner's theory as an applicable basic solution for regular waves.

Finally, if it is claimed that potential forces can only generate irrotational flow, one might ask how waves, with their surface curvature (cf. Sections 3.3 and 4.3), can be generated by potential forces alone. Since there is good reason to assume that surface gravity waves *are* mainly generated by potential forces, it is again reasonable to question the assumption that potential forces can only generate irrotational flow.

7.2.2 Superposition of linear Lagrangian components and transformation from the Lagrangian to the Eulerian frame of reference

Straightforward superposition of different wave components is mathematically correct only if the individual components are linear. A straightforward superposition model of irregular waves can therefore not include nonlinearities, and, since the governing equations are nonlinear, it will not be a physically complete model of irregular waves. Even if nonlinearities and nonlinear interactions are somehow accounted for, it is still not given that a superposition model represents real random seas satisfactorily. That depends on how close real random seas actually are to a sum of regular waves. Nonlinearities and interactions between spectral components can therefore not be expected to explain or account for all types of discrepancies between measurements and spectral models of irregular waves.

It is known that a 1st order (linear) Lagrangian solution corresponds to a 3rd order Eulerian solution with respect to the surface profile, cf. Eq. (4.41) and related comments. The reason for this is that the boundary conditions are satisfied in a more correct manner in the Lagrangian approach. Hence, even if it is still only a solution of the linearized problem, a linear Lagrangian model is superior to a linear Eulerian model. In Section 5.1 is shown that superposing linear wave components in the Lagrangian frame of reference is different from superposing linear wave components in the Eulerian frame of reference. Performing the superposition in the Lagrangian frame of reference is seen to automatically include interactions that appear as nonlinear from a purely Eulerian point of view, cf. Figure 5.1 - Figure 5.4. Such interactions may to some extent be included in Eulerian models also, e.g. as in the hybrid wave theory of Zhang et al. (1996). However, while these Eulerian approaches require quite complex additional models for the interaction between components, the analytical simplicity of the Lagrangian approach is striking.

The iteration methods in Sections 5.3 and 5.4 yield theoretically consistent values everywhere, also above the still water level, and as many frequency components as desired may be included. Their main advantage is that they eliminate the need for extrapolation of solutions and stretching of coordinates, and thus uncertainties due to violation of the governing equations and overprediction of high frequency contributions near and above the still water level. The iteration methods described in Section 5.3.4 were found to be sensitive to very low frequency contributions in irregular Miche waves. The reason for this is that the hyperbolic fraction in the expressions for x_{0t} and x_t in Eqs. (5.47) and (5.49) grow rapidly when k_n approaches zero, and the associated wave amplitudes may not be small enough to compensate for this, cf. Figure 6.34. These very lowest frequency components therefore cause an error in the output of the iteration, i.e. x_{0t} and z_{0t}, and thus an error in the calculated velocities. This is also the case for x_0 in Eq. (5.55), which will cause an error in η in Eq. (5.56). Since it is anyhow not physically correct to include the lowest frequency components in this way, cf. Eqs. (6.14) and (6.15) and related comments, a lower cut-off frequency should therefore be employed when performing iterations according to the hyperbolic expressions for finite depth.

The main problem with the Lagrangian approach presented here is comparing it with Eulerian measurements. In Skjelbreia et al. (1991), the Lagrangian orbital amplitude spectrum was not measured directly in the experiments, but it is found that the spectrum of the surface elevation measured at fixed Eulerian x-position is a reasonable approximation to the Lagrangian orbital amplitude spectrum, cf. Sections 5.4. This is discussed in more detail in Section 7.4.

However, comparisons with measurements in e.g. wave flumes are not the ultimate objective. Ocean waves are often measured by buoys, yielding wave spectra that may be considered more Lagrangian than Eulerian, and design spectra are anyhow subject to uncertainties, cf. Section 5.4 also.

Hence, even if perfect agreement between Eulerian measurements and calculations based on Lagrangian expressions may be difficult to obtain, the Lagrangian approach presented here should be of great practical and theoretical value, very well suited for simulations and design purposes. It applies to regular as well as broad-banded irregular waves, yielding equally consistent results everywhere, also in the splash zone. Simulations based on synthetic wave spectra may contribute to an improved understanding of certain physical phenomena, such as breaking of waves and 'ringing' of offshore structures. The potential for further theoretical development seems considerable, as is discussed in the following section.

7.2.3 Modelling nonlinear irregular waves by the Lagrangian approach

In Eqs. (4.8) and (7.3) it is seen that the Jacobian in Gerstner's exact analytical solution is a function of the wave amplitude and wave number. Therefore, regular Gerstner components of different amplitude and wavelength generally yield different Jacobians. From Eqs. (7.2) and

(7.3) we see that the Lagrangian frame of reference is determined by the Jacobian, and vice versa. A Lagrangian element defined by fixed values of Δx_0 and Δz_0 will therefore not represent the same material element for two different Gerstner components. The difference will depend on the differences in amplitudes and wavelengths. Therefore, different regular Gerstner components are associated with different Lagrangian frames of reference, which is also apparent from the vertical shift in Eq. (4.13). Hence, different individual Gerstner components cannot be directly compared or superposed. This is in fact a physical explanation why straightforward superposition cannot include nonlinearities.

If we realize this, however, we may also account for it. Nonlinear Lagrangian components may then possibly be superposed in a theoretically consistent manner. This may also be accounted for in the iteration methods described in Sections 5.3 and 5.4, yielding Eulerian quantities correct to higher orders. In other words, it appears that the Lagrangian approach makes irregularity and nonlinearity theoretically compatible. Note then that the most basic form of the equations of motion is linear, cf. Eqs. (2.11) - (2.14). The equations do not become nonlinear until the material derivative is invoked to have them on Eulerian form, or the chain rule is applied to have them on Lagrangian form. Hence, nonlinearity may be said to stem from differences between the frames of reference involved, and analytical problems caused by nonlinearity may be avoided or reduced by proper definition and interpretation of these frames of reference. However, cf. Section 7.2.1, such issues on nonlinear Lagrangian terms could not be pursued any further within the limited time frame of this thesis work.

For Miche waves, i.e. accounting for finite depth, the same inclusion of nonlinearities in the superposition and calculations should be possible. However, cf. Section 7.2.1, it is unclear how to best include nonlinearity on finite and varying depth.

In Section 5.1 it was shown that superposition of regular wave components may produce extreme waves and waves of extreme crest front steepness, if the values of the effective steepness in Eqs. (5.5) and (5.6) approach the limit value 1. Hence, the Lagrangian approach describes the kinematics in some types of extreme waves. If the limit value is reached or exceeded, continuity is violated and the wave will somehow break.

However, it does not seem that all types of extreme and breaking waves (in deep/intermediate water) can be modelled by superposition of spectral components alone, even if nonlinearities and interactions are somehow accounted for. It seems that any Lagrangian currents, i.e. real mass transport, must also be identified and included in the analysis. In Section 4.3 it was shown that interaction between regular waves and vertically non-uniform currents will eventually violate continuity in the Lagrangian sense, which must result in some sort of breaking and modulation of the waves. The currents may be local wind- or wave generated currents or underlying ocean currents. The kinematics in such extreme and breaking waves may be reasonably well modelled by superposing waves and current in a Lagrangian fashion, but only for a very short period of time, e.g. one wave period. Such interaction between waves and current should be further investigated in a Lagrangian frame of reference.

7.3 Results for Regular Waves

The regular wave cases considered pertain to intermediate water depth. Therefore, although the theoretical considerations in Sections 7.1 and 7.2 mainly consider Gerstner's theory, the calculations are performed according to Miche's theory.

7.3.1 Mean horizontal velocity in a vertical cross-section

This section pertains to the results presented in Section 6.2.1. Note that the mean horizontal velocity in Miche waves is calculated according to the approximate expression in Eqs. (4.77)

and (4.78), and that they therefore should not be expected to exhibit perfect agreement with the measurements.

The recordings of regular waves and wave kinematics show that two distinct transitions in the horizontal velocity take place during the experiments, yielding two distinctly different flow-field conditions. Such transitions are not observed for the surface elevation or vertical velocity, and these are also found to be practically unaffected by the transitions in the horizontal velocity.

The first transition, shown in Figure 6.5 and Figure 6.6, is associated with the wave front of the regular wave train. It takes place at $t \approx 14$ s in Case 9 and at $t \approx 17$ s in Case 8. This type of transition is also reported by Johnsen (1987) and Gudmestad et al. (1988) for other regular wave experiments, as will be discussed more closely in Section 7.3.5.

Skjelbreia (1991) observed a second type of transition in the experiments considered in Chapter 6, taking place when roughly 50 waves have passed wave gage 1, i.e. at $t \sim 100$ s. Closer investigations in Section 6.2.1 show that this transition takes place over some period of time, starting near the surface at $t \sim 75$ - 90 s and developing throughout the depth until $t \sim$ 120 - 135 s, eventually yielding a mean velocity profile as in Figure 6.9. This is still in agreement with the findings of Skjelbreia, who apparently only considered one case and one vertical level in this respect (Case 8, $z = 0.10$). The length of time until this transition takes place and develops throughout the depth appears to depend on the wave amplitude (i.e. the penetration of a wave into the fluid) and the water depth, rather than on the wave celerity and assumed Stokes drift velocity. These quantities are given in the introduction to Section 6.2. This suggests that it is not (mainly) a return current developing, but that it takes some time before regular waves as we expect them are fully developed throughout the depth.

The first disturbances in the surface elevation arrive at wave gage 1 a bit later in Case 9 than in Case 8, cf. Figure 6.4 and Figure 6.11, as might be expected due to the difference in the wave celerities in Eq. (6.18). However, the positive mean horizontal velocity associated with these very first disturbances is significantly higher in Case 9 than in Case 8, indicating that this effect is strongly influenced by depth. The difference in the negative mean velocity set up as the actual wave front passes is less, but still marked, cf. Figure B.1 - Figure B.13 and Figure B.24 - Figure B.32 in Appendix B.

In Figure 6.4 (Case 8), a distinct wave front can be identified as "wave number 6", and in Figure 6.11 (Case 9) a distinct wave front can be identified as "wave number 4". The first transition is associated with the wave front, and takes place a bit earlier in Case 9 than in Case 8 in spite of the lower wave celerity. The wave front in Figure 6.11 is not as pronounced as the wave front in Figure 6.4, but has more or less the same wave height as the subsequent waves. This difference in the nature of the wave front is found to be quite typical for these two cases, although some variations between the individual runs of each case occur.

The measured mean Eulerian horizontal velocity set up after the first transition, cf. Figure B.8 - Figure B.13 and Figure B.29 - Figure B.33 in Appendix B, resembles that often expected from Stokes drift and the associated vertically uniform return current, cf. Figure 6.2 and Figure 6.3. As the second transition takes place, the mean velocity profile takes on a form very similar to that predicted by Miche's theory, and remains more or less like this for the rest of the records, cf. Figure B.14 - Figure B.28 and Figure B.34 - Figure B.43 in Appendix B.

7.3.2 Instantaneous horizontal velocity in a vertical cross-section beneath individual crests and troughs

This section pertains to the results presented in Section 6.2.2. Figure 6.16 - Figure 6.19 show that large errors may be introduced if calculating the instantaneous Eulerian horizontal velocity according to the approximate Eulerian expressions in Sections 4.1.5 and 4.2.2. The

magnitudes of these errors depend on the wave steepness *ka* and the vertical coordinate *z*. The horizontal velocity in regular Miche waves is therefore calculated according to the iteration methods described in Sections 5.3 and 5.4. Wheeler's method is described in Section 5.2.

Figure 6.20 and Figure 6.21 show that Wheeler's method and Miche's solution yield identical values at the surface and at the bottom, as they should for regular waves, and the differences in the region in-between are qualitatively as expected due to the stretching of coordinates in Wheeler's method. These differences between Miche and Wheeler also show that the Lagrangian approach qualitatively accounts for the typically observed deficiency of Wheeler's method for the velocity beneath crests in irregular waves, cf. Section 5.2.

When compared with measurements, Miche's solution deviates from measurements made shortly after the first transition, as seen in Figure 6.22, Figure 6.23, Figure 6.26, Figure 6.27, Figure 6.30 and Figure 6.32. However, again, Miche's solution is found to compare very well with measurements made after the second transition, cf. Figure 6.24, Figure 6.25, Figure 6.28, Figure 6.29, Figure 6.31 and Figure 6.33.

7.3.3 Timeseries of the surface elevation and velocities in fixed spatial points

This section pertains to the results presented in Section 6.2.3. As for the instantaneous horizontal velocity, the timeseries in fixed Eulerian points were calculated according to the iteration methods described in Sections 5.3 and 5.4.

When considering the form of the surface elevation, the waves appear to be quite symmetric at $t \sim 45$ s, cf. Figure 6.30 and Figure 6.32, while a slight asymmetry about a vertical axis can be seen for $t \sim 150$ s in Figure 6.31 and Figure 6.33. This asymmetry is quite small and thus neglected with respect to the kinematics. However, the cause and effect of the asymmetry should be studied further. While the surface elevation in Case 8 generally exhibits a quite regular profile, the surface elevation records of Case 9 are clearly "non-regular", cf. Figure 6.4, Figure 6.7, Figure 6.8, Figure 6.11 and Figure 6.15. This "non-regularity" resembles a bound long wave, and is present from the very first waves and for the rest of the records.

The surface elevation is modelled quite well, but not perfectly, by Miche's solution. However, the level of the crests and troughs predicted by Miche's theory, accounting for the vertical shift, is in good agreement with the measured surface elevations, cf. Figure 6.22 - Figure 6.29, Figure 6.30, Figure 6.31, Figure 6.32 and Figure 6.33. Exceptions are Figure 6.26 and Figure 6.27. These happen to correspond to a crest of the apparent bound long wave, as seen for $t \approx$ 45 s in Figure 6.11, which explains these discrepancies. These are also the figures where the difference between applying the regular wave amplitude a from Table 6-1, Eq. (6.20) or (6.21), respectively, are seen to be most significant. These figures suggest, as expected, that Eq. (6.21) is a better choice than Eq. (6.20) as an appropriate local regular wave amplitude for calculations.

7.3.4 General findings for regular waves

The vertical velocity has not been studied very closely, since it is assumed that the results for the horizontal velocity are most descriptive with respect to the performance of the theory. The results in Section 6.2.3 show that the differences between measured and calculated velocities generally correspond to the differences in measured and calculated surface elevation. This is of special importance with respect to the vertical velocity, since this is out of phase with the surface elevation. A clear difference can be seen in the slope of w beneath crests and troughs, cf. Figure 6.30 and Figure 6.31. No transitions similar to those for the horizontal velocity are observed for the vertical velocity. There may seem to be a transition in the negative peak values of w from Figure 6.32 to Figure 6.33, but this is found to stem from quite local variations.

The creeping flow may have a marked influence on the entire mean velocity profile after a while, meaning that a real return current is set up due to the creeping flow. However, the creeping flow cannot be the cause of the second transition described above, since it does not "start" until after the second transition is more or less fully developed. This can be stated after reproduction and video-filming of a regular wave case identical to the one in Case 8, cf. Section 6.2.1. A run with regular waves of shorter wavelength was also filmed. The latter corresponds to deep water conditions, viz. $T = 1.2$ s, $\lambda = 2.25$ m, $ka = 0.25$ and $h = 1.3$ m. The second transition was observed visually for this case as well, taking place after a period of time comparable to that found for Case 8, while a creeping flow was not observed at all. The creeping flow is likely to be stronger and set up earlier in Case 9 than in Case 8, due to the different depth-to-wavelength ratios yielding higher velocities near the bottom in Case 9.

The comparisons in Section 6.2 focus on measurements made near $t \sim 45$ s and $t \sim 150$ s, since these are found to be representative for the two distinct situations identified. The results are verified for other time instants as well. Later on in the experiments, the measurements must be assumed to be more influenced by reflections, creeping flow and other undesired effects.

Hence, in the period after the first transition and prior to the second transition, the conditions are not unlike what would be expected from 2nd order Stokes waves including Stokes drift, while Miche's theory compares very well with measurements after the second transition and for the rest of the record. Note however that only the mean horizontal velocity has been considered for Stokes waves, that the measured maximum values are somewhat lower than predicted by Stokes drift in Figure 6.2 and Figure 6.3. Nor is there any reason to expect the positive mean velocity in the splash zone to be reduced if Stokes drift is real and a return current actually develops. Also, as apparent from Eq. (6.19), Stokes "particle"-drift would be quite strong and should be easily observable. Visual observations during reproduction and video-filming of some of the experiments in Skjelbreia et al. (1991) indicate that material elements are transported forward before the second transition, while they move in closed orbits after the second transition.

7.3.5 On the cause of the transitions in horizontal velocity in regular waves, and implications for the carrying out and interpretation of regular wave experiments

Johnsen (1987) suggests that the positive mean velocity associated with the very first disturbances stem from a positive pressure gradient caused by an apparent set-up of the mean water level ahead of the wave front of the regular wave train. Similarly, Johnsen (1987) and Gudmestad et al. (1988) suggest that the negative mean velocity associated with the actual wave front stem from a negative pressure gradient caused by a set-down that appears to follow the wave front itself. Calculations in Gudmestad et al. (1988) support this hypothesis. Gudmestad et al. (1988) also conclude that Wheeler's method is not suited for modelling regular wave kinematics, which is generally correct. However, Wheeler's method and Miche's solution give identical values at the very crest for regular waves. Also, the failure of Wheeler's method below the crest is predictable for regular waves, cf. Figure 6.20 and Figure 6.21, and Wheeler's method and Miche's theory may be considered comparable with respect to the other methods that are included in the comparisons of Gudmestad et al. (1988).

The results in Gudmestad et al. (1988) are based on results in Skjelbreia (1988) as well as Johnsen (1987). Johnsen (1987) analyzed data from experiments undertaken at Delft (Delft Hydraulics Laboratory, 1982), and Skjelbreia (1988) analyzed data from experiments undertaken at Caltech (Skjelbreia, 1987). The wave flumes in these experiments were of a type and dimensions comparable to that in Figure 6.1, and the wavemakers were of a horizontally acting flap/piston-type. The regular wave cases considered were also comparable to those in Table 6-1. The measurements chosen for comparisons were typically made as the first ten waves had passed the measurement point in Skjelbreia (1988), and near the beginning

of the uniform portion of the wave train before any reflected waves came back to the wave gage in Johnsen (1987).

The results and conclusions in Johnsen (1987) and Gudmestad et al. (1988) are all reasonable, although it is unclear if a pressure gradient due to a set-up or set-down explains the very clear *vertical uniformity* of the mean horizontal velocity after the first transition. However, it cannot be ignored that their considerations are based solely on measurements made before any second transition would have taken place. It is not obvious that the earliest part of a regular wave train represent regular waves satisfactorily, or that this early part is appropriate for comparisons with regular wave theory.

The question is therefore *what* causes these transitions and *when* the waves in a regular wave experiment are closest what we should expect them to be; before or after the second transition. It seems that the most crucial point is to determine whether Stokes drift is "true" or not, both in a theoretical as well as physical sense. It has been found that a Stokes-like drift exists early on in the experiments, but that small material elements eventually move in closed orbits as predicted by Gerstner's and Miche's wave theories. The analytical work in this thesis suggest that requiring irrotational flow may be incorrect, cf. Sections 7.1 and 7.2.1. Since Stokes drift itself violates continuity in the Lagrangian sense and is a direct consequence of requiring irrotational flow to second order, cf. Section 4.3, this suggests that the situation after the second transition is most appropriate for comparisons with regular wave theory. The initial Stokes-like drift is then not really Stokes drift, but "something else".

The initial effect of a horizontally acting wavemaker may be significant in this respect. The waves are generated by pressure acting horizontally on a vertical column of fluid, and not, as assumed for wind waves, mainly by pressure acting normally on the free surface. It must be assumed to take some time before the initially still water is adapted to the action of the wavemaker. A flap-type wavemaker may thus cause an initial transient forward mass transport in the upper region due to the "pushing" of the water, requiring an upwelling at the wavemaker and consequently a negative mass transport in the lower region. As the water eventually moves back and forth in a more periodic manner, i.e. has become more adapted to the action of the wavemaker, this initial circulation should vanish.

If, on the other hand, Stokes drift is found theoretically acceptable in spite of Sections 4.3, 7.1 and 7.2.1, Stokes drift must somehow be stopped or reduced because of the end-walls in the flume. However, since the creeping bottom flow is not stopped or prevented from being generated, there is no obvious reason why Stokes drift should be stopped or reduced. Recall that the second transition, i.e. when the apparent Stokes drift has stopped, takes place before a return flow caused by the creeping bottom flow could have influenced any Stokes drift.

However, these issues can hardly be resolved by further analysis of experiments in "short" wave flumes where waves are generated by horizontally acting flap-type wavemakers. The fundamental theoretical issues regarding vorticity and "particle"-drift should be resolved first, accompanied by regular wave experiments primarily carried out for deep-water conditions. A creeping bottom flow is thus avoided, or at least postponed, and the unfortunate bound long waves seen in Figure 6.11 and Figure 6.15 are minimized. The waves should preferably be generated by pressure acting normally on the free surface, in flumes long enough to avoid reflections for "long" periods of time. When the regular deep-water case is resolved, interactions with underlying and/or wave-generated currents may be included, as well as finite and varying depth. Irregular and three-dimensional wave conditions should be based on a proper understanding of regular two-dimensional waves and currents, cf. Section 7.2.3 also.

7.4 Results for Irregular Waves

Recall that irregular waves are modelled as a sum of linear (1st order) components. To first order, Stokes (Airy) waves may be replaced by Gerstner or Miche waves. The higher order (nonlinear) differences between the Lagrangian and Eulerian wave theories, such as the vorticity and vertical shifts in Gerstner and Miche waves and the 2nd order Stokes drift in Stokes waves, are therefore not of relevance here.

7.4.1 Mean horizontal velocity in a vertical cross-section

This section pertains to the results presented in Section 6.3.1. The mean horizontal velocity in irregular Miche waves is calculated according to the approximate expression in Eqs. (4.77) and (4.80).

For the long-term mean horizontal velocity in irregular waves, the narrow band assumption is found to compare very well with measurements above and below the typical level of the troughs. However, there is a clear underprediction at the typical trough-level itself, cf. Figure 6.37 - Figure 6.39. This should not be interpreted as an error in the underlying theory, but as an effect of the narrow band assumption as compared to broad-banded waves. This is apparent from Figure 6.35. Variations in the representative narrow band frequency is there seen to yield a marked increase/decrease in the calculated mean velocity at the typical trough-level, while the values above and below are practically unaffected. The simple expressions for the region always submerged, i.e. Eqs. (4.57), (4.58), (4.81) and (4.82), may be quite useful in order to estimate the magnitude of the mean Eulerian velocity (due to the waves) in irregular waves.

The development of the long-term mean horizontal velocity in irregular waves resembles the development in regular waves. In the early part of the records, there is a positive mean velocity in the splash zone and (quite roughly) a vertically uniform and negative mean velocity below the splash zone, cf. Figure 6.36. A marked transition then takes place within ~ 2-3 minutes, cf. Figure 6.37 - Figure 6.39. These figures are based on averaging timeseries-intervals of lengths corresponding to 80-100 peak periods, but the same results were found when considering somewhat shorter timeseries-intervals as well. This transition is believed to correspond to what is called the second transition in regular waves. The values of T_p and H_s in the irregular wave cases are quite similar to the wave parameters in the regular wave cases, cf. Table 6-1, and the transition takes place within a comparable time frame. Skjelbreia (1991) did not observe such a transition for irregular waves. However, it seems that he only considered relatively short excerpts of the timeseries in this respect, and that the irregularity itself would therefore have made it hard to identify distinct transitions. For the same reason, a transition equivalent to what is called the first transition in regular waves has not been studied for irregular waves, but similar effects are believed to be present here.

Studying short-term variations in the mean horizontal velocity is still useful in order to interpret the nature of the mean velocity. The quite strong variations seen in Figure 6.41 - Figure 6.43 suggest that the mean velocity is indeed a result of more or less closed orbital "particle"-paths of varying amplitudes. The waves in Figure 6.40 are here considered individual regular waves, and some uncertainty exist due to the choice of the averaging period of 1.5 s. Still, a higher individual wave is clearly associated with higher positive *and negative* values in the mean velocity profile, as predicted by Gerstner and Miche. A return-current, i.e. a real backward mass flow independent of the instantaneous wave, should not exhibit short-term variations of this nature or magnitude. Similar short-term variations are seen in Figure 6.44 - Figure 6.47.

No further efforts have been made to investigate the development and transitions of the mean horizontal velocity in irregular waves, since this issue should be resolved for the regular case

first. Creeping bottom flow is assumed to be negligible for the irregular wave cases considered in Section 6.3.

7.4.2 Instantaneous horizontal velocity in a vertical cross-section beneath individual crests and troughs

This section pertains to the results presented in Section 6.3.2. The horizontal velocity in irregular Miche waves is calculated according the iteration method described in Section 5.3.4, and the surface elevation is calculated according to Section 5.4. Wheeler's method is described in Section 5.2.

Calculations according to Miche are generally found to predict the horizontal velocity beneath crests quite well, and better than Wheeler's method does. The calculations generally compare better with measurements beneath crests than troughs, and the difference between Miche and Wheeler is less beneath troughs than crests, cf. Figure 6.50, Figure 6.52 - Figure 6.55, Figure 6.57 - Figure 6.59, Figure 6.61 - Figure 6.64 and Figure 6.66 - Figure 6.69.

The difference between Wheeler's method and calculations according to Miche is qualitatively the same as found for regular waves, cf. Figure 6.20 and Figure 6.21, and generally in accordance with the typical observed deficiency of Wheeler's method for the velocity beneath crests in irregular waves, cf. Section 5.2. In the previous section it was found that the mean horizontal velocity hardly can be interpreted as an underlying return current. The modification to Wheeler's method suggested by Gudmestad and Haver (1993) in Eq. (5.10) may therefore be questionable, since it is based on the assumption that such a return current exists. A modification of the same form but of lesser magnitude may be more appropriate, accounting for the stretching only and not for any return current. However, the Lagrangian approach yields theoretically consistent values everywhere, also in the splash zone, and eliminates the need for stretching methods and modifications.

The iteration methods in Sections 5.3.4 and 5.4 were found to introduce additional uncertainty when including the very lowest frequency components, i.e. $\omega << \omega_{20}$, cf. Section 7.2.2. This uncertainty is associated with the lowest values of k, and is estimated to 0.01 m/s for the figures pertaining to the frequency range $0 < \omega < 3\omega_{20}$ in Section 6.3.2. Note that this uncertainty only applies to calculations according to Miche's theory.

7.4.3 Timeseries of the surface elevation, effective steepness and velocities in fixed spatial points

This section pertains to the results presented in Section 6.3.3. The calculations are performed according the iteration methods described in Sections 5.3.4 and 5.4. As above, this introduces an additional uncertainty in the figures based on the frequency range $0 < \omega < 3\omega_{20}$, which is found to be of the order 0.01 m/s for the velocities and 0.01 m for the surface elevation.

Calculations according to Miche fail to reproduce the surface elevation perfectly, mainly because of the difference between an Eulerian surface elevation spectrum (i.e. measured at a fixed Eulerian x-position) and a Lagrangian orbital amplitude spectrum, cf. Section 5.4. The peak values of the surface elevation can still be expected to be reproduced quite well, while a difference in the form of the timeseries must be expected elsewhere. The calculated crests and troughs may also be slightly out of phase with the measured ones.

The peaks of the crests and troughs are generally very well reproduced, except for in the very highest waves of the records, cf. Figure 5.13, Figure 5.14, Figure 6.49, Figure 6.51, Figure 6.56, Figure 6.60, Figure 6.65, Figure 6.70 and Figure 6.72. The expected differences in the shapes of the timeseries intervals between the crests and troughs are also apparent in these figures.

Differences in calculated and measured timeseries of the velocities are generally found to correspond to the differences in the measured and calculated surface elevation when the *shape* of the timeseries is considered, cf. Section 6.3.3. However, differences in the actual *level* of the timeseries may be much smaller. This is apparent e.g. from Figure 6.65 and Figure 6.69, where the calculated peak value at of the surface elevation is in good agreement with the measured peak value, while the calculated horizontal velocity clearly exceeds the measured velocity. Also, Figure 6.67 shows a remarkable agreement between measurements and Miche's theory, while Wheeler's method overpredicts the velocity severely. However, studying the corresponding timeseries for u at $z = 0.10$ in Figure 6.72, we see that the peak of the measured values appear to be "cut off" and that a slightly higher peak value may be more correct, cf. Section 6.1.1 also.

In Figure 6.71 and Figure 6.73, the effective steepness can be seen to reach values close to 0.7 at the free surface. The steepness is found to be practically unaffected by applying Eq. (5.5) and Eq. (4.17) instead of Eqs. (5.6) and (4.66), meaning that it is not the difference between a hyperbolic and exponential expression causing these high values. The peak values of the steepness are also found to be the same when calculating them in accordance with Eq. (5.4), i.e. on Eulerian form. The experiments in Skjelbreia et al. (1991) hardly include the steepest waves ever, and the effective steepness in irregular waves may therefore be assumed to actually approach 1. Although this effective steepness may not be directly comparable to the steepness of regular waves, these results do question the common assumption that ka must be less than approximately 0.45 in regular waves. Recall that the limit steepness in regular Gerstner waves is given by $ka < 1$, and there are no obvious theoretical reasons why it should be less.

7.4.4 General findings for irregular waves

As for regular waves, the calculated and measured values of the vertical velocity in irregular waves will generally not compare well, since the vertical velocity is out of phase with the surface elevation and thus more subject to the differences between Eulerian measurements and calculations according to Lagrangian expressions, cf. Figure 6.72 and Sections 5.4 and 6.1.3. However, again, it is assumed that the results for the horizontal velocity are most descriptive with respect to the performance of the theory

The horizontal velocity at all depths seems to be in phase with the surface elevation. This seems to be the case in regular as well as irregular waves, in the early part of the timeseries as well as later on. However, this has not been studied closely, meaning that small phase lags may exist between different vertical levels.

All in all, superposition of regular Miche wave components compares quite well with the measurements of irregular waves in many cases, and better than Wheeler's method when the horizontal velocity beneath crests and troughs is concerned. The development of the mean horizontal velocity resembles that in regular waves, and, as stated for regular waves in Section 7.3.5, it is not obvious which parts of the experiments are best suited for comparisons with theory.

However, discrepancies clearly different from those to be expected are also observed, cf. e.g. Figure 6.62, Figure 6.64, Figure 6.66 and Figure 6.69. No attempts have been made to identify the exact cause of these discrepancies, or to determine the ideal timeseries-interval for the Fourier analysis or the ideal bandwidth for calculations. However, some possible reasons for the discrepancies are suggested in Section 7.4.5.

7.4.5 Uncertainties in the results for irregular waves

As stated in the previous sections, differences in the measured and calculated timeseries are to be expected when an Eulerian spectrum is used as input spectrum to the Lagrangian

expressions, and small additional errors may be introduced by including the very lowest frequency components in the iterations for Miche waves.

However, other and seemingly more fundamental discrepancies are also found to occur. Some possible explanations of these "unexpected" discrepancies are suggested in the following:

- Irregular waves in a wave flume do not consist of a sum of regular wave trains, as assumed in the superposition model. Instead, they consist of waves generated sequentially by one wavemaker, which do not result in series of persisting regular wave trains. Also, nonlinearities and bound waves are present. A Fourier analysis can therefore only to a limited extent identify the real surface elevation constituents.
- Which part of the timeseries the Fourier analysis is based on, and the bandwidth included in the analysis, is also of importance.
- Nonlinear terms are not included in the calculations.
- Effects similar to those associated with the initial wave front in the regular wave experiments are likely to exist for "wave fronts" in irregular waves also. This may include an "extra" positive mean velocity prior to the higher waves, as in Figure 6.5, followed by an "extra" negative mean velocity during and after the higher waves, as in Figure 6.6. However, interactions between such effects for different waves seem quite unpredictable, and it may therefore not be possible to recognize or identify such effects.
- Erroneous measurements.
- Other effects due to the flume, the wavemaker and the wave absorber.

Hence, so-called wave flume effects will be present, and a Fourier analysis will anyhow misinterpret the surface elevation to some extent. Also, it is likely that calculations will compare better with measurements if more effort is put into determining an ideal timeseries-interval for the Fourier analysis and an ideal bandwidth for calculations. The effect of neglecting nonlinear terms is unknown. However, any such uncertainties apply to e.g. Wheeler's method as well as to calculations according to Miche (or Gerstner).

Anyhow, these problems are mainly related to comparisons of theory with Eulerian measurements. As indicated in Sections 5.4, 7.2.2 and 7.2.3, the Lagrangian approach presented in this thesis should still be very well suited for simulations and practical design purposes.

CHAPTER 8

CONCLUSIONS AND RECOMMENDATIONS

The main subject of this thesis has been modelling of waves and wave kinematics based on the Lagrangian equations of motion. The Lagrangian approach is found to be very well suited for these purposes, offering certain fundamental advantages over the Eulerian approach. Also, it is found reason to question the common Lagrangian continuity requirement, namely that the Jacobian must be constant and equal 1, and to which extent we can speak of identifiable material particles in a continuum. The theorems of Helmholtz, Kelvin and others on the persistence of vorticity and circulation may therefore not be generally applicable, since these, when considered in a Lagrangian frame of reference, require that the Jacobian always equal 1.

8.1 Conclusions

8.1.1 The basic equations and vortex motion

- The basic equations of motion have been presented on Lagrangian as well as Eulerian form. The equations for conservation of linear momentum pertain to incompressible viscous flow, and include the general Lagrangian form of the Laplacian.

  The conservation laws apply to specific portions of matter, and are therefore Lagrangian by nature. A Jacobian may therefore always be determined, from an Eulerian as well as a Lagrangian solution, and the governing equations may be discussed from a Lagrangian point of view.

  With reference to Section 7.1, it is claimed herein that the common Lagrangian continuity requirement, i.e. J = *constant* (in time), is too restraining and neither necessary nor generally correct. For a continuum, continuity in a Lagrangian sense must involve the dimensions of a material element, allowing a change in the Jacobian accompanied by a corresponding change in the Lagrangian region defining the element, in particular if the state of deformation of the element changes.

  Correspondingly, the Eulerian material derivative can generally only be associated with an identifiable portion of matter if it is also associated with a region of some size. This does not have any consequences for the form of the basic equations of motion, only for

their interpretation with respect to material quantities. A specific Lagrangian point can only be interpreted as the same material particle in time *if* the Jacobian is constant.

The concept of "point-particles" is therefore unphysical and may be misleading. The Lagrangian frame of reference should be considered an instantaneously appropriate mathematical change of variables for a material region rather than a set of identifiable "point-particles".

- The relations governing vortex motion have also been presented. These include Cauchy's vorticity equations, Weber's transformation, Helmholtz' theorem on the rate of change of vorticity and Kelvin's theorem on the rate of change of circulation. Kelvin's theorem has been presented on Lagrangian form. In addition, a Lagrangian form of Helmholtz' theorem has been derived for the two-dimensional inviscid case in Section 3.2.5.

  These relations are traditionally assumed to be proofs of Lagrange's theorem, requiring irrotational motion in a flow that has only been subject to potential forces (assuming that the density is a function of the pressure only), e.g. as in incompressible inviscid flow. However, for any of the above relations to constitute a proof of Lagrange's theorem, it is absolutely necessary that the Jacobian initially and always equal 1, or in other words, that a Lagrangian point always represents the same identifiable material "point-particle", i.e. the same mass.

  However, according to the above, it is not generally correct to require that $J = constant = 1$. Also, requiring $J = 1$ is anyhow different from and more restraining than requiring $J = constant$, and it is not reasonable to compromize with regard to the continuity requirement, which is the most fundamental of the basic requirements in the continuum model, in order to satisfy secondary conditions on vortex motion. Note then that according to Cauchy's vorticity equations and Weber's transformation, $J = 1$ is necessary for the initial existence of an Eulerian velocity potential. Also, it has been shown that requiring $J = 1$ and incompressible potential flow simultaneously allows very simple forms of deformation only, if any at all.

  Lagrange's theorem is then generally applicable as an approximation assuming negligible deformations only. Recall that this is actually a common assumption to make for an infinitesimal material element, and that the deformation of a larger element is the integrated effect of the deformations of infinitesimal elements, cf. Section 7.1.3. Motion generated by potential forces only can then not generally be assumed or required to be irrotational to any order. The use of potential theory and conformal mapping in flow problems should therefore be reconsidered. This is reasonable with respect to e.g. D'Alembert's paradox.

  The derivations of Helmholtz and Kelvin still describe the *Eulerian* rate of change of vorticity and circulation. However, they can only be imposed physical conditions on and interpreted in a Lagrangian sense *while* the Jacobian is constant, meaning that vorticity and circulation in inviscid flow will only be constant as far as the Jacobian is constant. Vorticity will be of the same order as the Jacobian's deviation from 1, constant or not. The Jacobian will generally deviate from 1 in deforming motion, and the value of the Jacobian generally changes if the state of deformation of an element changes. The concepts of vortex lines and vortex tubes should therefore also be reconsidered.

  Still, there is one prevailing condition to be satisfied by the solution of inviscid incompressible flow problems, namely that *the curl of the acceleration must be zero*. This follows directly from the assumption of only potential forces acting.

Finally, it has been shown that rotation defined as half the vorticity does not describe how a fluid element actually rotates, in the sense of turning about itself. Expressions that do describe such motion more adequately have been presented. This also indicates that "point-particles" are unphysical and that a physical foundation for requiring irrotational flow may be lacking, since vorticity is often and incorrectly interpreted as an angular velocity (spin) of an element.

8.1.2 Basic wave theory

- The Lagrangian wave theories of Gerstner and Miche have been presented. Gerstner's theory is an exact analytical solution (of the nonlinear equations of motion and relevant boundary conditions) for waves of finite amplitude on infinite depth, and Miche's 2nd order perturbation solution applies to finite and uniform depth.

  By the use of Taylor-expansion, these regular wave theories have also been presented on Eulerian form, correct to second order, including expressions for mean Eulerian values of the velocities, accelerations and pressure. These also give mean values in the splash zone, accounting for the fact that points in the splash zone are not always submerged in water. Due to the closed orbital motion in Gerstner and Miche waves, the mean Eulerian horizontal velocity is negative beneath the splash zone and turns positive as we move upwards in the splash zone, positive being in the direction of wave propagation.

  In addition, expressions for the mean Eulerian horizontal velocity in narrow-banded irregular Gerstner and Miche waves have been presented. For Eulerian positions below the splash zone these appear as simple formulas, and are given as functions of the significant wave height, the peak period and the ratio between the representative narrow band frequency and the peak frequency. As in the regular wave case, a negative Eulerian current is present beneath the splash zone in irregular waves also. The magnitude of this current will be typically 0.1 - 0.2 m/s in real sea states, depending on the sea state parameters and the vertical position under consideration. Note again that this Eulerian current is not a mass transport.

  The derivations of the Eulerian expressions are to a large extent based on the work by Moe and Arntsen (1996).

- In spite of the constant negative vorticity in regular Gerstner and Miche waves, material elements in such waves do not have a net physical rotation about themselves. They appear to 'wiggle' back and forth, but the mean angular velocity of an element is zero. This behaviour is in accordance with the expressions referred to in Section 8.1.1 found to describe such motion.

- The difference between Stokes waves, which represents potential flow, and Gerstner and Miche waves, is Stokes drift. However, when studied from a Lagrangian point of view, Stokes waves are found to violate continuity and cause a vorticity at second order within less than one wave period, even for waves of small amplitudes. Recall that Stokes solution is a direct consequence of requiring zero vorticity. Stokes waves and Stokes drift are therefore theoretically inconsistent in the Lagrangian frame of reference. This questions the foundation for speaking of *identifiable material particles* in a continuum, and for how long and under which circumstances it may be relevant to do so. These results support those in Section 8.1.1, and question the correctness of requiring zero vorticity as well as Stokes waves as a basic solution for regular waves.

  Gerstner's wave theory is concluded to be an applicable basic solution for regular waves, in the limit of infinite depth and negligible viscosity. In intermediate water, Miche's solution applies. However, the physical relevancy of seeking a regular solution to second

order for such waves on finite depth may be questioned. The 2nd order solution on finite depth may instead be found by proper interpretation of the Jacobian and the Lagrangian frame of reference, and effects such as bound waves etc. may be inherent in such a solution. However, the validity or practical value of such an approach has not been verified or studied further.

8.1.3 Modelling of irregular waves and transformation from the Lagrangian to the Eulerian frame of reference

- The linear Lagrangian solution is superior to the linear Eulerian solution, since the boundary conditions are satisfied in a more correct manner in the Lagrangian solution. For the surface elevation, the linear Lagrangian solution (Gerstner waves) is equivalent to the 3rd order Eulerian solution (3rd order Stokes waves).

  Superposition of linear components in the Lagrangian frame of reference is seen to exhibit so-called nonlinear interactions when transferred to an Eulerian frame of reference. One example of this is how a short wave that rides on a longer wave becomes elongated and flattened in the trough of the longer wave, and correspondingly shortened and steepened in the crest of the longer wave. Also, when superposition is performed in the Lagrangian frame of reference, all frequency components are included in an equally consistent manner everywhere, also in the splash zone.

  The irregular model presented here is still only a solution of the linearized Lagrangian problem; it is not a model for nonlinear irregular waves in a mathematical sense. However, it seems that the Lagrangian approach may also open for theoretically consistent superposition of nonlinear irregular wave components, cf. Section 8.2.

- A Lagrangian solution alone may be of limited practical value. Therefore, iteration methods for transformation of the Lagrangian solutions to an Eulerian frame of reference have been developed, i.e. methods for determining which Lagrangian point occupies a specific Eulerian position at a specific instant in time. In the splash zone, the methods also determine whether the Eulerian position in question is submerged in water or not at this instant. These methods apply to 2D broad-banded irregular waves as well as regular waves, and the iterations converge quite fast. Assuming that the Lagrangian orbital amplitude spectrum of the free Lagrangian components is known, theoretically consistent values of any Eulerian as well as Lagrangian quantity anywhere in the fluid, also in the splash zone, may be calculated in a practical manner. As many frequency components as desired can be included. The need for extrapolation of solutions and stretching of coordinates, and therefore the common additional errors due to violation of the governing equations and overprediction of high frequency contributions near and above the still water level, are thus eliminated.

  The Eulerian quantities found by these iteration methods are correct to the same order as the original Lagrangian solution, assuming that the iteration itself is practically exact. Since Gerstner's solution for regular waves is exact, this means that also exact Eulerian quantities can be found for such waves. The very lowest frequency components should be excluded when employing the iteration methods for Miche waves, since the ratio [cosh kh/sinh kh] may then approach infinity (k being the wave number and h the water depth).

- The main problem with the Lagrangian approach presented here is direct comparisons with measurements of irregular waves made at fixed Eulerian positions. An amplitude spectrum of the surface elevation measured at a fixed Eulerian position will not be identical to the Lagrangian orbital amplitude spectrum of the process. The Eulerian spectrum is still a reasonable approximation of the Lagrangian spectrum, but certain types of discrepancies between calculated and measured values must be expected when using

component parameters based on an Eulerian spectrum as input to the Lagrangian expression.

However, comparisons with measurements in wave flumes are not the ultimate objective. Ocean waves are often measured by buoys, yielding wave spectra that may be considered more Lagrangian than Eulerian, and design spectra are anyhow subject to uncertainties.

Hence, even if perfect agreement between Eulerian measurements and calculations based on Lagrangian expressions may be difficult to obtain, the Lagrangian approach presented herein should be of great practical and theoretical value, very well suited for simulations and design purposes. The potential for further theoretical development seems considerable, cf. Section 8.2.

8.1.4 Comparisons of theory with measurements

- The Lagrangian approach has been compared with experimental measurements and, in a few cases, Stokes' 2nd order wave theory and Wheeler's method. The measurements are from the extensive experiments carried out by Skjelbreia et al. (1991). They include measurements of the surface elevation and LDV-measurements of horizontal and vertical water particle velocities, also in the splash zone. The experiments pertain to waves in intermediate water, and the measurements have therefore been compared with Miche waves. However, the differences between applying Gerstner's and Miche's expressions are of a minor quantitative nature, and the results for Miche's theory are therefore representative also for Gerstner's theory. Irregular as well as regular wave cases have been considered.

- For the regular wave cases, the development of the mean Eulerian horizontal velocity in a vertical cross-section was given particular attention. Two distinct transitions were found to take place.

  First, there is a transition associated with the arrival of the wave front. For a short period of time after this first transition, the mean velocity resembles what might be expected due to Stokes waves and associated Stokes drift and return current.

  After this short period of time a second transition takes place, resulting in a more steady state situation where the mean Eulerian horizontal velocity is very well predicted by Miche's theory. Comparisons were also made for the instantaneous Eulerian horizontal velocity in a vertical cross-section beneath individual crests and troughs. Again, Miche's theory compare very well with the measurements after the second transition. The agreement between calculations and measurements is equally good over the entire column of fluid, also in the splash zone.

  The results suggest that material elements eventually move in closed orbits, and that neither Stokes drift nor any significant return current is present. This is also supported by the results for irregular waves as well as by visual observations. It is not unlikely that the early Stokes-like drift is caused by the initial action of the wavemaker rather than the waves actually being Stokes waves. More specifically, it takes some time before the initially still water is adapted to the horizontal action of the flap-type wavemaker, which may cause a positive circulation in the early parts of such experiments.

  These results do to some extent support the suggested conclusions in Section 8.1.2. However, definite conclusions can hardly be drawn as long as the effects of the action of the wavemaker and the presence of the end-walls in a closed flume cannot be separated from the "pure" wave motion. Also, these results pertain to one set of experimental measurements only, although the first transition has been reported for other experiments

as well. However, the typical negative mean velocity below the splash zone in wave flume experiments is well known from literature.

- For the irregular wave cases, the same type of development of the mean Eulerian horizontal velocity was found as for the regular wave cases. In particular, when studying three consecutive individual waves of nearly identical period but markedly different amplitude, it was found that the mean Eulerian horizontal velocity varies in a way that can hardly be compatible with a return current, but indicates that material elements indeed move in (practically) closed orbits. The long-term mean Eulerian horizontal velocity predicted by the narrow-band approximation for Miche waves was found to compare well with the measurements.

  The results for irregular waves are more subject to uncertainties than the results for regular waves, and "unexpected" discrepancies between calculations and measurements were found to occur. It is likely that calculations would generally have compared better with measurements if more effort had been put into determining an ideal timeseries-interval for the Fourier analysis and an ideal bandwidth for the calculations, and if better estimates of the "true" Lagrangian orbital amplitude spectrum had been found. However, the effects of the action of the wavemaker and the presence of the end-walls is even more unpredictable for irregular waves than for regular waves, and a Fourier analysis will anyhow misinterpret the surface elevation to some extent. Also, nonlinear Lagrangian terms are left out of the calculations. Such experiments may therefore be of limited value with respect to verification of irregular wave models, even if the methods of analysis and calculations are optimized.

  However, the horizontal velocity beneath individual crests and troughs calculated according to the iteration method for irregular Miche waves was still found to compare quite well with the measurements, and better than Wheeler's method does. The difference between the iteration method and Wheeler's method accounts for the typical observed deficiency of Wheeler's method. Recall that due to the strecthing of coordinates, Wheeler's method does not satisfy the basic equations of motion, while the Lagrangian approach presented in this thesis yields theoretically consistent values everywhere, also in the splash zone, and eliminates the need for stretching and/or other modifications.

  Hence, in spite of uncertainties and discrepancies, the results for irregular waves still support the conclusions at the end of Section 8.1.3, namely that the Lagrangian approach is very well suited for simulations and practical design purposes. These results also support the findings for regular waves, namely that material elements indeed move in closed orbits rather than being transported by a Stokes-like current and a return current. It must still be noted that as for regular waves, these results also pertain to just one set of experimental measurements.

8.2 Recommendations for Further Work

- The fundamental theoretical issues on continuity and vorticity, and thus the concepts of point-particles and potential flow, should be further discussed and verified. For waves, it is of the utmost importance to determine whether a mass transport such as Stokes drift should be present or not, and to fully understand the actual generation of the waves.

- The Lagrangian approach may also offer an alternative method for finding higher order solutions in some cases. It could be that the 1st order solution applies to all orders, and that the higher order effects can be included by redefining the Lagrangian frame of reference according to the Jacobian resulting from the 1st order solution, satisfying conservation of a larger and well-defined material region. This is certainly the case for

Gerstner waves, and the same approach should be attempted with respect to the higher order terms for waves on finite depth. It is suggested that the general validity and practical value of such an approach be investigated further.

- Interactions between waves and currents, as well as between different wave components, should be investigated more closely from a Lagrangian point of view.

- A model for nonlinear irregular waves should be sought by realizing that each wave component has a unique Jacobian and Lagrangian frame of reference, and accounting for this in the superposition. Any interactions with currents should be included, since such interactions may lead to breaking or modulation of waves.

- The Lagrangian approach presented herein should be extended to the 3D case.

- The iteration methods for transforming the Lagrangian solution to an Eulerian frame of reference could possibly be refined, e.g. with respect to convergence and computation time. In accordance with the above, they should also be extended to account for nonlinearities and currents, and an extension to the 3D case should be attempted.

- With respect to comparisons of theory with measurements, ways of obtaining better estimates of the "true" Lagrangian orbital amplitude spectrum from Eulerian measurements should be sought. The approach in Zhang et al. (1996) and Zhang et al. (1998) may be relevant in this respect.

- Wave experiments should be carried out under conditions where the unfortunate effects of the wavemaker and tank walls are reduced or eliminated. Also, ways of measuring the long-term motion of a specific fluid "particle" could be considered. These issues may not be practically, technically or economically feasible to a satisfactory degree at present, but should be kept in mind for future work.

- Finally, the Lagrangian approach may be well suited for other and more complex wave problems also, such as waves on shallow water and varying depth, and may prove fruitful for other types of flow problems as well. One may e.g. study turbulence from a Lagrangian point of view, as well as the effect of viscosity, compressibility and non-uniform density in certain problems. Note that Lagrangian solutions exist for many problems, e.g. for waves on a sloping beach.

REFERENCES

Airy, G.B. (1845): "Tides and Waves", Encyclopaedia Metropolitana.

Aris, R. (1989): "Vectors, Tensors, and the Basic Equations of Fluid Mechanics", Dover Publications.

Baldock, T.E., C. Swan and P.H. Taylor (1996): "A laboratory study of nonlinear surface waves on water", Phil. Trans. Roy. Soc. A, Vol. 354, pp. 649-676.

Batchelor, G.K. (1967): "An Introduction to Fluid Dynamics", Cambridge University Press.

Biesel, F. (1952): "Study of wave propagation in water of gradually varying depth", in Gravity Waves, NBS Circular 521, pp. 243-254.

Carrier, G.F. and H.P. Greenspan (1958): "Water waves of finite amplitude on a sloping beach", Journal of Fluid Mechanics Vol. 4.

Cauchy, A.L. (1827): "Mémoire sur la Théorie des Ondes", Mém. de l'Acad. roy. des Sciences, i.

Cieslikiewicz, W. and O.T. Gudmestad (1993): "Stochastic characteristics of orbital velocities of random water waves", Journal of Fluid Mechanics, Vol. 255, pp. 275-299.

Cieslikiewicz, W. and O.T. Gudmestad (1994a): "Random water wave kinematics", Part I & II, Archives of Hydro-Engineering and Environmental Mechanics, Vol. 41, No. 1-2, pp. 3-85, Polish Academy of Sciences, Institute of Hydro-Engineering, Gdansk.

Cieslikiewicz, W. and O.T. Gudmestad (1994b): "Mass transport within the free surface zone of water waves", Wave Motion, Vol. 19, pp. 145-158.

Cieslikiewicz, W. and O.T. Gudmestad (1995): "Stochastic characterization of wave kinematics in laboratory-scale random waves", Coastal engineering, Vol. 26, No. 1&2, Sept. 1995, pp. 35-56.

Cieslikiewicz, W. and O.T. Gudmestad (1996): "Kinematics of random gravity waves in the free surface zone", Oceanology (English edition), Vol. 35, No. 4, Feb. 1996, pp. 445-455.

Corrsin, S. (1962): "Theories of turbulent dispersion", Colloques Internationeaux du Centre National de la Recherche Scientifique No. 108; Mécanique de la Turbulence, Université d'Aix Marseille, Aug. 28-Sept. 2., Éditions du Centre National de la Recherche, Paris.

Dean, R.G. and R.A. Dalrymple (1991): "Water Wave Mechanics for Engineers and Scientists", World Scientific.

Dean, R.G. (1970): "Relative Validities of Water Wave Theories", Journal of Waterways, Harbours, Coastal and Ocean Engineering Division, Proceedings of the American Society of Civil Engineers, Vol. 96 WW1, pp. 105-119.

Delft Hydraulic Laboratory (1982): "Wave kinematics in irregular waves", M1628/MaTS VM I-4.

Dubreil-Jacotin, M.-L. (1934): "Sur la détermination rigoureuse des ondes permanentes périodiques d'ampleur finie", J. Math. 13, pp. 217-291.

Edwards, C.H.jr. and D.E. Penney (1990): "Calculus and Analytic Geometry", 3rd ed., Prentice-Hall.

Faltinsen O.M. (1990): "Sea Loads on Ships and Offshore Structures", Cambridge University Press.

Gerber, R. (1949): "Sur la réduction à un principe variationnel des équations du mouvement d'un fluide visqueux incompressible", Annales de L'Institut Fourier, Université de Grenoble, Vol. I pp. 157-162.

Gerstner, F.J.v (1809): "Theorie der Wellen", Annalen der Physik 32, pp. 412-445.

Gerstner, F.J.v (1802): "Theorie der Wellen", Abh. d. k. bohm. Ges. d. Wiss.

Goldstein, S. (1960): "Lectures on Fluid Mechanics", Proceedings of the Summer Seminar "Lectures in Applied Mathematics" in Boulder 1957, Vol. II, Interscience Publishers.

Groeneweg, J. and G. Klopman (1998): "Changes of the mean velocity profiles in the combined wave-current motion described in a GLM formulation", Journal of Fluid Mechanics, Vol. 370, pp. 271-296.

Gudmestad, O.T. (1993): "Measured and Predicted Deep Water Wave Kinematics in Regular and Irregular Seas", Marine Structures, Vol. 6 pp. 1-73, Elsevier.

Gudmestad, O.T., J.M. Johnsen, J. Skjelbreia and A. Tørum (1988): "Regular Water Wave Kinematics", Proc. Int. Conf. on Behaviour of Offshore Structures BOSS '88, Trondheim, Norway, June 21-24, pp. 76-88.

Gudmestad, O.T. and S. Haver (1993): "Uncertainties in prediction of wave kinematics in irregular waves", Wave Kinematics and Environmental Forces, Vol. 29 pp. 75-99, Society for Underwater Technology.

Gudmestad, O.T. and D. Karunakaran (1994): "Wave Kinematics Models for Calculation of Wave Loads on Truss Structures", Proceedings of the 26th annual OTC, pp. 413-424, Houston, 2-5 May 1994.

Helmholtz, H. (1858): "Über Integrale der hydrodynamischen Gleichungen, welche den Wirbelbewegungen entsprechen", Journal für die reine und angewandte Mathematik (Crelle's Journal) ", Vol. 55.

Hudspeth, R.T. and W. Sulisz (1991): "Stokes drift in two-dimensional wave flumes", Journal of Fluid Mechanics, Vol. 230, pp. 209-229.

Johnsen, J.M. (1987): "Regular Water Wave Kinematics", Report OR 512008.00.02, MARINTEK, Trondheim, Norway.

Kelvin, Lord (W. Thomson) (1869): "On Vortex Motion", Transactions of the Royal Society of Edinburg, Vol. 25.

Kinsman, B. (1965): "Wind Waves; their generation and propagation on the ocean surface", Prentice-Hall.

Kochin, N.E., I.A. Kibel and N.V. Roze (1964): "Theoretical Hydromechanics", Interscience Publishers.

Kreyszig, E. (1988): "Advanced Engineering Mathematics", 6th ed., Wiley.

Lagrange, L. d. (1781): "Mémoire sur la Théorie du Mouvement des Fluides", Nouv. mém. de l'Acad. de Berlin.

Lamb, H. (1932): "Hydrodynamics", 6th ed., Cambridge University Press.

LeBlond, P.H. and L.A. Mysak (1978): "Waves in the Ocean", Elsevier.

Le Méhauté, B. (1976): "An Introduction to Hydrodynamics and Water Waves", Springer-Verlag (New York).

Levi, E. (1995): "The Science of Water; The foundation of Modern Hydraulics", ASCE Press.

Lighthill, J. (1989): "An Informal Introduction to Theoretical Fluid Mechanics", Reprint with corrections, Clarendon Press, Oxford.

Lin, C.C. and L.A. Segel (1988): "Mathematics Applied to Deterministic Problems in the Natural Sciences", Society for Industrial and Applied Mathematics (SIAM).

Liu, A.K. and S.H. Davis (1977): "Viscous attenuation of mean drift in water waves", Journal of Fluid Mechanics, Vol. 81, pp. 63-84.

Longuet-Higgins, M.S. (1953): "Mass transport in water waves", Phil. Trans. Roy. Soc. A 245(903), pp. 535-581.

Longuet-Higgins, M.S. (1960): "Mass transport in the boundary layer at a free oscillating surface", Journal of Fluid Mechanics, Vol. 8, pp. 293-306.

McClimans, T.A. (1980): "Wave Propulsion of Spar Buoys", Journal of the Waterway, Port, Coastal and Ocean Division, Proceedings of the American Society of Civil Engineers, Vol. 106, No. WW3, August 1980.

Mei, C.C. (1989): "The Applied Dynamics of Ocean Surface Waves", World Scientific.

Mei, C.C., P. L.-F. Liu and T.G. Carter (1972): "Mass Transport in Water Waves", Parsons Lab., MIT Report 146: 287.

Miche, M. (1944): "Mouvements ondulatoires de la mer en profondeur constante ou décroissante form limite de la houle lors de son déferlement. Application aux digues marine.", Annales des Ponts Chaussées 114, pp. 25-78, 131-164, 270-292, 369-406.

Milne-Thomson, L.M. (1996): "Theoretical Hydrodynamics", 5th ed., Dover Publications.

Moe, G. (2000): "Wave Kinematics – A Lagrangian Approach", Lecture at Offshore Technology Research Center (OTRC) Seminar, 27th of March 2000, College Station, Texas.

Moe, G. and Ø.A. Arntsen (1996): "Particle Velocity Distribution in Surface Waves", Proceedings of the 25th International Conference on Coastal Engineering (ICCE '96), Orlando, Florida, pp. 565-574.

Moe, G., Ø.A. Arntsen and S.H. Gjøsund (1998): "Wave Kinematics based on a Lagrangian Formulation", Proceedings of the 1998 International OTRC Symposium: Ocean Wave Kinematics, Dynamics and Loads on Structures (Ed.: J. Zhang), April 30th - May 1st 1998, Houston, ASCE Press, pp. 56-63.

Monin, A.S. and A.M. Yaglom (1971): "Statistical Fluid Mechanics; mechanics of turbulence", Vol. 1, MIT Press.

Monismith, S.G. (2000): Private communication.

Morison, J.R, M.P. O'Brien, J.W. Johnson and S.A. Schaaf (1950): "The force exerted by surface waves on piles", Pet. Trans. 189, AIME, pp. 149-154.

Naciri, M. and C.C. Mei (1992): "Evolution of a short surface wave on a very long surface wave of finite amplitude", Journal of Fluid Mechanics, Vol. 235, pp. 415-452.

Neumann, G. and W.J. Pierson Jr. (1966): "Principles of Physical Oceanography", Prentice-Hall.

Newland, D.E. (1993): "Random Vibrations, Spectral & Wavelet Analysis", 3rd ed., Longman Scientific & Technical.

Newman, J. N. (1977): "Marine Hydrodynamics", MIT Press.

Peregrine, D.H., J.W. Dold, K. Henderson, M. Jervis, D.J. Wood and C.C. Bird (1996): "Managed Programme on Uncertainties in Loads on Offshore Structures", Report, School of Mathematics, University of Bristol.

Pierson, W.J. jr. (1961): "Models of Random Seas Based on the Lagrangian Equations of Motion", Technical Report Prepared for the Office of Naval Research under contract Nonr-285(03), New York University, College of Engineering Research Division, Dept. of Meteorology and Oceanography, April 1961.

Pierson, W.J. jr. (1962): "Perturbation Analysis of the Navier-Stokes Equations in Lagrangian Form with Selected Linear Solutions", Journal of Geophysical Research, Vol. 67 No. 8, July 1962.

Sarpkaya, T. and M. Isaacson (1981): "Mechanics of Wave Forces on Offshore Structures", Van Nostrand Reinhold.

Segel, L.A. (1987): "Mathematics Applied to Continuum Mechanics; with additional material on elasticity by G.H. Handelman" (sequel to Lin and Segel, 1988), Dover

Publications.

Skjelbreia, J.E. (1987): "Observations of Breaking Waves on Sloping Bottoms by use of Laser Doppler Velocimetry", Ph.D. Thesis, California Institute of Technology, Pasadena.

Skjelbreia, J.E. (1988): "Measurements and observations of regular waves", Report STF60 F88046, MARINTEK, Trondheim, Norway.

Skjelbreia, J.E., G. Berek, Z.K. Bolen, O.T. Gudmestad, J.C. Heideman, R.D. Ohmart, N. Spidsø and A. Tørum (1991): "Wave Kinematics in Irregular Waves", Proceedings OMAE 1991, Vol. I-A Offshore Technology pp. 223-228, ASME.

Skjelbreia, J.E. (1991): "Kinematics in Irregular and Regular Waves", Draft Report, March 23 1991, MARINTEK.

Spell, C.A., J. Zhang and R.E. Randall (1996): "Hybrid wave model for unidirectional irregular waves - part II. Comparison with laboratory measurements", Applied Ocean Research 18, pp. 93-109.

Stansberg, C.T. (1994): "Second-order effects in random wave modelling", Proceedings of the International Symposium: Waves - Physical and Numerical Modelling, University of British Columbia, Vancouver August 1994, pp. 793-802.

Stansberg, C.T. and O.T. Gudmestad (1996): "Non-linear random wave kinematics models verified against measurements in steep waves", Proceedings OMAE 1996.

Stokes, G.G. (1845): "On the theories of the internal friction of fluids in motion, and the equilibrium and motion of elastic solids", Trans. Camb. Phil. Soc. 8, 287.

Stokes, G.G. (1847): "On the theory of oscillatory waves", Trans. Camb. Phil. Soc. 8, 441.

Stokes, G.G. (1880): "Supplement to a paper on the theory of oscillatory waves", Mathematical and Physical Papers, Vol. I, pp. 314-326, Cambridge University Press.

Swan, C., T. Bashir and O.T. Gudmestad (1998): Nonlinear Inertial Loading in Steep 2-D Water Waves", Proceedings of the 1998 International OTRC Symposium: Ocean Wave Kinematics, Dynamics and Loads on Structures (Ed.: J. Zhang), April 30th - May 1st 1998, Houston, ASCE Press, pp. 126-133.

Thomson, W.; see (Lord) Kelvin.

Tick, L.J. (1963): "Nonlinear probability models of ocean waves", in Ocean Wave Spectra, pp. 163-169, Prentice-Hall.

Tokaty, G.A. (1994): "A History and Philosophy of Fluid Mechanics", Dover Publications.

Truesdell, C. and R.A. Toupin (1960): "The Classical Field Theories", Encyclopedia of Physics, Vol. III/1, Springer-Verlag.

Trulsen, K. and K. B. Dysthe (1996): "A modified nonlinear Schrödinger equation for broader bandwidth gravity waves on deep water", Wave Motion 24, pp. 281-289.

Trulsen, K., J.-M. Temmos, K.B. Dysthe, O.T. Gudmestad and M.G. Velarde (1998): "The

Schrödinger method for water wave kinematics", Proceedings of the 1998 International OTRC Symposium Ocean Wave Kinematics, Dynamics and Loads on Structures (Ed.: J. Zhang), April 30th - May 1st 1998, Houston, ASCE Press.

Tørum, A. and O.T. Gudmestad (Eds.) (1990): "Water Wave Kinematics", Nato ASI Series, Series E: Applied Sciences - Vol. 178, Kluwer Academic Publishers

Tørum, A. and J.E. Skjelbreia (1990): "Irregular Water Wave Kinematics", in Water Wave Kinematics (Eds.: A. Tørum and O.T. Gudmestad), Nato ASI Series, Series E: Applied Sciences - Vol. 178, Kluwer Academic Publishers.

Ünülata, Ü and C.C. Mei (1970): "Mass Transport in Water Waves", Journal of Geophysical Research, Vol. 75, No. 36, Dec. 20 1970.

Weber, H. (1868): "Über eine Transformation der hydrodynamischen Gleichungen", Journal für die reine und angewandte Mathematik (Crelle's Journal) ", Vol. 68.

Wehausen, J.V. and E.V. Laitone (1960): "Surface Waves", Encyclopedia of Physics, Vol. IX/Fluid Dynamics III, Springer-Verlag.

Wheeler, J.D. (1970): "Method for Calculating Forces Produced by Irregular Waves", Journal of Petroleum Technology, March 1970, pp. 359-367.

White, F.M. (1988): "Fluid Mechanics", 2nd ed., McGraw-Hill.

White, F.M. (1991): "Viscous Fluid Flow", 2nd ed., McGraw-Hill.

Wiegel, R.L. (1964): "Oceanographical Engineering", Prentice-Hall.

Woltering, S. and K-F Daemrich (1994): "Mass Transport and Orbital Velocities with LAGRANGEian frame of reference", ICCE '94, Kobe, Japan.

Woltering, S (1996): " Eine LAGRANGEsche Betrachtungsweise zur Bescreibung von Seegang", Mitteilungen des Franzius-Instituts für Wasserbau und Küsteningenieurwesen der Univeristät Hannover, Heft 77.

Zhang, J., L. Chen, M. Ye and R.E. Randall (1996): "Hybrid wave model for unidirectional irregular waves - part I. Theory and numerical scheme", Applied Ocean Research 18, pp. 77-92.

Zhang, J., J. Yang, J. Wen and I. Prislin (1998): "Deterministic Decomposition and Prediction of Irregular Ocean Waves", Report 98A9475, Offshore Technology Research Center, College Station, Texas.

Zhang, J. (Ed.) (1998): "Proceedings of the 1998 International OTRC Symposium: Ocean Wave Kinematics, Dynamics and Loads on Structures", April 30th - May 1st 1998, Houston, ASCE Press.

APPENDIX A

INVERSE PARTIAL DERIVATIVES

Inverse Partial Derivatives, 2D (x, z)-plane:

$$\frac{\partial x}{\partial x}=\frac{\partial x}{\partial x_0}\frac{\partial x_0}{\partial x}+\frac{\partial x}{\partial z_0}\frac{\partial z_0}{\partial x}=1 \tag{A.1}$$

$$\frac{\partial x}{\partial z}=\frac{\partial x}{\partial x_0}\frac{\partial x_0}{\partial z}+\frac{\partial x}{\partial z_0}\frac{\partial z_0}{\partial z}=0 \tag{A.2}$$

$$\frac{\partial z}{\partial x}=\frac{\partial z}{\partial x_0}\frac{\partial x_0}{\partial x}+\frac{\partial z}{\partial z_0}\frac{\partial z_0}{\partial x}=0 \tag{A.3}$$

$$\frac{\partial z}{\partial z}=\frac{\partial z}{\partial x_0}\frac{\partial x_0}{\partial z}+\frac{\partial x}{\partial z_0}\frac{\partial z_0}{\partial z}=1 \tag{A.4}$$

(A.1) yields:

$$\frac{\partial x_0}{\partial x}=\frac{1-\dfrac{\partial x}{\partial z_0}\dfrac{\partial z_0}{\partial x}}{\dfrac{\partial x}{\partial x_0}} \tag{A.5}$$

(A.2) yields:

$$\frac{\partial x_0}{\partial z}=\frac{-\dfrac{\partial x}{\partial z_0}\dfrac{\partial z_0}{\partial z}}{\dfrac{\partial x}{\partial x_0}} \tag{A.6}$$

(A.3) yields:

$$\frac{\partial z_0}{\partial x}=\frac{-\dfrac{\partial z}{\partial x_0}\dfrac{\partial x_0}{\partial x}}{\dfrac{\partial z}{\partial z_0}} \tag{A.7}$$

(A.4) yields:

$$\frac{\partial z_0}{\partial z}=\frac{1-\dfrac{\partial z}{\partial x_0}\dfrac{\partial x_0}{\partial z}}{\dfrac{\partial z}{\partial z_0}} \tag{A.8}$$

(A.5) and **(A.7)** then yields

$$\frac{\partial x_0}{\partial x}\frac{\partial x}{\partial x_0} = 1 - \frac{\partial x}{\partial z_0}\left(-\frac{\dfrac{\partial z}{\partial x_0}}{\dfrac{\partial z}{\partial z_0}}\right)\frac{\partial x_0}{\partial x}$$

$$\Downarrow$$

$$\frac{\partial x_0}{\partial x}\left[\frac{\partial x}{\partial x_0} - \frac{\dfrac{\partial x}{\partial z_0}\dfrac{\partial z}{\partial x_0}}{\dfrac{\partial z}{\partial z_0}}\right] = 1$$

$$\Downarrow$$

$$\frac{\partial x_0}{\partial x} = \frac{1}{\dfrac{\partial x}{\partial x_0} - \dfrac{\dfrac{\partial x}{\partial z_0}\dfrac{\partial z}{\partial x_0}}{\dfrac{\partial z}{\partial z_0}}} = \frac{\dfrac{\partial z}{\partial z_0}}{\dfrac{\partial x}{\partial x_0}\dfrac{\partial z}{\partial z_0} - \dfrac{\partial x}{\partial z_0}\dfrac{\partial z}{\partial x_0}} = \frac{1}{J}\frac{\partial z}{\partial z_0} \tag{A.9}$$

Similarly

$$\frac{\partial z_0}{\partial x} = -\frac{\dfrac{\partial z}{\partial x_0}}{\dfrac{\partial x}{\partial x_0}\dfrac{\partial z}{\partial z_0} - \dfrac{\partial x}{\partial z_0}\dfrac{\partial z}{\partial x_0}} = -\frac{1}{J}\frac{\partial z}{\partial x_0} \tag{A.10}$$

$$\frac{\partial z_0}{\partial z} = \frac{\dfrac{\partial x}{\partial x_0}}{\dfrac{\partial x}{\partial x_0}\dfrac{\partial z}{\partial z_0} - \dfrac{\partial x}{\partial z_0}\dfrac{\partial z}{\partial x_0}} = \frac{1}{J}\frac{\partial x}{\partial x_0} \tag{A.11}$$

$$\frac{\partial x_0}{\partial z} = -\frac{\dfrac{\partial x}{\partial z_0}}{\dfrac{\partial x}{\partial x_0}\dfrac{\partial z}{\partial z_0} - \dfrac{\partial x}{\partial z_0}\dfrac{\partial z}{\partial x_0}} = -\frac{1}{J}\frac{\partial x}{\partial z_0} \tag{A.12}$$

where J is the two-dimensional Jacobian defined in Chapter 2, Eq. (2.19).

Inverse Partial Derivatives, 3D (x, y, z)-space, cf. Eq. (2.28):

$$\frac{\partial x_0}{\partial x} = \frac{1}{J}\frac{\partial(y,z)}{\partial(y_0,z_0)} \tag{A.13}$$

$$\frac{\partial x_0}{\partial y} = \frac{1}{J}\frac{\partial(z,x)}{\partial(y_0,z_0)} = -\frac{1}{J}\frac{\partial(x,z)}{\partial(y_0,z_0)} \tag{A.14}$$

$$\frac{\partial x_0}{\partial z} = \frac{1}{J}\frac{\partial(x,y)}{\partial(y_0,z_0)} \tag{A.15}$$

$$\frac{\partial y_0}{\partial x} = \frac{1}{J}\frac{\partial(y,z)}{\partial(z_0,x_0)} = -\frac{1}{J}\frac{\partial(y,z)}{\partial(x_0,z_0)} \tag{A.16}$$

$$\frac{\partial y_0}{\partial y} = \frac{1}{J}\frac{\partial(z,x)}{\partial(z_0,x_0)} = \frac{1}{J}\frac{\partial(x,z)}{\partial(x_0,z_0)} \tag{A.17}$$

$$\frac{\partial y_0}{\partial z} = \frac{1}{J}\frac{\partial(x,y)}{\partial(z_0,x_0)} = -\frac{1}{J}\frac{\partial(x,y)}{\partial(x_0,z_0)} \tag{A.18}$$

$$\frac{\partial z_0}{\partial x} = \frac{1}{J}\frac{\partial(y,z)}{\partial(x_0,y_0)} \tag{A.19}$$

$$\frac{\partial z_0}{\partial y} = \frac{1}{J}\frac{\partial(z,x)}{\partial(x_0,y_0)} = -\frac{1}{J}\frac{\partial(x,z)}{\partial(x_0,y_0)} \tag{A.20}$$

$$\frac{\partial z_0}{\partial z} = \frac{1}{J}\frac{\partial(x,y)}{\partial(x_0,y_0)} \tag{A.21}$$

where J is the three-dimensional Jacobian defined in Chapter 2, Eq. (2.24).

APPENDIX B

DEVELOPMENT OF THE MEAN EULERIAN HORIZONTAL VELOCITY IN THE REGULAR WAVE EXPERIMENTS

The figures in this appendix show the measured (*) and calculated (-) mean horizontal velocity in a vertical cross-section at the longitudinal position of wave gage 1 for the regular wave cases 8 (R15B) and 9 (SR15), cf. Sections 6.1.1 and 6.2.1.

Figure B.1 - Figure B.23 show the development of the mean horizontal velocity in Case 8 (R15B), while Figure B.24 - Figure B.43 show the development in Case 9 (SR15).

The measured values are averaged over one wave period in the initial part of the experiments, and over ten wave periods later in the experiments. The specific timeseries-interval is given in each of the figures.

The calculations are performed according to Miche's solution as given by Eqs. (4.77) and (4.78) in Section 4.2.2, and the calculated profile is identical in all figures pertaining to the same wave case.

The Eulerian frame of reference is defined by $z = 0$ at the initial still water level.

Recall that the total duration of the records is 819.2 seconds, and that the regular wave periods are 1.5 seconds.

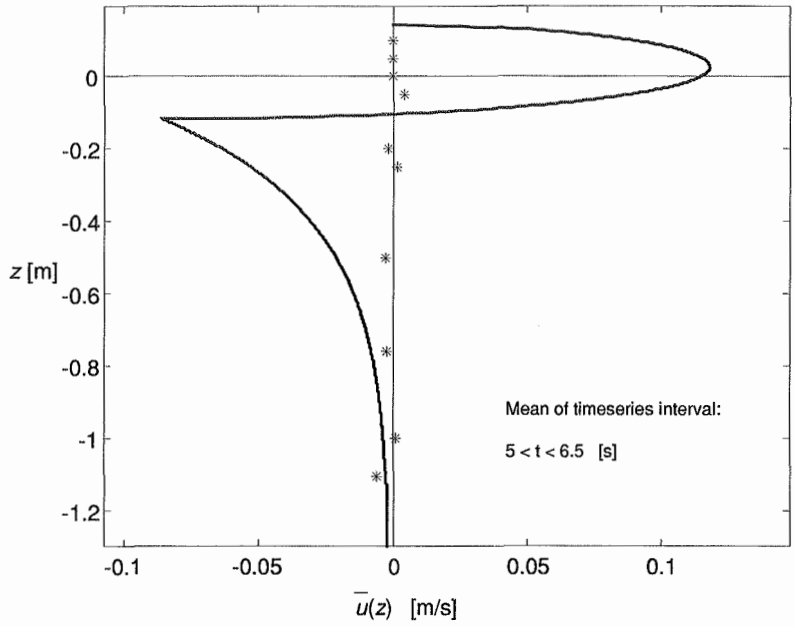

Figure B.1 Case 8 (R15B), $5 < t < 6.5$ [s].

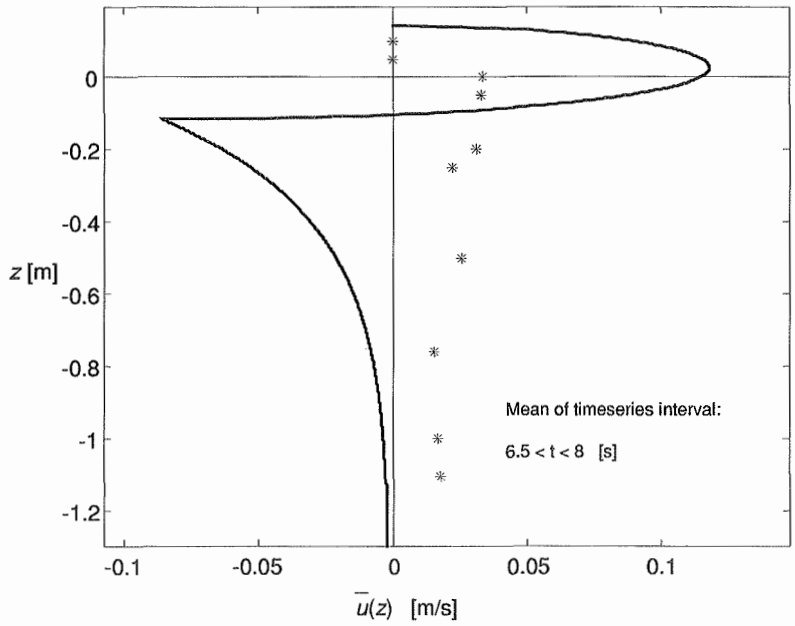

Figure B.2 Case 8 (R15B), $6.5 < t < 8$ [s].

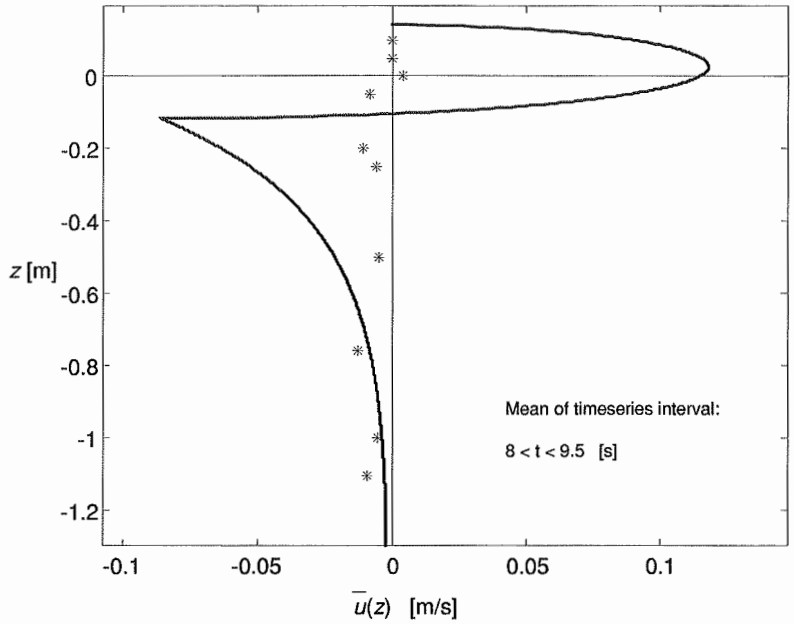

Figure B.3 Case 8 (R15B), $8 < t < 9.5$ [s].

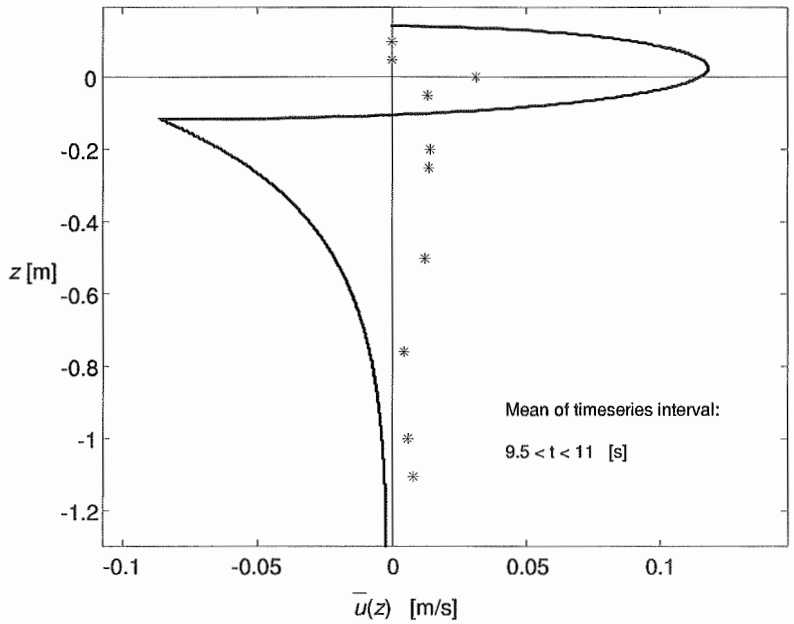

Figure B.4 Case 8 (R15B), $9.5 < t < 11$ [s].

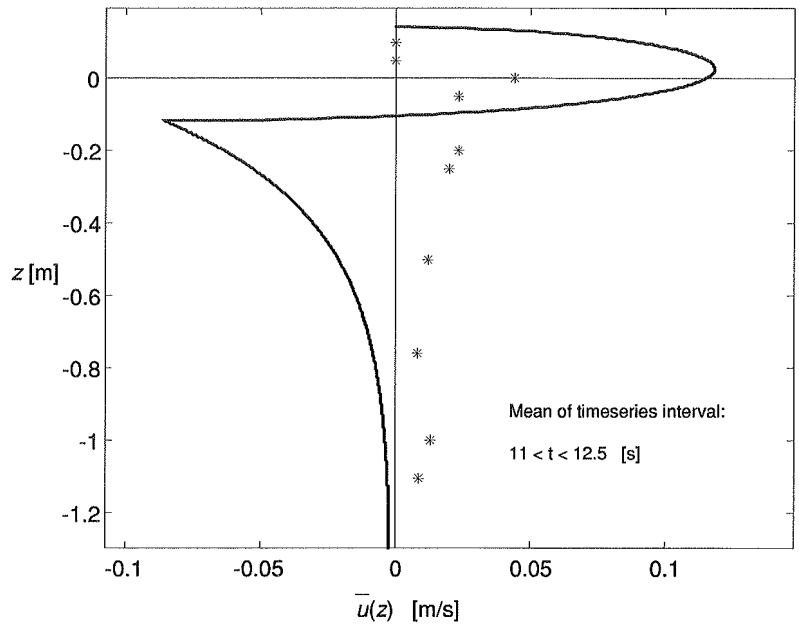

Figure B.5 Case 8 (R15B), $11 < t < 12.5$ [s].

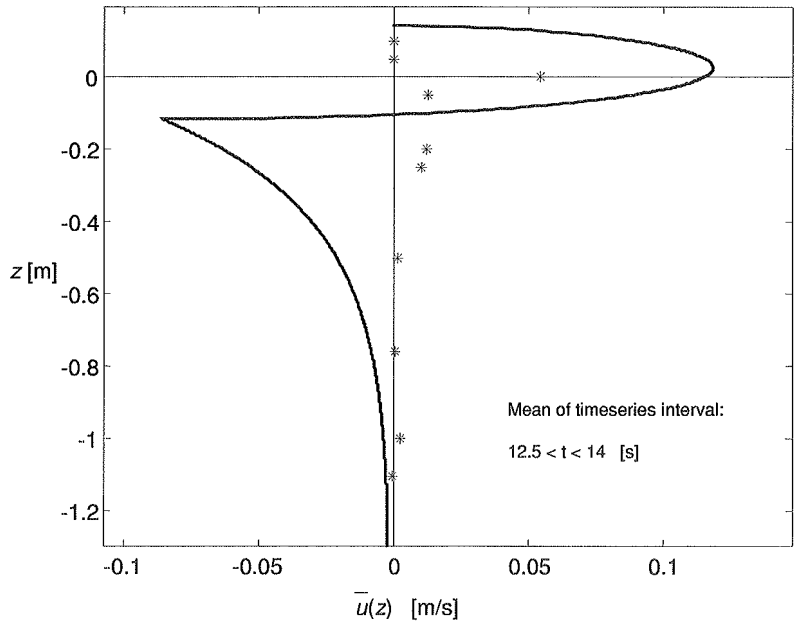

Figure B.6 Case 8 (R15B), $12.5 < t < 14$ [s].

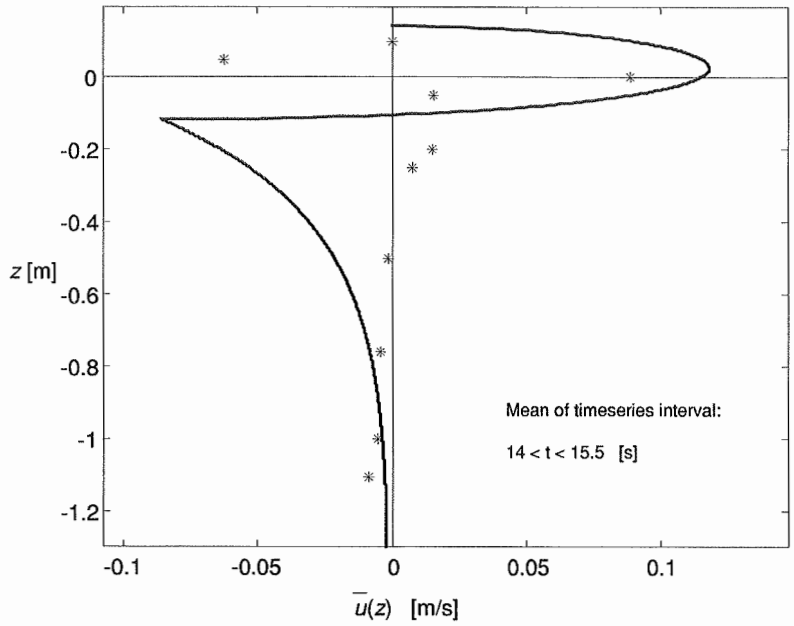

Figure B.7 Case 8 (R15B), $14 < t < 15.5$ [s].

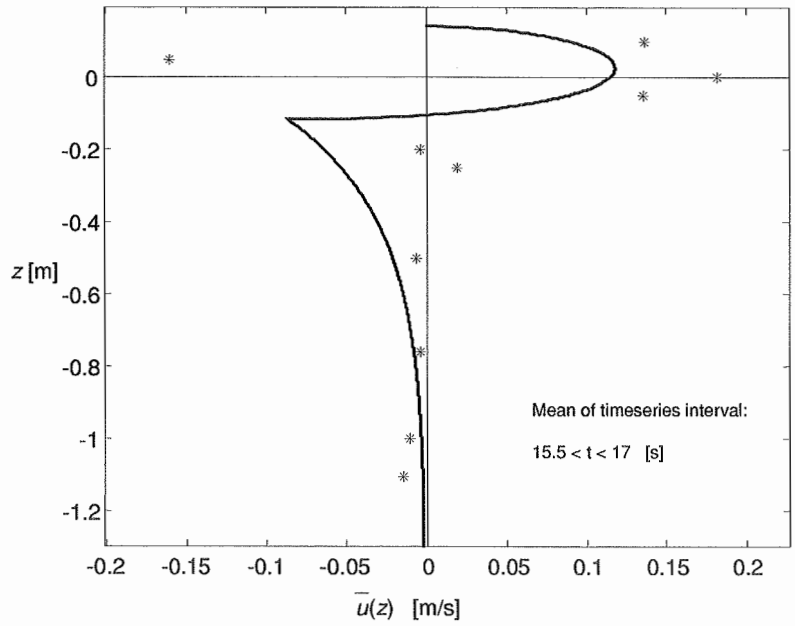

Figure B.8 Case 8 (R15B), $15.5 < t < 17$ [s].

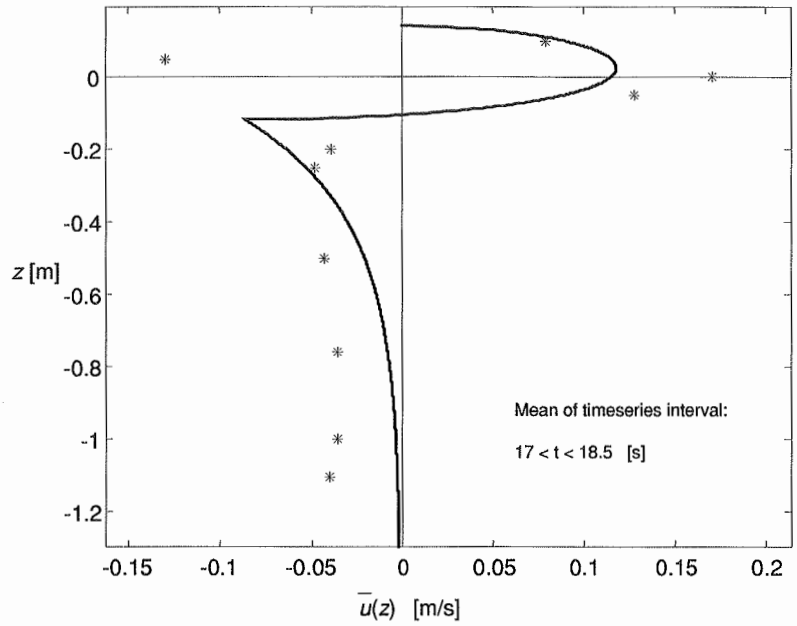

Figure B.9 Case 8 (R15B), $17 < t < 18.5$ [s].

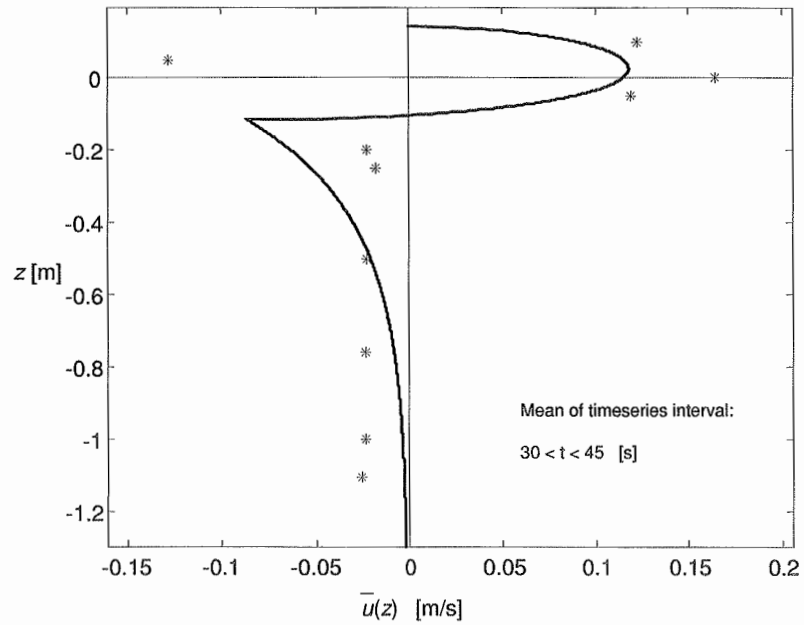

Figure B.10 Case 8 (R15B), $30 < t < 45$ [s].

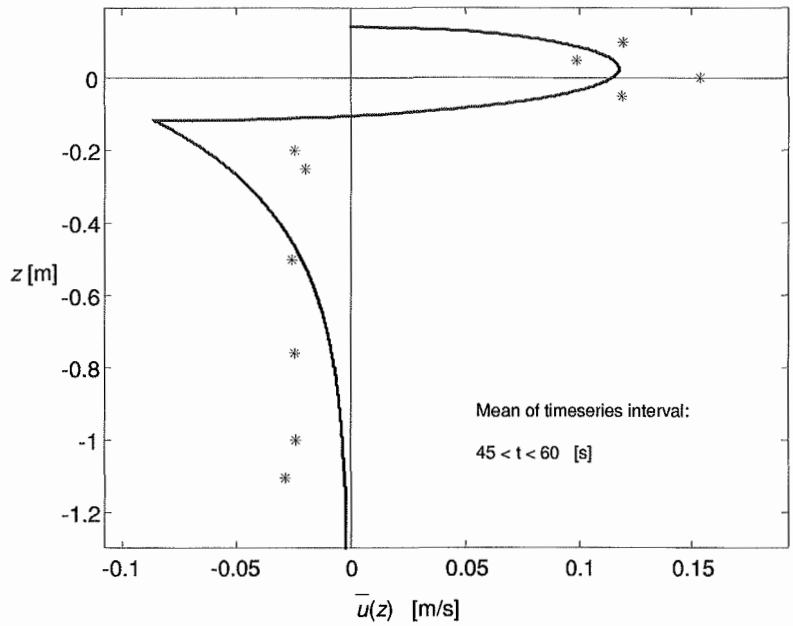

Figure B.11 Case 8 (R15B), $45 < t < 60$ [s].

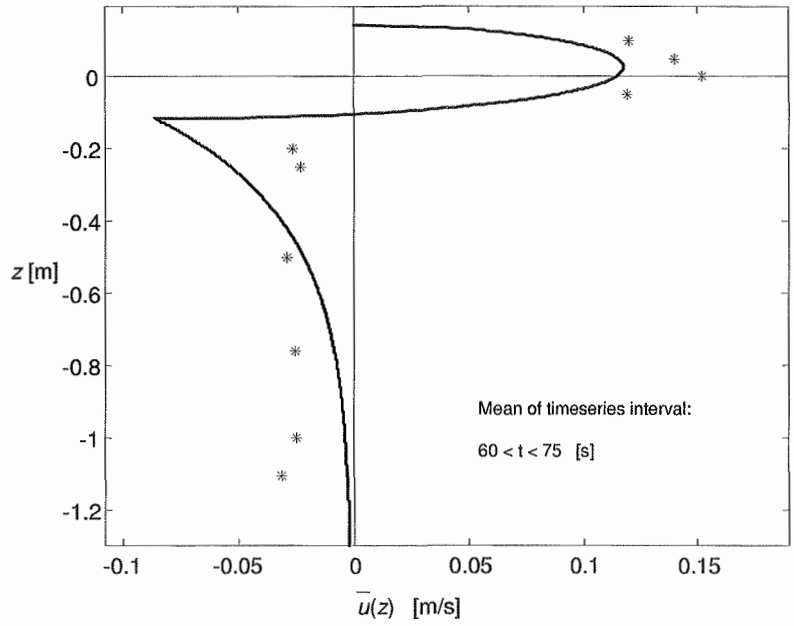

Figure B.12 Case 8 (R15B), $60 < t < 75$ [s].

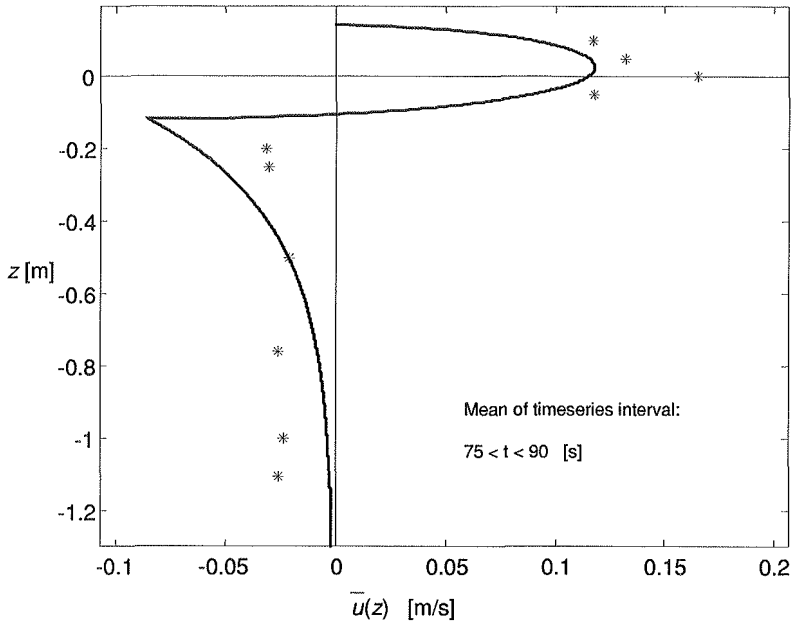

Figure B.13 Case 8 (R15B), $75 < t < 90$ [s].

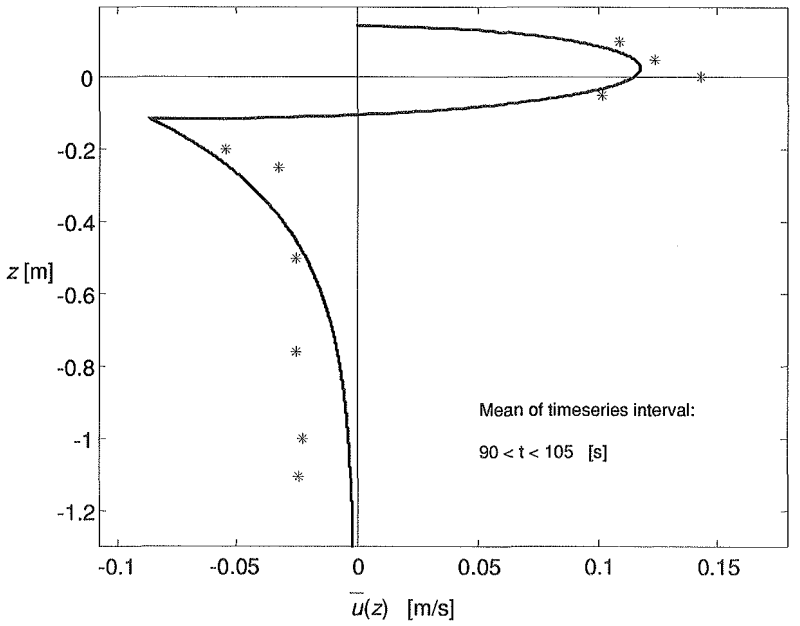

Figure B.14 Case 8 (R15B), $90 < t < 105$ [s].

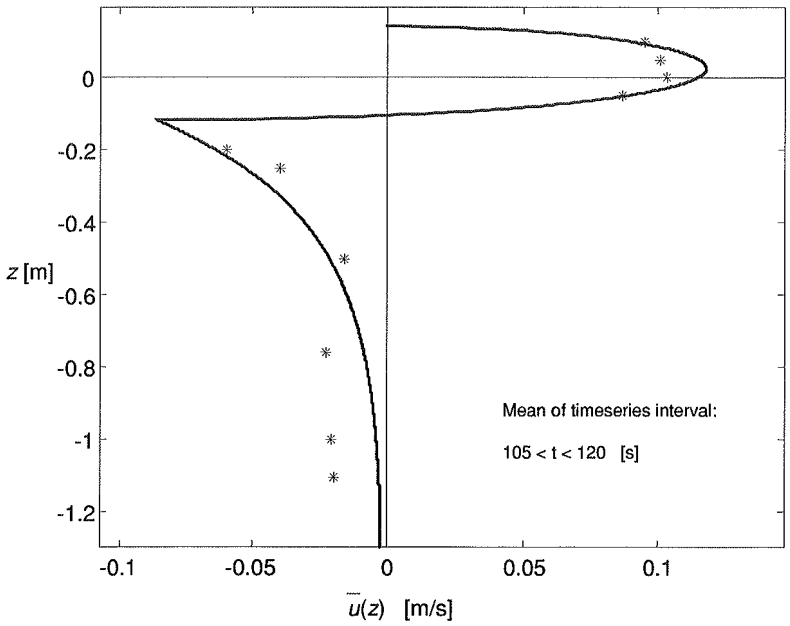

Figure B.15 Case 8 (R15B), $105 < t < 120$ [s].

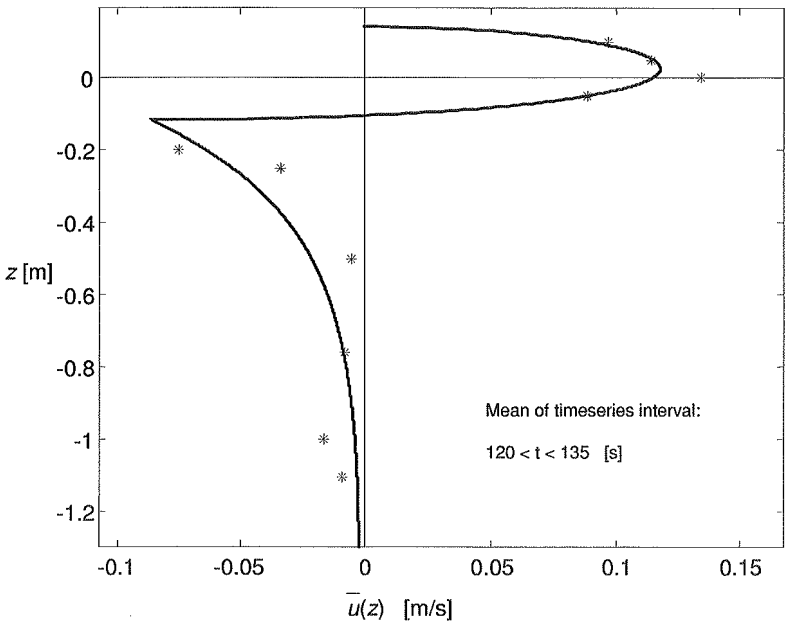

Figure B.16 Case 8 (R15B), $120 < t < 135$ [s].

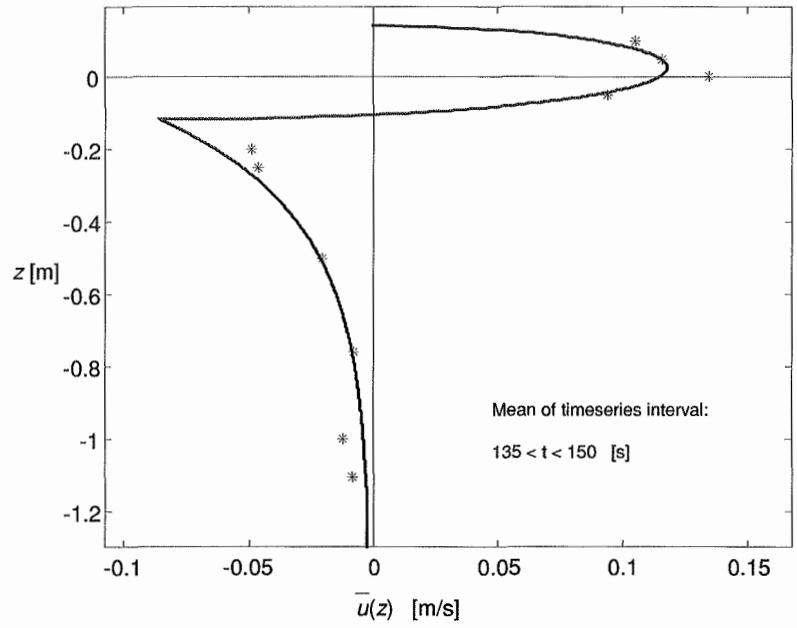

Figure B.17 Case 8 (R15B), $135 < t < 150$ [s].

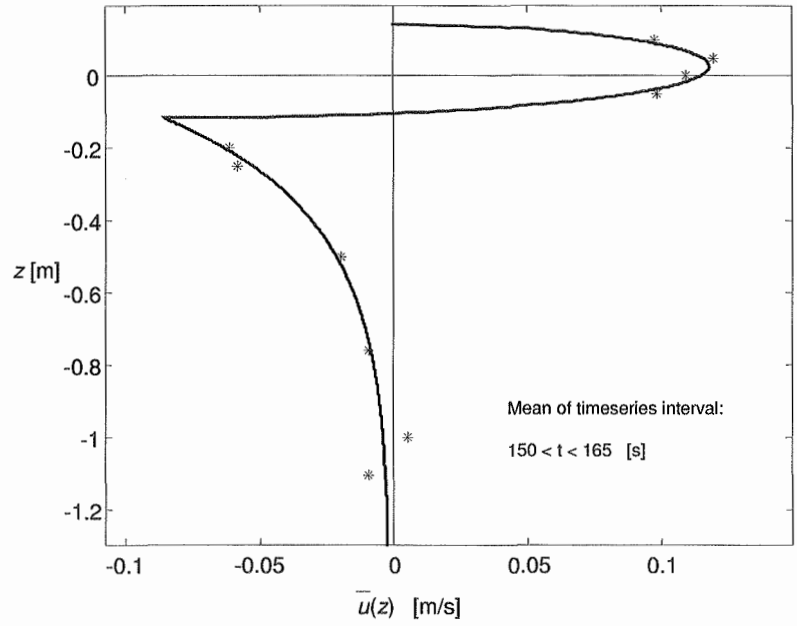

Figure B.18 Case 8 (R15B), $150 < t < 165$ [s].

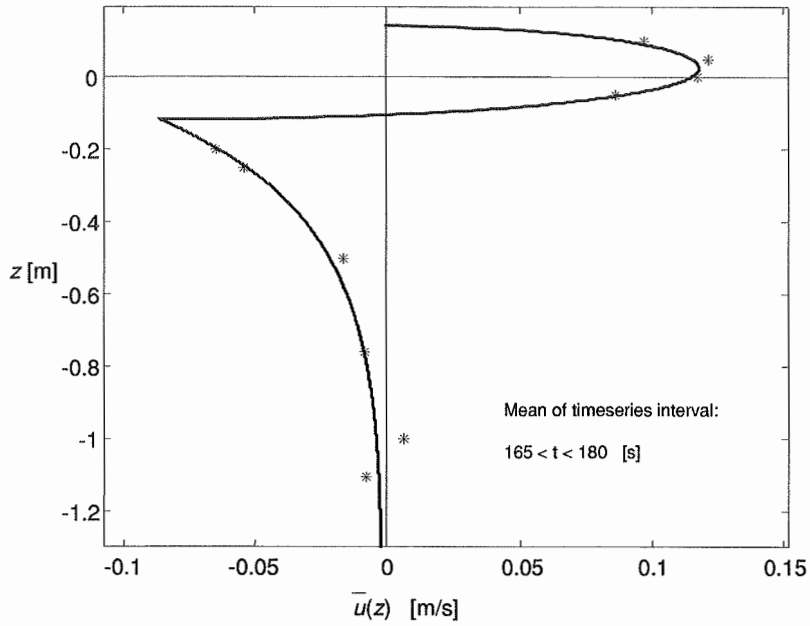

Figure B.19 Case 8 (R15B), $165 < t < 180$ [s].

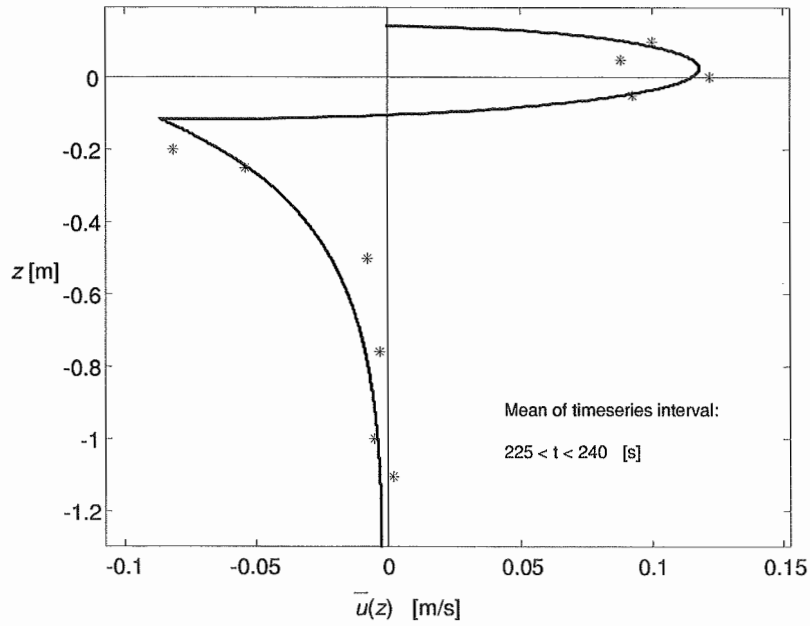

Figure B.20 Case 8 (R15B), $225 < t < 240$ [s].

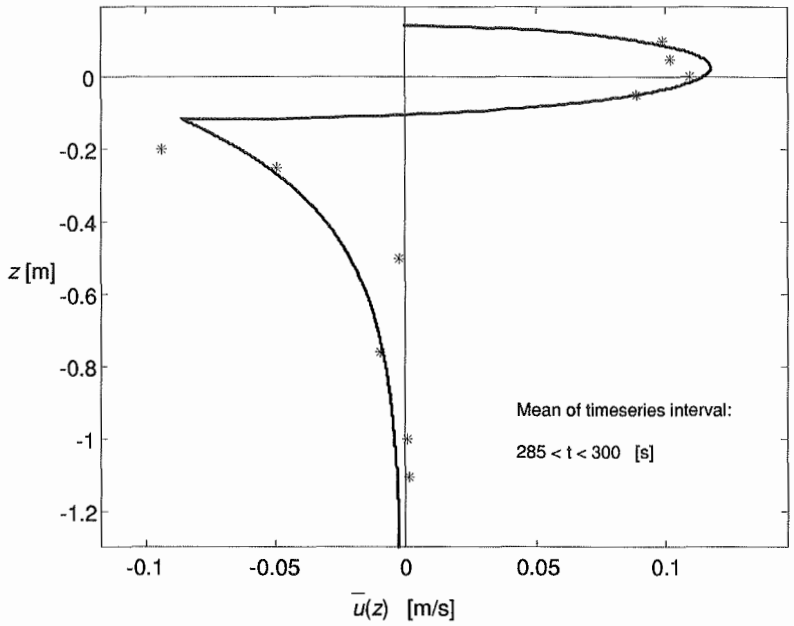

Figure B.21 Case 8 (R15B), $285 < t < 300$ [s].

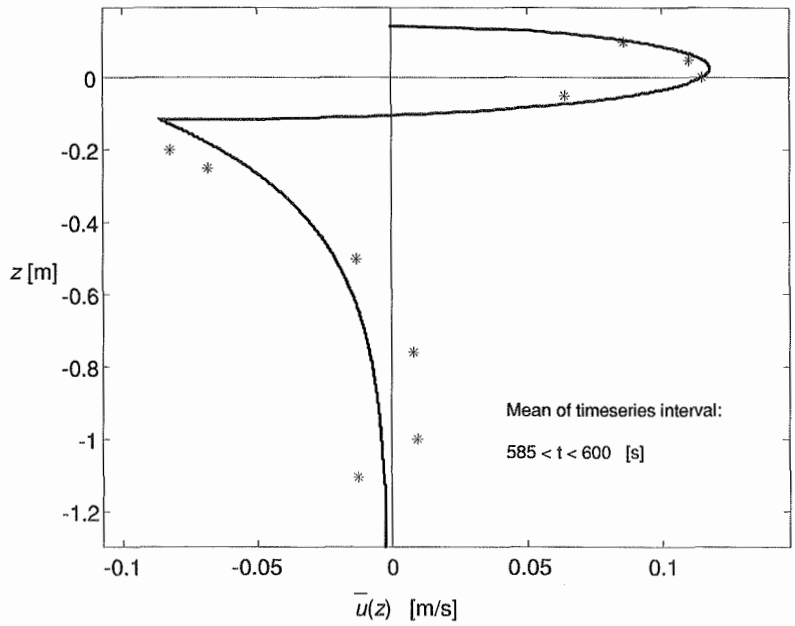

Figure B.22 Case 8 (R15B), $585 < t < 600$ [s].

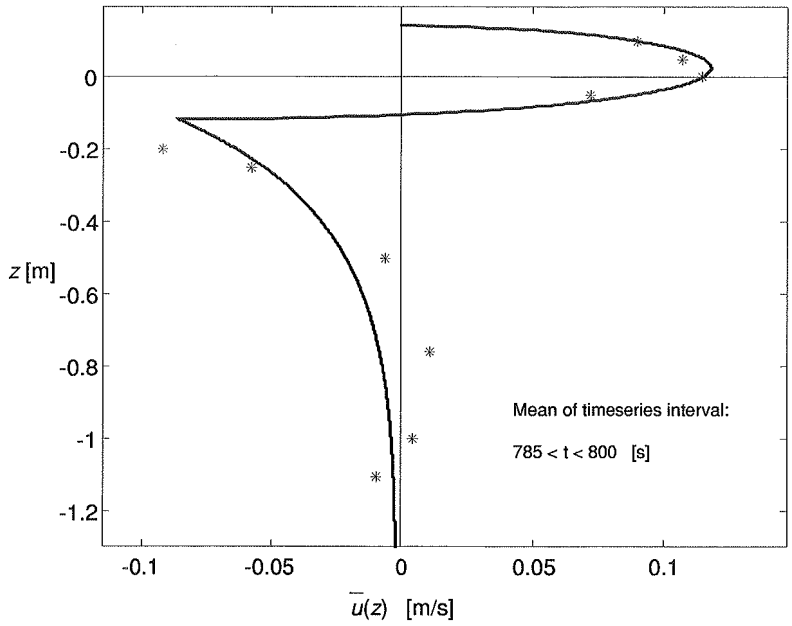

Figure B.23 Case 8 (R15B), $785 < t < 800$ [s].

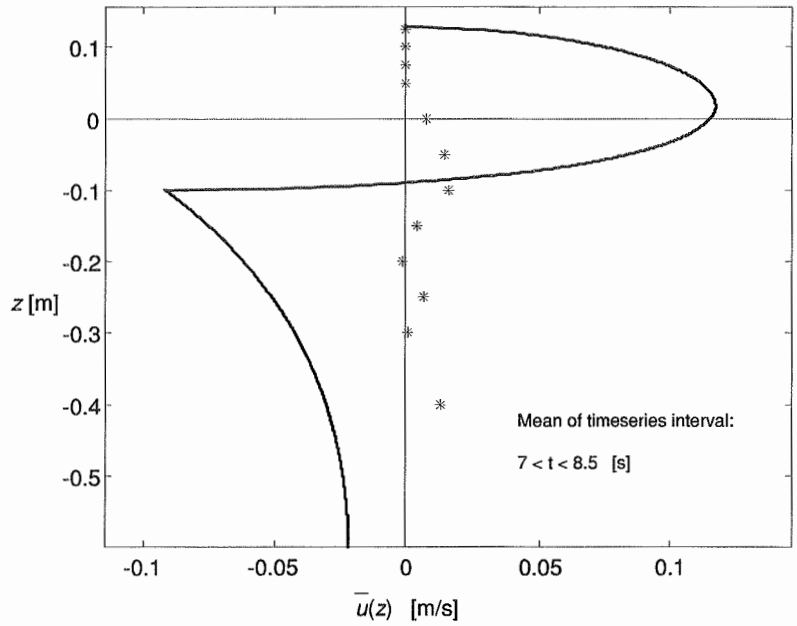

Figure B.24 Case 9 (SR15), $7 < t < 8.5$ [s].

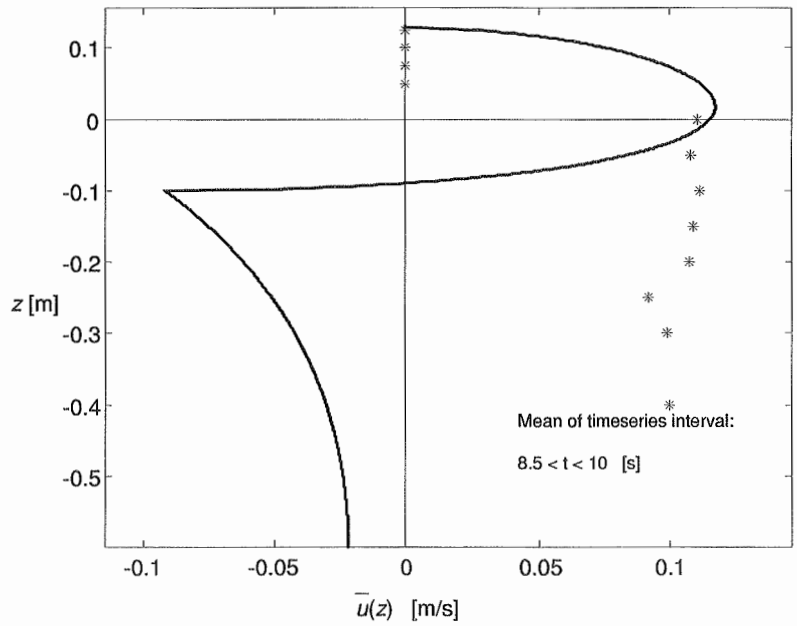

Figure B.25 Case 9 (SR15), $8.5 < t < 10$ [s].

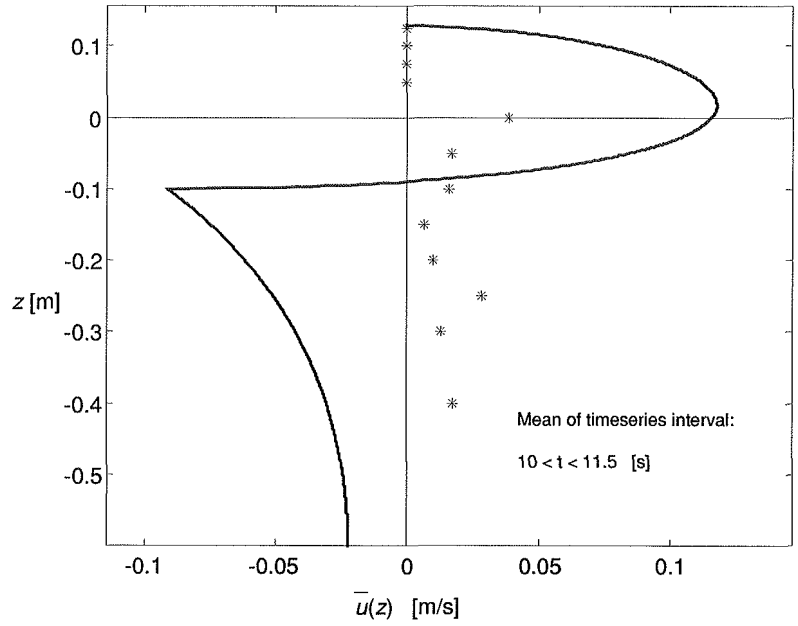

Figure B.26 Case 9 (SR15), $10 < t < 11.5$ [s].

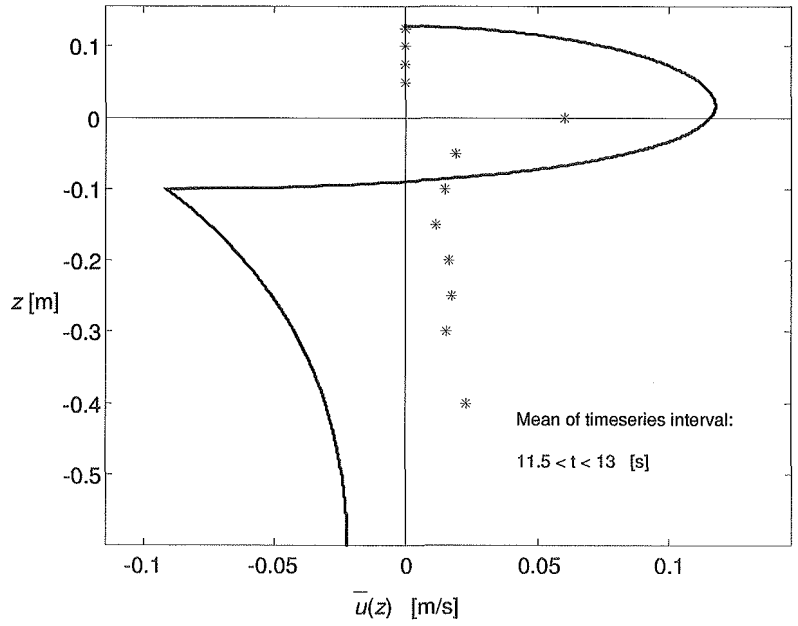

Figure B.27 Case 9 (SR15), $11.5 < t < 13$ [s].

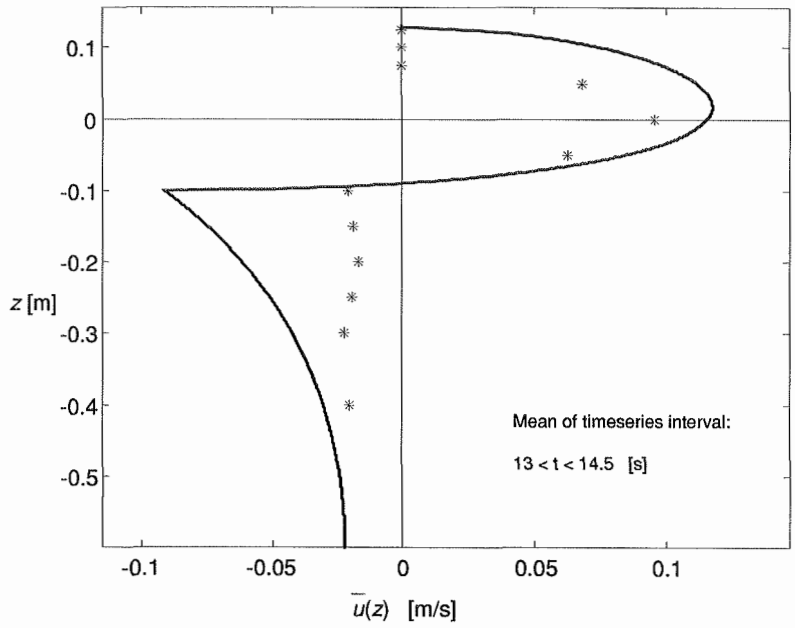

Figure B.28 Case 9 (SR15), $13 < t < 14.5$ [s].

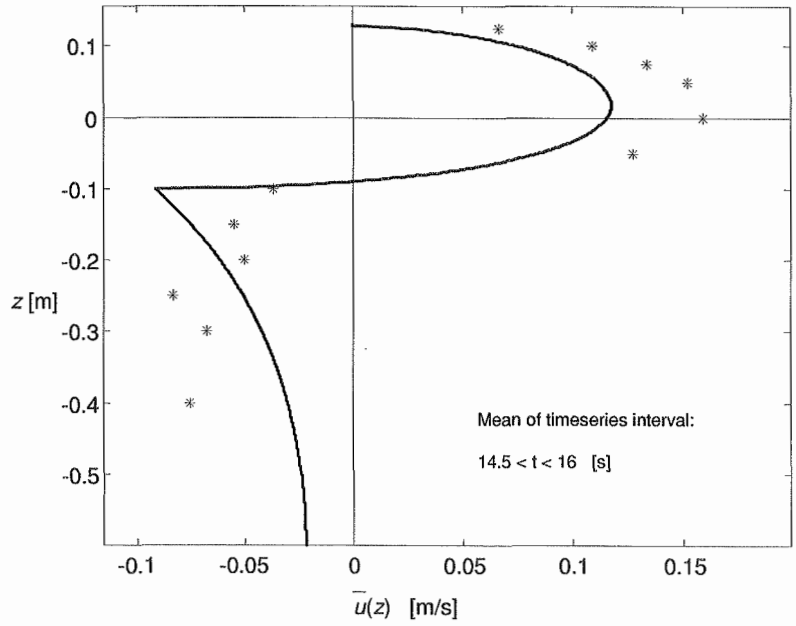

Figure B.29 Case 9 (SR15), $14.5 < t < 16.5$ [s].

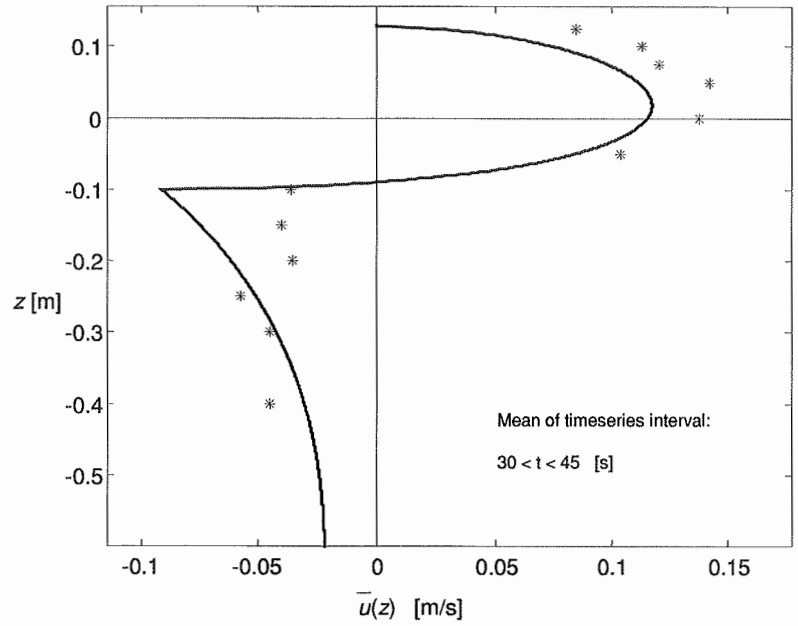

Figure B.30 Case 9 (SR15), $30 < t < 45$ [s].

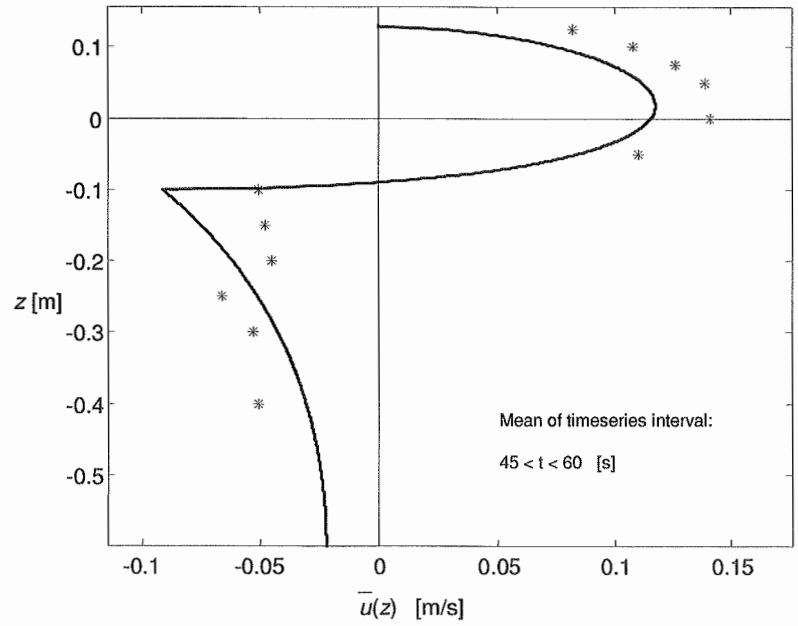

Figure B.31 Case 9 (SR15), $45 < t < 60$ [s].

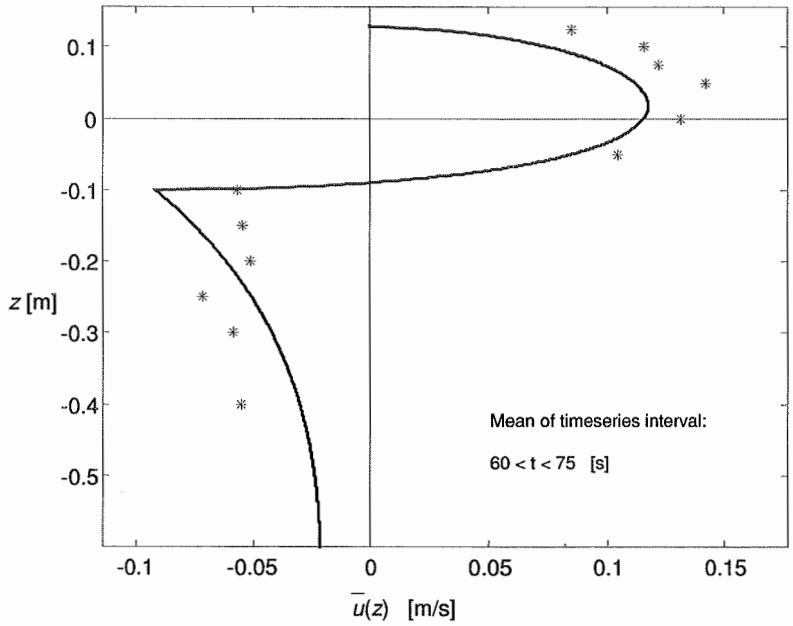

Figure B.32 Case 9 (SR15), $60 < t < 75$ [s].

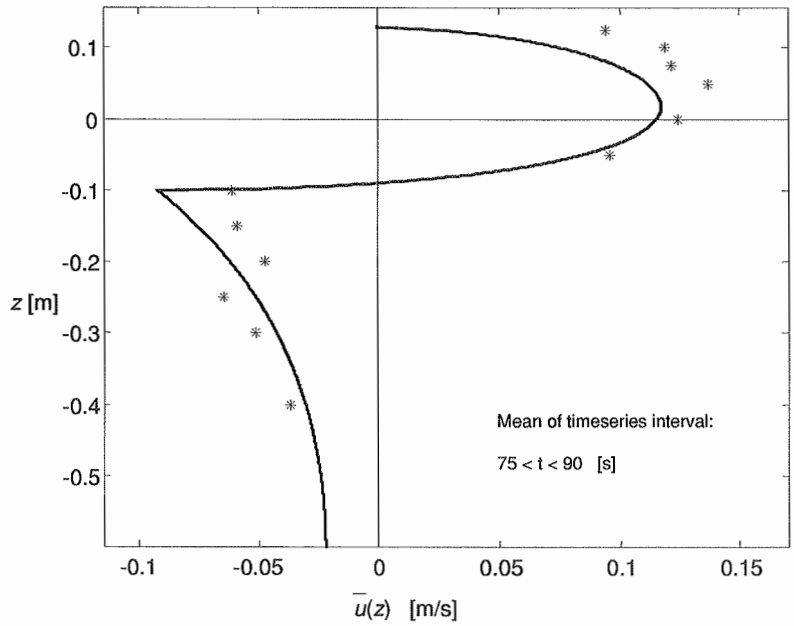

Figure B.33 Case 9 (SR15), $75 < t < 90$ [s].

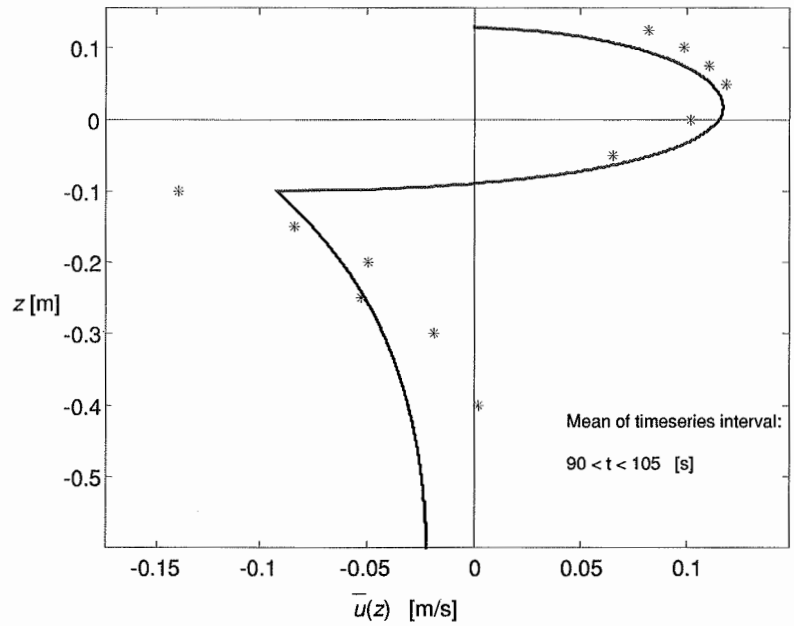

Figure B.34 Case 9 (SR15), $90 < t < 105$ [s].

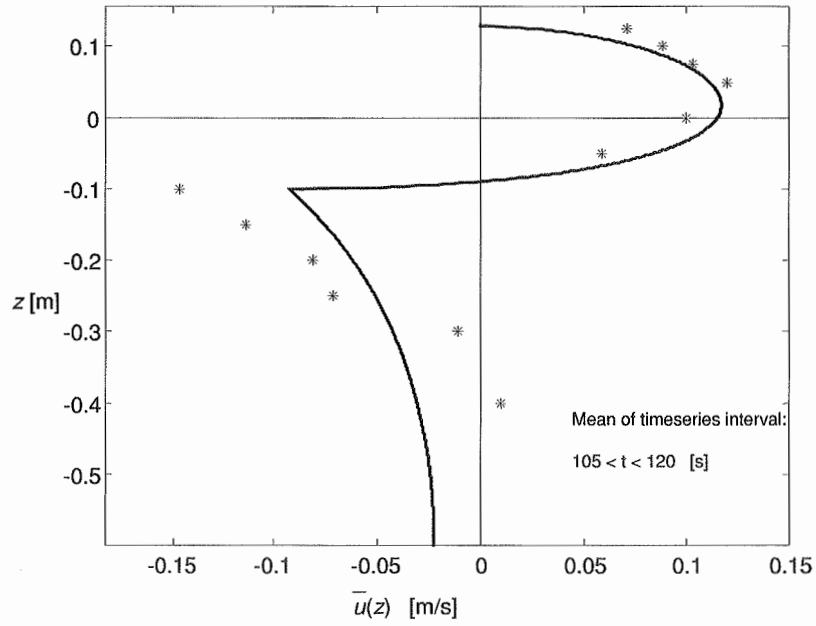

Figure B.35 Case 9 (SR15), $105 < t < 120$ [s].

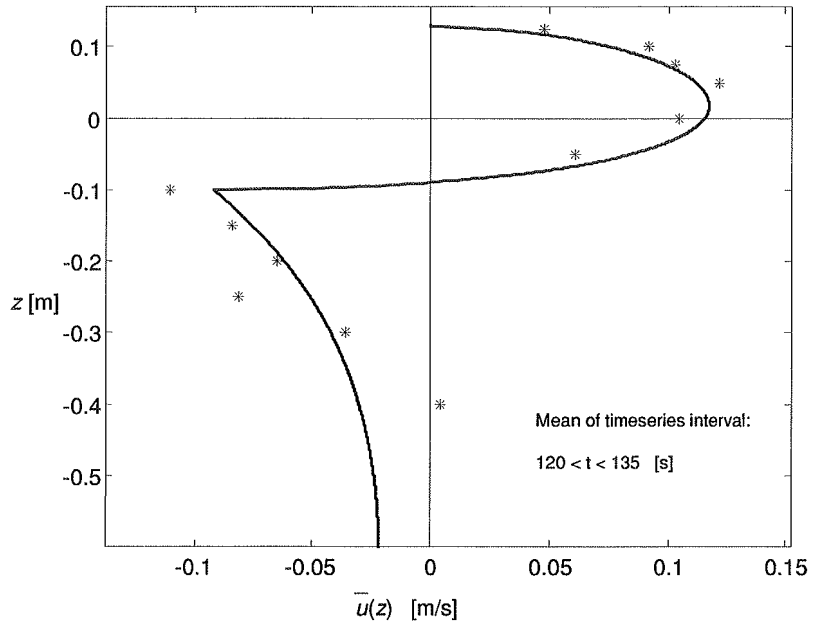

Figure B.36 Case 9 (SR15), $120 < t < 135$ [s].

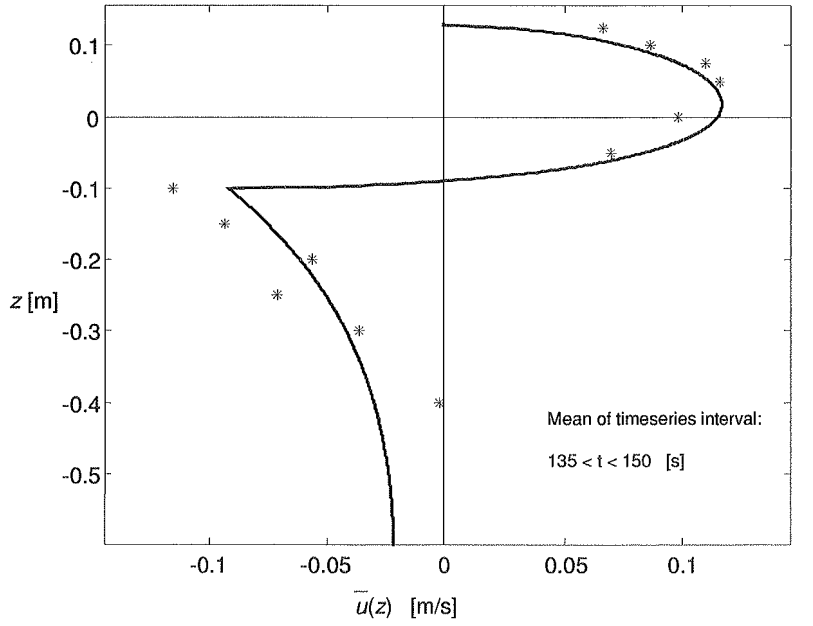

Figure B.37 Case 9 (SR15), $135 < t < 150$ [s].

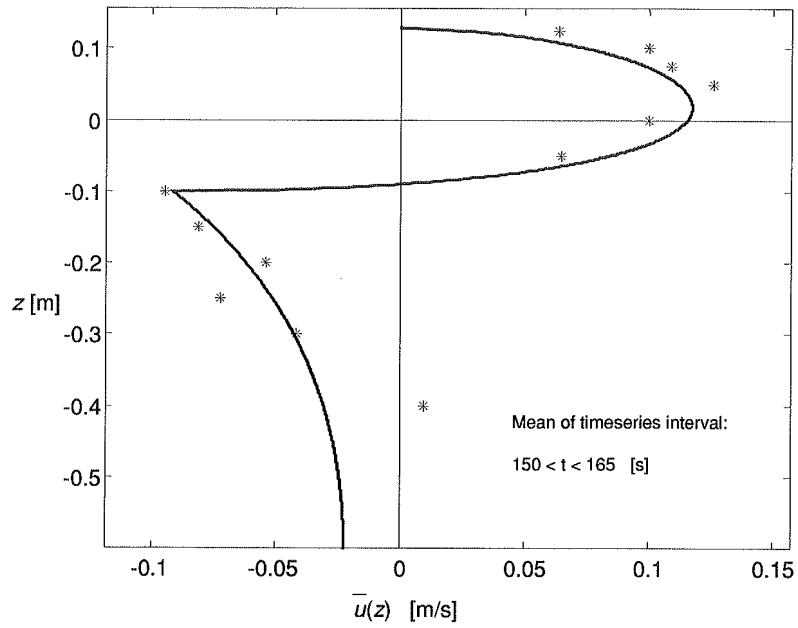

Figure B.38 Case 9 (SR15), $150 < t < 165$ [s].

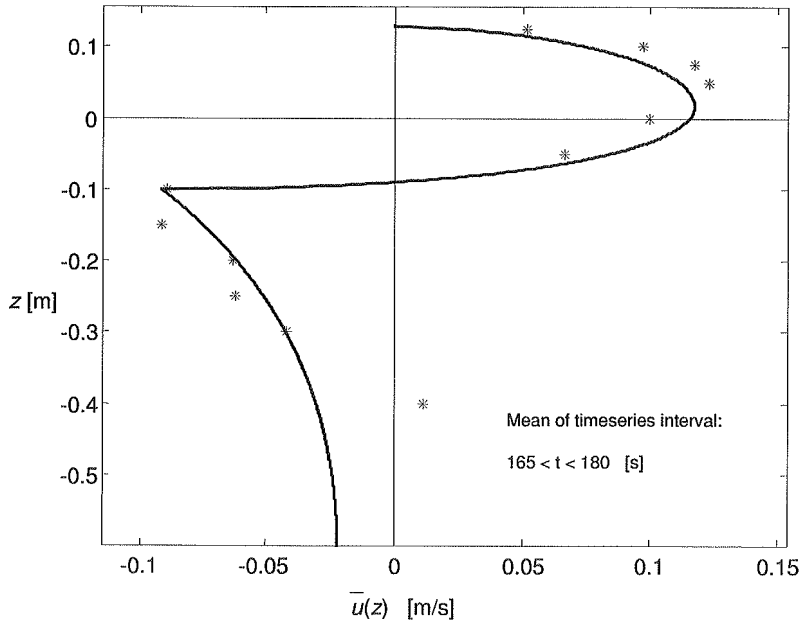

Figure B.39 Case 9 (SR15), $165 < t < 180$ [s].

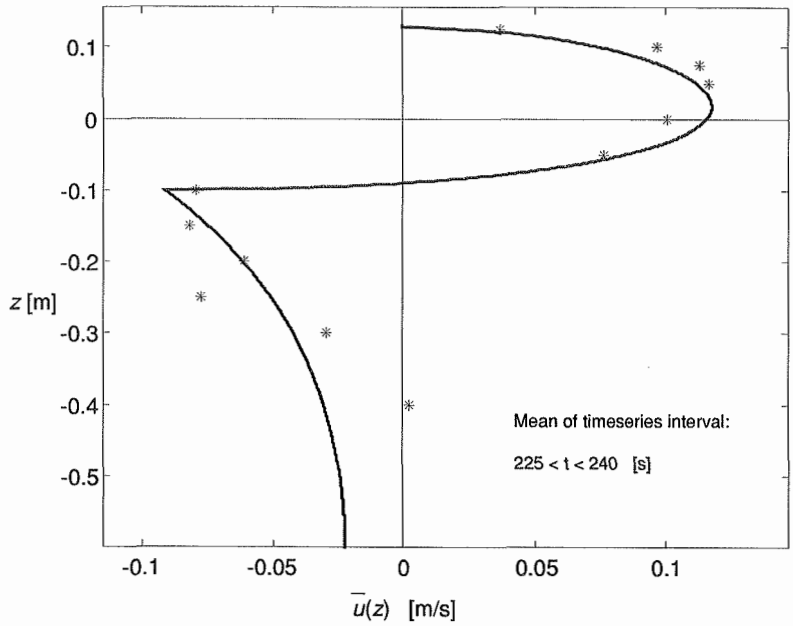

Figure B.40 Case 9 (SR15), $225 < t < 240$ [s].

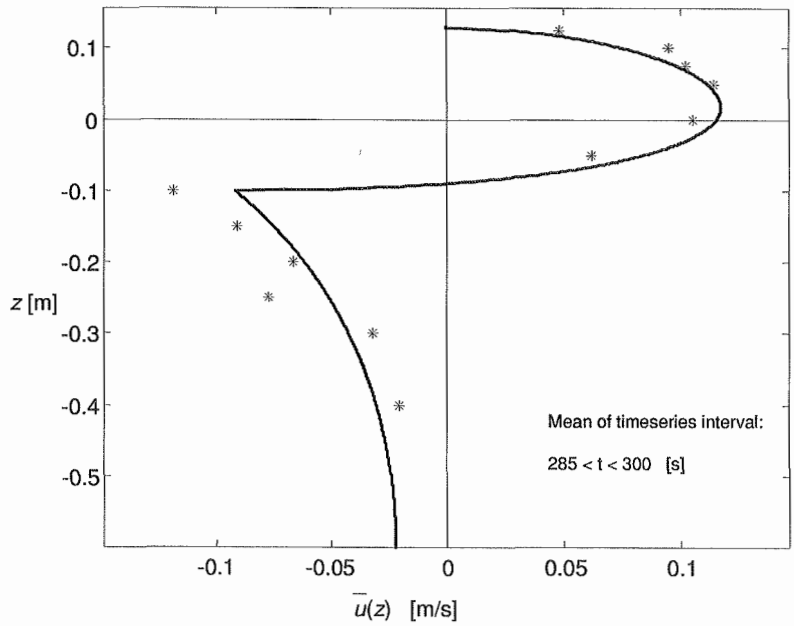

Figure B.41 Case 9 (SR15), $285 < t < 300$ [s].

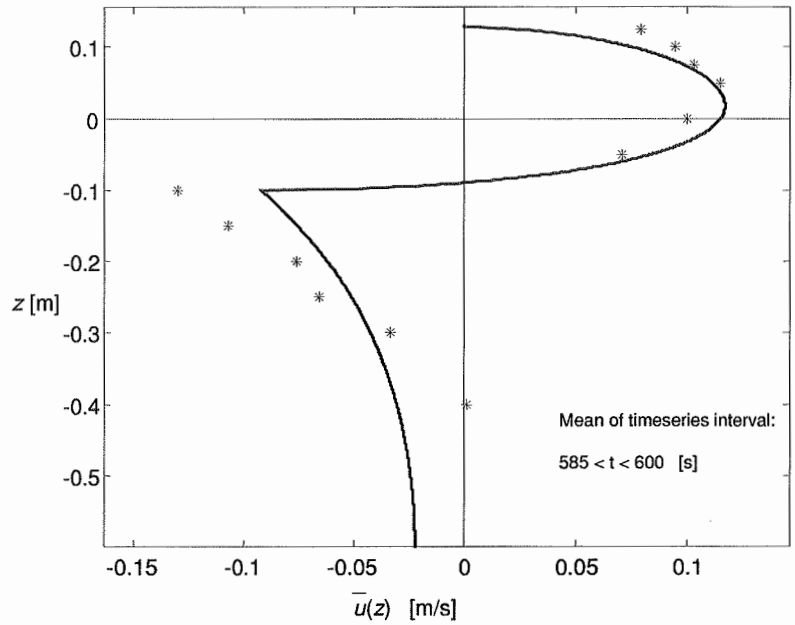

Figure B.42 Case 9 (SR15), $585 < t < 600$ [s].

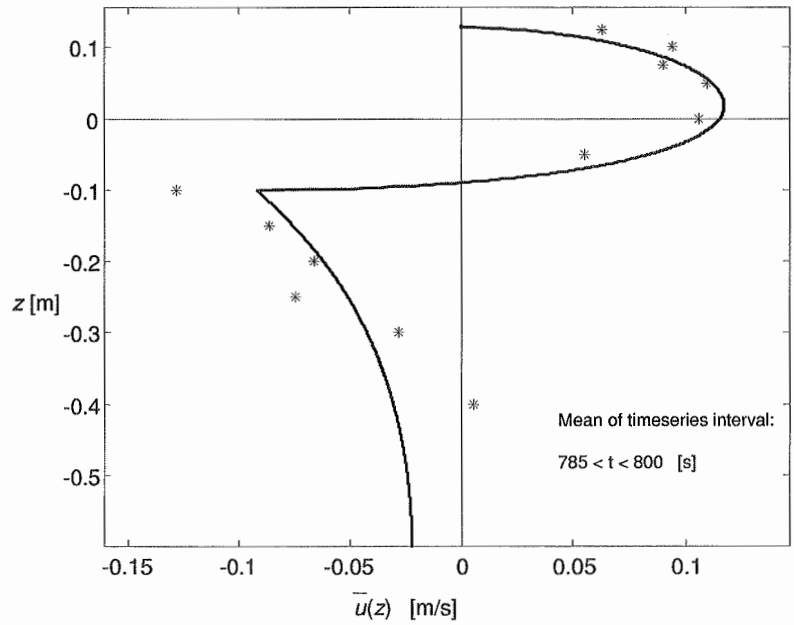

Figure B.43 Case 9 (SR15), $785 < t < 800$ [s].

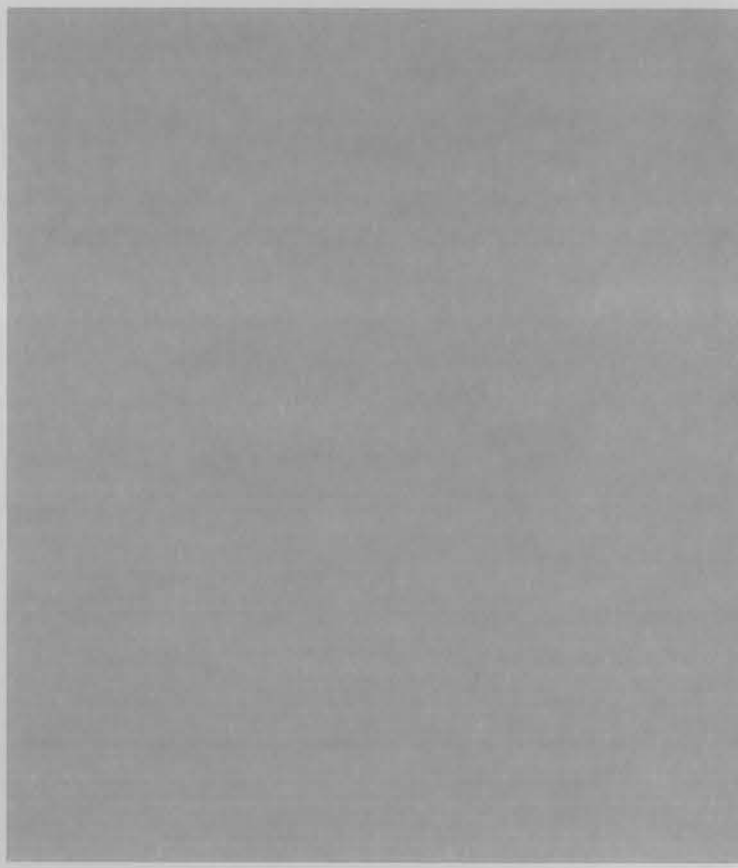

ISBN 82-7984-112-1
ISSN 0809-103X